

Master's thesis

2019

Steinar H. H. Møkkelgjerd

Master's thesis

**NTNU**  
Norwegian University of  
Science and Technology  
Faculty of Engineering  
Department of Geoscience and Petroleum

Steinar H. H. Møkkelgjerd

Metamorphic and magmatic  
evolution near Mandal, Vest-  
Agder; a key area for elucidating  
Sveconorwegian orogenesis

August 2019





Norwegian University of  
Science and Technology

# Metamorphic and magmatic evolution near Mandal, Vest-Agder; a key area for elucidating Sveconorwegian orogenesis

**Steinar H. H. Møkkelgjerd**

Submission date: August 2019

Supervisor: Trond Slagstad

Co-supervisor: Bjørn E. Sørensen and Anette Granseth

Norwegian University of Science and Technology  
Department of Geoscience and Petroleum



## Abstract

The study area lies between the villages Øyslebø and Try in Vest-Agder southern Norway; located within the Telemark lithotectonic unit (believed to be < 1.52 Ga) along the eastern margin of the Sirdal Magmatic Belt (SMB), a 1070-1010 Ma voluminous granitic batholith. The area lies between rocks that underwent continuous 1070-920 Ma ultra-high temperature metamorphism in Rogaland and more discrete short-lived metamorphic events in the east (i.e. 1140-1130 Ma Bamble high-temperature metamorphism, 1050-1020 Ma Idefjord high-pressure metamorphism, and 970 Ma Eastern Segment eclogite facies metamorphism). The aim is to describe magmatic and metamorphic events in the area and relate them to the regional geology; this by U-Pb geochronology and Lu-Hf isotope measurements of zircons with *Laser Ablation – Split Stream – Inductively Coupled Plasma -Mass Spectrometry* (LA-SS-ICP-MS) and *Sensitive High-Resolution Ion Microprobe* (SHRIMP) analysis. The lithologies found in the area include a disperse (relations between biotite and quartzofeldspathic minerals) migmatite and two gneiss units with tectonic relations. These lithologies are intruded by SMB and hornblende-biotite granite (HBG), pegmatites, and mafic rocks.

Three different samples of disperse migmatite yields ages older than the Telemarkian orogen (1.52-1.48 Ga), that is believed to be the earliest rock formation event in the Telemark lithotectonic unit; these measured ages are  $1566 \pm 7$  Ma,  $1565 \pm 11$  Ma, and  $1532 \pm 38$  Ma. This questions the validity of using Gothia- and Telemarkia- orogens as a spatial divide between 1.66-1.52 Ga, and 1.52-1.48 rocks in Southern Norway. Porphyric magmatism at  $1210 \pm 31$  Ma and  $1208 \pm 16$  Ma resulted in two gneiss units; this coincides with a pre-Sveconorwegian period of rifting from 1.34 to 1.10 Ga.

$1078 \pm 14$  Ma and  $1066 \pm 67$  Ma granitic intrusions found close to the edges of SMB at Øyslebø marks one of the earliest found onsets of SMB. Further within the SMB-batholith ages yields between 1050 and 1025 Ma, which fits well with the known peak of SMB magmatism. SHRIMP analysis of zircon rims in migmatite shows migmatisation at  $1011 \pm 9$ , Ma coeval with late-SMB magmatism; this closely followed with end of foliation. HBG-suite magmatism in the area yields at  $945 \pm 14$  Ma, and is the source of local pegmatites.

Lu-Hf isotope measurements of zircons reveals that the rocks are a result of crustal reworking with little to no juvenile input after 1.5 Ga.

## Sammendrag

Feltområdet ligger mellom tettstedene Øyslebø og Try i Vest-Agder, lokalisert i Telemark litotektoniske enhet (menes å være < 1.5 Ga) langs den østre margin av Sirdal Magmatiske Belte (SMB), et 1070-1010 Ma volumøst granitisk batholitt. Området ligger imellom b.a. som gjennomgikk kontinuerlig 1070-920 Ma ultra-høytemperatursmetamorfose i Rogaland, og med diskrete kortlevde metamorfoseeventer i øst (dvs. 1140-1130 Ma høytemperatursmetamorfose i Bamble-Kongsberg, 1050-1020 Ma høytrykksmetamorfose i Idefjord, og 970 Ma Eastern Segment eklogitt-facies). Målet med oppgaven er å beskrive magmatiske og metamorfosiske eventer i området og relatere de til regionalgeologien i Sørnorge. Dette med hjelp av U-Pb geokronologi og Lu-Hf isotop målinger av zircon med *Laserablasjon – delt strøm -Induktivt Koblet Plasma – Massespektrometer* (eng.: LA-SS-ICP-MS) og *Sensitive Høyresolusjon Ionmikroprobe* (eng.: SHRIMP) analyser. Bergartene funnet i feltområdet inkluderer dispers (forholdet mellom biotitt og quartzofeltpastiske mineraler) migmatitt og to gneiss-enheter med tektonsk relasjon. Disse blir intrudert av SMB og hornblende-biotite-granitt (HBG), pegmatitter, og mafiske bergarter.

Tre forskjellige migmatittprøver gir en alder eldre en det Telemarkiske orogenet (1.52-1.48 Ga), dette er den tidligste bergformeringsperioden funnet i Telemark litotektoniske enhet; disse er  $1566 \pm 7$  Ma,  $1565 \pm 11$  Ma, og  $1532 \pm 38$  Ma. Dette setter spørsmål med validiteten i å bruke det gotiske- og telemarkiske orogen som geografiske skiller mellom 1.66-1.52 og 1.52-1.48 Ga gamle bergarter i Sørnorge. Porfyrisk magmatisme ved  $1210 \pm 31$  Ma, og  $1208 \pm 16$  Ma resulterte i to gneisenheter, disse sammenfaller med pre-sveconorwegisk riftin fra 1.34 til 1.10 Ga.

$1078 \pm 14$  Ma og  $1066 \pm 67$  Ma granitiske intrusjoner nær grensen til SMB ved Øyslebø markerer en av de eldste påbyggingene av SMB funnet. Lengre inni SMB-batholitten zirconprøver gir en alder mellom 1025 og 1050 Ma, dette passer med den kjente toppen av SMB-magmatisme mellom 1050 og 1030 Ma. SHRIMP-analyser av zirconrammer i migmatitt tilsier en migmatisering på  $1011 \pm 9$  Ma, sammenfallende med den siste SMB-magmatismen; dette ble kjapt etterfulgt av foliering. HBG-suite magmatisme i området gir en alder på  $945 \pm 14$  Ma, og er kilden til lokale pegmatitter.

Lu-Hf-isotopemålinger av zircon viser at bergartene er et resultat av skorpeomarbeiding med lite juvenil inngang etter 1.5 Ga

## Acknowledgements

This thesis is a collaboration between *Norwegian University of Science and Technology* (NTNU), and *Norwegian Geological Survey* (NGU), as a part of my MSc in geology. Dr Trond Slagstad (NGU) has been the main supervisor, while associate professor Bjørn E. Sørensen (NTNU) and PhD student Anette Granseth has been co-supervising the project. During the last year, I've had offices at both NTNU and NGU's department for mineral resources; one semester was spent at *Texas Tech University* in Lubbock, Texas.

I want to thank my supervisors for their, feedback, engagement in the project, bureaucratic help, endless patient, help in the field, and an open-door policy well beyond what is expected for a master degree. Also, thanks to Nolwenn Coint and Trond Slagstad for giving me access to their samples from the field area.

I would also like to thank NTNU, NGU, and GEMMS, who helped fund the project. GEMMS stands for *Green Management of Mineral Resources* and is a co-project by NTNU and Texas Tech funded by *the Centre for International Cooperation in Education* (SIU).

A big thanks goes to the Mineral lab at NGU letting me use their equipment preparing the samples, and a special thanks to Benjamin Berge, Anne Nordtømme, and Øyvind Skår for lab introductions. Thanks to Kjetil Eriksen and Arild Monsøy at the NTNU thin section lab for preparing my thin section and letting me work as a lab assistant during the last year. Thanks to Chris Kirkland and Bradley McDonald at the *John de Laeter Centre* at *Curtin University*, Australia for assisting and facilitating the SHRIMP and LA-SS-ICP-MS analysis done in this project.

Thanks to the late Arnfinn Villa, who piqued my first interest in geology as a pupil in his class at Molde Secondary School. And thanks to Grammarly, without you, my dyslexia would make this thesis littered with spelling errors (even more than it probably is right now). At last, thanks to my fellow students at NTNU and TTU, you made everything more fun.

Steinar Halvdan Hansen Møkkelgjerd

Trondheim, August 2019

# Table of Content

<b>Abstract.....</b>	i
<b>Sammendrag.....</b>	ii
<b>Acknowledgements.....</b>	iii
<b>Table of Content.....</b>	iv
<b>List of figures and tables.....</b>	vii
Figures .....	vii
Tables .....	viii
Equations.....	viii
<b>Abbreviations .....</b>	ix
<b>1. Introduction.....</b>	1
1.1 Background and aims for study.....	1
1.2 Description of the study area .....	2
1.3 Previous mapping in the field area.....	2
<b>2 Regional geology.....</b>	4
2.1 The Fennoscandian Shield .....	4
2.2 Transscandinavian Igneous Belt (TIB) 1.86-1.66 Ga .....	4
2.3 Gothian-Telemarkia 1.66-1.48 Ga .....	6
2.3.1 Gothian orogeny.....	6
2.3.2 Telemarkian orogeny.....	7
2.4 Pre-Sveconorwegian 1.48-1.15 Ga evolution.....	7
2.5 The Sveconorwegian orogeny 1140-920 Ma, a long-lived accretionary margin.....	8
2.6 The Sveconorwegian orogeny 1140-920 Ma as a four-phased model.....	13
<b>3 Theory .....</b>	16
3.1 U-Pb Geochronology .....	16
3.1.1 U-Th-Pb.....	16
3.1.2 U-Pb Concordia plots.....	17
3.2 Zircon Lu-Hf Isotopes.....	18
3.3 REE-Spider plot .....	20
3.4 Mass Spectrometry methods .....	20
3.4.1 ICPMS (LA-SS-ICP-MS) .....	20
3.4.2 SIMS (SHRIMP).....	21
3.5 Zircon .....	22
<b>4 Methods.....</b>	24
4.1 Fieldwork .....	24

4.2 Sample preparation .....	24
4.2.1 Thin sections .....	24
4.2.2 Geochronological and geochemical preparation .....	25
4.3 Geochronological and geochemical analysis .....	28
4.3.1 SHRIMP II .....	28
4.3.2 LA-SS-ICP-MS .....	28
4.3.3 Data reduction .....	29
4.4 Map digitalization .....	29
4.5 Additional software used .....	30
<b>5 Results .....</b>	<b>31</b>
5.1 Lithological units .....	31
5.1.1 Migmatites .....	33
5.1.2 Augen-gneiss .....	35
5.1.3 Flaser-gneiss .....	37
5.1.4 Deformed granite .....	39
5.1.5 Undefomed granites .....	41
5.1.6 Amphibolites .....	43
5.2 Structural geology of the area .....	44
5.3 U-Pb data .....	47
5.2.1 Migmatites .....	48
5.3.2 Eastern gneisses .....	55
5.3.3 Deformed granites .....	60
5.2.4 Magmatic intrusions .....	68
5.4 Lu-Hf data .....	72
<b>6 Discussion .....</b>	<b>73</b>
6.1 The Gothian-Telemarkian orogenic evolution .....	73
6.1.1 Gothian age rocks in the Telemark lithotectonic unit .....	73
6.1.2 The crustal evolution of the Telemark lithotectonic unit .....	74
6.2 Ca. 1200 Ma magmatism .....	76
6.3 SMB in the field area .....	78
6.3.1 1070-1010 Ma Magmatism .....	78
6.3.2 Late SMB migmatization .....	78
6.4 HBG-suite in the field area .....	79
6.4.1 Widespread granitic intrusion .....	79
6.4.2 HBG-suite as the source of pegmatites .....	80
6.5 Mafic magmatism .....	81

6.5 Structural data.....	82
<b>7. Conclusions.....</b>	<b>83</b>
<b>8 References.....</b>	<b>84</b>
<b>Appendix.....</b>	<b>91</b>
Appendix A – Samples and localities.....	92
Appendix B – Geochronological data from SHRIMP.....	96
Appendix C – Geochronological data from LA-SS-ICP-MS.....	97
Appendix D – Trace element data .....	109
Appendix E - Lu-Hf data.....	117
Appendix F – Zircon data sampling map.....	125
Appendix G – Thin section notes .....	135

## List of figures and tables

### Figures

<b>1.1</b>	Geological map of southern Norway, including a square indicating the field area	1
<b>1.2</b>	Pictures of the field area	2
<b>1.3</b>	Falkum (1985)'s map of the field area	3
<b>2.1</b>	Geological map of Sweden	4
<b>2.2</b>	Geological map of the Fennoscandian shield	5
<b>2.3</b>	Summarised geochronological data by Slagstad et al. 2018	10
<b>2.4</b>	Structural data from SW Telemark lithotectonic unit presented in Slagstad et al. 2018	13
<b>2.5</b>	Schematic model of the four-phase model from Bingen et al. 2008a of Sveconorwegian orogeny	15
<b>3.1</b>	Illustration of U-Th-Pb decay chains	17
<b>3.2</b>	Illustration of $\delta^{176}\text{Hf}/\delta^{177}\text{Hf}$ -ratio differences between solid and liquid after magma formation	18
<b>3.3</b>	Illustration of $\epsilon(\text{Hf}(i))$ -ratio differences between solid and liquid after magma formation	19
<b>3.4</b>	Illustration of Laser Ablation (LA) systems	21
<b>3.5</b>	Schematic layout of SHRIMP II at John de Laeter Centre at Curtin University	22
<b>4.1</b>	Step-by-step illustration of mineral separation done in this study	27
<b>4.2</b>	Image illustrating the digitalisation of the sketched map	29
<b>4.3</b>	Image illustrating the digitalisation based on the horizontal magnetic gradient	30
<b>5.1</b>	Geological of the field area produced by this study, including locations from the field book	31
<b>5.2</b>	Disperse migmatite	34
<b>5.3</b>	Augen-gneiss	36
<b>5.4</b>	Flaser-gneiss	38
<b>5.5</b>	Deformed granite	40
<b>5.6</b>	Undeformed granite	42
<b>5.7</b>	Amphibolite	43
<b>5.8</b>	Tectonic foliation measurement from the field area presented in a stereonet	44
<b>5.9</b>	Horizontal magnetic gradient with the two folds highlighted	44
<b>5.10</b>	Tectonic foliation measurement from the field area presented in the horizontal magnetic gradient map. Including the four main anomalies.	46
<b>5.11</b>	VAG 128018	51
<b>5.12</b>	HAL 193062	52
<b>5.13</b>	HAL 193073	53
<b>5.14</b>	VAG 084363	54
<b>5.15</b>	VAG 128016	57
<b>5.16</b>	VAG 128017	58
<b>5.17</b>	VAG 128019	59

<b>5.18</b>	VAG 128011	63
<b>5.19</b>	VAG 084362	64
<b>5.20</b>	HAL 193061	65
<b>5.21</b>	HAL 193063	66
<b>5.22</b>	VAG 128010	67
<b>5.23</b>	HAL 193052	70
<b>5.24</b>	HAL 193066	71
<b>5.25</b>	Lu-Hf data from the field area	72
<b>6.1</b>	Lu-Hf-vectors from Petersson et al. 2015a and Bingen et al. 2011	75
<b>6.2</b>	Lu-Hf-vector from this study presented together with previous calculated vectors	76
<b>6.3</b>	Impact of high temperature on quartzofeldspathic aggregates	77
<b>6.4</b>	CL-image of HAL 193073-N	79
<b>6.5</b>	Pegmatite-granite relations at location 123	81
<b>6.6</b>	Amphibolite-flaser gneiss-granite-relations at location 129	82

## Tables

<b>5.1</b>	List of mineral abbreviations	32
<b>5.2</b>	Results from the U-Pb geochronological measurements	47

## Equations

<b>3.1</b>	$238\text{U} \rightarrow 206\text{Pb}$	16
<b>3.2</b>	$235\text{U} \rightarrow 207\text{Pb}$	16
<b>3.3</b>	$232\text{Th} \rightarrow 208\text{Pb}$	16
<b>3.4</b>	Discordance	17
<b>3.5</b>	$176\text{Lu} \rightarrow 176\text{Hf}$	18
<b>3.6</b>	$176\text{Lu} \rightarrow 176\text{Yb}$	18
<b>3.7</b>	$i_{\text{CHUR}}$	19
<b>3.8</b>	$i_{\text{Sample}}$	19
<b>3.9</b>	$\epsilon_{\text{Hf}(i)}$	19

## Abbreviations

<b>BKSK</b>	Bjerlreim-Sokndal Layered Intrusion
<b>BSE</b>	Backscatter Electron
<b>CL</b>	Cathodoluminescent
<b>E##</b>	Europavei (eng. Europa road)
<b>Fm</b>	Formation
<b>Fv###</b>	Fylkesvei (eng. County road)
<b>GAB</b>	Göteborg-Åmål Belt
<b>GEMMS</b>	Green Management of Mineral Resources
<b>HAOM</b>	high-alumina orthopyroxene megacrysts
<b>HBG</b>	Hornblende Biotite Granite
<b>HREE</b>	Heavy Rare Earth Element
<b>LA-SS-ICP-MS</b>	Laser Ablation - Split Stream - Inductively Coupled Plasma - Mass Spectrometry
<b>LREE</b>	Light Rare Earth Element
<b>MC</b>	Multi Collector
<b>MZ</b>	Mylonite Zone
<b>NGU</b>	Norges Geologiske Undersøkelse (Eng.: Geological Survey of Norway)
<b>NTNU</b>	Norges Tekniske og Naturvitenskapelige Universitet (Eng.: Norwegian University of Science and Technology)
<b>PPL</b>	Plane Polarized Light
<b>RAP</b>	Rogaland Anorthosite Province
<b>REE</b>	Rare Earth Element
<b>RIC</b>	Rogaland Igneous Complex
<b>SC</b>	Single Collector
<b>SEM</b>	Scanning Electron Microscope
<b>SHRIMP</b>	Sensitive High-Resolution Ion Microprobe
<b>SIMS</b>	Secondary Ion Mass Spectrometry
<b>SLM</b>	Stora Le-Marstrand
<b>SMB</b>	Sirdal Magmatic Belt
<b>TIB</b>	Transcandinavian Igneous Belt
<b>TTU</b>	Texas Tech University
<b>UHT</b>	Ultra-High temperature
<b>XPL</b>	Cross Polarized Light
<b>Ma</b>	Millions of years
<b>Ga</b>	Billions of years

## 1. Introduction

### 1.1 Background and aims for study

This study elucidates a previously uninvestigated area located between two units with distinct metamorphic evolution (Rogaland and Bamble-Kongsberg) of the Sveconorwegian Orogen (1140-920 Ma) along the eastern border of Sirdal Magmatic Belt (SMB). The aim is to determine the age of local

metamorphism/magmatism structural evolutions related to regional geology and give a detailed description of the lithological units in the field area.

Regionally the orogen separates between long-lived (1070-920) ultra-high temperature metamorphism in the Rogaland (Slagstad et al., 2018) and more discrete shortlived pressure metamorphic events further east. These include 1140-1130 Ma Bamble high-temperature(Bingen and Viola, 2018, Clough and Field, 1980, Njiland et al., 2014), 1050-1020 Ma Idefjord high-pressure (Söderlund et al., 2008), and 970 Ma Eastern Segment eclogite facies metamorphism (Hegardt et al., 2005, Johansson et al., 2001, Möller, 1998).

1070-1010 Ma magmatism resulted in a NNW-SSE trending major granitoid batholith coined Sirdal Magmatic Belt referred to as SMB from now on (Slagstad et al., 2013a). This is followed by emplacement of geographically widespread 990-930 Ma Hornblende-Biotite granite referred to as HBG (Jensen and Corfu, 2016, Vander Auwera et al., 2011, Vander Auwera et al., 2003) and the 950-920 Ma Rogaland Igneous Complex (Schärer et al., 1996, Vander Auwera et al., 2011, Bybee et al., 2014).

There are four major Lithotectonic units within the Sveconorwegian orogen; these are Telemarkia, Bamble-Kongsberg, Idefjord, and the Eastern Segment. The Gothian (1.66-1.52 Ga) (i.e., Bamble-Kongsberg, Idefjord, and the Eastern Segment) and Telemarkian (1.52-1.48 Ga) were previously believed to be two separate orogens. However, later geochronological

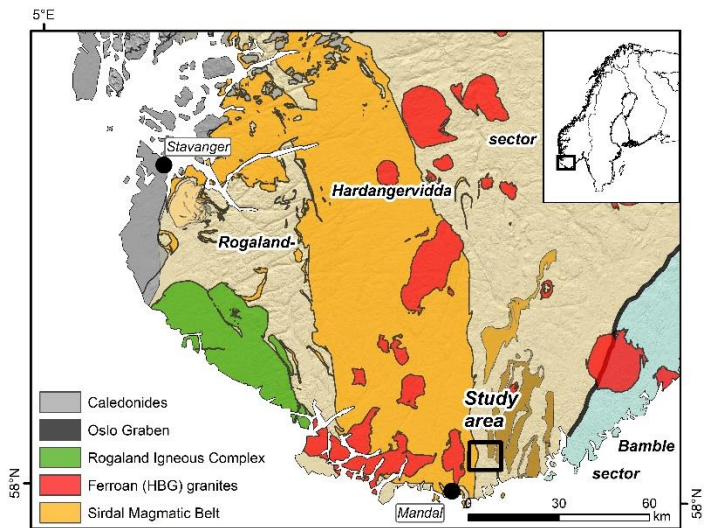


*Figure 1.1 : Modified map from Slagstad et al. (2018). Shows the study area situated between Rogaland and Bamble on the eastern border of SMB.*

research suggest these two orogens comes from one long-lived accretionary arc (Roberts and Slagstad, 2014).

### 1.2 Description of the study area

The study area is approximately 70 km<sup>2</sup> and lies north of Mandal, Vest-Agder, situated in a quadrant with Øyslebø and Tryfjorden as end corners. Though not highly populated the area has a well-distributed road network partly due to a high number of cabins and summer houses. The road cuts presented many good localities with easy access by car. Private roads closed to cars presents an easy hike towards areas not found along any fylkesvei (en. County road). Fv302 and Fv459/E39 gives good opportunities for East-West profiles for the southern and northern part respectively, Kleivsetveien and Svemmelandsveien follows the eastern portion from south to north, while Fv151 and Kjærsvægen gives access to the interior.

Lakes and densely forested hills dominate the area. Due to geology, the area north of Kleivsetvannet is less forested and easy to map, the rest of the area is often too densely forested to be mapped. The large number of lakes also gives a good mapping opportunity. Areas around Tryfjorden and Nomedalsvatnet has cliffs that can be difficult to map without any special gear.



Figure 1.2: (A) lake Krokvatnet, one of many lakes in the area, on the opposite side, there is a well-forested similar gentle hill to the terrain that dominates the study area. (B) Road cut along a private side road to Fv302, road cuts like these provided the best opportunity for mapping.

### 1.3 Previous mapping in the field area

Falkum (1985) divides the field area into three different, broadly described units (see figure 1.3). The first one is coloured in dark orange and is described as “*Augen gneiss, mainly deformed porphyritic granites and granodiorites with large phenocrysts (1-20 cm) of alkali feldspar*”. This unit description is given to three separate bodies, one stretching all along the western border of the field area, and two found in the eastern part of the field area. Bingen

## 1. Introduction

---

and Van Breemen (1998) interprets the western body to be a part of the Mandal-Svirdal units that yields to  $1049 +2/-8$  Ma. This unit is a part of the larger Feda suite, a biotite  $\pm$  hornblende augen gneiss. The same paper interprets the two eastern gneisses to be of coeval to the Gjerstad suite found in Telemark; a biotite  $\pm$  hornblende augen gneiss that locally yields to a grey charnockite augen gneiss. The Gjerstad suite is comprised to 1.19-1.18 Ga.

The Light orange unit that is found in central parts of the field area is described by Falkum (1985) as “*Banded gneiss, partly migmatitic, amphibolite, biotite gneiss banded with light coloured gneiss, locally with garnet-sillimanite-cordierite biotite gneiss in layers of quartzite*”.

The last unit is coloured in pink and if found along the easternmost of the Gjerstad bodies. It is described as “*Granitic gneisses, variable fine- to mediumgrained quartzo-feldspathic gneisses*”.

It is worth noting that Falkum (1985) mapped a much larger area than the field area, and some of the observations used to make the description may not be from the field area.

(Falkum, 1985) found that the general tectonic foliation has a N-S strike with a westward dip. Also, a Antiform with a N-S axial trace line is cutting the western Gjerstad unit (see figure 1.3).

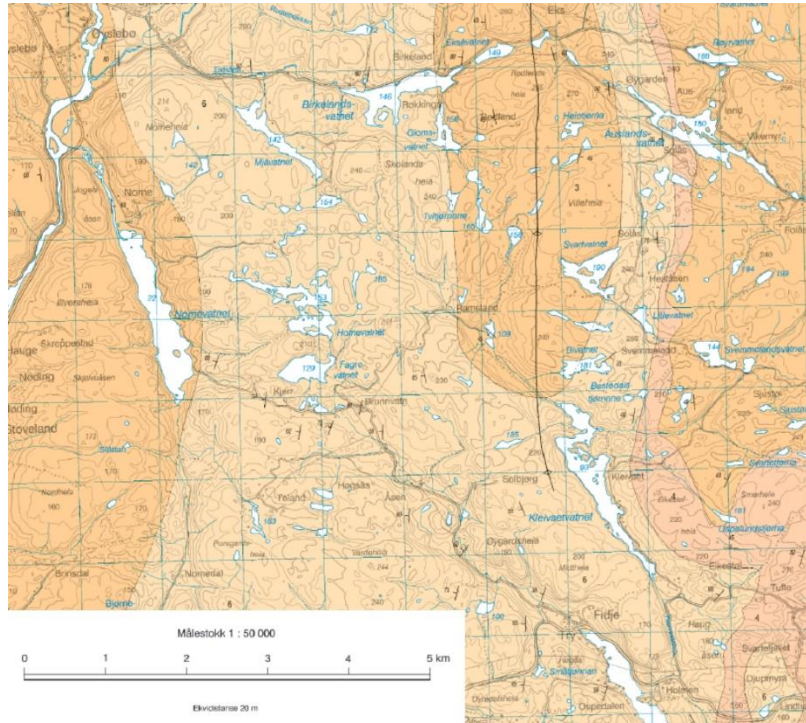


Figure 1.3: Falkum (1985)'s map of the field area.

## 2 Regional geology

### 2.1 The Fennoscandian Shield

The field area lies along the eastern border of the Sirdal Magmatic Belt (SMB) (1.07-0.92 Ga) a large granitic belt found in Gothaian-Telemarkian at the southwest margin of the Fennoscandian Shield (often referred to as Fennoscandia) (Slagstad et al., 2013a, Slagstad et al., 2018). Fennoscandia formed during Columbian supercontinental amalgamation of Archaean crusts at 1.9-1.85 Ga. Coeval to this several periods of continental growth and accretion from 2.0 to 1.8 Ga created what we now call the Svecofennian domain. In the late stages of Svecofennia, the Svecobaltic orogeny (1.83-1.79 Ga) resulted in a collision with the already conjoined cratons of Sarmatia and Volgo-Uralia creating the East European Craton (Roberts and Slagstad, 2014).

The Archaean fragments, Svecofennian (2.0-1.8 Ga), Transscandinavian Igneous Belt (TIB) (1.86-1.66), and Gothian-Telemakian (1.66-1.48) makes up the four main subgroups of Fennoscandia and can be found geographically from northeast to southwest as mentioned.

### 2.2 Transscandinavian Igneous Belt (TIB) 1.86-1.66 Ga

TIB is a belt of alkali-rich, alkali-calcic I- and A-type granitoids stretching from Blekinge in southern Sweden and up to Dalarna-Herjedalen-Hedmark where it meets the Caledonides. The Revsund granitoids in northern Sweden and pockets within the Caledonian belt as far north as Tromsø are all believed to be a part of TIB (Högdahl et al., 2004). Usually divided into three subgroups: TIB-0 (1.86-1.84 Ga), TIB-1 (1.88-1.77 Ga), and TIB-2/3 (1.72-1.62 Ga). The Belt represents a continental arc with voluminous alkaline-rich granitoid emplaced as a result of mafic underplating of Svecofennian and juvenile crust. It represents a shift in dip-direction from a

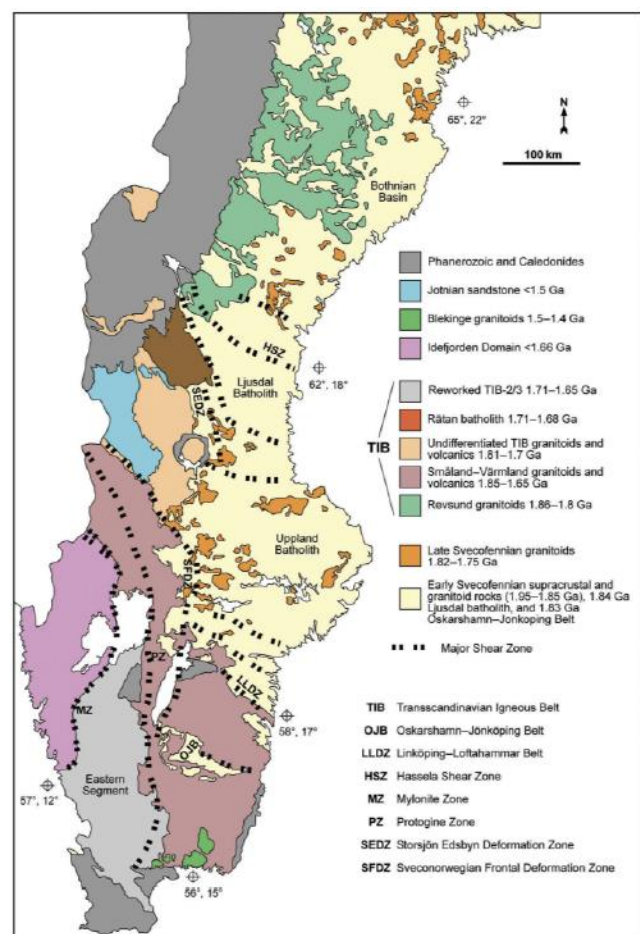


Figure 2.1: Sketched map of the Transscandinavian Igneous Belt from Roberts and Slagstad (2014), modified after Högdahl et al. (2004).

north dipping (1.86–1.81 Ga) subduction zone, to a east (1.81–1.76 Ga), and later to a northeast (1.76–1.66 Ga) dip-direction, where the magmatism comes from nearby extensional and transtension/transpression environments within the craton (Roberts and Slagstad, 2014, Andersson et al., 2004). The western part of TIB is referred to as the Eastern Segment, situated west of TIB but considered to be an extension of TIB-2/3 reworked by the Sveconorwegian orogeny (Söderlund et al., 1999).

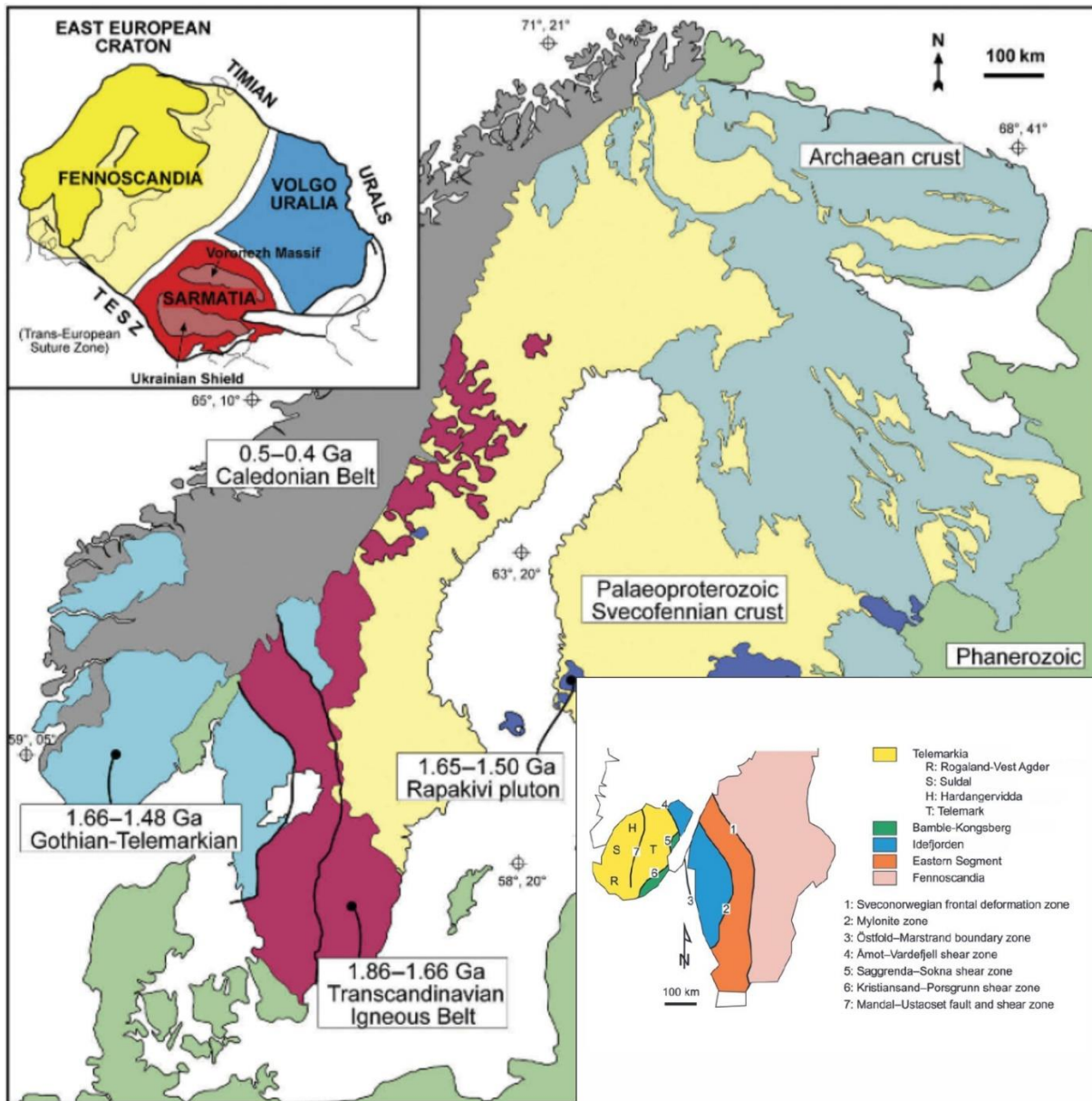


Figure 2.2: Sketched map of Fennoscandia showing the four mentioned sub-groups and more. The top inset shows the three cratons Fennoscandia, Sarmatia, and Volga-Uralia that makes up the East European Craton. The lower inset shows the Lithotectonic units of Southern Fennoscandia. The main sketch and upper inset is taken from Roberts and Slagstad (2014) (modified from Bingen et al. (2008b), Korja et al. (2006), and Bogdanova et al. (2008); the lower inset is taken from Bingen et al. (2005a).

### 2.3 Gothian-Telemarkia 1.66-1.48 Ga

Gothian-Telemarkian has previously been referred to as two separate orogens formed in the same region; first the Gothian orogeny from 1.66 Ga to 1.52 Ga, and then the Telemarkian orogeny from 1.52 to 1.48 Ga. Later research suggests that they come from the same long-lived accretionary orogen (Roberts and Slagstad, 2014) and can be viewed as part of the same orogenic event that grew westward with time. However, the two subdomains are often separated spatially where Gothian (1.66-1.52 Ga) occupies the southern Norway-Sweden border areas and coastal regions of Telemarkian and Aust-Agder while Telemarkian (1.52-1.48 Ga) occupies Southern Norway and North Western-Norway. The boundary between Gothia and Telemarkia is situated along the Bamble Kongsberg tectonic wedge that was created during early Sveconorwegian orogen (1140-920 Ma); it divides the Telemark lithotectonic unit from the Bamble-Kongsberg-, Idefjord, and Eastern Segment lithotectonic units. The geographical area of Telemark lithotectonic unit is the same as the believed extent of the Telemarkia orogeny; the same goes for Bamble-Kongsberg- and Idefjord- lithotectonic units and the Gothian orogeny.

#### 2.3.1 Gothian orogeny

Gothian orogen has been separated into three distinct units, i.e. the Horred Fm (1.66 Ga), the Åmål Fm (1.63-1.59 Ga), and the Stora Le-Marstrand (SLM) (1.59 Ga) (Brewer et al., 1998). The Horred Fm is described to be metamorphosed magmatic rocks ranging from felsic to mafic in composition; a small portion of metasedimentary rocks(<1%) is also part of the formation. The Åmål Fm is a set of greenschist- to amphibolite-facies volcanites and sediments. While the Stora Le-Marstrand consists of Amphibolite and greywackes from an oceanic or back-arc setting (Åhäll and Daly, 1989, Brewer et al., 1998).

Further research combines the Åmål Fm with the contemporary calc-alkaline granitoid intrusions of the Göteborg suite to a single continental arc belt called the Göteborg-Åmål belt (GAB). While the Stora Le-Marstrand is divided into two packages: SLM1 (1.59 Ga), and SLM2 (1.57-155 Ga), contemporary to SLM 2 Hisingen (1.59-1.52 Ga) suite granitoid intrusions magmatism takes place, marking the end of craton margin magmatism in the Gothian domain (Åhäll and Connelly, 2008).

In the same paper, Åhäll and Connelly (2008) discuss nine stages of oceanward-stepping growth in south-west Fennoscandia, four of which describing Gothian domain.

Stage 6 (1.66 Ga) forms the Horred Fm from an island arc, abundant “*andesitic and rhyolitic composition implies either a mature island arc or arc founded on attenuated continental crust that allowed mafic magma ascent without significant assimilation*” (Åhäll and Connelly, 2008).

Stage 7 (1.63-1.59 Ga) includes the Göteborg suite and the Åmål Fm resulting in the Göteborg-Åmål belt. Unlike the Horred Fm that is only found locally in south-east Idefjord close to the Mylonite Zone (MZ), the Göteborg-Åmål belt is found in large quantities along the whole eastern part of Idefjord lithotectonic unit. It comes as a result of alkaline continental arc magmatism.

Stage 8 (1.59 Ga) and 9 (1.59-1.52 Ga) describes SLM1/2 and the Hisingen suite as mentioned earlier to be a result of an oceanic back-arc. Coeval to Gothian domain continental margin magmatism. Inland magmatism occurs in the Svecofennian domain in form of Rapakivi suite magmatism (see figure 2.2) moving westward with time (Åhäll et al., 2000). Equal to this the Horred Fm, the Göteborg-Åmål belt, and the Hisingen Belt all young to the west (Roberts and Slagstad, 2014).

### 2.3.2 Telemarkian orogeny

Telemarkian orogeny refers to voluminous magmatic event resulting in major continental growth from 1.52 to 1.48 Ga that settled over a large area. Different suites at different locations suggests several settings took places during this 40 Ma period. For instance, the Suldal sector west in Telemarkia indicates continental margin setting while the Rjukan group further east in Telemarkia suggest a “within-plate” continental rift system (Bingen et al., 2005a). In Setesdal, about 50 km north of the field area and within Telemarkia tonalites has been dated to 1.55 Ga, 35 million years before what is thought to be the age of Telemarkian orogen (Pedersen et al., 2009).

### 2.4 Pre-Sveconorwegian 1.48-1.15 Ga evolution

The time between 1.48 Ga to Sveconorwegian orogeny at 1.15 Ga in south-west Fennoscandia are by many described as anorogenic, interorogenic, or intracratonic, with Gothian-Telemarkia being in an extensional environment east of a westward migrating east-dipping subduction zone. Slagstad et al. (in prep.) suggests that extensional rifting between 1.34 and 1.10 Ga resulted in the division of the Gothian-Telemarkian orogeny into three separate lithotectonic units that later took part in the Sveconorwegian orogeny; i.e. Idefjord-, Bamble-Kongsberg-, and Telemark- lithotectonic units.

Events in this region (excluding Idefjord) is constrained to 1.48-1.46 Ga and <1.3 Ga. Central southern-Norway has meta-magmatic units settled during this later period, e.g. Tromøy complex (1.20-1.18 Ga) (Knudsen and Andersen, 1999), Gjeving suite ( $1152 \pm 2$  Ma) (Kullerud and Machado, 1991), Iveland-Gaustad (1285-1271 Ma) (Pedersen et al., 2009), Aletthei Augen gneiss (1279-1264 Ma) (Pedersen et al., 2009) and Gjerstad suite (1.19-1.15 Ga) (Bingen et al., 1998). Bingen and Van Breemen (1998) suggest that the Gjerstad suite is coeval to rocks mapped by Falkum (1985) within the field area. In Telemark, sedimentary sequences are as young as 1110 Ma, overlapping with the early stages of the Sveconorwegian orogeny (Bingen et al., 2003, Lamminen, 2011, Spencer et al., 2014).

The Hallandian-Danopolonian orogeny refers to 1.47-1.38 Ga tectonothermal events from a convergent margin that for the most part affected southern Sweden, but also resulted in magmatic intrusions in Gothian-Telemarkia. There is also geographically difference with felsic intrusion more common to the south, while mafic intrusion becomes more prevalent, suggesting a thinning northward (Brander and Söderlund, 2009). Coeval metamorphism occurs within the Eastern Segment, but this does not extend west of the Mylonite Zone, and is not present in Gothian-Telemarkian indicating that Gothian-Telemarkian may not have been adjacent to the Eastern Segment at this point. Zircon data indicates that Gothian-Telemarkia and the Eastern Segment did not get the spatial relationship they have today before mid to late Sveconorwegian orogeny (Andersson et al., 2002). Brander (2011) suggest a three-stage model for the events of this period. First a pre-collisional environment (>1.45 Ga) with a north dipping convergent margin resulting in volcanic arcs. Second a collisional environment (1.45-1.42 Ga) resulting in metamorphism and migmatization. Last a post-collisional environment (1.42-1.38 Ga) giving way to magmatism and pegmatite emplacement. The shift from an east-dipping subduction zone in the Telemarkian period to a North-dipping continental margin indicates a change in geometry during this period.

## 2.5 The Sveconorwegian orogeny 1140-920 Ma, a long-lived accretionary margin

The Sveconorwegian orogeny is a period of convergence between 1140 and 920 Ma (Slagstad et al., 2018); its tectonic setting is debated. The traditional view is that it's a continuation of the Greenville orogen in eastern Canada (Gower et al., 1990, Karlstrom et al., 2001); a Himalayan style orogen created by a collision between Laurentia and an unknown continent from 1050 to 980 Ma (Hynes and Rivers, 2010, Bingen et al., 2008a). Slagstad et al. (2013a) challenges this view. Based on new extensive mapping; it argues that the orogen is a result of a long-lived Andean style accretionary margin, created without interference from

Greenville. The Sveconorwegian domain comprises of pre-Caledonian rocks west of the Sveconorwegian Frontal Deformation Zone (SFDZ) (see figure 2.1) (Roberts and Slagstad, 2014); this means that the Sveconorwegian domain extends beyond Gothian-Telemarkia lithotectonic units and well into the Transscandinavian Igneous Belt (TIB).

The first recorded metamorphism is a high-pressure metamorphism in Bamble, constrained to 1140-1130 Ma by Bingen and Viola (2018). The event is characterised by amphibolite- to granulite- facies towards the ocean in the Bamble area (Njiland et al., 2014). Bingen et al. (2008a) infers this to reflect crustal thickening after a collision of Bamble-Kongsberg-, and Telemarkia-, and possibly Idefjord -lithotectonic units; the collision resulted in the formation of the Bamble and Kongsberg tectonic wedges (Andersson et al., 1996, Ebbing et al., 2005). Continued convergence resulted in high-grade metamorphism in the whole of Bamble-Kongsber lithotectonic unit and parts of Idefjord lithotectonic unit at 1110 to 1080 Ma. It resulted in the Bamble(Bingen et al., 2008a).

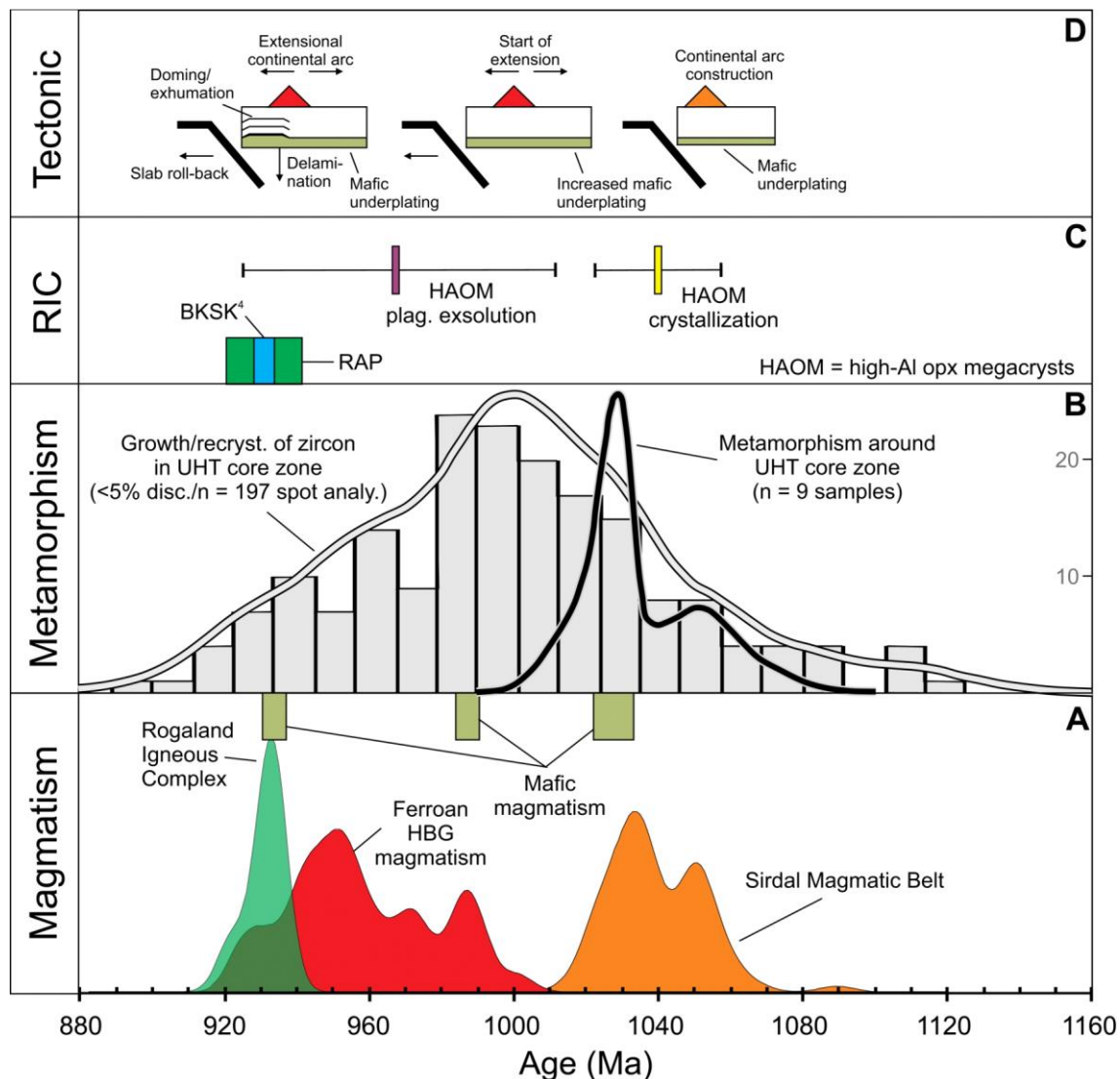


Figure 2.3: Illustration taken from Slagstad et al. (2018) that summarises available geochronological data. (A) Shows the age range, and frequency of the main Sveconorwegian magmatic events described in the text. (B) Shows high-grade, and ultra-high-grade metamorphism in and around the “core area”. The “core-area” is loosely defined as the area in which samples contain evidence of long-lived continuous growth close to Rogaland Igneous Complex. (C) Shows the timing of geochronological data found in Rogaland Igneous Complex = RIC. Other abbreviations are, BKS = Bjerkreim-Sokndal Layered Intrusions, RAP = Rogaland Anorthosite Province, HOAM = High-Al Orthopyroxene Megacrysts. (D) Illustration of the intrepid tectonic evolution of southwest Sveconorwegian province by Slagstad et al. (2018)

1070-1010 Ma magmatism in Telemarkia resulted in the formation of the Sirdal Magmatic Belt (SMB), a voluminous ~50 km wide, 150 km long batholith in Telemarkia, first presented in Slagstad et al. (2013a). It consists of magnesian calc-alkaline granites (mainly porphyritic), described in detail by Slagstad et al. (2013a) and Coint et al. (2015). The Feda- and Fennefoss- suite augen gneiss described by Bingen and Van Breemen (1998) that yields an age of 1051 Ma is implemented into the SMB; in Bingen and Van Breemen (1998), the Feda suite is interpreted to reflect a short-lived subduction event before the continent-continent

collision. Metamorphism is commonly associated with SMB magmatism; this includes migmatization (Coint et al., 2015, Slagstad et al., 2018). Syn-kinematic emplacements resulted in large scale N-S-striking xenolith belt (Stormoen, 2015). It has been speculated if mafic underplating is the heat source of SMB (Slagstad et al., 2013a), Bybee et al. (2014) argument that high-Al orthopyroxene megacrysts (HAOM) in Rogaland Igneous Complex crystallised from mantle-derived mafic magma at  $1041 \pm 17$  Ma supports this.

Geochronological data from diorites presented by Slagstad et al. (2018) at Flåt ( $1025 \pm 13$  Ma) and Gyadalen ( $1031 \pm 5$  Ma) proves that there was mafic magmatism during SMB emplacement.

At 1010 Ma SMB magmatism ceases, marking a tectonic regime change; Slagstad et al. (2013a) suggest that this is due to a shallowing of a subducting slab and results in crustal thickening (Collins, 2002). Although Slagstad et al. (2018) points out that there is no evidence for crustal thickening in the area at the time, they points to a probability plot (see figure 2.3 B) taken from 197 spot analysis from different geographically spread lithological units that there is a peak at ca. 1000 Ma, and argues that it must have a geologic significance. An age at 1000 Ma, coincides with the majority of the published U-Pb zircon ages from the area (Bingen et al., 2008c, Drüppel et al., 2012, Möller et al., 2002).

Renewed magmatism at ca. 990 Ma (Jensen and Corfu, 2016) marks a shift in the character of the Sveconorwegian. It marks the onset of a widespread ferroan A-type hornblende-biotite that lasted until ca. 930 Ma, first described by Vander Auwera et al. (2003); this suite will from now on be referred to as HBG (see figure 1.1). Granseth et al. (2019) showed that SMB and HBG found outside SMB are chemically similar, whereas HBG inside SMB is more ferroan and enriched in incompatible elements, giving it an A-type composition. They infer this to be due to a similar source of 50 % partial melt of 1.5 Ga crust. While HBG inside SMB is a result of 5-20 % remelting of SMB residue. Furthermore, isotopic composition of Flå-Iddefjord-Bohus suite (925 Ma) from the eastern part of the Sveconorwegian province suggests an older source; this supports the claim from 2.3 that Gothian-Telemarkia migrated westwards. Development of major extensive shear zones (Viola et al., 2011) and mafic dikes (Söderlund et al., 2005) is evidence that the Sveconorwegian orogen experienced divergent movement at ca. 970 to 940 Ma; either from a post-orogenic collapse (Vander Auwera et al., 2003) or as extension behind an active continental margin(Slagstad et al., 2013a)

The youngest documented magmatism in the Sveconorwegian orogen is the Rogaland Igneous Complex (RIC) (see figure 1.1); dated between 950 Ma and 920 Ma (Bybee et al., 2014, Vander Auwera et al., 2011). It comprises the Rogaland Anorthosite Province (RAP), and the Bjerkreim-Sokndal Layered Intrusion (BKS), as well as associated charnockitic and fayalite-bearing granites. Rogaland Anorthosite Province divides further into the Egersund-Ogna, Håland-Helleren-and Åna-Sira-massifs. The Bjerkreim-Sokndal Layered Intrusion is a large ( $230 \text{ km}^2$ ) anorthosite intrusion constrained at ca. 930 Ma (Vander Auwera et al., 2011, Wilson et al., 1996). Rogaland Anorthosite Province is thought to be of the same age (Westphal et al., 2003, Schärer et al., 1996).

All the anorthosites have plagioclase and high-alumina orthopyroxene megacrysts (HAOM). Zircons found in RIC are related to HAOM but their relationship has never been observed, leaving the meaning of the 930 Ma age uncertain. As mentioned earlier, Bybee et al. (2014) argues that HAOM formed from a 1041 Ma mafic source. The same study finds exsolution lamellas of plagioclase to yield an age of  $968 \pm 43 \text{ Ma}$ . Previously, Schärer et al. (1996) has suggested that the zircons may have grown from a evolved melt, late in the magmatic evolution of RIC. This implies that RIC may be older than the measured zircons. HBG comes from a much more hydrous source (Vander Auwera et al., 2003); Vander Auwera et al. (2011) suggests that this is due to RIC coming from a lower crustal anhydrous source, while HBG comes from a hydrous underplated to slightly depleted mafic source.

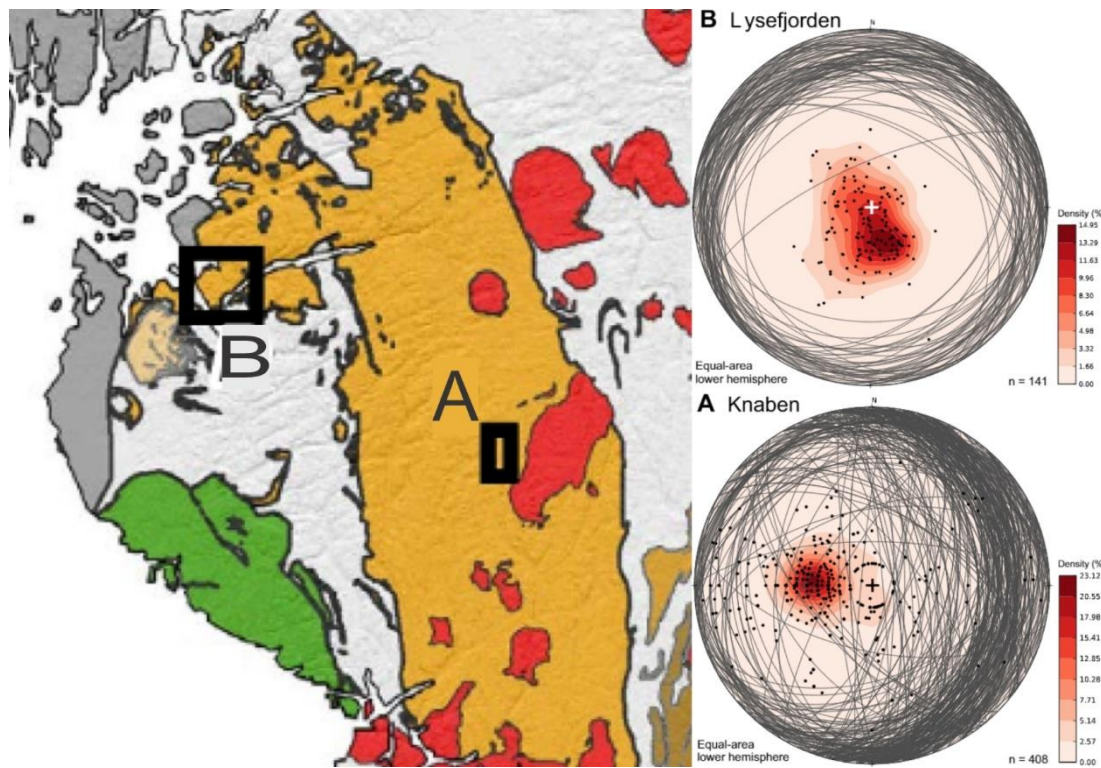


*Figure 2.4: Structural data presented by Slagstad et al. (2018). The map to the left indicates where the samples were gathered. Colours indicate the different suites, HBG Pre-sveconorwegian rocks in light-grey, SMB in orange, HBG in red, RIC in green, and Caledones in dark-grey. The stereoplots are lower-hemisphere stereoplots of foliations (tectonic and magmatic). The measurements are collected from Stormoen (2015), Marker and Slagstad (2018), Marker et al. (2012)*

Blereau et al. (2017) estimates contact metamorphoses at 950 Ma to be ~5kbar close to RIC, and at 3-4 kbar 10 km away from RIC; Slagstad et al. (2018) suggests that this is due a dome-like structure limited to the southwestern part of Rogaland/Vest-Agder sector. This is supported by structural data (Stormoen, 2015, Marker and Slagstad, 2018, Marker et al., 2012) seen presented in figure 2.4. U-Pb geochronology of zircons in ultra-high-temperature rocks reveals ongoing metamorphism in Rogaland from 1080 to 920 Ma within the doming (Slagstad et al., 2018). This long-lived metamorphism is coeval with the emplacement of SMB, HBG, and RIC.

## 2.6 The Sveconorwegian orogeny 1140-920 Ma as a four-phased model

The Sveconorwegian orogen has often been linked up to the Greenvilian orogen, a Himalayan style orogen found in eastern Canada. Bingen et al. (2008a) describes a four-phase model for assembly of the orogen as a continental-continental tectonic event. The four phases are the Arendal phase, the Agder phase, the Falkenberg phase, and the Dalane phase; they are summarised underneath from Bingen et al. (2008a).

During the Arendal phase between 1140 and 1080 Ma, a northwest-trending subduction of an oceanic basin resulted in the collision between the Telemarkia and Idefjord lithotectonic units that formed the Bamble-Kongsberg tectonic wedge (Andersson et al., 1996, Ebbing et al., 2005). The 30 Ma that followed was a period of apparent tectonic quiescence. The Agder phase lasted from 1050 to 980 Ma and is described as the main phase when Fennoscandia collided with a large continent. Tectonic imbrication and crustal thickening in the central part of the orogen corresponds with this period. In Idefjord, burial resulted in high-grade metamorphism up to granulite-facies (Bingen et al., 2008c, Söderlund et al., 2008). 1050–1030 Ma a short-lived subduction event resulted in the calc-alkaline plutons of the Feda and Fennefoss plutons (Bingen and Van Breemen, 1998); Slagstad et al. (2013a) implements these in the Sirdal Magmatic Belt. The Falkenberg phase lasted from 980 to 970 Ma and reflects a high-grade metamorphism in the Eastern Segment. Here eclogites ( $972 \pm 12$  Ma) represents the last indisputable evidence of convergence in the sveconorwegian belt. The last phase, the Dalane phase that lasted from 970 to 900 Ma, represents gravitational collapse driven by extension and is characterised by voluminous post-collisional magmatism, peaking at 920-930 Ma with the emplacement of Rogaland Igneous Complex, and the Bohus and Flå plutons in iddefjord.

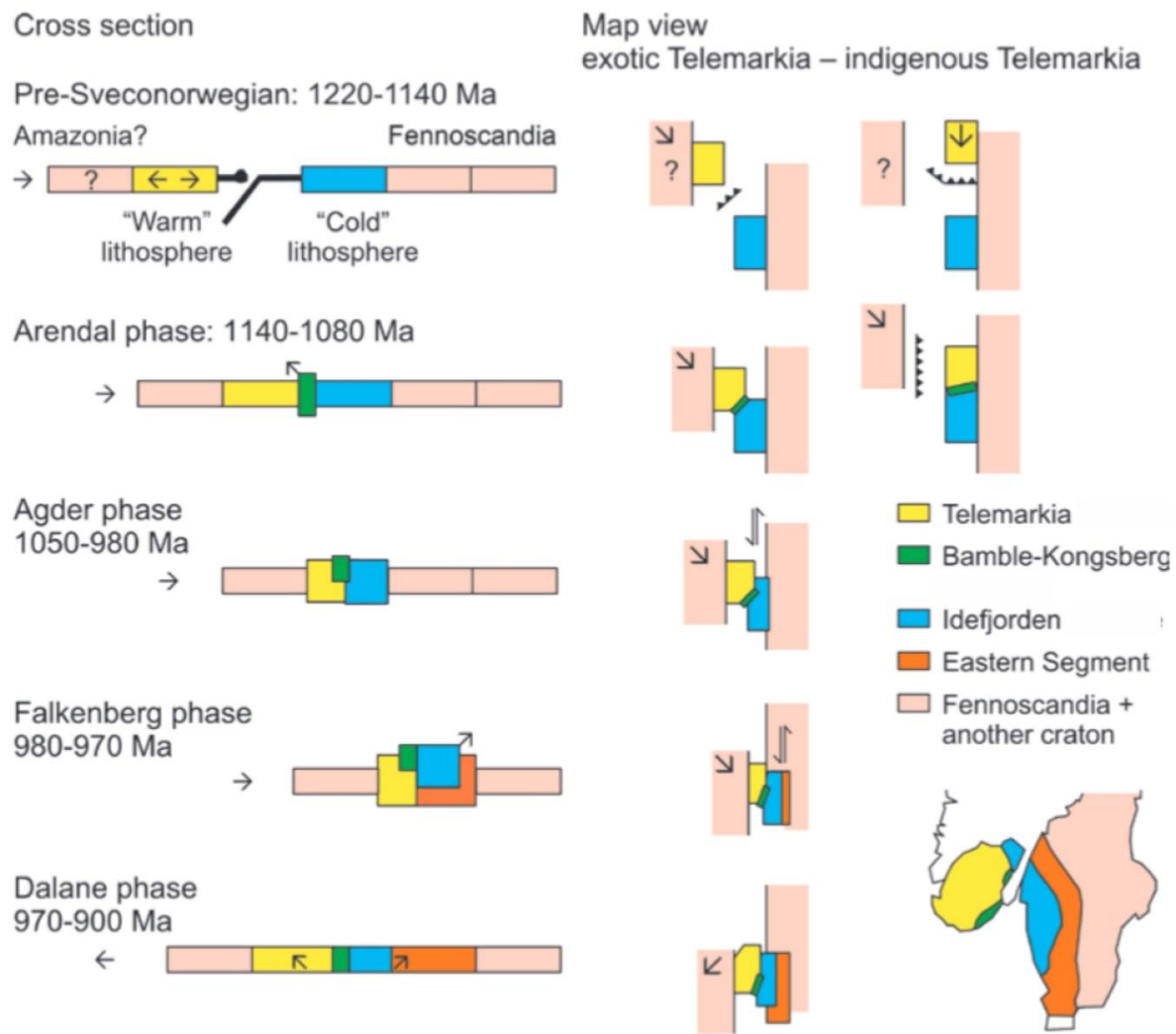


Figure 2.5: Schematic model of the four-phase model. In the model, Fennoscandia collides with an unknown continent (possibly Amazonia) resulting in the Sveconorwegian orogeny. The sketch is taken from (Bingen et al., 2008a).

Slagstad et al. (2017) suggest that the Sveconorwegian orogen happened separately from the Greenvillian, but may be linked through the behaviour of Amazonia. They interpret the Sveconorwegian orogeny to consist of “*a series of geographically and tectonically discrete events*”. In short, these are, thrusting and high-grade metamorphism between 1140 and 1080 Ma, and arc magmatism and ultra-high-temperature metamorphism from 1060 to 920 Ma

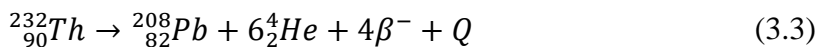
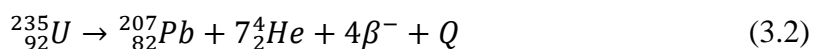
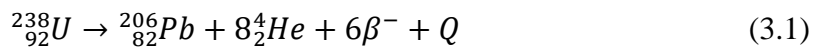
### 3 Theory

A central part of the study are U-Pb geochronology, trace elements, and Lu-Hf Isotope measurement of Zircons taken with *Laser Ablation – Split Stream – Inductively Coupled Plasma – Mass Spectrometry* (LA-SS-ICP-MS) analysis. For two migmatite samples, U-Pb geochronology was performed with *Sensitive High-Resolution Ion Microprobe* (SHRIMP) analysis. The theory behind will be discussed in this chapter.

#### 3.1 U-Pb Geochronology

##### 3.1.1 U-Th-Pb

One common way to establish an age is by measuring the decay of uranium (U) and thorium (Th) to lead (Pb). A reason for this is that it involves several different parent isotopes with different half-lives that results in different stable lead, giving it a broader usage (Schoene, 2014). In nature, uranium occurs as  $^{234}\text{U}$ ,  $^{235}\text{U}$ , and  $^{238}\text{U}$  all radioactive, thorium mainly as  $^{232}\text{Th}$ , and lead as  $^{204}\text{Pb}$ ,  $^{206}\text{Pb}$ ,  $^{207}\text{Pb}$ , and  $^{208}\text{Pb}$ .  $^{204}\text{Pb}$  is non-radiogenic and sometimes referred to as common lead (Passarelli et al., 2009). Neither thorium nor uranium decays directly to lead but does through a sequence of alpha and beta decays described in figure 3.1 end up as lead;  $^{238}\text{U}$  to  $^{206}\text{Pb}$  as shown in equation (3.1),  $^{235}\text{U}$  to  $^{207}\text{Pb}$  as shown in equation (3.2), and  $^{232}\text{Th}$  to  $^{208}\text{Pb}$  as shown in equation (3.3) (Schoene, 2014). Q is energy liberated in the process,  $\beta^-$  is beta radiation, and  $^4\text{He}$  are alpha particles. The different half-life for the different parent isotopes are  $4.468 \cdot 10^9$  years for  $^{238}\text{U}$ ,  $0.7038 \cdot 10^9$  years for  $^{235}\text{U}$ , and  $14.010 \cdot 10^9$  years for  $^{232}\text{Th}$  (Steiger and Jäger, 1977). The decay chains of  $^{238}\text{U}$ ,  $^{235}\text{U}$ , and  $^{232}\text{Th}$  are in secular equilibrium, i.e., all the abundance of the parental isotopes and their decay products are equal among all the intermediate daughter isotopes. Because of this, all three can be treated as if they decay directly to lead (Schoene, 2014).



Since both parental elements concentrates into the liquid phase during partial melting and incorporates into the silica-rich products, Uranium and Thorium gets enriched in the crust (Faure and Mensing, 2005). For this reason, minerals commonly used for U-Th-Pb dating such as allanite, apatite, baddeleyite, monazite, perovskite, rutile, titanite (sphene), and zircon (Passarelli et al., 2009) are commonly found in continental crusts.

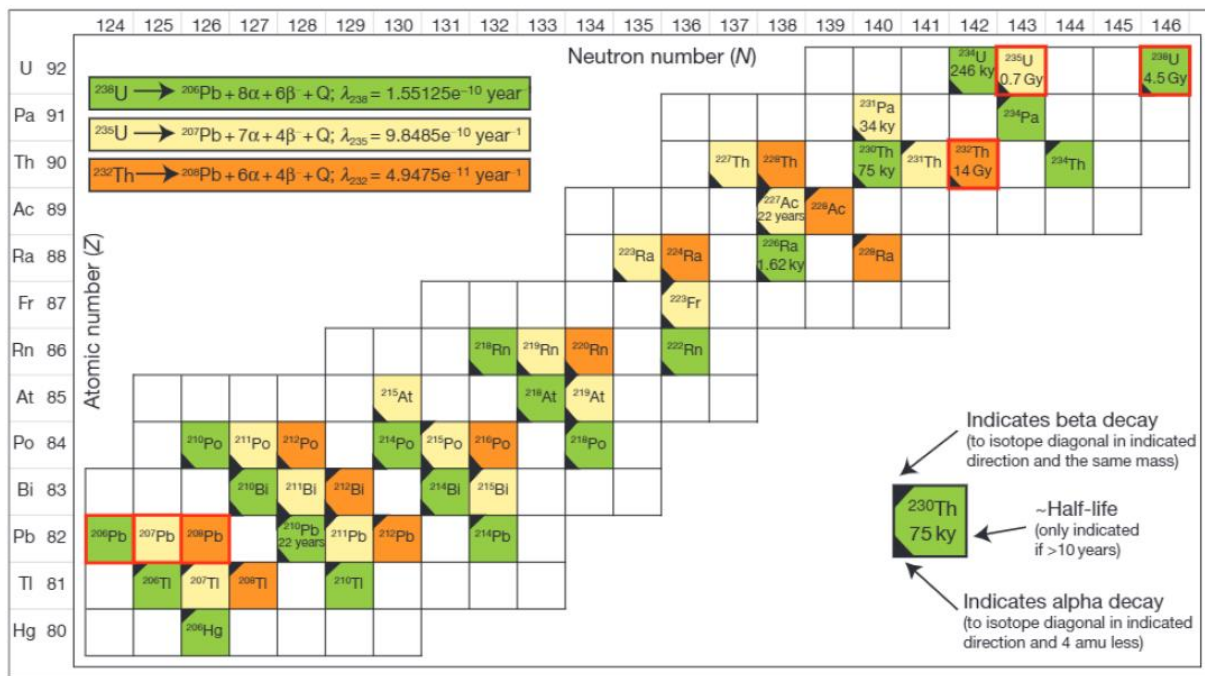


Figure 3.3 An illustration of the U-Th-Pb decay chains where each occurring isotope is colour-coded according to its parental isotope outlined in red. (Schoene, 2014)

### 3.1.2 U-Pb Concordia plots

Concordia plots help visualise the measured values of parent and daughter isotopes. The two most commonly used are the Wetherill plot ( $x = {}^{207}\text{Pb}/{}^{235}\text{U}$ ,  $y = {}^{206}\text{Pb}/{}^{238}\text{U}$ ,  $z = {}^{204}\text{Pb}/{}^{238}\text{U}$ ) (Wetherill, 1956) and the Tera-Wasserburg plot ( $x = {}^{238}\text{U}/{}^{206}\text{Pb}$ ,  $y = {}^{207}/{}^{206}\text{Pb}$ ,  $z = {}^{204}\text{Pb}/{}^{206}\text{Pb}$ ) (Tera and Wasserburg, 1972);  $z$  is used for 3-dimensional visualisation which is less common. A key element of the plot is the calculated curved line representing the natural decay of U-Pb where age of the y-axis equals the age of the x-axis; this line is a Concordia. If an analysis plots away from the Concordia, it is referred to as discordant, and it implies that the U-Pb system in the material may have been disturbed at some point; due to things like later weathering, inaccuracies during measurements, Pb loss, Inheritance, etc.. The amount of discordance is calculated from equation (3.4).

$$Discordance = 100 - 100 \frac{\frac{{}^{206}\text{Pb}}{{}^{238}\text{U}} \text{age}}{\frac{{}^{207}\text{Pb}}{{}^{206}\text{Pb}} \text{age}} \quad (3.4)$$

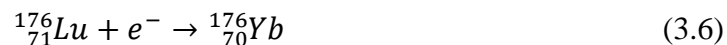
This thesis uses Tera-Wasserburg plots; the advantages of this plot is that you easily can detect high common-lead-values and fractionation. Since a Tera-Wasserburg plot uses Pb/Pb instead of U/Pb in the x-axis high common lead will appear as a vertical trend from the Concordia line while fractionation can appear as a horizontal array. Also,  ${}^{235}\text{U}$  in a Wetherill

plot is calculated from  $^{238}\text{U}$  and is thus an uncertain measurement. Lead loss will appear as an increase in  $^{238}\text{U}/^{206}\text{Pb}$ , and analysis will form a horizontal line.

A Discordia line is when discordant measurement plots on a straight line that intersects Concordia in two places; these intersections are then interpreted as two events influencing the same sample.

### 3.2 Zircon Lu-Hf Isotopes

Lu-Hf method is a useful method for determining proportions of mantle in original melt, which can help explain the magmatic evolution of a region. Lutetium (Lu) occurs naturally as the non-radioactive  $^{175}\text{Lu}$  and the radioactive to  $^{176}\text{Lu}$  that decays  $^{176}\text{Hf}$  by emitting a  $\beta$ -particle and  $^{176}\text{Yb}$  by electron capture (Faure and Mensing, 2005); shown in equation (3.5) and (3.6).



Since  $^{177}\text{Hf}$  is stable and  $^{176}\text{Lu}$  decays to  $^{176}\text{Hf}$ , the  $^{176}\text{Hf}/^{177}\text{Hf}$ -ratio will increase over time; the amount of  $^{176}\text{Lu}$  present determines this rate. Since Lutetium (0.93 Å) has a larger ionic radius than Hafnium (0.81 Å) (Faure and Mensing, 2005) Lu will stay in the mantle (solid) at a larger extent than Hf during magma formation, meaning that there will be more  $^{176}\text{Lu}$  in the mantle relative to the crust, resulting in more  $^{176}\text{Hf}$  over time and a higher  $^{176}\text{Hf}/^{177}\text{Hf}$ -ratio.

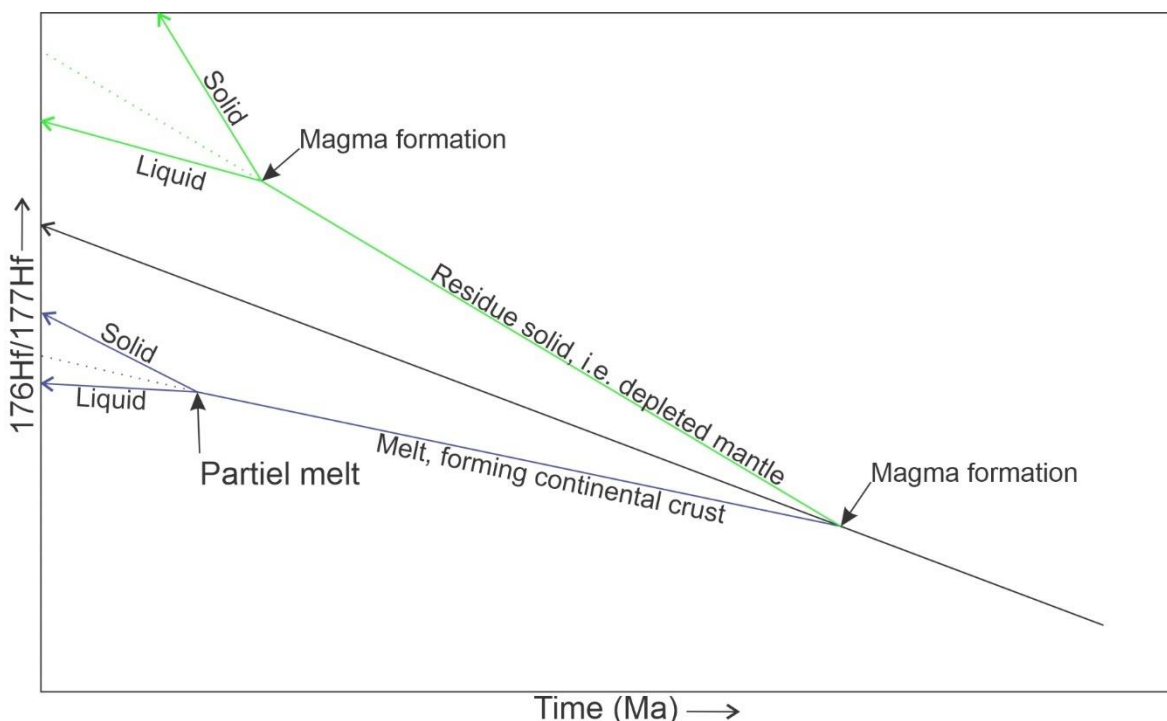


Figure 3.4: Illustration of how the  $^{176}\text{Hf}/^{177}\text{Hf}$ -ratio will increase over time after a magma formation with the green line following the path of the residue magma, and the blue line following the path of the newly formed melt. The rate is determined by the amount of  $^{176}\text{Lu}$  distribution in melt and solid; the rate will then stay fixed until any further fractionation.

The ratio between  $^{176}\text{Hf}$  and  $^{177}\text{Hf}$  is relatively minor, meaning differences can be difficult to visualise. One way to combat this is to calculate epsilon with the *Chondritic Uniform Reservoir (CHUR)* (Bouvier et al., 2008) set as zero, as seen in equation (3.7), (3.8), and (3.9).

$$\left( \frac{^{176}\text{Hf}}{^{177}\text{Hf}} \right) i_{\text{CHUR}} = \left( \frac{^{176}\text{Lu}}{^{177}\text{Hf}} \right)_{\text{CHUR}} - \left( \frac{^{176}\text{Hf}}{^{177}\text{Hf}} \right)_{\text{CHUR}} \cdot (e^{\lambda t} - 1) \quad (3.7)$$

$$\left( \frac{^{176}\text{Hf}}{^{177}\text{Hf}} \right) i_{\text{Sample}} = \left( \frac{^{176}\text{Lu}}{^{177}\text{Hf}} \right)_{\text{Sample}} - \left( \frac{^{176}\text{Hf}}{^{177}\text{Hf}} \right)_{\text{Sample}} \cdot (e^{\lambda t} - 1) \quad (3.8)$$

$$\varepsilon_{\text{Hf}_i} = \left[ \frac{\left( \frac{^{176}\text{Hf}}{^{177}\text{Hf}} \right) i_{\text{Sample}}}{\left( \frac{^{176}\text{Hf}}{^{177}\text{Hf}} \right) i_{\text{CHUR}}} - 1 \right] \cdot 10^4 \quad (3.9)$$

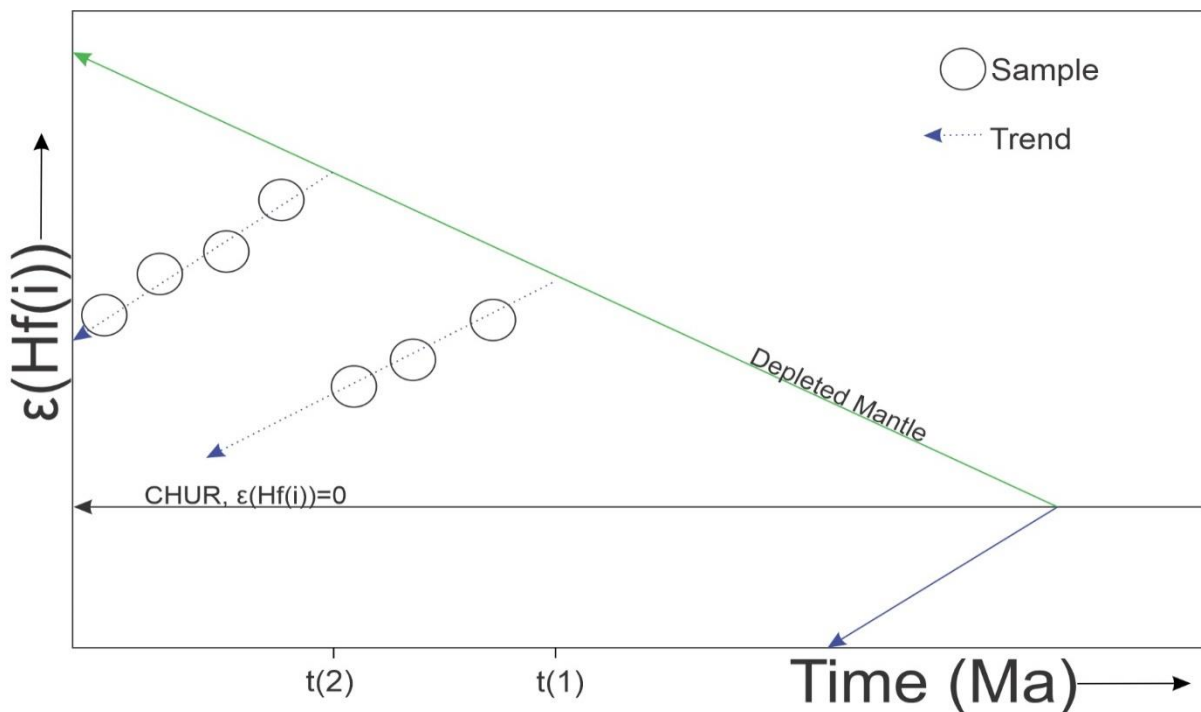


Figure 2Figure 3.3: Seven hypothetical samples from one location showing two trends. At time  $t(1)$  a continental crust was formed from the depleted mantle, the first three samples are formed from melts originating from this crust. At time  $t(2)$  juvenile magma for

Continental crust that forms from a depleted mantle will form a negative trend like the ones you see in figure X; this trend can be used to determine the age of the continental crust.

### 3.3 REE-Spider plot

A REE-Spider plot is used to represent the abundance of Rare Earth Elements (REE) in a rock or mineral. In a Spider plot, the sample-values is normalised by dividing it to values calculated from a chondrite. A chondrite is a meteor that consists of chondrules; chondrules are small spherical silicate inclusions that disappears under differentiation caused by high temperatures; thus, chondrites are considered undifferentiated and preferable for normalisation (Winter, 2001). Trace elements (elements with < 0.1 wt%) are positioned along the x-axis based on compatibility. Light Rare Earth Elements (LREE) to the left, Heavy Rare Earth Elements to the Right; they are placed in order so that each element is more compatible than the one to the left. Rock types that favours incompatible elements relative to the standard will have a trend that shows high LREE and low HREE, and vice versa for a rock type that favours compatible elements relative to the standard.

### 3.4 Mass Spectrometry methods

Mass Spectrometers are used to measure quantities of different isotopes (e.g.  $^{238}\text{U}$ ,  $^{176}\text{Hf}$ ,  $^{176}\text{Yb}$ ) by measuring its mass-to-charge ratio. There are many different methods of mass spectrometry, all with different advantages based on price, accuracy, availability, etc. The three main methods are *Thermal Ionization Mass Spectrometry* (TIMS), *Inductively Coupled Plasma Mass Spectrometer* (ICPMS), and *Secondary Ion Mass Spectrometry* (SIMS); the ones used in this thesis are LA-SS-ICP-MS (ICPMS), and SHRIMP (SIMS).

#### 3.4.1 ICPMS (LA-SS-ICP-MS)

Laser Ablation Inductively Coupled Plasma (LA-ICP) is often used because of its high spatial resolution, rapid analysis time less than 60 seconds (Košler et al., 2013), and affordability relative to SIMS (Schoene, 2014). A sample placed in a closed chamber filled with Helium gas; in our case, the samples are individual zircon grains on a polished mount. A laser beam ablates elements, and the Helium gas transports it into a second chamber where it's mixed with Argon gas before it's further transported into the ICP. ↴

The ICP heats the elements and converts them into positive charged elements (ions) by removing one electron from its orbital; this means that elements that are naturally negatively charged like Cl, I, and F are difficult to determine in an ICP (Wolf, 2005).

Before sending the ions into the mass spectrometer (MS), a Split Stream (SS) divides the number of atoms in two and sends them in separate collectors. This means two analyses can be done from the same analytical spot; this also means the analytical spot needs to be double the size. The types of collectors varies; in this case, it was on multiple collector (MC) and one

single collector (SC). A multiple collector tends to be larger and more precise, a greater effort is put into decreasing the pressure from the ICP to the analyser, decreasing then number of collisions. The increased precision comes from that each isotope can be counted simultaneously in different collectors (Kylander-Clark, 2017). A single collector is designed for rapid mass switching and is used when analysing a large quantity when precision is less important (Kylander-Clark, 2017).

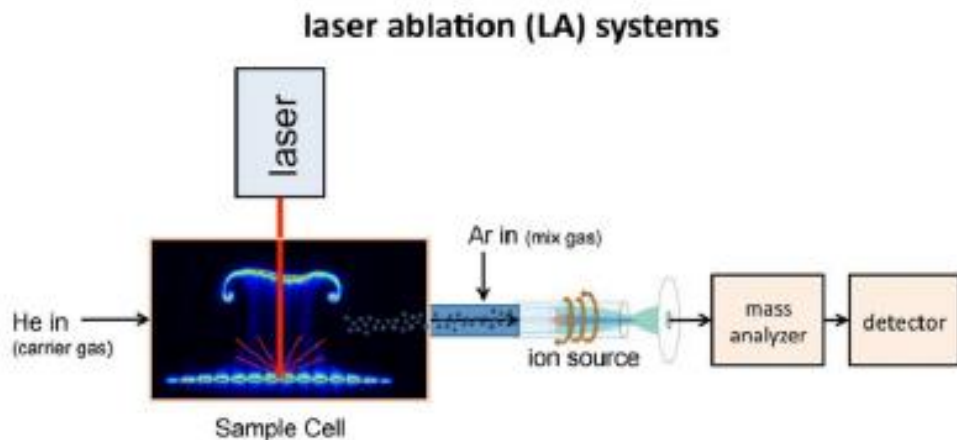
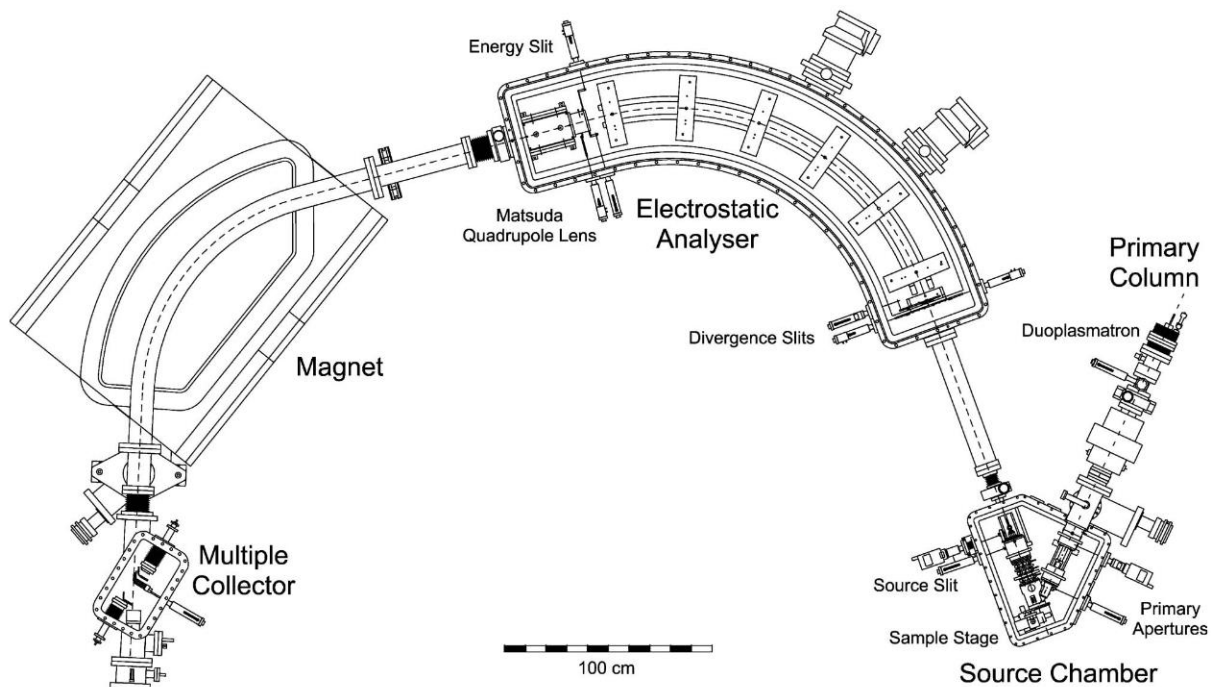


Figure 3.4 From Kylander-Clark and Cottle (2014). A laser shot at the sample cell that releases elements. The Helium gas transports the elements into a second chamber where Argon gas is introduced. The ICP then ionises the elements ready to be counted in the detector.

### 3.4.2 SIMS (SHRIMP)

SHRIMP is a variant of SIMS. In SIMS a beam of ions gets shot on the surface of a polished sample; if the beam is positive charge negative charged ions are favoured, and opposite if the beam is negative. In the case of SHRIMP, an  $O_2^-$  beam hit the surface at an angle of  $45^\circ$  releasing secondary ions that are transported to an electrostatic analyser. The electrostatic analyser ionises that allows passage for specific charged ions. A magnet then sorts the ions based on their ionic mass before a multiple collector counts the desired ions. The layout of the SHRIMP (SHRIMP II) used can be seen in figure 3.5. The advantages of using the SHRIMP over the LA-SS-ICP-MS is a smaller data point radius, which is useful in rocks with several growths present within one single zircon grain (e.g. migmatite). Also, a more gentle SHRIMP does not hit as deep within the grain, meaning, less elements get trapped surpassing other elements on the way out.



*Figure 3.5: The Schematic layout of SHRIMP II found at John de Laeter Centre at Curtin University. The ionic beam is produced in the Primary Column. The beam is aimed at the sample stage in the source chamber. Secondary ions are transported to the Electrostatic analyser where it's ionised before it's sorted in the magnet and finally counted in the multiple collector. The sketch is originally published in Ireland et al. (2008)*

### 3.5 Zircon

Zircons is the most commonly used mineral for geochronological research because of both chemical properties and abundance. It is found in most silica-rich rocks, in sedimentary, igneous, and metamorphic rock; it is less common in mafic and ultramafic rocks. The high density ( $4.66 \text{ g/cm}^3$ ) (Finch et al., 2001), small size ( $<250 \mu\text{m}$ ), and characteristic look means they are easy to separate.

Resistance to weathering and slow element diffusion makes them less likely to reset; one single grain can often retain several generations of thermal history (Cherniak and Watson, 2003). The Uranium content in zircon is much higher than in a host rock average making it a good candidate for U-Pb geochronology; also, Zircon discriminates against  $\text{Pb}^{2+}$  because of its high ionic radius resulting in a high  $\text{U}/\text{Pb}$  ratio (Davis et al., 2003, Schoene, 2014). The high closure temperature of zircon ( $>900^\circ\text{C}$ ) (Dodson, 1973) prevents the magmatic zircons from being reset by later metamorphic events. Textures seen in cathodoluminescent imaging reflects its geological history; visible zoning reflects variations in U and Th (as well as many other elements) and indicates episodic growth in a magmatic or metamorphic environment (Corfu et al., 2003). The low  $\text{Lu}/\text{Hf}$  ratio in zircon ( $\sim 0.002$ ) gives a low  $^{176}\text{Lu}/^{177}\text{Hf}$  ratio after fractionation meaning that in situ decay of  $^{176}\text{Lu}$  impact on the  $^{176}\text{Hf}/^{177}\text{Hf}$  ratio is negligible

(Kinny and Maas, 2003) and a good candidate for Lu-Hf measurements. A high incorporation of minor and trace elements gives zircon the ability to retain a substantial chemical and isotopic information (Finch and Hanchar, 2003).

## 4 Methods

### 4.1 Fieldwork

Fieldwork was done over two two-week periods in 2018, one in June/July and one in September. Field equipment included: topographic maps, colour pencils, notebooks, a sledgehammer, a mason hammer, 360° compass, a Olympus TG-5 digital camera, a Windows Linx tablet with included GPS and ArcPad, a hand lens, a rental car to get around, and amazingly nice weather.

The structural measurements are noted as dip/dip-direction for tectonic foliation and trend/plunge for fold axis.

To cover the whole field area the mapping was focused along roads and pathways, only deviating into the forest to map special interest points. In the preliminary phase, NGU's 1:50.000 map done by Falkum (1985) helped plan out areas of interest. After the first period, horizontal magnetic gradient mapping (NGU-COOP-project, 2017) gave further information especially helpful pointing out areas interesting for structural research. The mapping was done by hand on several 1:10,000 in the field and copied onto a 1:20,000 later to be scanned and digitalised. All in all, 103 localities are noted down in two field books that are available alongside the thesis, most of these has an emphasis on lithological outcrop description. Also, an unknown number of outcrops is mapped given a colour for its lithological unit. All localities, 169 structural measurements, and 23 sample locations were noted down in ArcPad. Borders between the lithological units were drawn based on mapped outcrops; areas that were not mapped was drawn on best estimate based on topography.

### 4.2 Sample preparation

In addition to the 23 samples collected during the fieldwork, 16 samples were collected in 2014/2015 by N. Coint and T. Slagstad. These have the prefix VAG, while the new ones are given the prefix HAL. All VAG-samples have been prepared as thin sections ( $\sim 30\mu\text{m}$  thickness), and minerally separated ( $<250\mu\text{m}$ ,  $>3.3\text{g/cm}^3$ ) by the lab at NGU before the research.

#### 4.2.1 Thin sections

15 of the 23 HAL-samples were prepared into thin sections, these can be found in Appendix A. Sample HAL193062, and HAL193071 were made into two thin sections, each making it a total of 17. The chosen rocks were photographed with marked lines before cut and handed over to lab at NTNU where they were prepared and polished down to  $30\mu\text{m}$ .

#### 4.2.2 Geochronological and geochemical preparation

8 HAL-samples were prepared in the NGU lab: three migmatites, two undeformed granite, two deformed granites, and one amphibolite. The mineral separations of Zircons from the rock sample are based on three qualities: grain size ( $<250\text{ }\mu\text{m}$ ), density ( $4.55\text{ g/cm}^3$  (Finch et al., 2001)), and magnetism (non-magnetic). For each step, the machined used are thoroughly washed between the samples to avoid any contamination.

First, all samples are sawed into fist size pieces, and all weathering removed; this, to ensure they fit in the small crusher. For the three migmatite samples, the mesosome and leucosome are separated into two different samples and given the suffixes -P (Paleosome/mesosome) and -N (Neosome/leucosome). Before subjected to the jaw crusher, the samples are scrubbed and washed in water to remove any biological material and loose gravel. The jaw crusher pulverises the rock twice. At this point, none of the sample has removed; a 200 g and a 50 g sample was taken from each sample and stored (except for HAL193066). The samples were placed on vibrating sieves for 20 minutes each to separate all grains  $<250\text{ }\mu\text{m}$ .

The  $<250\text{ }\mu\text{m}$  grains were subjected to a Wishley washing-table to separate away the high density. Since the samples had a high zircon content, this was sufficient separation. Normally the remaining samples are further separated with heavy liquid (diiodomethane,  $3.3\text{ g/cm}^3$ ); only for HAL193062-N was this necessary. Vertical and horizontal Frantz isodynamic magnetic separated removed any magnetic grains.

Around 45-55 zircons from both VAG and HAL were picked from each sample if feasible and mounted in epoxy in four different mounts; Halvdan A, B, and C for LA-SS-ICP-MS, and Halvdan SHRIMP for SHRIMP II. The mounts were polished down to bring the zircons to the surface ideally cut in half. Since the SHRIMP II machine don't contain any standards, two standards were added to the mounts; these are Temora 2 (Black et al., 2004) and 91500 (Wiedenbeck et al., 1995).

A Leo 1450 VP Scanning Electron Microscope with a Wolfram emitter at NGU was used to image the zircons in both BSE- and CL-imaging to map out the samples, describe the grains, and determine its origin. The images were taken with a working distance 19-22 mm, accelerating voltage at 15 kV. To have get all the zircons in a high mag picture, the CL imaging was done in the Scandium software that takes several individual images that can be patched together to one image.

Halvdan SHRIMP was cleaned and gold-coated at Curtin University a few days before the analysis. It was cleaned in the following step-by-step process: wiping it with petroleum spirits, 5-minute ultrasonic bath, wiping it with propanol, 5-minute ultrasonic bath, wiping it with soap solution, 3-minute ultrasonic bath, and then drying it for minimum 30 minutes in >60°C. For the LA-SS-ICP-MS samples, a quick wash with ethanol was all that was needed. To avoid charging in the SHRIMP a 40 nm coat of high-purity gold was added to give a resistance of 15-25 Ω (Windgate and Kirkland, 2015).

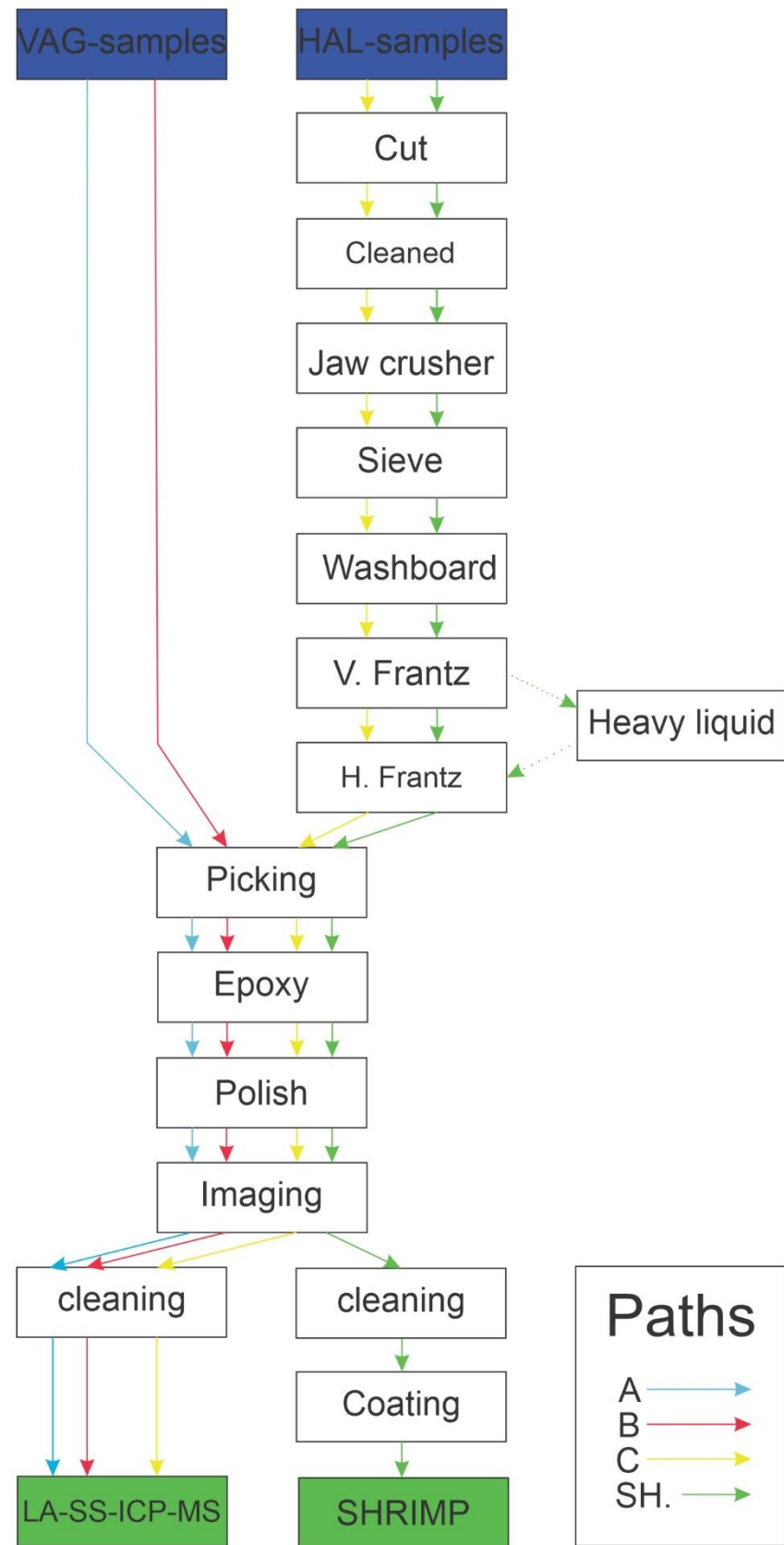


Figure 4.1: Schematic presentation of each step in the mineral separation as described in chapter 4.2.2. Each of the four amount is given a coloured path, light blue for Halvdan A, red for Halvdan B, yellow for Halvdan C, and green for Halvdan SHRIMP. Heavy liquids were used only for HAL193062-N represented by a striped line.

### 4.3 Geochronological and geochemical analysis

#### 4.3.1 SHRIMP II

HAL 193073 and HAL 193062 underwent U-Pb zircon geochronology using the SHRIMP II at *John de Laeter Centre* at Curtin University. Because of time constraint and grain loss during polishing, HAL 193053 was not analysed. Procedures for measurements of U, Th, and Pb were done based on descriptions from Compston et al. (1984), Claoué-Long et al. (1995), and Williams (1998). A 28  $\mu\text{m}$   $\text{O}_2^-$  ion beam spattered at the grains at 10 keV purified by a Wien filter. The net primary ion current leaving the sample normally lied within 1.5 and 2.1 nA and was then accelerated to 10 keV. Passing through a cylindrical 85° electrostatic analyser with a turning radius of 1.27 m, then mass-filtered with a magnet sector of 72.5° and a turning radius of 1 m.

The secondary beam of interest was focused magnetically towards a electron multiplier, used in pulse-counting mode. The secondary ion analyser was set to  $\geq 3000$  to resolve lead isotopes from most potential molecular interference. The following sequence: 196 (species [90Zr216O]+), 204 (204Pb+), 204.1 (background), 206 (206Pb+), 207 (207Pb+), 208 (208Pb+), 238 (238U+), 248 ([232Th16O]+), and 254 ([238U16O]+) was set to the magnetic field in cycles. The SHRIMP was left overnight taking 42 sample points from the four samples (neosome and paleosome); in between sample points measurements from the standards Temora-2(Black et al., 2004) and 91500 (Wiedenbeck et al., 1995) at an interval of each third sample point. All SHRIMP data lies in Appendix B.

#### 4.3.2 LA-SS-ICP-MS

Twenty-one samples underwent U-Pb geochronology, trace elements geochemistry, and Lu-Hf geochemistry with LA-SS-ICP-MS at *John de Laeter Centre* at Curtin University. An Agilent 7700 quadrupole inductively coupled plasma mass spectrometer (QICP-MS) measured trace elements and U-Pb, and a Resonetics Resolution M-50A measured Lu-Hf. The data points were set to 50  $\mu\text{m}$  to get sufficient numbers to both collectors. For each sample point two cleaning pulses and a 40 seconds analyses at 10 Hz and laser energy at 2.2 J/cm<sup>2</sup>, ending with a 15 seconds baseline after ablation. Ultra-high purity He (320 ml/min) and N<sub>2</sub> (1.2 mL/min) and transports the ablated isotopes into the Argon chamber where it is mixed with Ultra-purity Ar. Standards used were 91500 (Wiedenbeck et al., 1995), OG1 (Stern et al., 2009), Plesovice (Sláma et al., 2008), and GJ-1 (Jackson et al., 2004). The following trace elements were measured: Si, Ti, La, Ce, Pr, Nd, Sm, Eu, Gd, Dy, Yb, Lu, Pb, Th, and U;

rock/chondrite-values were made using chondrite-values for REE based on Sun and McDonough (1989).

#### 4.3.3 Data reduction

The data was reduced on excel with the add-in software Squid.xls and Isoplot. (Ludwig, 2003)

#### 4.4 Map digitalization

The sketched map was digitalised in ArcMap 10.6. The map was added as a layer, and polygons were drawn along the mapped borders like seen in figure 4.2. Two lithological border (Augen gneiss/ Migmatite, and SMB/migmatite) could be determined within high certainty with the horizontal magnetic gradient; these borders were re-drawn like seen in figure 4.3. In areas with mapped outcrops, a higher trust was kept to the worked done in the field and the borders were not re-drawn. Structural measurements and locations were transferred from ArcPad and added as individual layers.

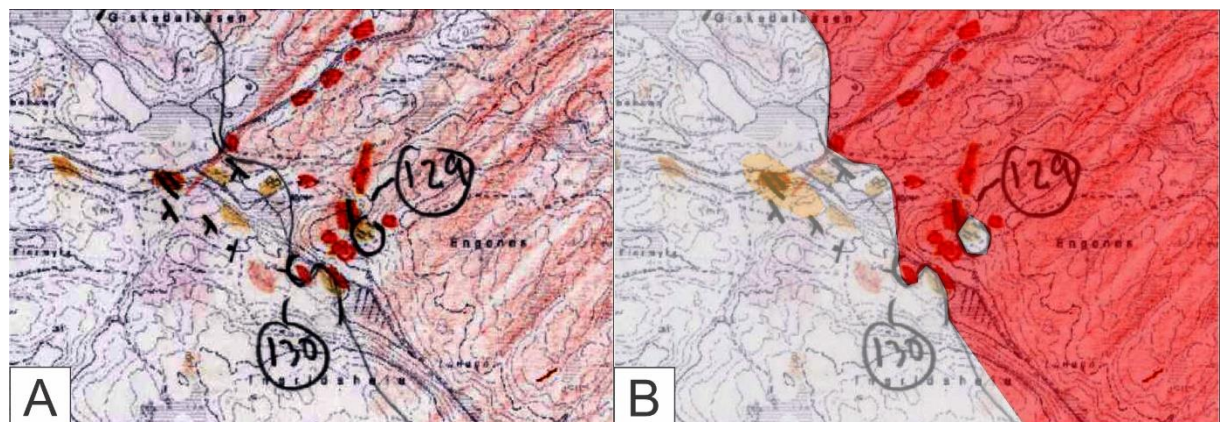


Figure 4.2: (A) shows a scanned image of the border between Flaser gneiss (red) and Migmatite (beige/colourless). Locality 129 and 130 are also marked, in addition to structural markings indicating dip and dip-direction of tectonic foliation. One outcrop within the migmatite along the road is coloured orange with two straight lines; orange symbolises undeformed granite and the straight lines indicates xenoliths of migmatite. The direction indicates the dip/dip-direction of the xenoliths. (B) Shows the same map with polygons drawn, notice the migmatite (White/Beige) outcrop within the Flaser gneiss (red), and granite (orange) outcrop within the Migmatite (white/beige).

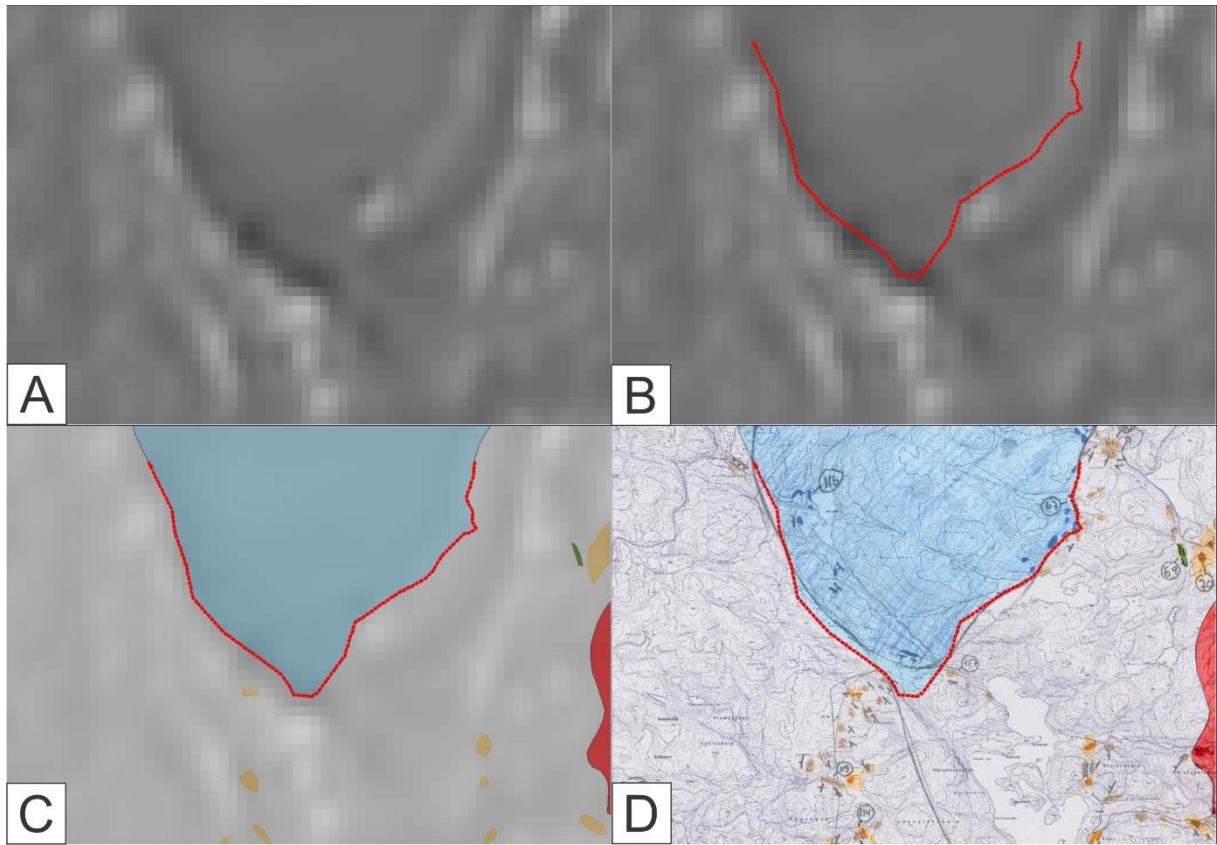


Figure 4.3: (A) shows the horizontal magnetic gradient. A Homogenous body with clear border is visible; mapping reveals this body to be the Augen Gneiss. The left (western) border is clear, the right (eastern) border has two candidates; mapping reveals that the inner one of these is the correct one. (B) Shows a re-drawn border. In (C) the border to Flaser gneiss (red), and granitic (orange) Amphibolite (green) intrusions is shown; these are not visible in the A and B. In (D) we can see that the new border fits with the mapped outcrops.

#### 4.5 Additional software used

Structural data are represented in a stereonet using *Stereonet 10* a free stereonet software from Allmendinger (2019). Spider charts of trace elements were produced by *Igpet* (Rockware, 2007); chondrite/rock was calculated based on Sun and McDonough (1989). Figures are made and/or prepared in *CorelDraw 2019* (Corel, 2019). Imaging of thin sections was done with both AxioVision (Zeiss, 2009) and LAS EZ (Leica, 2011).

## 5 Results

### 5.1 Lithological units

This sub-chapter contains references to difference localities; locality description can be found in the field books that will be brought to the Falkum (1985) defence. There are seven lithological units in the field area, in chronological order, they are: disperse migmatite, augen-gneiss, flaser-gneiss, deformed granite, amphibolite, undeformed granite, and pegmatite; their distribution can be seen in figure 5.1.

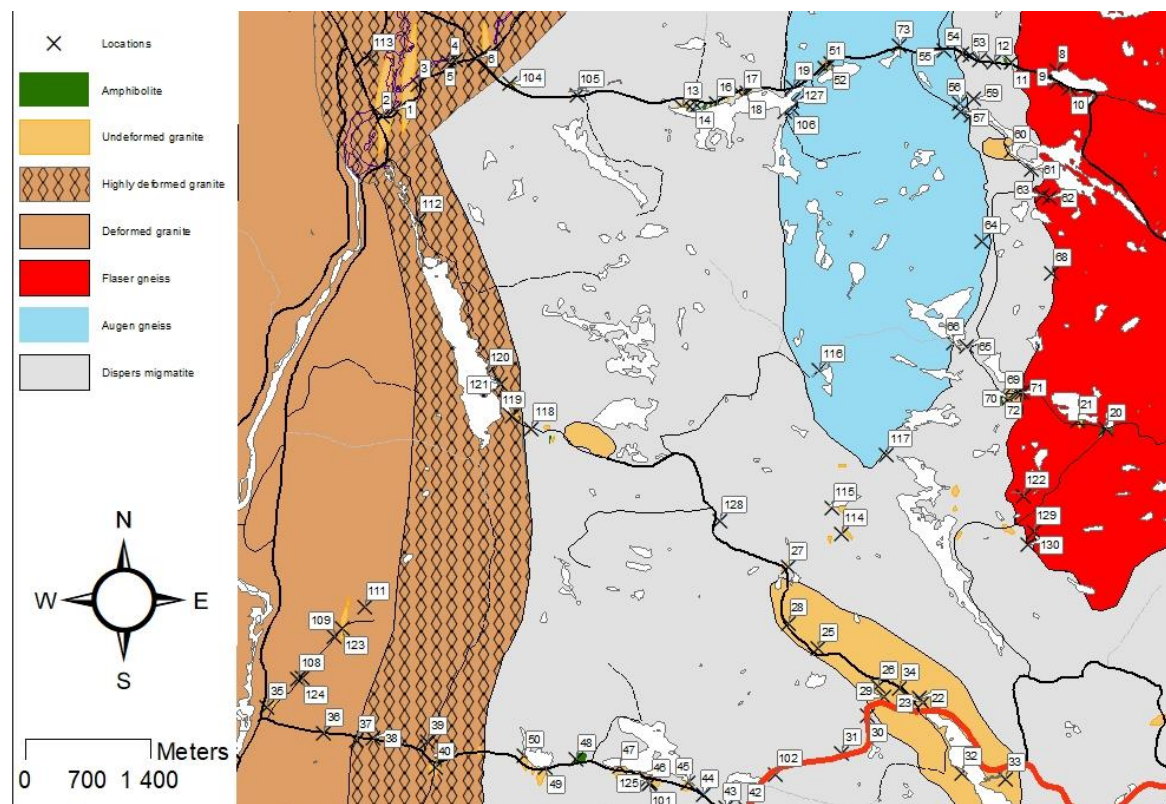


Figure 5.1: Geological map showing the six of the seven units. Pegmatite never appears large enough to be visible in this scale, and they are believed to be related to the undeformed granite. An area of highly deformed granite is highlighted, U-Pb geochronology shows that this is the same unit as the deformed granite.

Mineral abbreviations	
Apa	Apatite
Plg	Plagioclase
A-Fds	Alkalifeldspar
Qtz	Quartz
Zrn	Zircon
Amp	Amphibole
Bt	Biotite
Ser	Sericite
Aln	Allanite
Fds	Feldspar
Msc	Microcline

Table 5.1: mineral abbreviations used in the thin section images

### 5.1.1 Migmatites

The area east of the proposed SMB is dominated by a fine- to medium-grained layered migmatite (see figure 5.1). The mesosomes consists of medium-grained quartzofeldspathic minerals (mostly plagioclase) disperse fine-grained amphibole and biotite with a common orientation resulting in a clear foliation. Zircon, titanite, and apatite occurs as accessory minerals. Foliated with a westward dip.

The leucosomes are quartzofeldspathic fin- to medium-grained and with an orientation similar to the melanocratic minerals in the mesosome. Medium-grained aggregates of amphibole and biotite occurs within the leucosomes possibly as a result of amalgamation of two or more leucosomes. At several localities (e.g., 11 and 14) a second generation of coarse-grained leucosomes cuts foliation (see figure 5.2 (A)). Its melanosomes are  $<1/2$  cm thick and consists of medium-grained amphibole and biotite. Depending on the thickness of the leucosomes, it is not always visible in the field.

In the thin section myrmekite, recrystallisation of quartz, intergrowth textures of plagioclase in feldspar, seritization, bulging, and granoblastic textures can be found.

Layers of porphyritic migmatite at two locations (i.e., location 30 and 105 (see figure 5.2 (E)) suggest that the protolith is not a homogenous batholith, but could itself a more complicated history of batholiths, intrusions, and possibly sediments. Also, horizontal magmatic gradient suggest that the migmatite consist of two main units folded together (see chapter 5.2); these units might differ in protolith age (see chapter 5.2.1), inside  $1469 \pm 45$  Ma (HAL193073), outside  $1565 \pm 11$  Ma (HAL193062).

Undeformed granite and amphibole cuts the migmatite; also, migmatites are found as xenoliths and ghost textures within both undeformed and deformed granite. This suggest that the border is thermal and not tectonic. While the border between the migmatite and the augen- and flaser-gneiss units has no cutting relationship, and the borders is often marked by heavy folding, indicating a tectonic border.

Seven samples were collected; out of these HAL193062, and HAL193073 underwent SHRIMP analysis, and VAG128018 underwent LA-SS-ICP-MS.

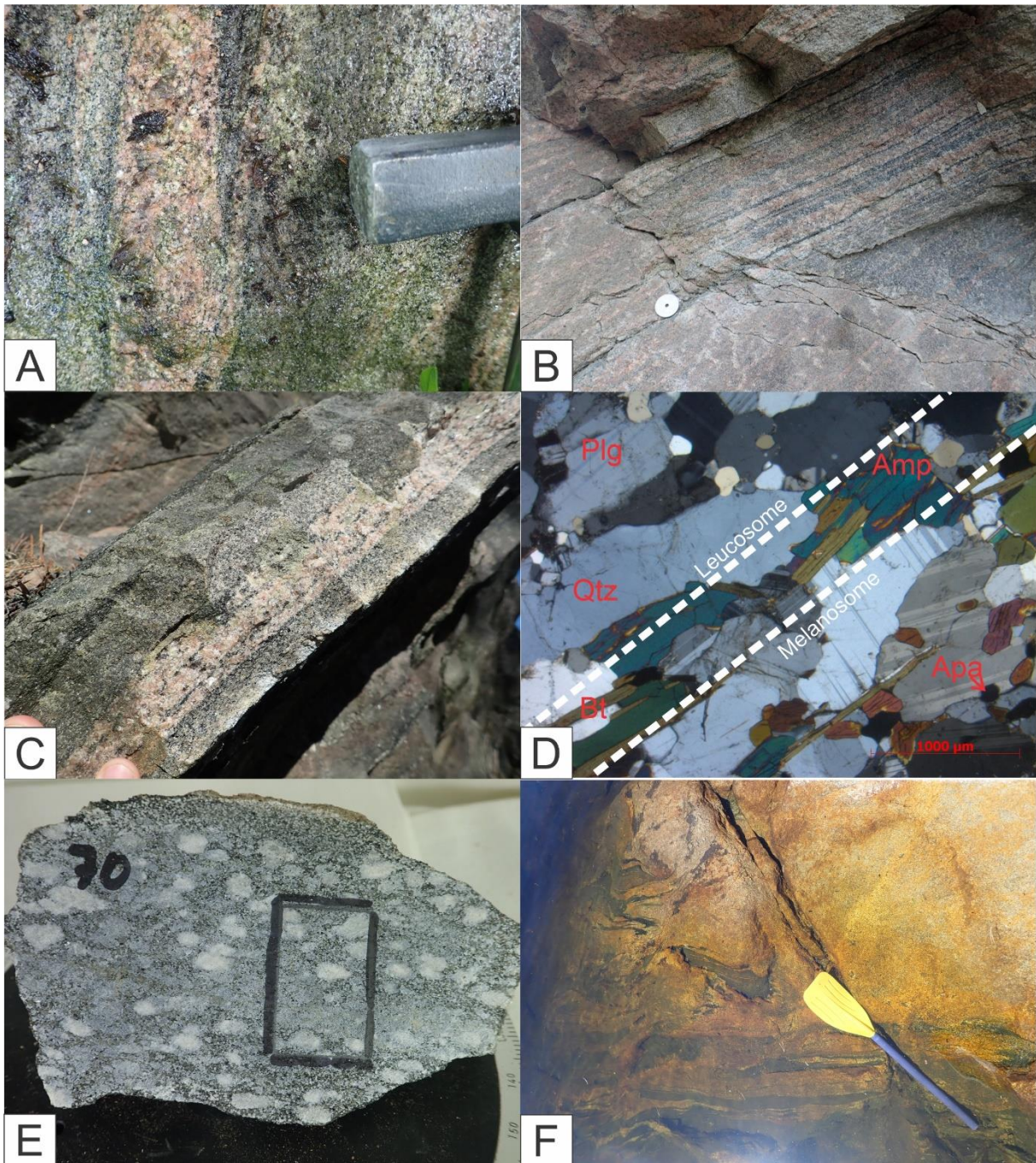


*Figure 5.2: (A) 3-5 cm thick coarse-grained leucosomes cutting the foliation of the mesosome and a < 1 cm thick fine-grained leucosome; found in locality 11. (B) Migmatite with high density of 1-3 cm thick leucosomes surrounded by thin melanosomes and fine-grained mesosomes; found in location 42. (C) Close-up of an ~2cm thick fine-grained leucosome with fine-grained amphiboles on the edges and as lined clusters within; found at locality 128. (D) XPL-image of HAL193073. The sample has a thin leucosome that can be seen in the upper corner, while the mesosome lies in the lower corner. In between lies a thin layer of amphibole and biotite. (E) Sample gathered from a ~10 cm thick layer within the migmatite; Sample HAL 193070 from locality 30. Its phenocrysts is most possible feldspars, but a high weathering makes it difficult to see in an optical microscope; now consist of white micas. (F) Xenoliths of fine- to medium-grained disperse migmatite found within an undeformed fine-grained granite at locality 13.*

### 5.1.2 Augen-gneiss

Found from its southern point just west of Kleivsetvannet northern tip continuing northwards and beyond the field area (see figure 5.1). Consists of a fine-grained gneissos groundmass of quartz, alkali feldspar (microcline and perthite), plagioclase, amphibole, and biotite; zircons, and apatite appears as accessory minerals. The 1-6 cm phenocrysts consists mostly of aggregates of coarse-grained quartz, that are occasionally altered to sericite. The Phenocrysts are often dragged along foliation; in extreme cases, it forms leucocratic layers (see figure 5.3 (C)). Myrmekite, bulging, and recrystallisation appears among the quartzofeldspatic minerals in the groundmass. Radiogenic halos from zircons are found in biotite, while amphibole appears in one sample (HAL 193070) to be retrograde. Migmatization is present but rear. Weak westward foliation similar to that found in the migmatite

The augen-gneiss unit is less forested than the rest of the unit with a much higher degree of outcrops; in such a extent that it is visible on google earth (see figure 5.3 (E)). Also, the magnetism is highly homogenous relative to the other units (see figure 5.3 (D)). Undefomed-granite cut the augen-gneiss, but no amphibolite was found.

Four samples collected; out of these VAG128016, and VAG128017 underwent LA-SS-ICP-MS.

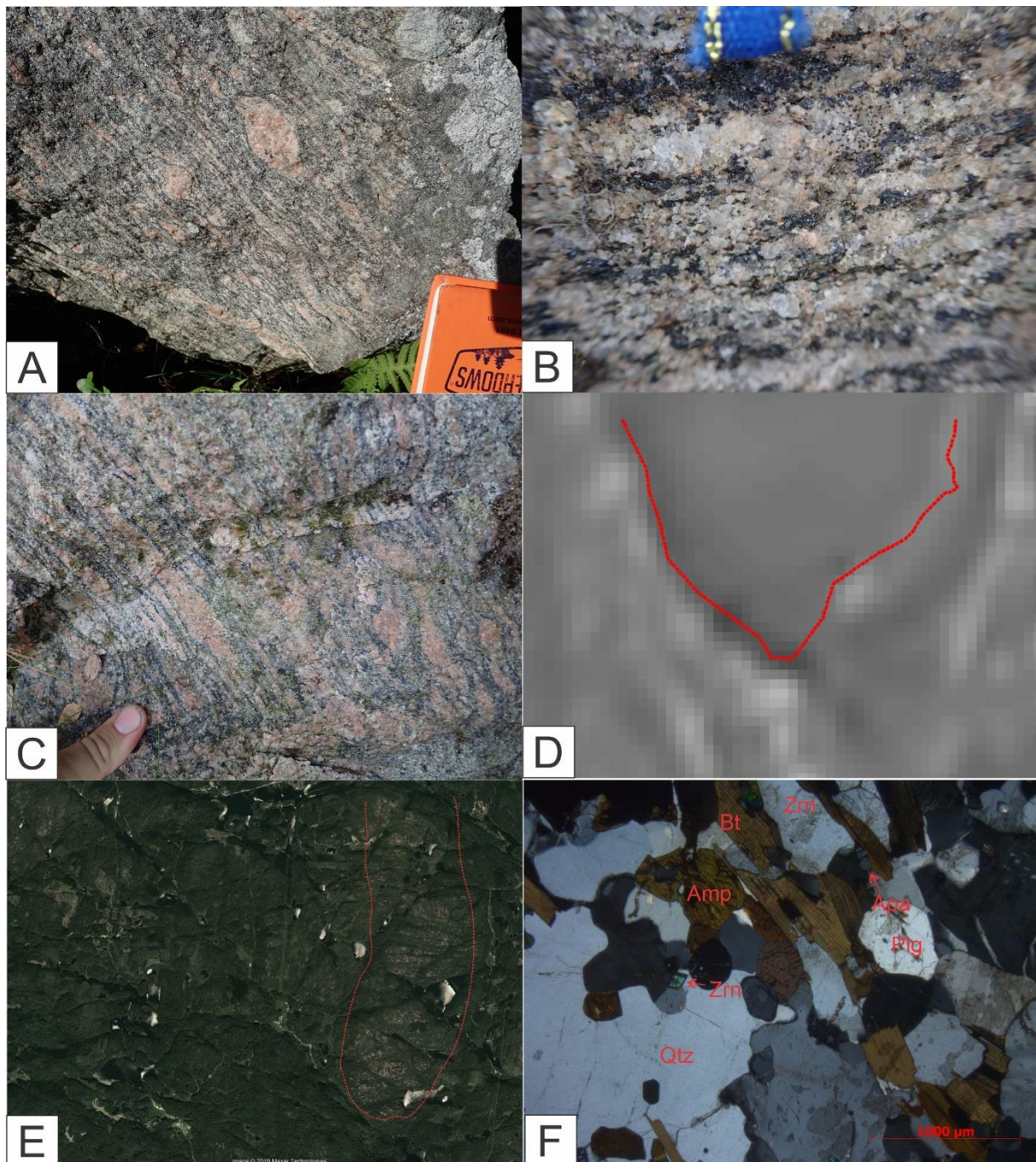


*Figure 5.3: (A) Augen-gneiss found at location 66, large 5-6 cm sigma-clasts, two medium-grained leucocratic veins with thin melanocratic edged cuts foliation, possible migmatization. (B) Close-up on the gneissos texture of the groundmass at location 19, leucocratic and melanocratic minerals are segregated into layers. (C) Example of several phenocrysts now layered at location 64. (D) Image taken from the Horizontal Magmatic Gradient map (NGU-COOP-project, 2017). The red line indicates the visible border. (E) Map gathered from Google Maps (Google, 2018), the red line highlights the less forested area that fits well to the mapped Augen-gneiss unit. (F) XPL-image of HAL193016. Melanocratic and laucocratic minerals are separated in a gneissos texture where Biotite and Quartz forms along oriented bands.*

### 5.1.3 Flaser-gneiss

The northeastern corner consists of a flaser-gneiss that extends outside the field area to the north and east (see figure 5.1). To the west and south it borders the migmatite, this border is folded (see figure 5.4 (C)) and difficult to follow in the terrane especially in the south. Because of time constraint, the border represented on the map is much less detailed than reality, but it is the best estimation based on Falkum (1985) and the Magnetic Horizontal Gradient (NGU-COOP-project, 2017). Migmatite has been found within the flaser-gneiss, most likely due to the heavy folding of the flaser-Migmatite-border, amphibolites, granites, and pegmatites shows cutting relationship to flaser-gneiss. Has a westward foliation similar to that seen in the migmatite, and augen-gneiss.

Characterised by 1-5 cm leucocratic partly or fully recrystallised leucocratic phenocrysts surrounded by fine-grained melanocratic bands; this texture is often referred to as *Tiger Stripes*. For the most part, the phenocrysts have recrystallised into varies quartzofeldspathic minerals such as: medium grain quartz partly recrystallised, ålagioclase with alkali-feldspar intergrowths, microcline, and myrmekite. VAG 128019 (See figure 5.17) shows phenocrysts of microcline up to 1 cm with inclusions of quartz and biotite and perthite intergrowth; these are interpreted to remains of the original phenocrysts. The melanocratic bands consists of a mixture of amphibole and biotite; these bands also seem to be relative rich in apatite. Titanite and zircon also appears as accessory minerals.

Locally the phenocrysts are less recrystallised and resembles an augen-gneiss texture, at location 21 this co-exists whit a structural anomaly, indicating that these textures could be due to less stress inflicted on the rock.

Two samples collected; out of these VAG128019 underwent LA-SS-ICP-MS.

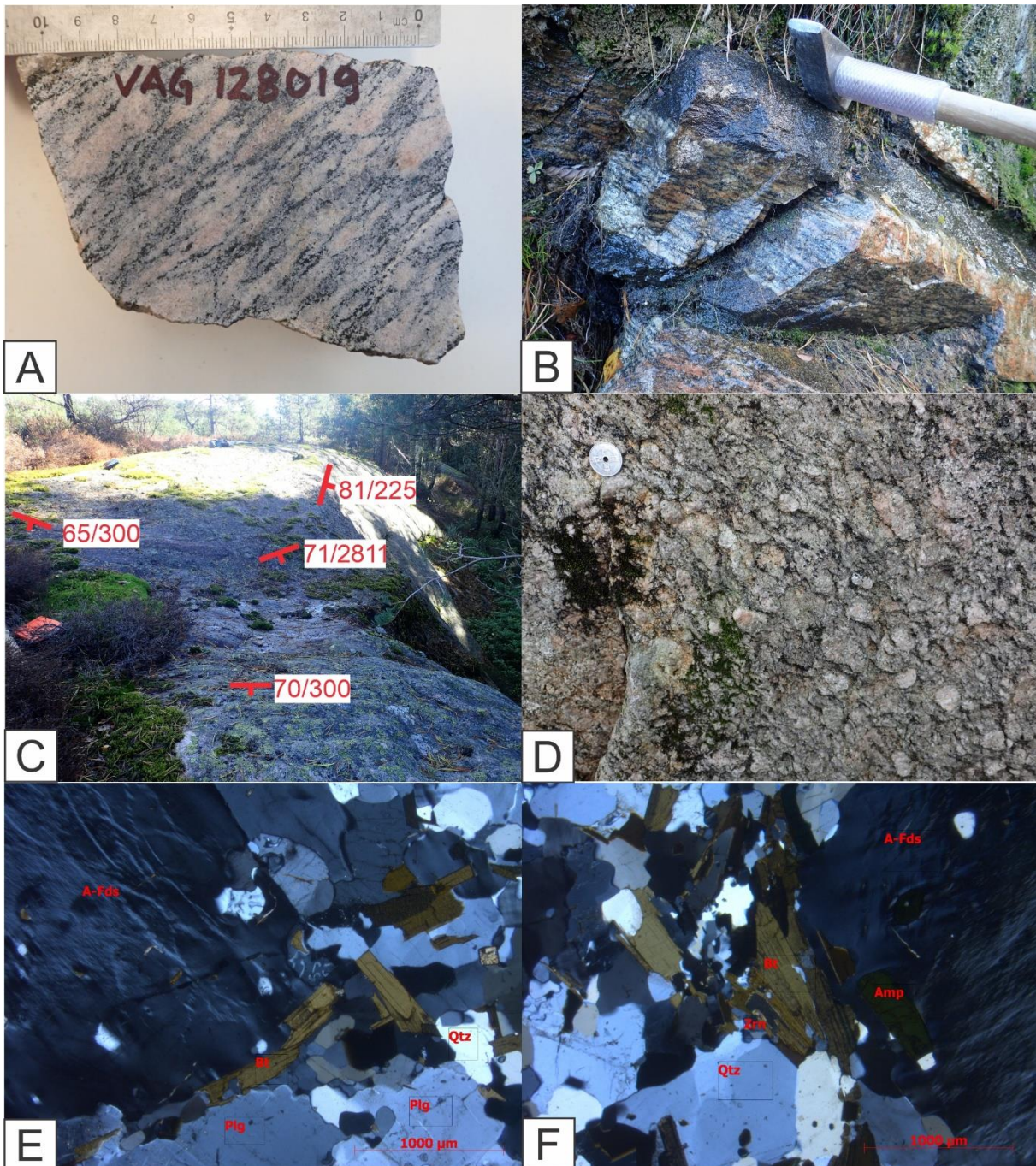


Figure 5.4: (A) Sample VAG 128019 taken from locality 8, consists of 1-3 cm large aggregates of recrystallised leucocratic minerals and fine-grained leucocratic and melanocratic bands. (B) 10-15 cm amphibolite layers that cuts the flaser texture at location 20, sample HAL 193071 is taken from this rock. (C) Flaser gneiss outcrop close to the border to the disperse migmatite at locality 130; the tectonic foliation changes 75 degrees in just a few meters. This is represented with many outcrops along the border. (D) Augen-gneiss texture found at location 21; structural anomaly suggests that we may be within a strain shadow. (E)(F) XPL-images taken along a alkali-feldspar phenocryst.

#### 5.1.4 Deformed granite

Deformed granite found along the eastern border of field area (see figure 5.1); believed to be SMB. Eastwards the deformation increases, and pockets of migmatization occurs. The mapped border falls along a visible line in the horizontal magnetic gradient (NGU-COOP-project, 2017) that has been interpreted to be the border. Along the border xenoliths of migmatite is common, indicating a transitional thermal border. The deformation follows a westward dip similar to the earlier units. Although porphyritic textures is most common, locally, it can appear as co-magmatic with both porphyritic and fine- to medium-grained equigranular melts. The nomenclature “deformed” is used to separate it from the relatively less deformed granite described in 5.1.5.

Characterised by 1-5 cm leucocratic rectangular phenocrysts of mostly alkali-feldspar (some quartz), and a fine- to medium-grained groundmass of feldspar, quartz, amphibole, biotite; zircon, titanite, and apatite occurs as accessory minerals. Metamorphic features as granoblastic textures, grain boundary migration, recrystallisation of quartz, and seritization of the phenocrysts is common. From the protolith myrmekite, intergrowths in feldspars, and melt textures remains. Coarse leucocratic veins cuts foliation similar to those found in the disperse migmatite (see figure 5.5).

The unit is cuts migmatite, and is cut by amphibolite, undeformed granite; there is no contact between it and the augen-gneiss and flaser-gneiss units.

Seven samples collected, out of these HAL193061, HAL193063, VAG084362, VAG128010, and VAG128011 underwent LA-SS-ICP-MS

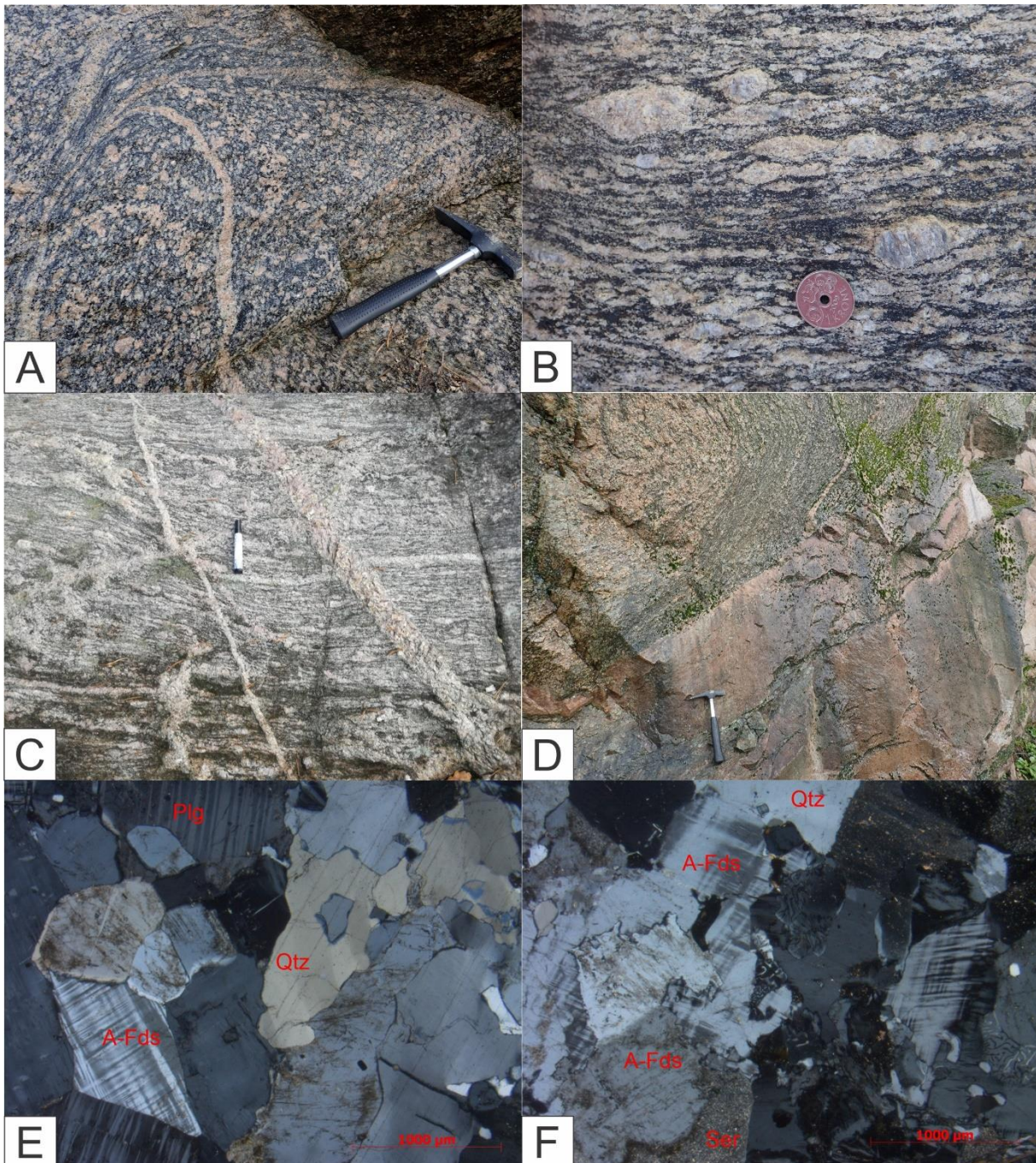


*Figure 5.5: (A) Deformed granite at location 111; 1-2 cm leucocratic phenocrysts and a fine-grained melanocratic groundmass. Fine-grained 1-2 cm thick deformed leucocratic veins cuts the rock. The same outcrop is cut by 60-70 cm thick fine-grained undeformed granite. The deformation seen in the image is not uncommon for the unit. (B) Highly deformed granite (see figure 5.1) at location 38. At the eastern limit of the deformed granite, it becomes more deformed and partly migmatized. (C) Highly deformed granite (see figure 5.1) at location 120 cut by coarse-grained leucocratic veins. The phenocrysts is the source of the grains along foliation. (D) folded deformed granite cut by undeformed granite at location 109. (E) XPL-Image of VAG128011 showing granoblastic textures. (F) XPL-imaging of VAG128011 showing melt-texture, myrmekite bulging, and seritization.*

### 5.1.5 Undeformed granites

Undeformed equigranular fine- to medium-grained granitoid found all over the field area as intrusions; believed to be HBG-suite. Around Tryfjorden in the southwestern corner, lies a larger body coined Fidje-granite (see figure 5.1) rich in biotite-rich xenoliths of migmatites; the granite that stretches along the valley for at least 2 km. Other than the Fidje-granite, the intrusions does not gel larger than a 100 meters. Unlike the earlier unit, there is no clear foliation or preferred direction in the hand specimen. Xenoliths and ghost textures of migmatite is common (see figure 5.2 (E)). It is important to note the nomenclature “undeformed” is to separate it from the “deformed granite” described in 5.1.4; The undeformed granite shows some deformation on micro-scale but is relatively undeformed in relation to the deformed granite.

Build up of alkali-feldspars, plagioclase, quartz, biotite, amphibole, and accessory minerals such as allanite, apatite, titanite, and zircon, in addition to sericite alteration of feldspars. Allanite is not found in any of the other units. Magmatic textures like melt textures and myrmekite is the most common in addition to recrystallisation of quartz. Other metamorphic textures like bulging and granoblastic textures appears but is not as common.

The undeformed granite has a cutting relationship to all other units (see figure 5.6 (A) and 5.5(D)) found except pegmatite. At location 123 a 10 cm thick pegmatite vein originates from the undeformed granite (see figure 5.6 (B)), suggesting that HBG could be the possible source to the many pegmatites found in the Agder region of southern Norway.

Seven samples collected; of these HAL 193056, HAL193066, VAG128014, and VAG128015 underwent LA-SS-ICP-MS

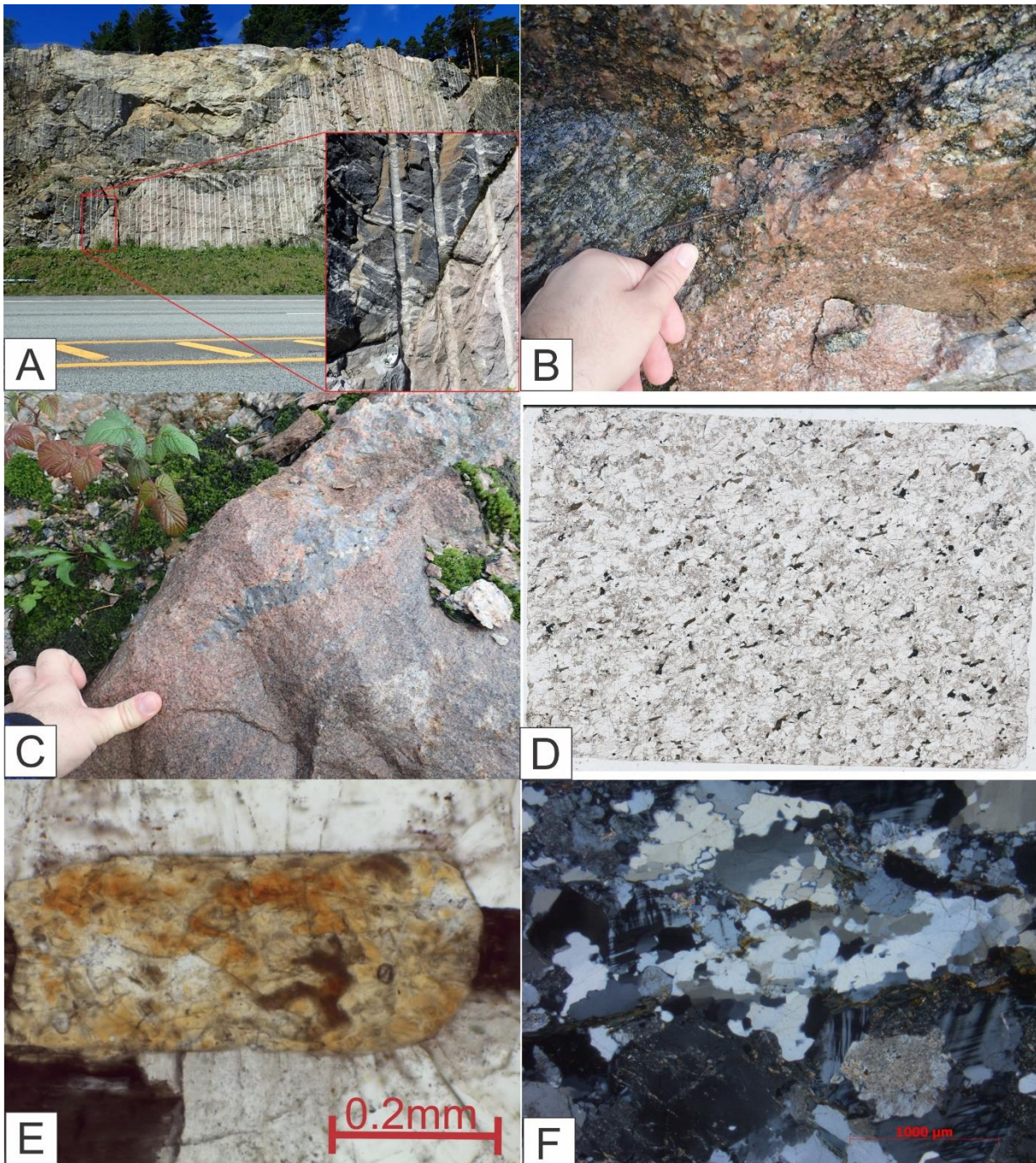


*Figure 5.6: Large 10-15 m intrusion of undeformed granite cutting melanocratic migmatite at location 30 along E39. (B) A fine-grained undeformed granite at location 123 that gradually transforms to a pegmatite, indicating that undeformed granite could be the source of the pegmatites found in the area. (C) Fine-grained undeformed granite at location 123. (D) PPL-scan of HAL193066. The biotite is well distributed in with no clear orientation. The dimensions of the thin sections are 28x48 mm (E) PPL-image from VAG128015 of an allanite grain surrounded by feldspars. Allanite is only found within the undeformed granite. (F) XPL-image of HAL193056 showing recrystallisation of quartz. Although the undeformed granite is dominated by magmatic features, recrystallisation of quartz is common. In addition to quartz, there is microcline and sericite-alteration of feldspars in the image.*

### 5.1.6 Amphibolites

Intrusions of fine-to medium-grained equigranular amphibolite, a clear orientation is visible in the thin section. Varies from 10 cm in thickness to 20-30 meters in thickness. Distributed all over the field as injections in migmatite and flaser-gneiss, and as xenoliths in the deformed granite. The amphibole itself is at one locality (123, see figure 5.7 (A)) cut by a coarse-grained leucocratic vein similar to the ones found in the deformed granites and disperse migmatite. In the same image, you can see a granitic intrusion cutting them both.

Dominated by amphibole, biotite, and plagioclase, minor minerals includes quartz; zircon, alkali-feldspars, and apatite occurs as accessory minerals; titanite occurs as a major mineral phase in HAL193071, and as an accessory retrograde mineral in HAL193052. Quartz sometimes acts as inclusions in the amphibolite. Carlsbad twinning occurs in amphibolite.

Three samples collected; of these, HAL193052 and VAG084363 underwent LA-SS-ICP-MS

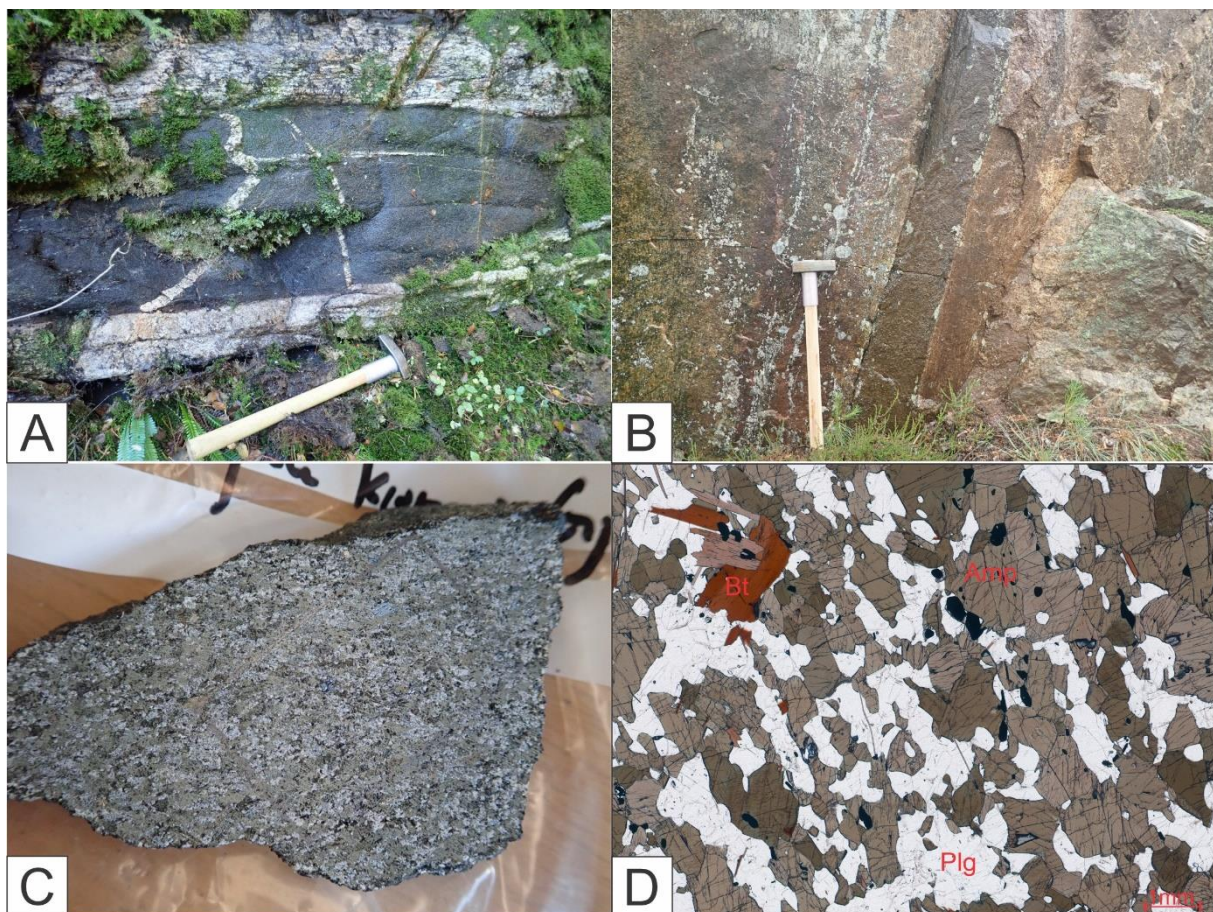


*Figure 5.7: (A) Amphibolite at location 129, cutting a flaser-gneiss. It is cut by a granitic intrusion and coarse-grained leucocratic veins. The granitic intrusion appears to cut both the amphibolite and coarse-grained leucocratic vein. (B) 10 cm thick amphibolite cutting along foliation of the flaser-gneiss in location 8. (C) Image of sample HAL193052. (D) PPL-scan of HAL193052. The sample is dominated by amphibole (amp) and plagioclase.*

## 5.2 Structural geology of the area

Based on the Horizontal magnetic gradient, two large-scale folds where one cuts the other are present in the field area (see figure 5.9).

Fold number one is only present in the migmatite. The fold closes at Systadsnavnet were also the dip-direction shifts from westwards to northwards. West of four z-folds (looking north) have been measured (trend→plunge) to: 17→168, 20→200, 25→235, and 25→225. While on the east side one s-fold (looking north) measures at xx→180. The interpretation is that Fold 1 is a antiform plunging south.

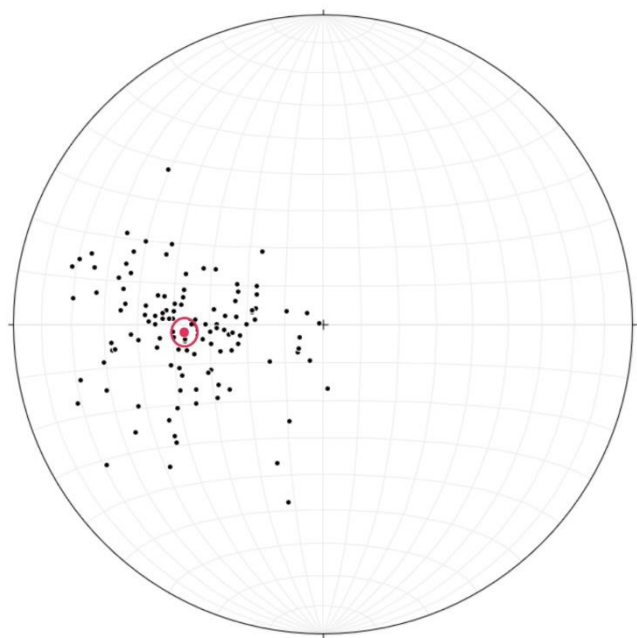


Figure 5.8: Stereonett of measured tectonic foliation excluding the anomalies seen in figure 5.10. The mean vector is indicated as a red point with a red circle around, it sits at 266/53 dip/dip-direction; this is based on 119 measurements. Each black dot represents a dip/dip-direction measurement. The software used is stereonet 10 (Allmendinger, 2019).

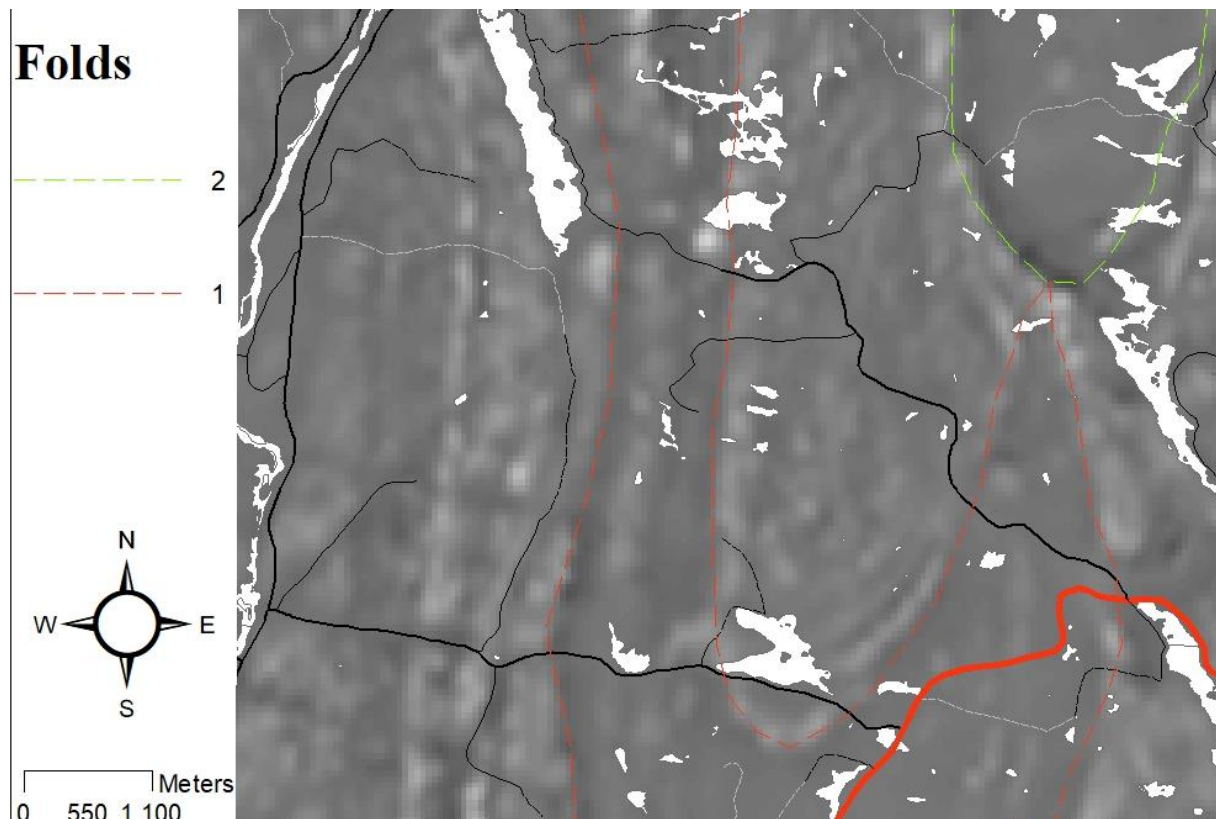


Figure 5.9: Horizontal magnetic gradient map of the area (NGU-COOP-project, 2017) where the two folds are lined up and colour-coded; red for fold 1 and green for fold 2.

Fold 2 cut Fold 1 just north of Lillevann, which is visible through di/dip-directions seen in figure 5.10. The fold fits well with the presence of the augen-gneiss unit. This fold is already noted down by Falkum (1985) as a antiform.

Dip/dip-direction measurements of tectonic foliations taken all over the field area indicates a overall westward dip with a mean vector of 266/53.

There are four main anomalies to this trend shown in figure 5.10. These are coined: Nomevatnet anomaly, Slemmedsvannet anomaly, Systadvatnet anomaly, and Lillevann anomaly.

1. Nomevatnet anomaly shows a step eastward dip approximately with the same strike as the mean vector.
2. Slemmedsvannet anomaly are two measurements that has a northward dip. This coexist with a lower degree of deformation in the flaser unit.
3. Systadvatnet anomaly locates where fold 1 closes, and it affects the dip-direction for over 2 km. moving from E39 along the FV459 the dip-direction switches from westwards to a southwards dip-direction; influenced by the closing of fold 1
4. Lillevann anomaly locates where fold 2 cuts fold 1. Gradually moving towards the border, the dip-direction switches from westwards to a north-northwest direction.

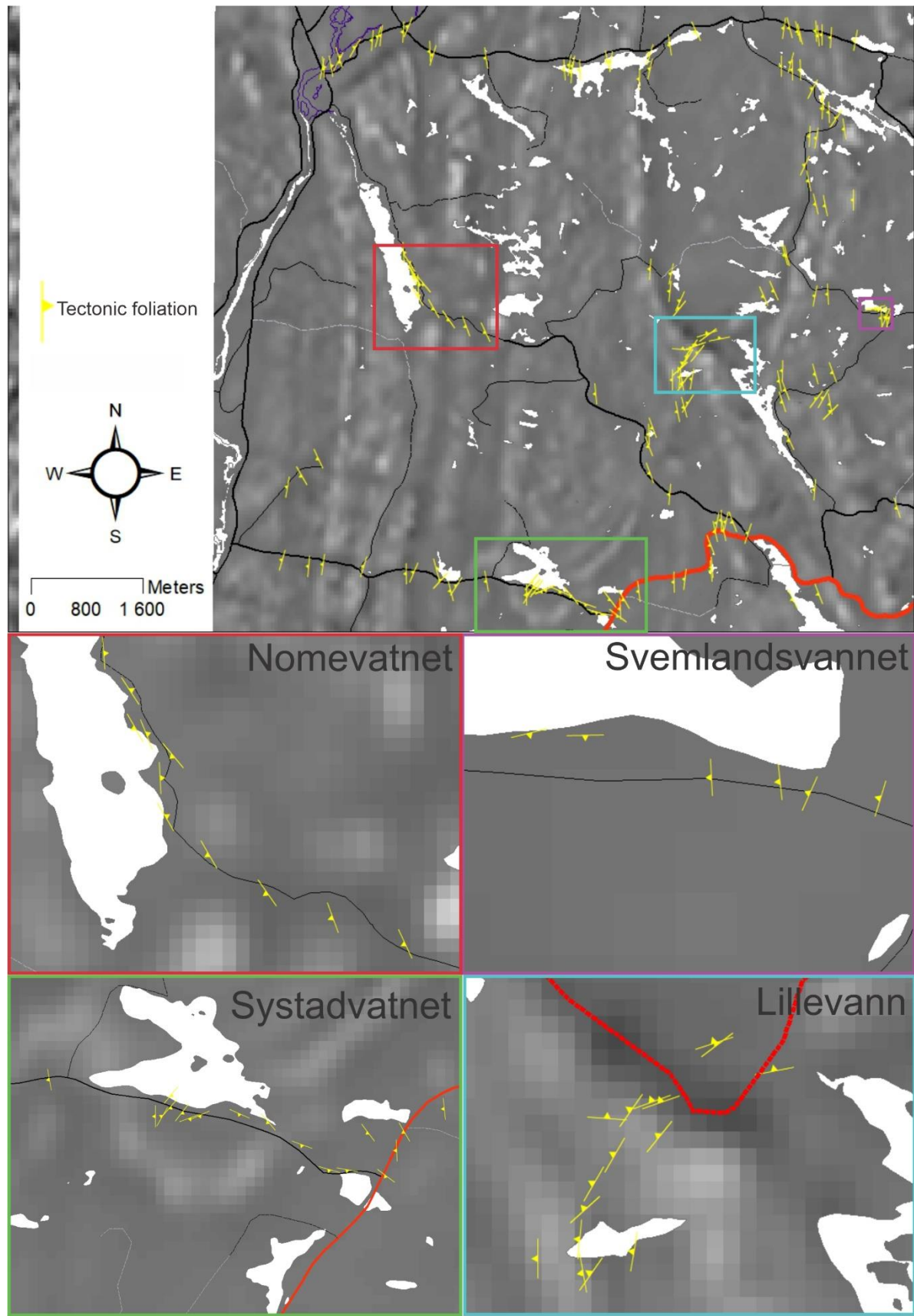


Figure 5.10: Map of the field area showing all the measurements of tectonic foliation with the horizontal magnetic gradient as a background (NGU-COOP-project, 2017). Beneath, the four main anomalies mentioned in the text have been zoomed in.

### 5.3 U-Pb data

Sixteen samples were dated at Curtin University, two by SHRIMP analysis, and fourteen by LA-SS-ICP-MS. Samples that were collected in connection with this study have the prefix “HAL”, while samples with the prefix “VAG” were sampled back in 2014/2015 by Nolwenn Coint and Trond Slagstad. The results will be presented in this sub-chapter. All coordinates are *UTM WGS 1984 EPSG*. Notes from the thin sections can be found in Appendix G.

Sample	Locality	32N		Rock type	Method	Data points	Age (Ma)	I/M/U*
		East	North					
HAL 193052	10	422818	6448003	Amphibolite	LA-SS-ICP-MS	5	968 ± 14	U
HAL 193056	34	420923	6441265	Undeformed granite	LA-SS-ICP-MS	5	No clear result	I
HAL 193061	37	414826	6440679	Deformed granite	LA-SS-ICP-MS	20	1038 ± 28	I
HAL193062	105	417304	6447923	Migmatite	SHRIMP	10	1565 ± 11 1011 ± 20 560 ± 40	I/M/U
HAL193063	111	414918	6442172	Deformed granite	LA-SS-ICP-MS	34	1025 ± 20	I
HAL193066	123	414667	6441936	Undeformed granite	LA-SS-ICP-MS	9	945 ± 14	I
HAL193073	128	418910	6443145	Migmatite	SHRIMP	31	1469 ± 45 1011 ± 9	I/M
VAG 084362	b 35-36	414488.59	6440759	Deformed granite	LA-SS-ICP-MS	25	1050 ± 6	I
VAG 084363	c 41	416346	6440569	Migmatite	LA-SS-ICP-MS	32	1532 ± 38 1011 ± 50	I/M
VAG 128010	c 2	415158	6447684	Deformed granite	LA-SS-ICP-MS	21	1066 ± 67	I
VAG 128011	b 1-3	415410	6447899	Deformed granite	LA-SS-ICP-MS	30	1078 ± 14	I
VAG 128012	c 4	415849	6448254	granite	LA-SS-ICP-MS	16	No clear result	U
VAG 128014	c 104	416616	6448012	Undeformed granite	LA-SS-ICP-MS	20	Uncertain source	U
VAG 128015	13	418482	6447780	Undeformed granite	LA-SS-ICP-MS	27	No clear result	U
VAG 128016	c 51	420005	6448159	Augen gneiss	LA-SS-ICP-MS	39	1241 ± 41	I
VAG 128017	c 51	420031	6448181	Augen gneiss	LA-SS-ICP-MS	31	1210 ± 31	I
VAG 128018	c 53	421718	6448384	Migmatite	LA-SS-ICP-MS	23	1566 ± 7	I
VAG 128019	8	422671	6448199	Flaser gneiss	LA-SS-ICP-MS	47	1208 ± 16 1063 ± 18	I

\*I = Igneous, M = Metamorphic, U = Unknown

Table 5.2: All results from the U-Pb geochronology at Curtin University. Sample HAL193056, VAG128012, VAG128015 showed no clear results. Sample VAG128014 gave a  $^{207}\text{Pb}/^{206}\text{Pb}$  age mean average of  $1586 \pm 26$  ( $\text{MSWD}=0.63$ , probability = 0.88), but due to a uncertain source, it is excluded from this chapter. c = close to, b = between.

### 5.2.1 Migmatites

Four samples underwent geochronological testing, two from VAG and two from HAL. LA-SS-ICP-MS was used for the two VAG-samples, while SHRIMP was used for the two HAL-samples. Images and charts are found after description.

#### VAG 128018

32N 421718E 6448384N

Found within disperse migmatite close to location 53. A fine-grained disperse mesosome consisting of amphibole, biotite, feldspars, and quartz. It has a clear foliation where amphibole and biotite are oriented similar to the leucosomes. This quartzofeldspathic leucosomes are no more than 1 cm thick and divided from the mesosome by a < 1mm melanosome consisting of amphibole and biotite. A thin section was made with >90 % mesosome, with the rest consisting with <1 cm thick quartzofeldspathic leucosomes and a thin amphibole/biotite melanosome. Both magmatic and metamorph textures are present. The amphibole/biotite in follows an orientation similar to that of the leucosomes. Minerals present are plagioclase (40%), quartz (30%), amphibole (20%), biotite (5%), alkali-feldspars (5%), and zircon as a accessory mineral.

The zircons colourless to slightly brown, most are rounded but a few prismatic, with a variant size 50-200 µm. U-Zoning in the CL images indicates magmatic origin.

Twenty-three data points were analysed with LA-SS-ICP-MS, which gives a Concordia that intercepts at  $787 \pm 430$  and  $1555 \pm 26$  Ma (MSWD = 1.4). Most of the analysis are grouped, removing the data points outside gives  $288 \pm 1200$  and  $1558 \pm 19$  Ma (MSWD = 1.2). Further removing five more data points three with higher  $^{238}\text{U}/^{206}\text{Pb}$  and two with less, a possible Concordia age at  $1566 \pm 7$  Ma (MSWD = 1.2, P = 0.15).

The interpretation is that the protolith crystallised at  $1566 \pm 7$  Ma, any age of migmatization is not possible to determine.

#### HAL 193062

32N 417304E 6447923N

Migmatite sample taken from a 20 meters wide outcrop at location 105. The mesosome is fine to medium-grained disperse evenly proportioned with melanocratic and leucocratic minerals that has an orientation following a westward dip direction. One layer < 10 cm shows elongated leucocratic fine-grained aggregates and a melanocratic matrix. The leucosomes are sparse and < 1 cm, while the melanosomes are for all except one non-visible. 50-60 cm thick

granitic intrusion with ghost structures are also found on the location. Furthermore Small < 1cm thick folds with amphibolite-aggregates in the hinge with a N-S strike. The thin sections reveals a later alteration in form of seritization of leucocratic minerals. Both magmatic and metamorph textures are present. Minerals present are quartz (50%), amphibole (25%), plagioclase (15%), biotite (5%), alkali-feldspars (5%), an apatite, zircon, and sericite as accessory minerals.

The zircons are prismatic, brownish, 100-200  $\mu\text{m}$ , and has a U-zoning reflecting a magmatic origin. One grain differs from these and shows a clear rim and a clear core reflecting two stages of mineralisation.

Ten grains were dated by Shrimp analysis, the rim/core twice once of the rim and once of the core. One of the analysis were rejected because of high common Pb deeming it invalid. For the rim/core grain the rim is dated to  $1011 \pm 20$  Ma (MSWD = 0.046, P = 0.83), while the core looks to have hit both the rim and the core. Six of the magmatic zircons groups together to form a Concordia age at  $1565.4 \pm 11$  Ma (MSWD = 4.2, P = 0.040). Two magmatic outliers form a line that, together with the grouped analysis that intercepts at  $560 \pm 40$  Ma and  $1548 \pm 15$  Ma (MSWD = 0.75).

The interpretation is that the protolith crystallised at  $1565 \pm 11$  Ma, migmatized at  $1011 \pm 20$  Ma, and a possible third event at  $560 \pm 40$  Ma.

*HAL 193073  
32N 418910E 6443145N*

Disperse migmatite from a ca 15-meter outcrop along the road at location 128. Leucosomes are in general 5-6 cm with 1 cm melanosome. The mesosome is fine-grained and contains biotite and quartzofeldspathic minerals, while the melanosome contains medium-grained amphibole. The leucosome consists of mainly quartz and alkali-feldspar up to 4 mm. Plagioclase occurs as intergrowths in the alkali feldspars. Myrmekite, quartz-recrystallisation, and bulging are common textures. Minerals present are quartz (60%), alkali-feldspar (30%), amphibolite (5%), biotite (2%), and plagioclase, zircon, and apatite as accessory minerals.

The zircons are prismatic, brownish, and with a high variance in size from up to 250  $\mu\text{m}$  to < 50  $\mu\text{m}$ . In CL, a clear separation of core and rim, likely reflecting the age of the rock and the age of the migmatization.

Thirty-one data points were dated by SHRIMP analysis from 15 grains. Two of these were discarded due to no U being measured during sampling. Discarding further eight discordant

analysis gives a line that intercepts  $998 \pm 24$  Ma and  $1469 \pm 45$  Ma (MSWD = 1.4). Ten of the rim analysis groups together possible, giving a more correct age of the migmatization at  $1011 \pm 9$  Ma (MSWD = 0.35, P = 0.55).

The interpretation is that the protolith crystallised at  $1469 \pm 45$  Ma with a migmatization at  $1011 \pm 9$  Ma.

VAG 084363

32N 414918E 6442172N

An alternation between migmatite and amphibolite found close to location 41 within the area mapped as disperse migmatite. Split into four zones: Zone 1 consist of coarse-grained Qtz. Zone 2 consist of fine-grained amphibolite with amphibole (60%), biotite(<1%), quartz (20%), plagioclase(20%), apatite(<1%). Zone 3 medium-grained quartz and plagioclase with some biotite. Quartz is recrystallised and bulged. Zone 4 is biotite (50%) rich, with some amphibole (20%), quartz (25%) plagioclase (5%), and apatite (<1%).

The zircons are rectangular and range from colourless to brown, and from 50  $\mu\text{m}$  to 250  $\mu\text{m}$ . In CL most grains show oscillatory zoning, while some are dark and without variance.

Thirty-two data points were captured with LA-SS-ICP-MS. The results are discordant ranging from 1550 to 1200 Ma suggesting a possible discordia line, eleven data points are discordant from this line and are thus rejected. Since the sample is found within the disperse migmatites, it is possible that the discordia line will intercept with the migmatization age found in VAG 128018 and HAL 193073. By assuming a interception at  $1011 \pm 50$  Ma, the Discordia line intercepts at  $1532 \pm 38$  Ma (MSWD = 0.98).

The interpretation is that the data reflect a protolith crystallisation at  $1532 \pm 38$  Ma with a migmatization at  $1011 \pm 50$  Ma.

## VAG 128018

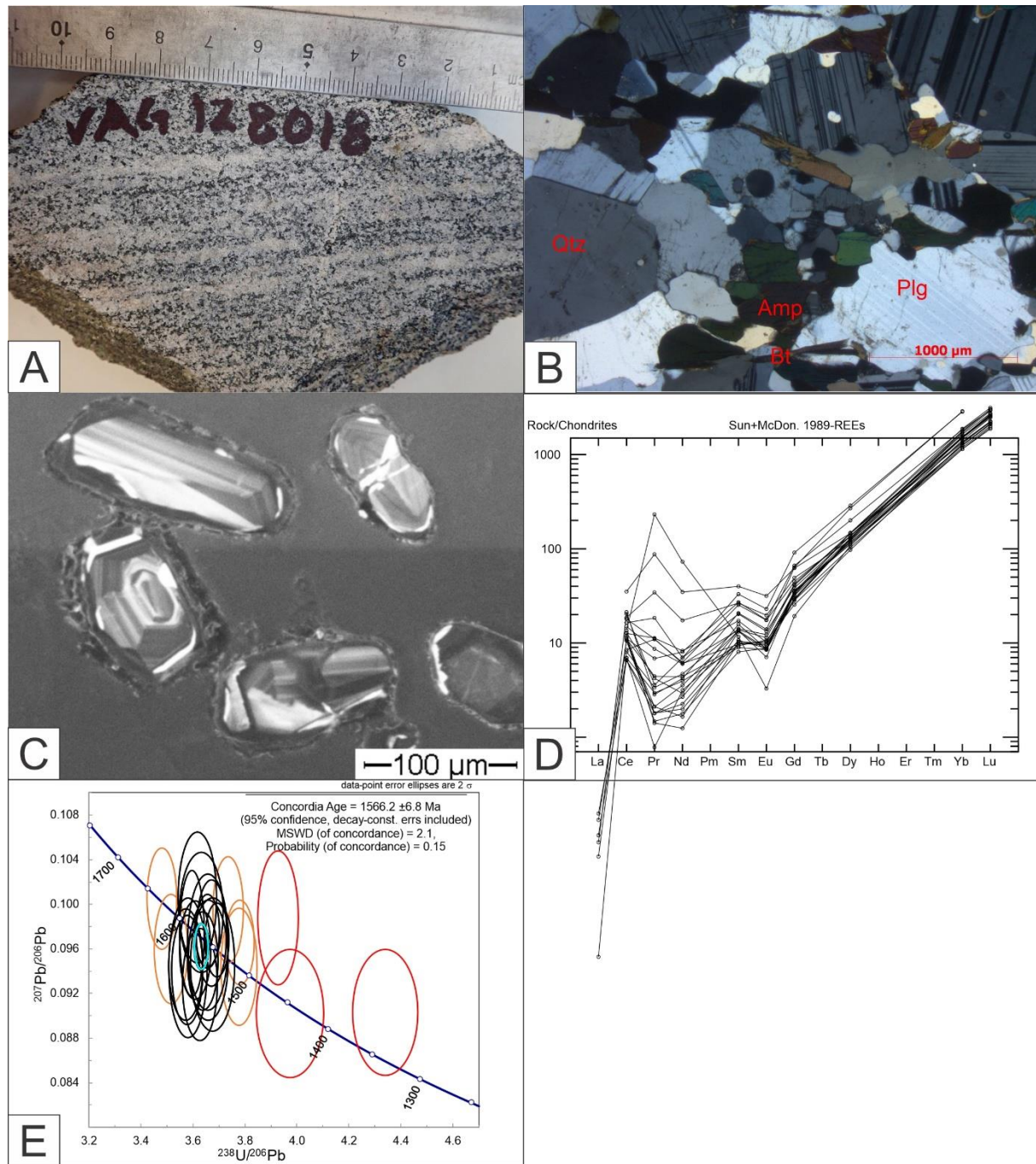


Figure 5.11: (A) An image of the collected sample, a mesosome-rich sample with thin leucosomes. (B) XPL-image of VAG128018 with granoblastic texture, and bulging of plagioclase (C) Example of zircons collected from the sample. (D) Spider diagrams of the trace elements measured in the zircon. (E) Terra-Wasserburg-plot of the U-Pb geochronology. The black circles are the measurements used to calculate the Concordia age that is highlighted in blue. The red and orange circles are outlier not used in the calculation.

HAL 193062

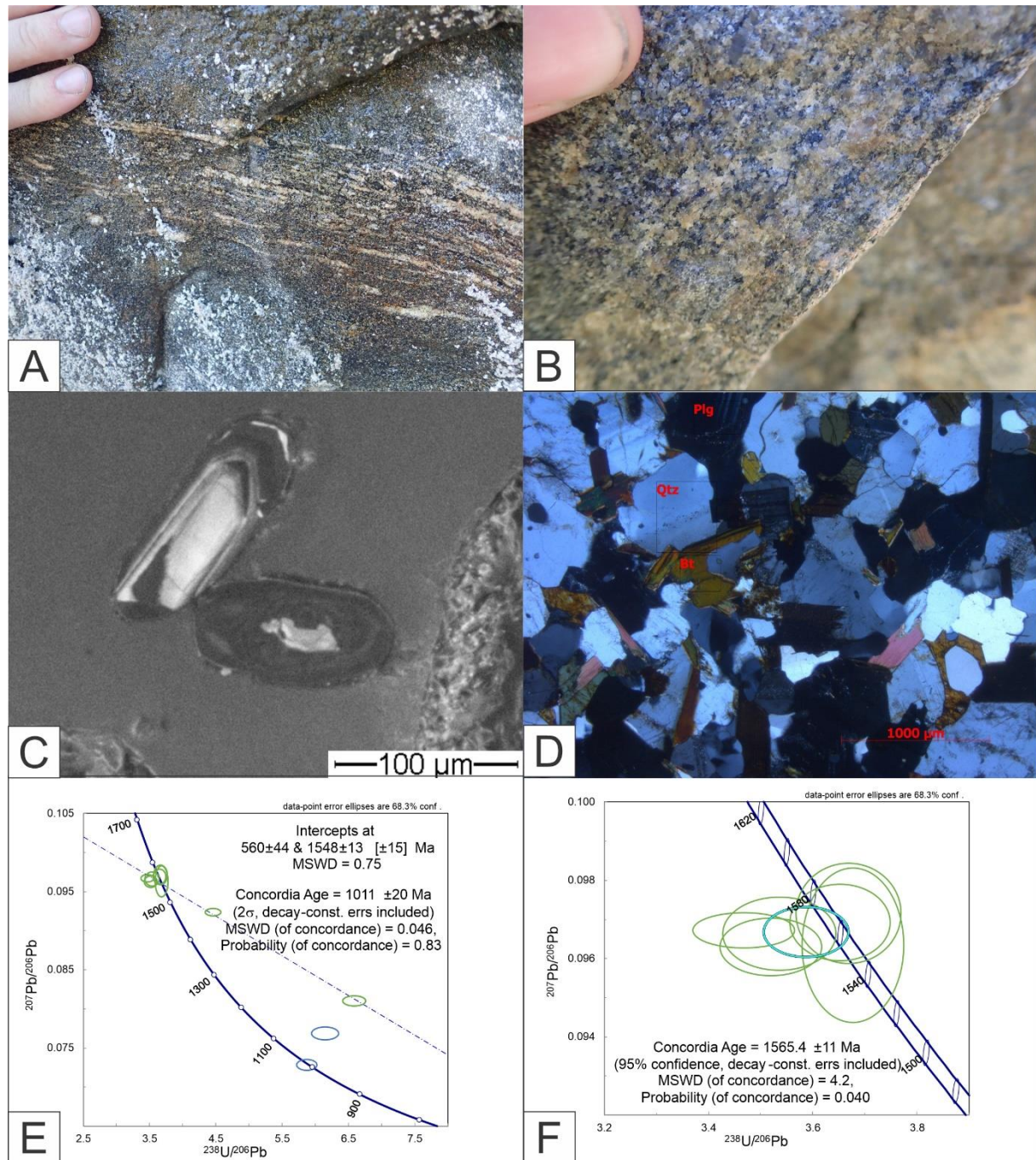


Figure 5.12: (A) a < 10cm layer showing elongated leucocratic aggregates at the locality. (B) Example of a mesosome found at the locality. (C) CL-imaging of two of the zircons that were measured. The zircon to the right is the one showing core/rim zoning, while the one to the left shows magmatic zoning (D) XPL-image of the mesosome. (E) Terra-Wasserburg-plot based on the U-Pb geochronology. The green circles are the measurements from the magmatic zircons used to calculate the 1548 Ma, and 560 Ma interception. The blue circles come from the core/rim zircon; the rim-measurement gives a age at 1011 Ma. (F) Shows the Concordia age calculation that the 1565 Ma age is based on. The blue circle represents the Concordia age.

## 5 Results

HAL 193073

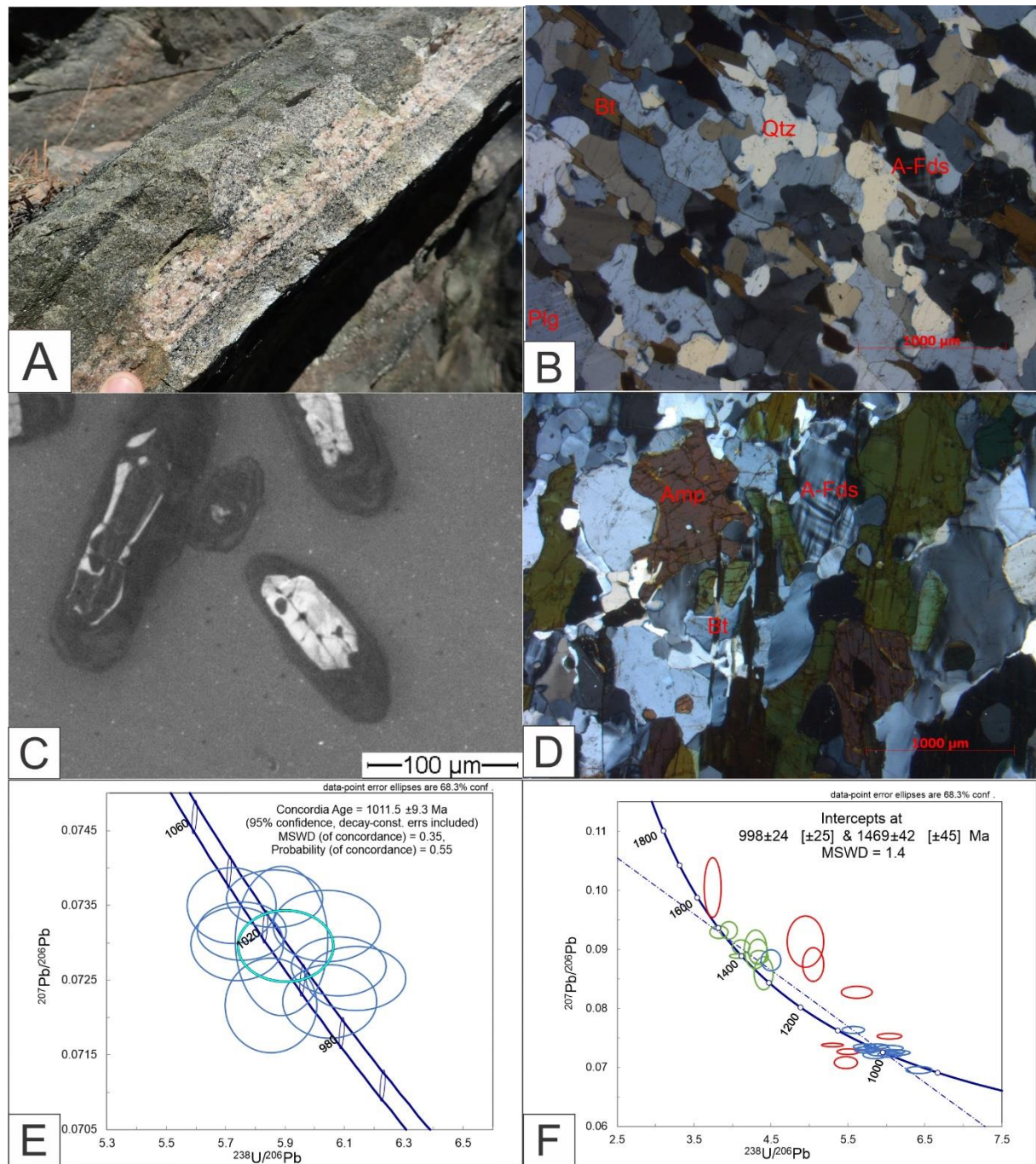


Figure 5.13: (A) Image of a clear leucosome from the locality, a thin layer of melanosome on each side. (B) XPL-image of the mesosome. (C) CL-imaging of the zircons showing a rim/core texture. (D) XPL-image of the melanosome (E, F) Terra-Wasserburg plot of the U-Pb geochronology. Red circles are discarded outliers, green circles are measurements of the core, while blur circles are measurements of the rim. The plot gives two interceptions with a protolith age of 1469 Ma. (E) Shows a more accurate age calculation with a Concordia age in light blue at 1011 Ma.

## VAG 084363

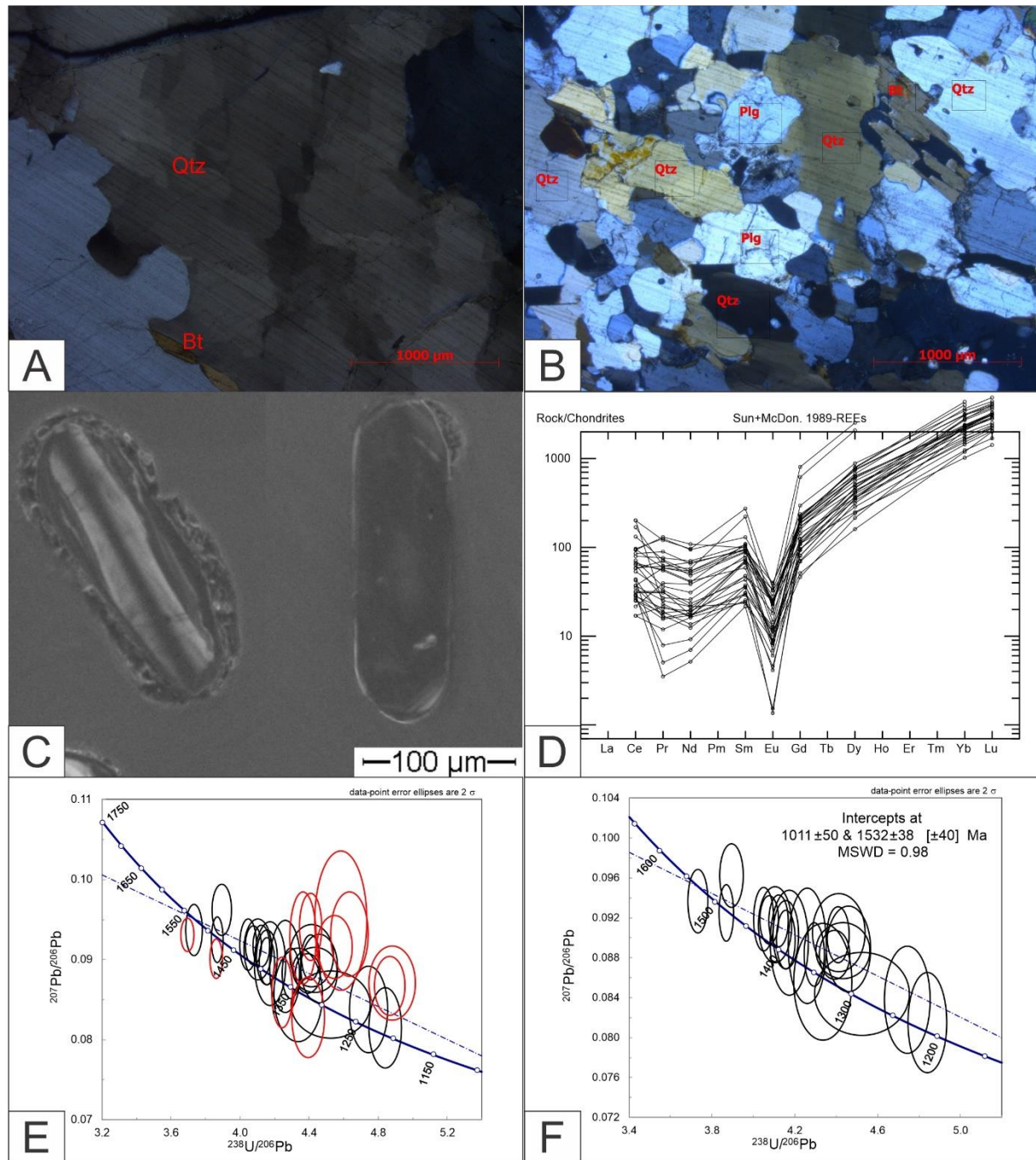


Figure 5.14: (A) XPL-image of zone 1, a zone of coarse-grained quartz. (B) XPL-image of zone 3. (C) CL-images of two zircons showing the two kinds of zircons in the sample as described in the text. (D) Spider diagram of trace element measurements from the zircon. (E,F) All U-Pb data creating a Concordia line that intercepts the Concordia at 1532 Ma and 1011 Ma. The circles in red are discarded as outliers.

### 5.3.2 Eastern gneisses

The eastern gneisses consists of one augen-gneiss body and one Flaser-gneiss body separated by disperse migmatite. These units has previously been speculated to be associated with Gjerstad Suite, a 1.15-1.19 Ga augen-gneiss found in Telemark (Bingen et al., 1998, Bingen and Van Breemen, 1998). Two augen-gneiss samples and one flaser-gneiss sample underwent LA-SS-ICP-MS at Curtin University.

#### *VAG 128016 (Augen-gneiss)*

32N 420005E 6448159N

VAG 128016 is a augen-gneiss collected by Eiksåvann lake. Described in the fields as migmatic granitic gneiss by earlier fieldwork. In the thin section, it is leucocratic with aggregates of amphibole and biotite. Both magmatic and metamorphic features are present. Mineral assemblage is quartz (80%), plagioclase (30%), alkali-feldspar (15%), amphibole (10%), biotite (2%), and zircon and apatite as accessory minerals.

The zircons are colourless to spatially brownish, prismatic with a variant size from 100 to 250 µm. CL-imaging shows magmatic zoning with most being oscillatory.

39 data analysis were taken with LA-SS-ICP-MS. There is a high variance of LREE, but there is seems to be no special correlation with these and age. All data points with discordance > 10 are removed, as well 5 concordant outliers, weighted average of  $^{207}\text{Pb}/^{206}\text{Pb}$  age then becomes  $1241 \pm 22$  (MSWD = 0.52, P = 0.97).

The interpretation is that this age reflects the crystallisation age at  $1241 \pm 41$  Ma. The large number of concordant outliers yielding an younger age indicates that the age may be younger than 1241 Ma.

#### *VAG 128017 (Augen-gneiss)*

32N 420031E 6448181N

Collected at the same locality as VAG 128016. Leucocratic fine- to medium-grained rocks with bands of amphibole and biotite. Phenocrysts of quartz and plagioclase takes up almost half of the space. Quartzofeldspatic groundmass with some fine-grained biotite. Metamorphic textures such as bulging is present. Mineral assemblage is quartz (45%), alkali-feldspar (30%), plagioclase (20%), biotite (5%), and amphibole, zircon, sericite, and apatite as accessory minerals

The zircons colourless rectangular, variant in size from 50 to 250 µm. CL-imaging shows both normal and oscillatory zoning.

Out of thirty-one data-points, seven data-points with  $^{207}\text{Pb}/^{206}\text{Pb} > 0.085$  were removed. The remaining data-points are within 0.074 and 0.083  $^{207}\text{Pb}/^{206}\text{Pb}$  but vary in  $^{238}\text{U}/^{206}\text{Pb}$ , possibly due to lead loss. To achieve a  $^{207}\text{Pb}/^{206}\text{Pb}$  weighted average, twelve additional data points were removed; this gave an age of  $1210 \pm 31$  Ma (MSWD = 1.2, P = 0.26)

We interpret this age to reflect the protolith age.

*VAG 128019 (Flaser gneiss)*

32N 422671E 6448199N

VAG 128019 is a flaser-gneiss collected by Røyrvatnet lake at location 8. Fine- to medium-grained flaser gneiss with 5 cm aggregates intruded by pegmatites and amphibolite. Variations from flaser gneiss to porphyritic structure occurs. Mineral assemblage of the thin section is alkali-feldspar (40%), plagioclase (35%), quartz (20%), amphibole (5%), biotite (1%), and zircon as a accessory mineral.

The zircons are colourless, prismatic, and 150-79  $\mu\text{m}$ . Clear magmatic zoning is visible in CL-imaging.

Forty-eight data points are distributed evenly along Concordia. High amount of reverse discordant samples makes it difficult to determine any reasonable Discordia line, but out of the data, one population can be singled out. Alpha-dose calculations reveal an increase with younger age that ends around 1.05 Ga; here, three data points lies that is located away from the rest that becomes population 2; with a Concordia age of  $1063 \pm 18$  Ma (MSWD = 4.6, P = 0.032). Five discordant data-points are removed from the remaining data-points, a  $^{207}\text{Pb}/^{206}\text{Pb}$  weighted average of the remaining data points gives a age of  $1208 \pm 16$  Ma (MSWD = 0.94, P = 0.57).

The interpretation is that protolith crystallisation happened at  $1208 \pm 16$  Ma, and later metamorphisation happened at  $1063 \pm 18$  Ma.

## VAG 128016

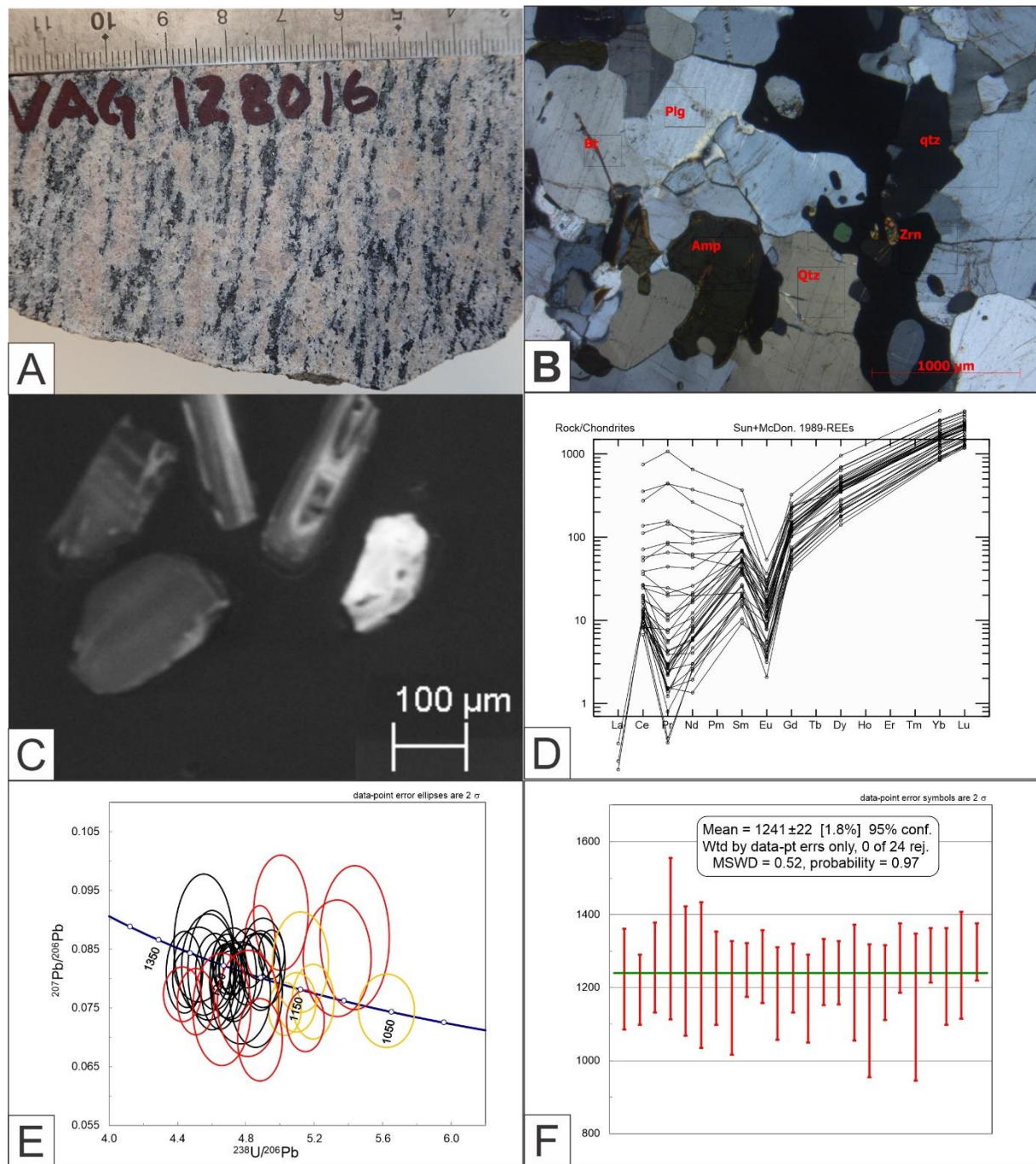


Figure 5.15: (A) Hand specimen of the sample. Leucocratic aggregates surrounded by gneissos matrix. (B) XPL-image of VAG128016 showing metamorphic features such as granoblastic textures, and bulging. (C) CL-image of the zircons with magmatic zoning. The grain to the right is an apatite. (D) Spider diagram of trace elements from the sample. There is a high variance in LREE, but there are no found correlation between this and age and/or discordance. (E) Terra-Wasserburg plot of the U-Pb geochronology. Red circles are discordant data, while yellow circles are concordant outliers. The black circles indicates those used to calculate the age. (F)  $^{207}\text{Pb}/^{206}\text{Pb}$  weighted average of the black circles giving a age of 1241 Ma.

Vag 128017

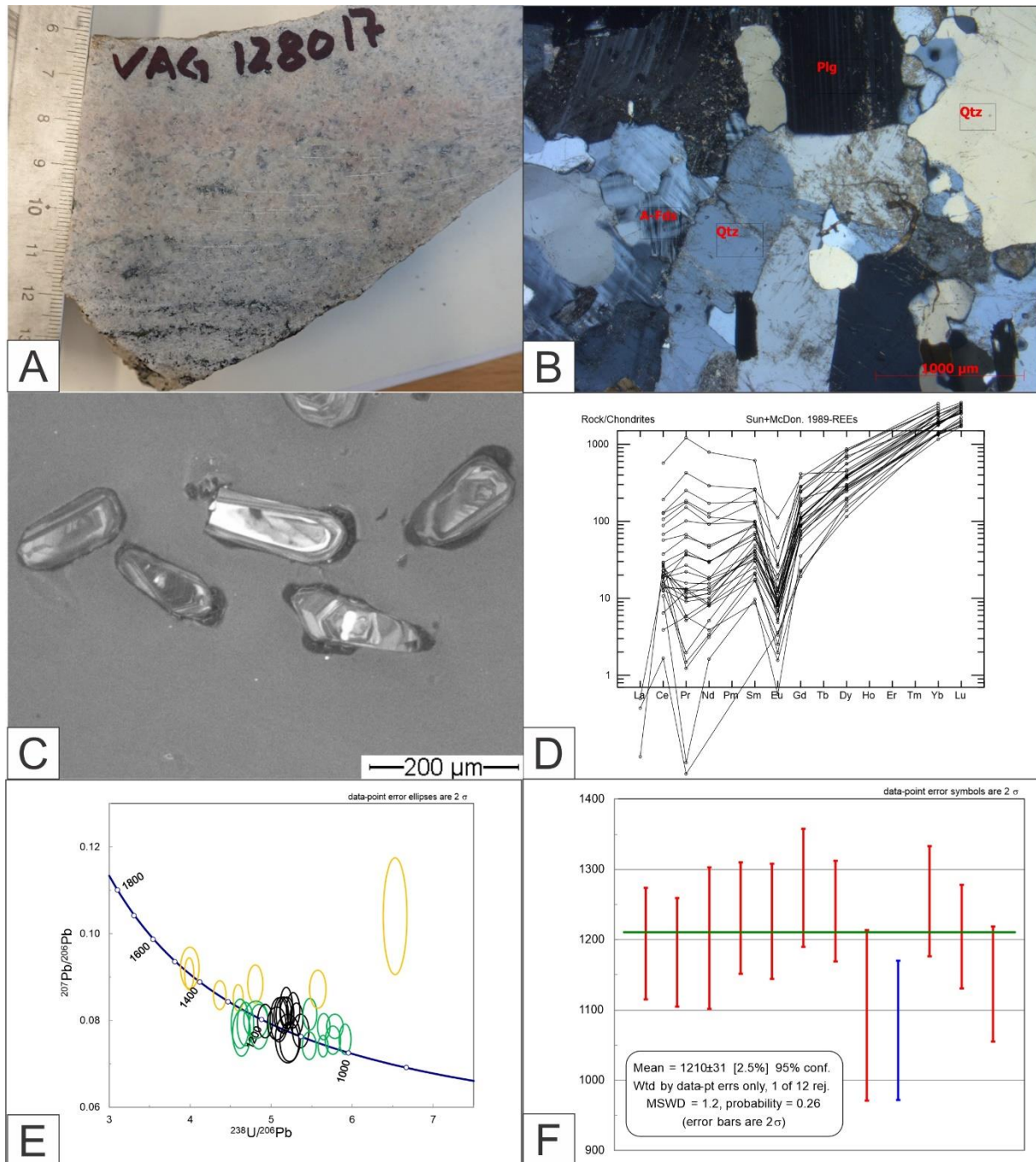


Figure 5.16: (A) Hand specimen of VAG 128017. (B) XPL-image of VAG 128017. (C) Magmatic zircons from VAG 128017. (D) Spider diagram of trace elements from VAG 128017. (E) Terra-Wasserburg plot of the U-Pb geochronology, the yellow circles indicate with  $^{207}\text{Pb}/^{206}\text{Pb} > 0.085$ , green circles are outliers, while black circles are data-points used in the weighted average. (F)  $^{207}\text{Pb}/^{206}\text{Pb}$  weighted average yielding a age of 1210 Ma

## 5 Results

### VAG 128019

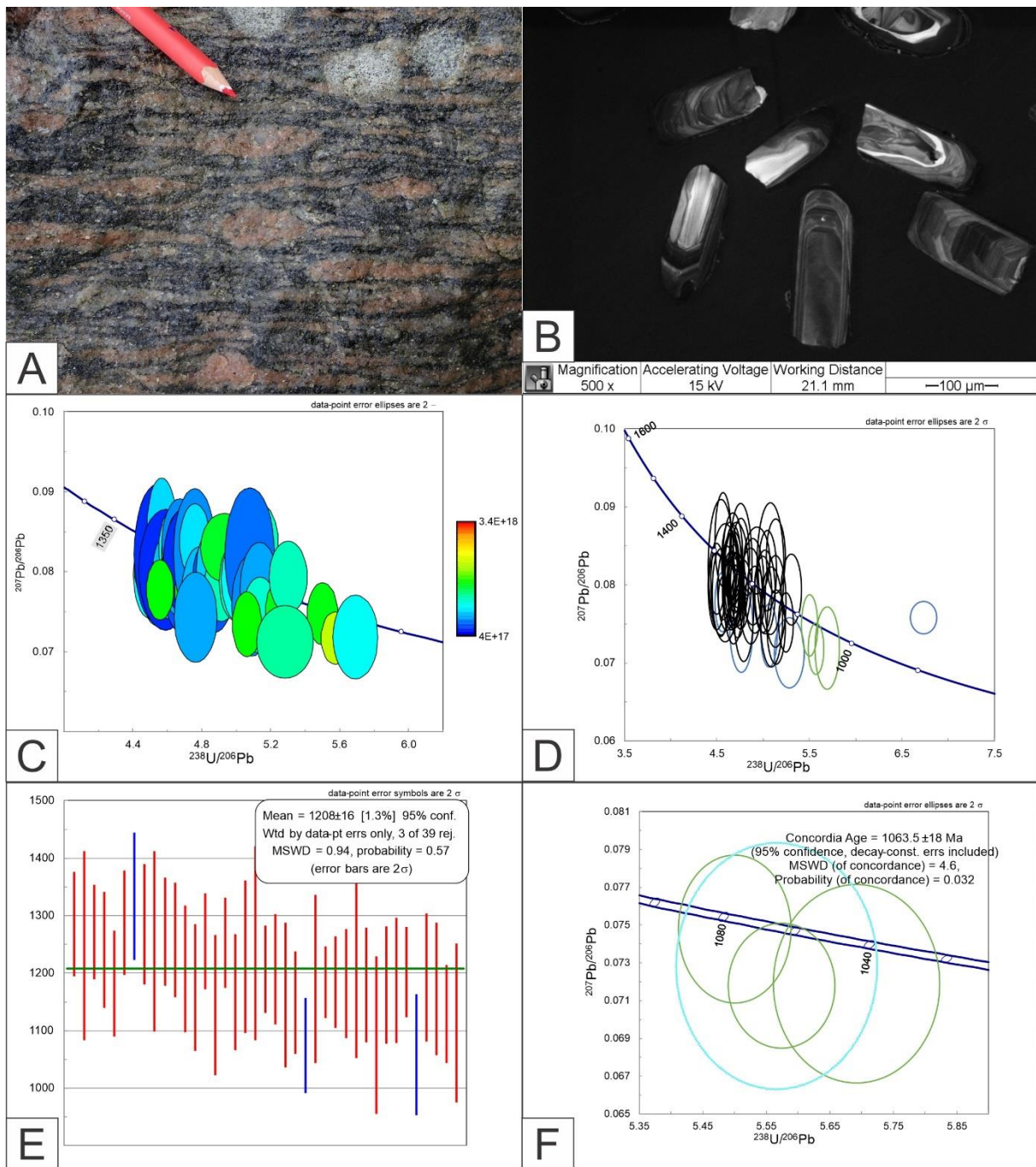


Figure 5.17: (A) Image of flaser gneiss taken on the other side of Røyrfjellsvatnet lake. (B) CL-imaging of magmatic zircons. (C) Terra-Wasserburg plot with each data point coloured after its alpha-dose. With alpha-dose increasing with increasing  $^{238}\text{U}/^{206}\text{Pb}$ . (D) Terra-Wasserburg plot. population 2 in green. While blue circles indicate discordant data points (E)  $^{207}\text{Pb}/^{206}\text{Pb}$  weighted average of remaining data points gives a mean age at  $1208 \pm 16$  Ma. (F) A calculated Concordia age of population 2 yields an age of  $1063 \pm 18$  Ma.

### 5.3.3 Deformed granites

Three VAG-samples and two HAL-samples underwent LA-SS-ICP-MS at Curtin University. A description of the unit can be found in 5.1.4. The term “deformed” is used to separate it from the undeformed granites.

#### VAG 128011

(32N 415410E 6447899N)

Megacrystic foliated granite sampled by Fv303 along Marna river close to Øyslebø. The sample area is dominated by undeformed granitic intrusions with xenoliths possibly host rocks of migmatite and deformed granite; the sample is from the latter. Large alkali-feldspar crystals with and interstitial amphibolite and biotite. Perthite and carlsbad is common in the feldspar. The mineral assemblage consists of alkali-feldspar (80%), quartz (15%), plagioclase (5%) amphibole (1%), and biotite, zircon, apatite and muscovite as accessory minerals. The muscovite is associated with amphibole.

The zircons show two different populations. One that is round brown up to 200 µm, and one that's brownish to colourless up to 100 µm. Both populations show zoning in CL, often with a light rim that is too thin to be measured that could originate from deformation.

Thirty data points were captured: seven rejected for being discordant and seventeen rejected because of common Pb loss. That leaves 4 data point left at Concordia with a Concordia age at  $1078 \pm 14$  Ma (MSWD = 1.12, P = 0.29).

The age is interpreted to come from crystallisation of the protolith granite.

#### VAG 084362

(32N 414489E 6440759N)

Previously described as “granitic gneiss” sampled within deformed granite between location 35 and 36. These locations consist of deformed granites with 1-3 cm prismatic Fds and a Bt-rich matrix. It's cut by a fine- to medium-grained biotite-rich granite. Phenocrysts appear as fine-grained aggregates of plagioclase and recrystallised quartz. Small scale folding is characterised by medium-grained aggregates of amphibole. In between, there are bands of fine-grained amphibole and biotite. Mineral assemblage is quartz (40%), plagioclase (35%), amphibole (20%), biotite (5%), and apatite, zircon and opaque as accessory minerals.

The zircons are colourless, prismatic, and >100 µm. CL imaging shows Oscillatory zoning indicating magmatic origin.

Results from LA-SS-ICP-MS gives uncertainty. High amount of discordance makes it difficult to find a weighted average. Since the discordant measurement is grouped together

and not along any line, a Concordia line is not a good explanation. The most likely reason for this is some event resulting in an increase in  $^{207}\text{Pb}/^{206}\text{Pb}$ , possibly loss in common Pb. Out of twenty-five data points, fourteen are removed due to high LREE, differentiated by  $\text{Pr}/\text{chondrites}$ (Sun and McDonough, 1989) = 10. Additional five outliers are removed to get a Concordia age at  $1050 \pm 6$  Ma (MSWD = 5.6, P = 0.018) which is believed to be the best estimate. This age is further supported by similar estimates from other samples (i.e., HAL 193061). It is worth noting that the uncertainty given is most likely lower than the real uncertainty.

The interpretation is that  $1050 \pm 6$  Ma reflects the age of protolith crystallisation.

*HAL 193061*

32N 414826E 6440679N

A deformed porphyritic granite found at location 37 cut by fine-grained 1-5 cm thick granitic veins. Phenocrysts are highly deformed and recrystallised along shear direction creating new veins and possibly migmatization. The Mineral assemblage consists of alkali-feldspar (70%), quartz (10%) amphibolite (10%), plagioclase (5%), biotite (5%), and apatite, sericite, and zircon as accessory minerals.

The zircons are colourless to brownish, 100-200  $\mu\text{m}$  rectangular. CL-imaging shows magmatic oscillatory zoning.

Twenty data points were measured with LA-SS-ICP-MS. Of these, three discordant points (discordance > 10) were rejected. The remaining seventeen data points gives a  $^{207}\text{Pb}/^{206}\text{Pb}$  weighted average at  $1038 \pm 28$  (MSWD = 1.3, P = 0.16).

The interpretation is that  $1038 \pm 28$  reflects crystallization age.

*HAL 193063*

32N 414918E 6442172N

Deformed porphyritic granite found at location 111. The rock is cut by 1-2 cm fine-grained leucocratic veins that follows deformation. Larger 60-70 cm undeformed granitic intrusions are found on the other side of a small creek meters away.

The zircons are colourless, prismatic, 100-200  $\mu\text{m}$ . CL-imaging shows magmatic oscillatory zoning.

Thirty-four data points were collected by LA-SS-ICP-MS, of these nine discordant results where rejected. The remaining twenty-five data points gives a  $^{207}\text{Pb}/^{206}\text{Pb}$  weighted average of  $1025 \pm 20$  Ma (MSWD = 1.12, P = 0.31).

The interpenetration is that  $1025 \pm 20$  Ma reflects granitic crystallisation.

VAG 128010  
32N 415158E 6447684N

Foliated porphyritic Bt granite sampled along Fv303 along Marna river close to Øyslebø. The sample area is dominated by undeformed granitic intrusions with xenoliths possibly host rocks of migmatite and deformed granite; the sample is from the latter. The sample is weakly foliated with phenocrysts of microcline. Both metamorphic and magmatic textures is seen in the thin section. The mineral assemblage is alkali-feldspar (60%), quartz (30%), plagioclase (5%), biotite (5%), and zircon, opaque grains, and apatite as accessory minerals.

The zircons are colourless to brownish, rectangular, variant in size from 50  $\mu\text{m}$  to 250  $\mu\text{m}$ . CL-imaging magmatic zoning.

Twenty-one data points were gathered with LA-SS-ICP-MS; most of these were discordant and rejected. Of the four concordant (discordance < 10), one outlier where rejected while the three remaining gave a  $^{207}\text{Pb}/^{206}\text{Pb}$  weighted average of  $1066 \pm 67$  Ma (MSWD = 1.3, P = 0.27). This age is similar to other porphyritic granites in the field area.

The interpretation is that  $1066 \pm 67$  Ma reflect crystallization age.

## VAG 128011

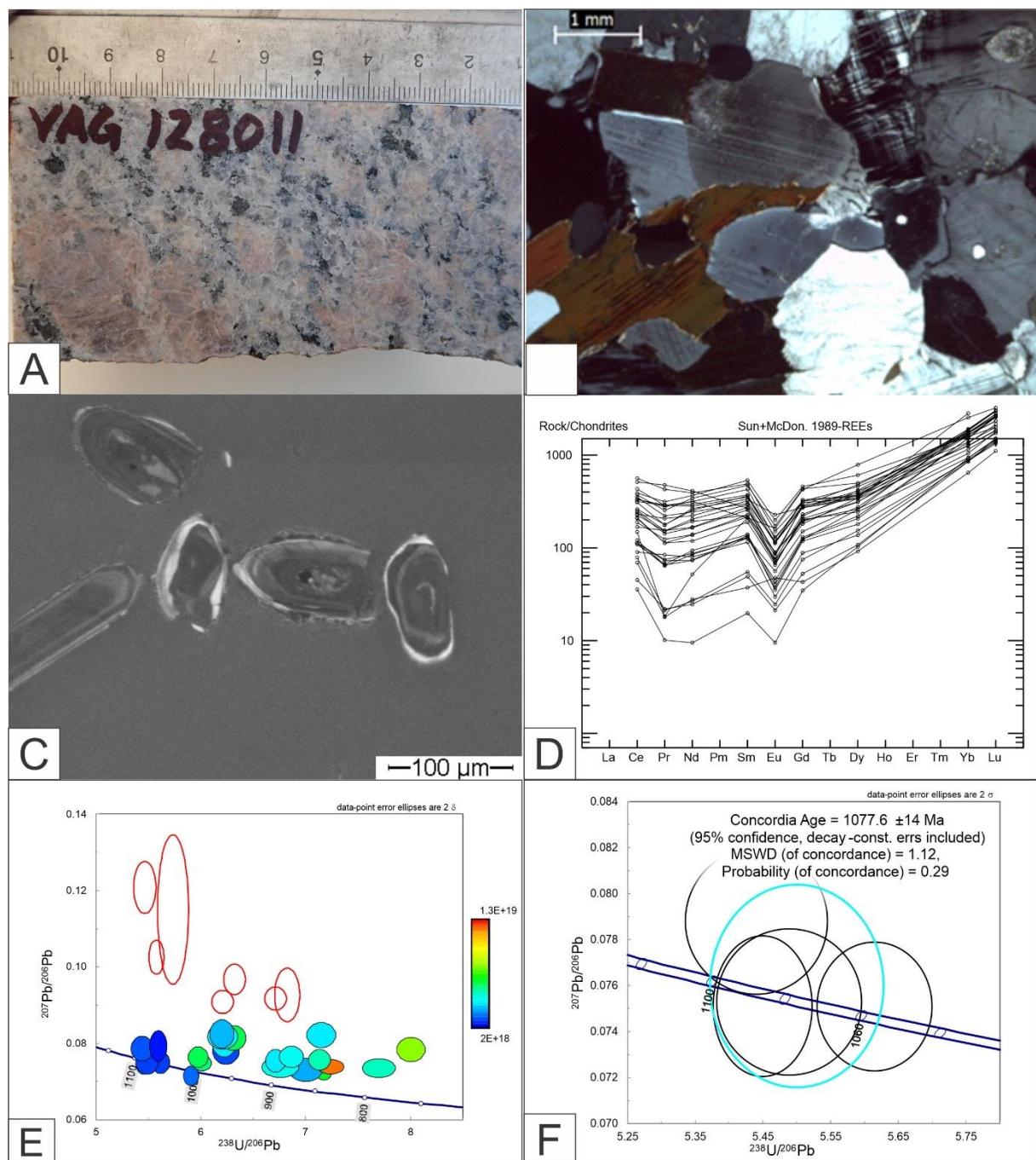


Figure 5.18: (A) Hand specimen of VAG 128011. (B) XPL image taken of VAG 128011 with the amphibole forming a melt texture. Also, in the middle of the image, there is a myrmekite. Both clear examples for magmatic features. (C) CL-imaging of magmatic zircon. (D) Spider diagram of trace elements. (E) Terra-Wasserburg plot colour-coded after common lead, the trend indicates lead loss. The red circles are discordant samples with a high  $^{204}\text{Pb}$ -value. (F) Concordia age at 1078 Ma of the remaining four samples.

## 5 Results

### VAG 084362

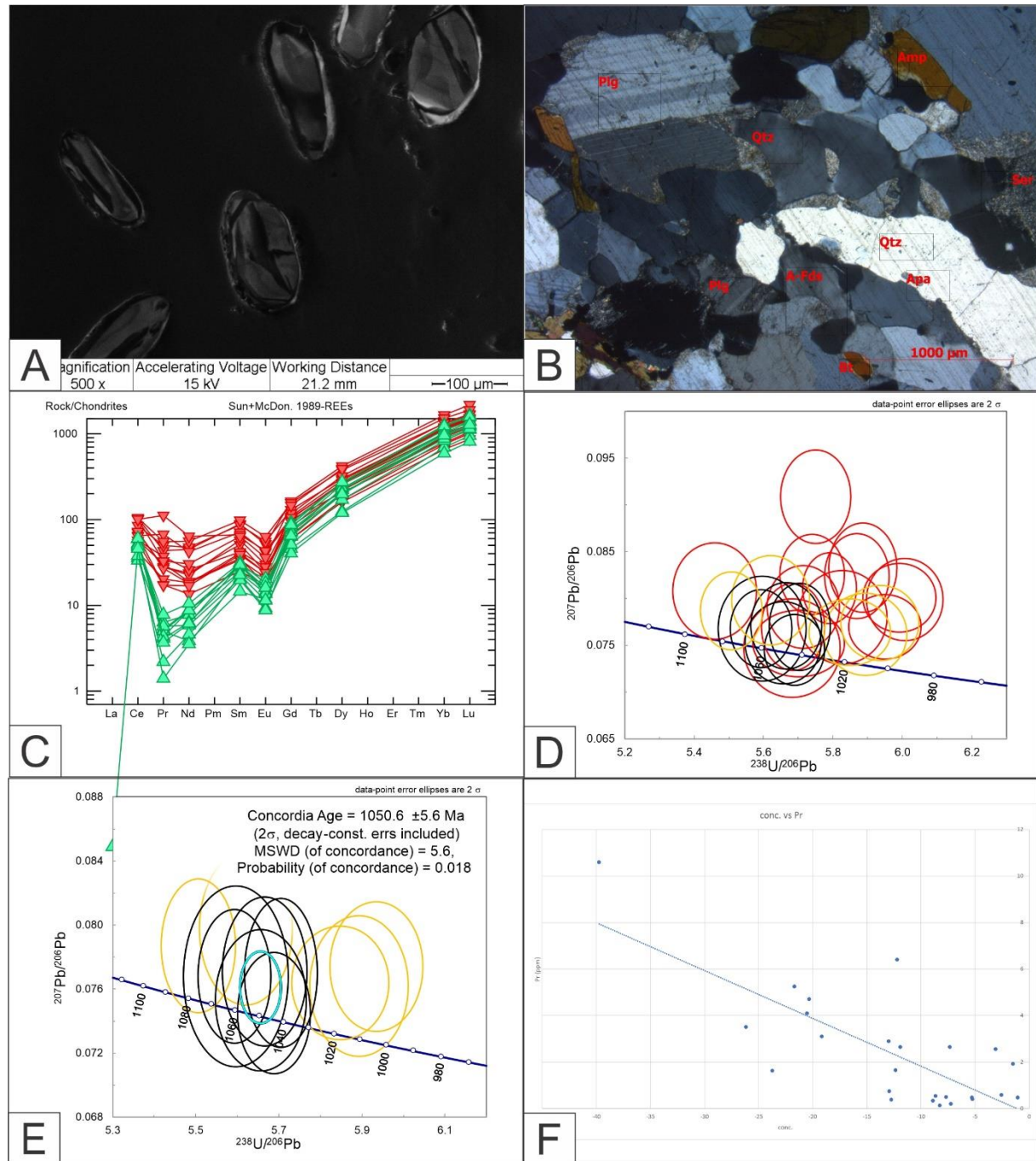


Figure 5.19: Images associated with VAG 084362. (A) CL-imaging of zircons. (B) XPL-Image of VAG084362. (C) Spider diagram over trace elements in the zircon. Green lines are for low LREE data points, while red line is for high LREE data points. The difference is set to  $\text{Pr/Chondrite} = 10$ . (D) Terra-Wasserburg plot. High LREE samples are in red, while outliers are marked in yellow. Black circles represents data point used in the final calculation (E) Concordia plotted against Pr (ppm). With an increase in negative discordance, follows an increase in Pr ppm.

HAL 193061

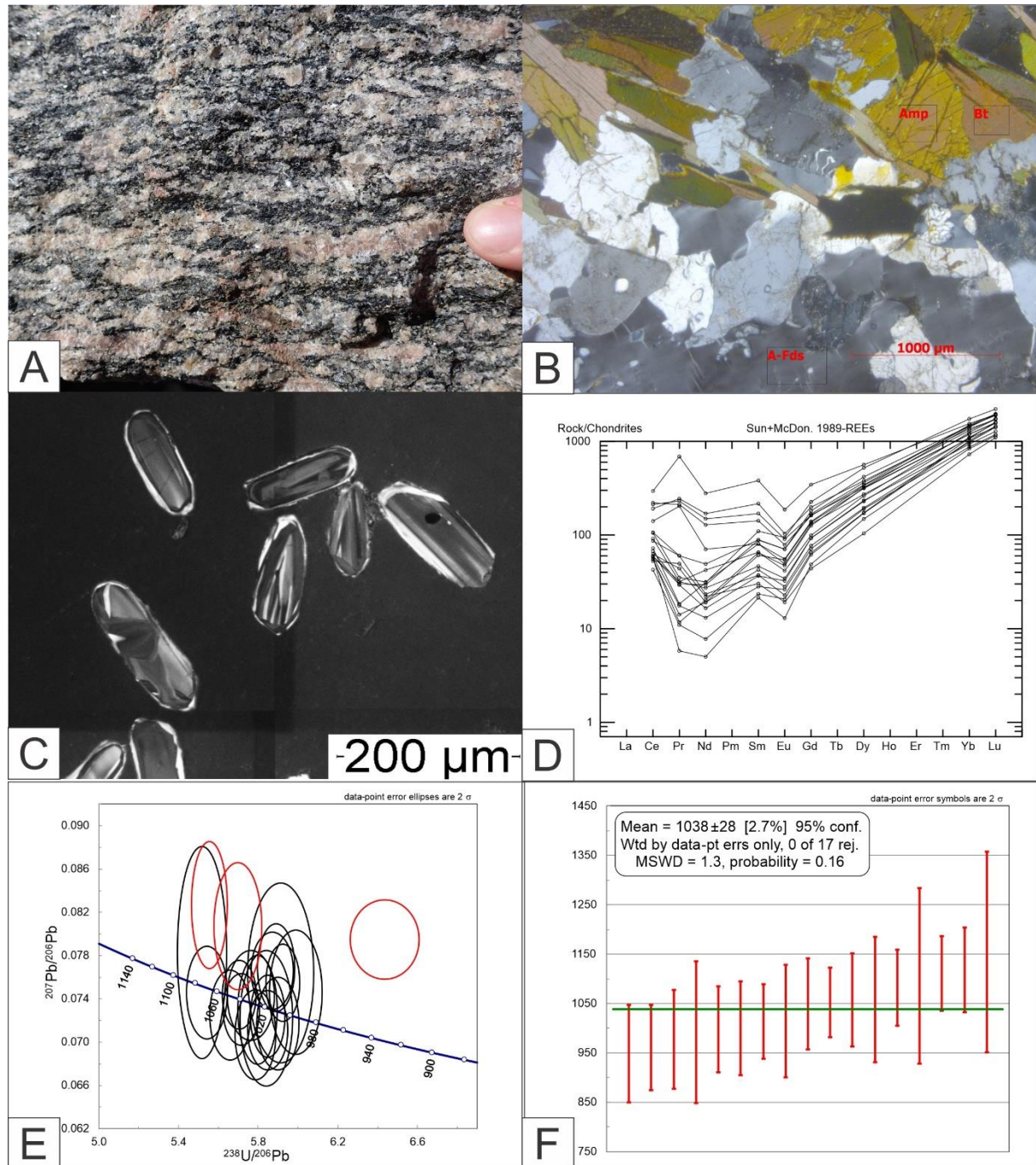


Figure 5.20: (A) Image taken from location 37, the same location as were HAL 193061 is taken from. (B) XPL-image of HAL193061. (C) CL-images of magmatic oscillatory zoned zircons. (D) Spider diagram of trace elements in the zircons. (E) Terr-Wasserburg plot, the three rejected discordant data points are marked in red. (F)  $^{207}\text{Pb}/^{206}\text{Pb}$  weighted average of the remaining 17 data point; giving an age at 1038 Ma

## HAL 193063

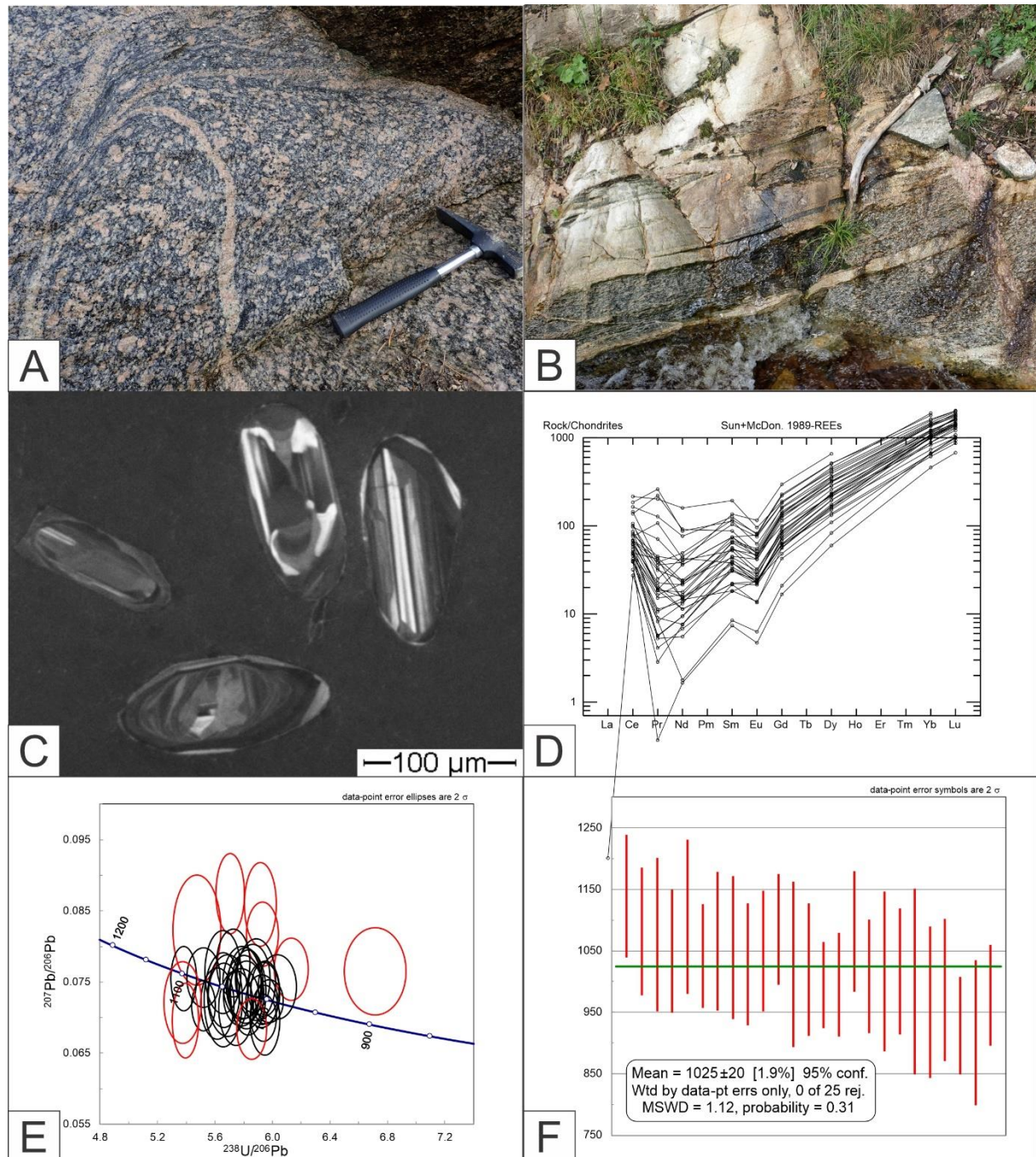


Figure 5.21: (A) Image taken at the same location as HAL 193063. Large phenocrystic aggregates with a melanocratic matrix. (C) CL-image of oscillatory zoned magmatic zircons. (D) Spider diagram of trace elements shows now clear variations among the zircons. (E) Terra-Wasserburg plot of the data points from HAL 193063. The red circles are discordant data that were rejected. (F)  $^{207}\text{Pb}/^{206}\text{Pb}$  weighted average gives an age at 1025 Ma.

VAG 128010

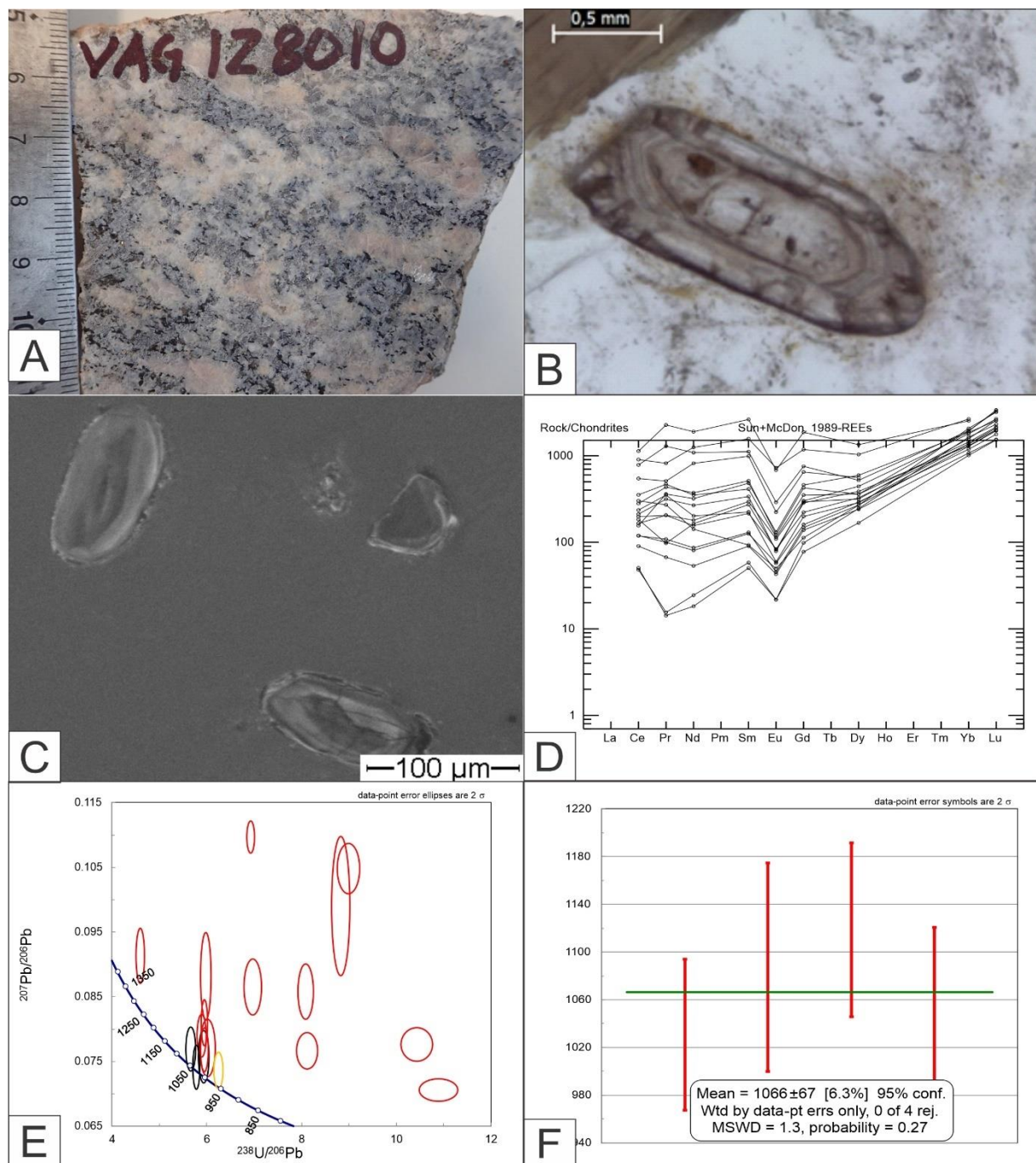


Figure 5.22: (A) Hand specimen of VAG 128010 showing large alkali-feldspar phenocrysts and a disperse mesocratic groundmass. (B) Image of a zircon in ppl. The zoning is clear even without CL. (C) CL-image of the grains used. (D) Spider diagram of the trace elements, no clear diffraction were found. (E) Terra-Wasserburg plot of the data point. Red circles represents data points that were rejected due to high discordance; yellow circle indicates outliers. (F)  $^{207}\text{Pb}/^{206}\text{Pb}$  average mean of the four remaining data points gives a age at 1066 Ma.

#### 5.2.4 Magmatic intrusions

*HAL 193052 (Amphibolite)*

32N 422818E 6448003N

Found on location 10 on the south side of Røyrvatnet. A 20-meter-wide amphibolite body found within flaser gneiss. Change in grain size from fine to medium towards the middle is interpreted to be a chilled margin in an intrusive mafic body. Accessory retrograde titanite is associated with amphibole. The mineral assemblage is amphibole(55%), plagioclase (45%), and titanite, quartz, biotite, zircon, apatite, opaque grains and alkali-feldspars as accessory minerals.

The zircons are  $<100\text{ }\mu\text{m}$ , rectangular with a brownish colour. CL-imaging shows weak zoning in all but one grain, it is uncertain if the grains are from the protolith or later metamorphic events.

Five data points were taken, two rejected due to high LREE. The three remaining points give a Concordia-age at  $968 \pm 14\text{ Ma}$  ( $\text{MSWD} = 0.64$ ,  $P = 0.43$ ). The two rejected data points are both concordant, and a higher sampling collection could reveal these to reflect real events. Afterall both are similar or close to other ages found in the area. Calculated Concordia-age of these are:  $1183 \pm 17\text{ Ma}$  and  $1032 \pm 8\text{ Ma}$ .

The interpretation is that  $968 \pm 14$  reflects crystallisation of a mafic intrusion while the  $1183 \pm 17\text{ Ma}$  and  $1032 \pm 8\text{ Ma}$  possibly are relict zircons from other units. Since there are only one data point of each of the outliers, the uncertainty is likely higher than calculated.

*HAL 193066 (undeformed granite)*

32N 414667E 6441936N

Undeformed granite cutting deformed granite like that of HAL 193063. Pegmatites cutting the deformed granite has grain size gradient relationship with the undeformed granite suggesting it as a source. The undeformed granite is fine-grained with pockets of coarser material. The thin section shows that there are metamorphic textures present such as bulging, seritization, and granoblastic textures, and a slight preferred orientation. The mineral assemblage is alkali-feldspar (45%), quartz (33%), plagioclase (20%), biotite (green and brown) (2%), and apatite, and zircon as accessory minerals.

The zircons are colourless,  $<150\text{ }\mu\text{m}$ , rounded rectangular and with a clear magmatic zonation in CL.

## 5 Results

---

Nine data points were gathered with LA-SS-ICP-MS, four discordant results where rejected. Four of the five remaining data points together gives a Concordia-age at  $945 \pm 14$  Ma (MSWD = 0.18, P = 0.67). One lonely concordant outlier gives a Concordia-age of  $1084 \pm 15$  Ma.

The interpenetration is that  $945 \pm 14$  Ma reflects the crystallisation age of the undeformed granite while  $1084 \pm 15$  Ma might reflect relict zircons of the deformed granite. The fact that there is only one data point of this outlier may suggest that the uncertainty is higher than calculated.

## HAL 193052

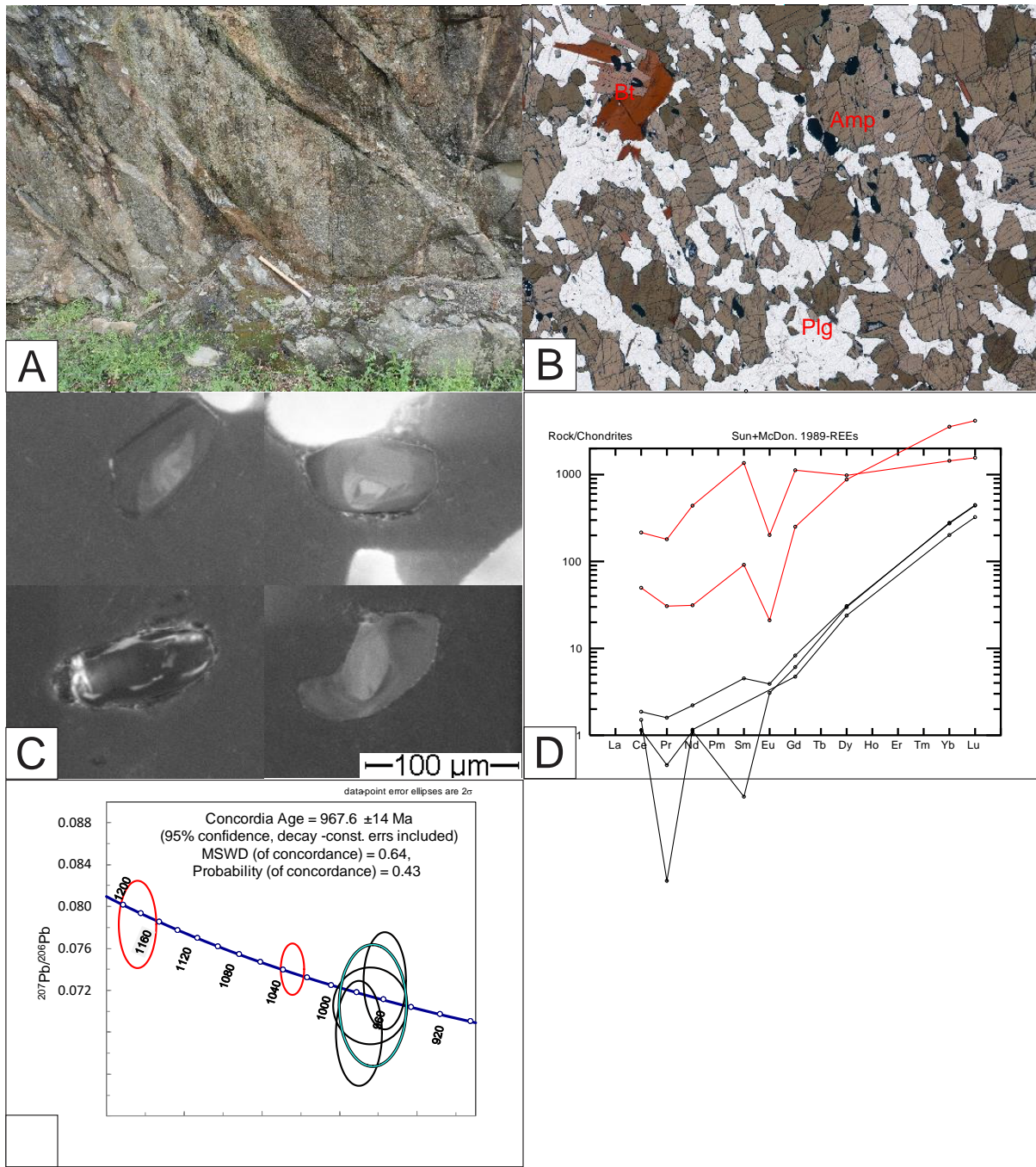


Figure 5.23: (A) image from the samples locality. (B) PPL-scan of HAL193052. (C) CL-image of the zircons, three examples of weak zoning, and one example of one grain lacking zoning. (D) Spider diagram of trace elements, the two red lines are the data points rejected for HIGH REE. (E) Terra-Wasserburg plot with calculated Concordia age at 968 Ma highlighted in light blue. The two red circles represents the high REE data points.

## HAL 193066

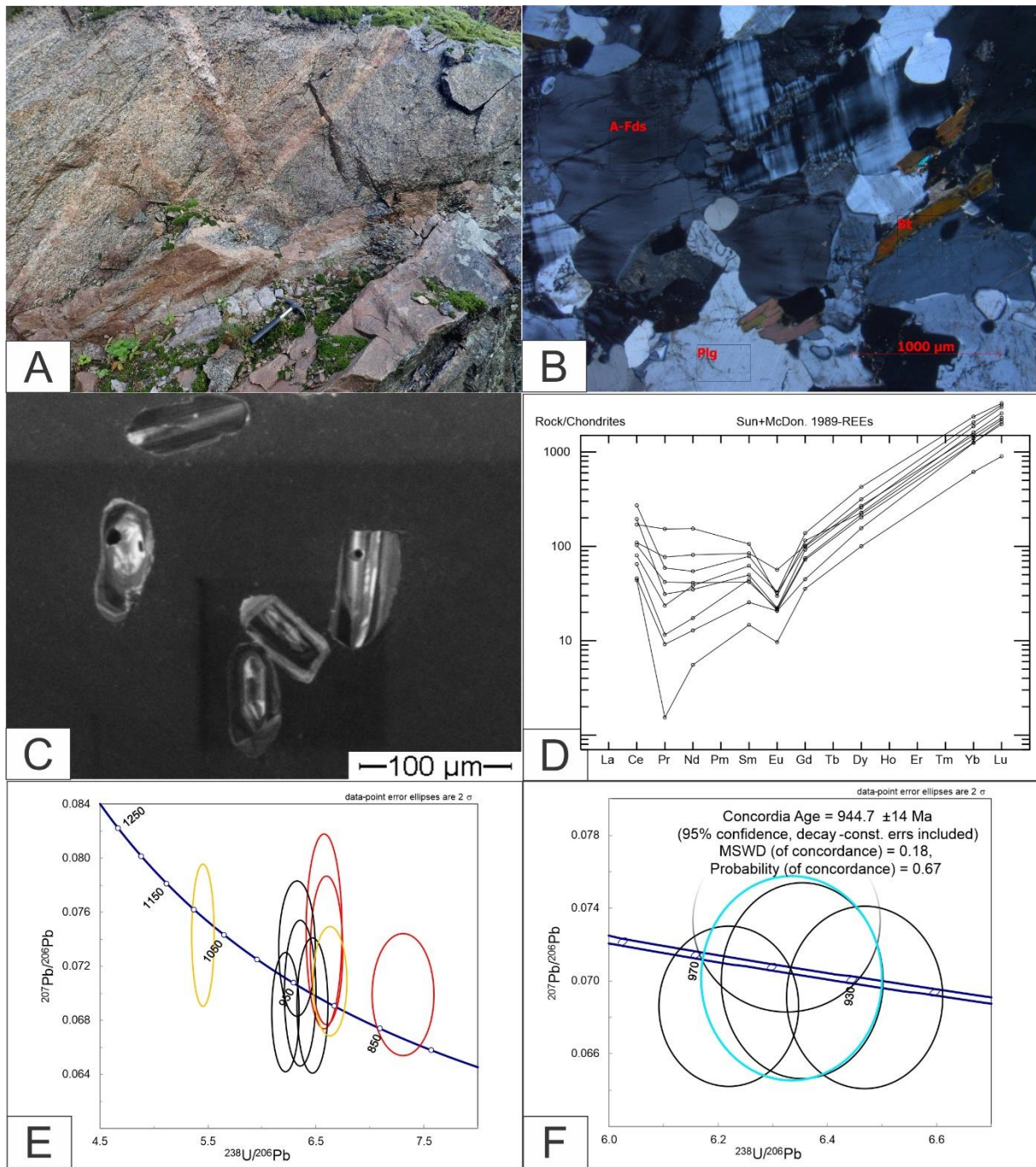


Figure 5.24: (A) Image taken at location of an undeformed granite cutting a deformed granite. (B) XPL-image of HAL193066. CL-image of the sample showing a clear magmatic zonation. (D) Spider diagram of trace elements from the sample. (E)Terra-Wasserburg with discordant data points in red and outliers in yellow; data points used in the calculation is in black. (F) Close up of the Terra-Wasserburg with Concordia age calculation shown in light blue. Age calculated to 945 Ma.

#### 5.4 Lu-Hf data

All samples that underwent LA-SS-ICP-MS underwent Lu-Hf measurements; i.e. all samples described in 5.3 except for HAL 193073, and HAL 193062. Also, HAL 193056, VAG 128012, and VAG 128015 got good Lu-Hf results, since they did not get any clear results from U-Pb geochronology they are given an best-estimated age; i.e. 1050 Ma for VAG 128012 and VAG 128015, and 950 Ma for HAL 193056. All Lu-Hf data can be found in appendix E.

The samples from this study falls along a  $^{176}\text{Lu}/^{177}\text{Hf} = 0.015$  that starts at 1.75 Ga. This is interpreted as the age of creation of the continental crust. HAL 193053 plots above the line, it is uncertain that if these zircons represents the protolith age or a metamorphic age; this could be the reason for the anomaly. Also, the mafic content could mean that the anomaly represent a influx of juvenile mantle.

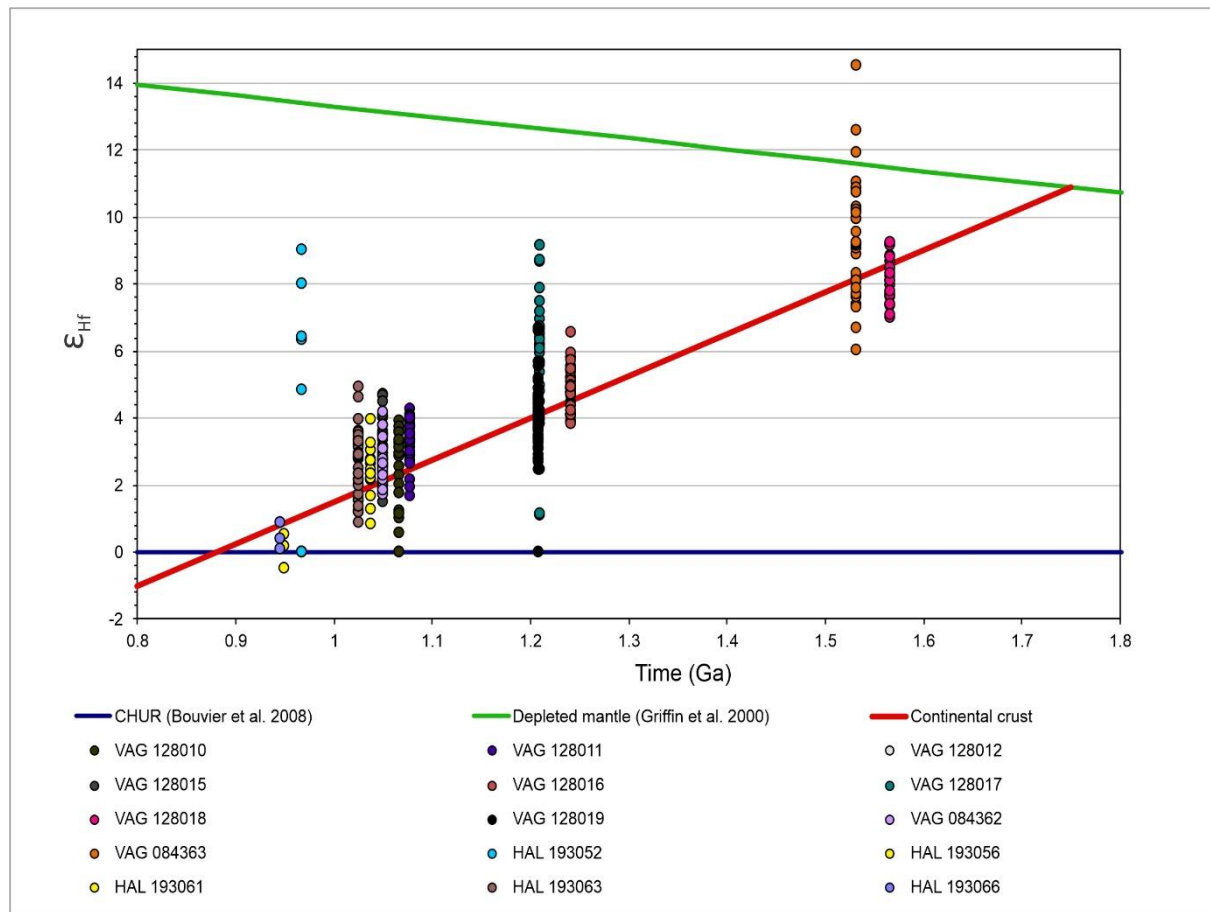


Figure 5.25:  $\epsilon_{\text{Hf}}$  vs time in Ga. A trend is calculated from 1.75 Ga with  $^{176}\text{Lu}/^{177}\text{Hf} = 0.015$ . The depleted mantle is calculated by Griffin et al. (2000), and the CHUR by Bouvier et al. (2008).

## 6 Discussion

The aim is to determine age of local metamorphism/magmatism structural evolutions related to regional geology.

### 6.1 The Gothian-Telemarkian orogenic evolution

#### 6.1.1 Gothian age rocks in the Telemark lithotectonic unit

The Gothian-Telemarkian orogen refers to a long period of build-up along the southwestern reach of Fennoscandia from 1.66 to 1.48 Ga. The separation of Gothia and Telemarkia into two separate orogens is probably obsolete, as new data appears to suggest a continuous orogenic evolution; however, Gothia (1.66-1.52 Ga) and Telemarkia (1.52-1.48 Ga) is still in use since rocks of Gothian age is thought to be spatially constrained to the Bamble-Kongsberg- and Idefjord- lithotectonic units (Roberts and Slagstad, 2014). Between the last Gothian-Telemarkian orogen and the Sveconorwegian orogen, Gothian-Telemarkia split-up into three separate lithotectonic units, i.e. Telemark, Bamble-Kongsberg, and Idefjord. The three lithotectonic units collided during early phases of the Sveconorwegian orogeny (Slagstad et al., in prep.). Since the field area lies within the Telemark lithotectonic unit, there should not be any rocks that yield an older age than 1.52 Ga. Telemark lithotectonic unit is geographically constrained with Caledonian rocks to the north-northwest, and the Bamble-Kongsberg tectonic wedge and Oslo rift to the east. It is referred to as Telemarkian domain in Roberts and Slagstad (2014), and Telemarkia terrane in Bingen et al. (2008c), Bingen et al. (2005a), while it consists of the Hardangervidda-Rogaland, and Telemark blocks of Andersen (2005). The current age definition of Telemarkia lithotectonic units is constrained by Roberts et al. (2013), Bingen et al. (2008c) to 1485-1521 Ma. In Evje, Setesdal, U-Pb geochronology measurements of a metatonalite yields an age at  $1555 \pm 29$  Ma (Pedersen et al., 2009) 34 million years older than the current age constraint of Telemark lithotectonic unit; this age, however, is poorly constraint with a small data point selection and a large uncertainty (Pedersen et al., 2009).

The disperse migmatite is the oldest rock found in the area based on field relations; its mesosome is fairly homogenous fine- to medium-grained, equigranular with a few rare porphyritic layers. Horizontal magnet gradient mapping (NGU-COOP-project, 2017) of the disperse migmatite shows a folding event that does not affect any of the other units. It also reveals that the disperse migmatites may be divided into two or more layers. However, thin sections of samples collected inside and outside the fold does not show any major petrographic differences worth noting. However, based on three samples, two from outside

the fold (HAL 193062, and VAG 128018), and one from inside the fold (HAL 193072), there is a age difference of ca. 100 million years; noting that the HAL 193073 protolith age yields a large uncertainty at  $\pm 45$  Ma.

U-Pb geochronology of three samples of disperse migmatite yields to  $1566 \pm 7$  Ma,  $1565 \pm 11$  Ma and  $1532 \pm 38$ ; this is 44 million years older than the age constraint set by Roberts et al. (2013) and Bingen et al. (2005a). This gives a higher validity to the poorly constrained 10 million years younger 1555 Ma metatonalite in Evje (Pedersen et al., 2009). This questions the use of the Gothian- and Telemark domains as spatial dividers of 1.66-1.52 Ga and 1.52-1.48 Ga rocks. Gothian-Telemarkia should rather be viewed as one 180 million year-long orogen younging to the west with no clear divide. Gothia and Telemark can still be used when discussing different lithotectonic units involved in the break-up of the Gothian-Telemarkian orogen and the subsequent Sveconorwegian orogeny.

#### 6.1.2 The crustal evolution of the Telemark lithotectonic unit

Petersson et al. (2015a) uses U-Pb and Lu-Hf isotopes to map the evolution of growth in the eastern parts of the Sveconorwegian orogen (i.e. the Eastern Segment). The study shows that the Eastern Segment is formed by a 40-50% reworked Archean crust and 2.1-1.9 Ga juvenile mantle-derived magma. This corresponds with the onset of crust generation in proto-Svecofennia (Gaál and Gorbatshev, 1987, Nironen, 1997, Patchett et al., 1987). From 1.9 to 1.7 Ga Lu-Hf measurements (Andersen et al., 2009b, Andersson et al., 2011, Petersson et al., 2015a) shows a increase in the juvenile component; Petersson et al. (2015a) estimates that it increases from 50% at 1.9 Ga to 60-65% at 1.7 Ga.; after 1.7 Ga, there is no evidence of an Archean contributing as a source of new melt. From 1.7 Ga and onwards, Petersson et al. (2015a) estimates that the Eastern Segment rocks follows a  $^{176}\text{Lu}/^{177}\text{Hf} = 0.018$  vector. This fits with a model of steady-state with no new juvenile input (see figure 6.1).

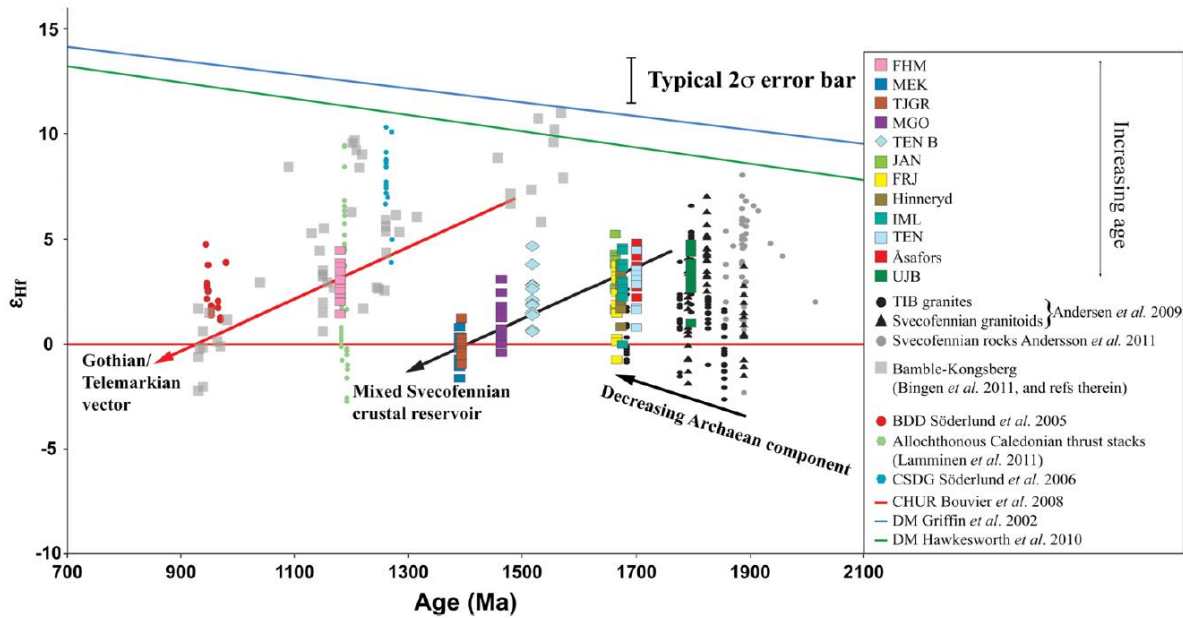


Figure 6.1: Figure from Petersson et al. (2015a) that shows the crustal evolution from 1.9 to 0.9 within the Sveconorwegian domain. From 2.1 to 1.9 Ga crustal growth is based on increasing amount of juvenile input; crustal rocks in the Eastern Segment from 1.7 to 1.4 Ga follows a vector  $^{176}\text{Lu}/^{177}\text{Hf} = 0.018$  that is broadly equivalent to felsic continental crust (Hawkesworth et al., 2010, Rudnick and Gao, 2003). Coevally, crustal rocks in Gothia-Telemarkia follows a vector ( $^{176}\text{Lu}/^{177}\text{Hf} = 0.015$ ) that is approximately  $\epsilon_{\text{Hf}} = 5$  above the ones in the Eastern Segment (Bingen et al., 2011). CHUR is calculated by Bouvier et al. (2008), and the depleted mantle is calculated by Griffin et al. (2002), Hawkesworth et al. (2010). Samples are from Andersen et al. (2009b), Andersson et al. (2011), Bingen et al. (2011), Lamminen (2011), Petersson et al. (2015a), Söderlund and Ask (2006)

Bingen et al. (2011) presents a  $^{176}\text{Lu}/^{177}\text{Hf}$  vector for Gothia-Telemarkia (see figure 6.1) based on samples from Telemarkia, Bamble-Kongsberg, and Svecofennian dolerites. The Gothian-Telemarkian vector follows a  $^{176}\text{Lu}/^{177}\text{Hf} = 0.015$  with a juvenile signature offset at around  $\epsilon_{\text{Hf}} = 5$  above the mixed Svecofennian reservoir. At 1.2 Ga, Petersson et al. (2015a) discusses a possible new juvenile input based on the FHM sample that plots at ca. 1-5  $\epsilon_{\text{Hf}}$  (see figure 6.1), well above the assumed evolution. Here we suspect there has been a miscalculation; the values given for FHM in the supplementary appendix to Petersson et al. (2015a), actually plots well below the assumed evolution, at  $\epsilon_{\text{Hf}} (-6 \text{ to } -10)$ . Due to the uncertainty, we don't put much emphasis on FHM. Further west, in Sauda-Suldal, Roberts et al. (2013) shows that rocks yielded between 1521 and 1485 Ma is a result of mixing of juvenile mantle, a young low-temperature altered material, and older low-temperature altered material. The studies mentioned above indicate a trend of juvenile influx followed by a steady crustal environment; their age and spatial relations is compatible with an westward migrating orogen.

Mafic magmatism in Telemarkia (Slagstad et al., 2018) may have given a juvenile component to the granitic melts in the Sirdal Magmatic Belt (SMB); Granseth et al. (2019) calculates that

the proportion bay be as much as 50% and it still would not impact the  $\epsilon_{\text{Nd}}$  within uncertainties; in theory, this will be similar for  $\epsilon_{\text{Hf}}$ .

The vector found in this study is similar to that found by Bingen et al. (2011). It has a  $^{176}\text{Lu} / ^{177}\text{Hf} = 0.015$ , and intercepts the depleted mantle line calculated by Griffin et al. (2000) at 1.75 Ga. This reflects that the magmatism seen in the field area is due to crustal recycling. The presence of mafic intrusions in the flaser-gneiss unit indicates that there might be some juvenile input around 1200 Ma; such a trend is not seen in our  $\epsilon_{\text{Hf}}$ -values.

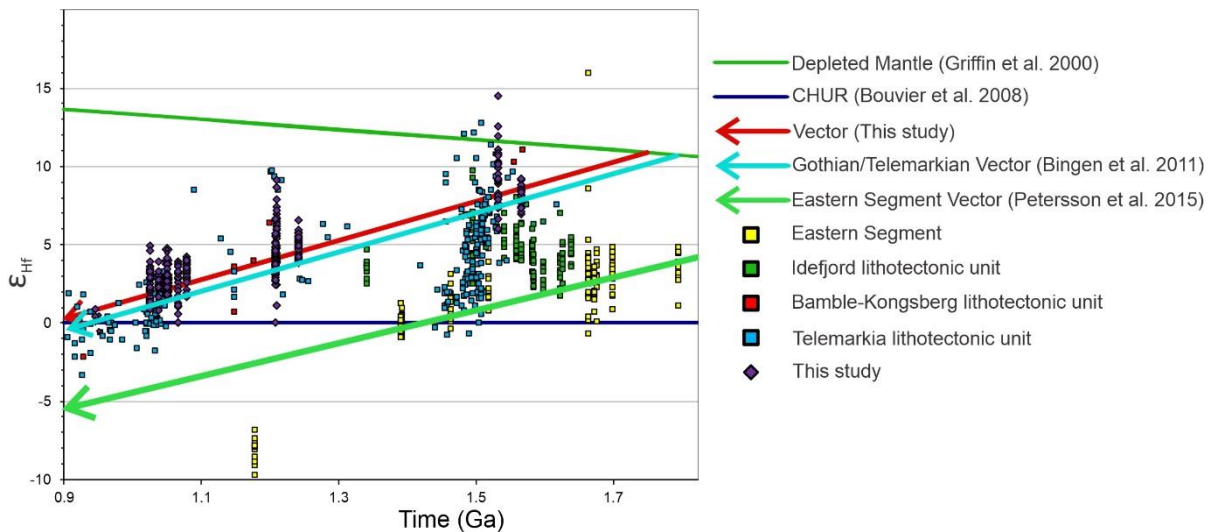


*Figure 6.2: Illustration of the vector found in this study with that of Bingen et al. (2011) and Petersson et al. (2015a). Samples collected from other studies is marked with a square colour-coded after the lithotectonic unit it belongs to; the Eastern Segment (Petersson et al., 2015a) in yellow, Idefjord (Andersen et al., 2002, Petersson et al., 2015b) in green, Bamble-Kongsberg (Andersen et al., 2004, Andersen et al., 2002) in red, Telemarkia (Andersen et al., 2009b, Andersen and Griffin, 2004, Andersen et al., 2002, Andersen et al., 2007, Roberts, 2010) in blue, and samples from this study in purple diamond. The Vector in this study follows a trend similar to the Gothian-Telemarkian vector described by Bingen et al. (2011). The depleted mantle is calculated by Griffin et al. (2000), and CHUR by Bouvier et al. (2008).*

## 6.2 Ca. 1200 Ma magmatism

The period between the end of the Gothia-Telemarkian orogen (1.48 Ga) and the onset of the Sveconorwegian orogen (1.14 Ga) is by many authors viewed as anrogenic, or at least tectonically quiet; they advocate for a back-arc or behind-arc setting related to a subduction margin west of present-day Norway (Roberts and Slagstad, 2014, Brewer et al., 2004).

Roberts and Slagstad (2014) suggests that the inboard events resulting in the Rapakivi suite (Åhäll et al., 2000) continued beyond 1.65 and migrated westwards, it may explain the evolution seen in southern Norway around this time. Between 1.34 and 1.10 Ga the Gothian-Telemarkian orogen experienced extensional rifting that likely resulted in the formation of the Idefjord-, Bamble-Kongsberg-, and Telemark lithotectonic units (Slagstad et al., 2017).

The two gneiss units in the eastern part of the field area has previously been linked to the Gjerstad suite in Telemark (Bingen and Van Breemen, 1998); a 1.19-1.12 Ga (Bingen and Van Breemen, 1998, Heaman and Smalley, 1994) pink hornblende  $\pm$  biotite augen gneiss. This study has mapped them as two different units in the field; one is a fairly homogenous augen-gneiss while the other is a heterogenous heavily folded flaser-gneiss that often can appear as augen-gneiss. U-Pb geochronology of these samples yields to  $1241 \pm 41$  Ma (VAG128016), and  $1210 \pm 31$  Ma (VAG128017) for the two augen gneisses; the samples are taken from the same location and similar rocks, they are believed to be of the same age. As mentioned in 5.3.2,  $1241 \pm 41$  Ma probably is older than true age; we interpret  $1210 \pm 31$  Ma to reflect the protolith age of the augen-gneiss. The flaser-gneiss yields an age of  $1208 \pm 16$  Ma (VAG128019); the closeness in age reflects that the two units are from the same event. It is still uncertain why the two units shows different degree of deformation, but it may suggest that the flaser gneiss unit was deep in the crust, relative to the augen-gneiss before the Sveconorwegian orogeny. Passchier and Trouw (2005) suggests that the flaser texture of quartzofeldspathic aggregates reflects high-grade temperature ( $<600^\circ\text{C}$ ) conditions, while the augen gneiss texture reflects low- to medium-grade temperatures.

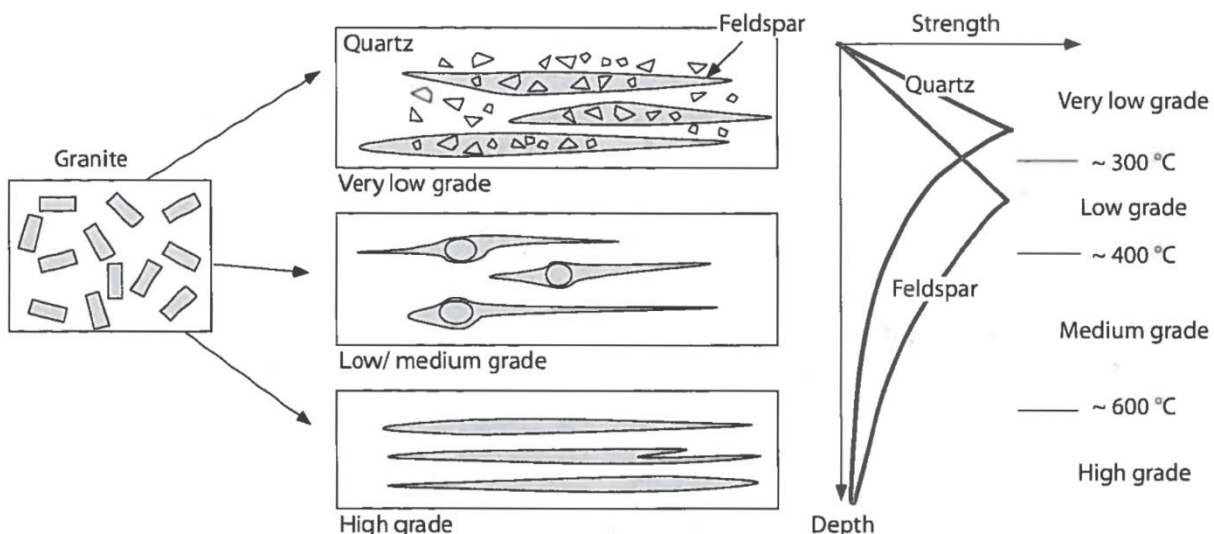


*Figure 6.3: Sketch indicating how temperature quartzofeldspathic phenocrysts and aggregates taken from Passchier and Trouw (2005). At very-low grade, feldspar is weaker than quartz (Chester and Logan, 1987, Evans, 1988), possibly due to cleavage in feldspar; parts of the feldspar (especially potassium-feldspar) will be elongate and may recrystallise into kaolinite or sericite. At low/medium grade quartz becomes ductile, while feldspar stays brittle; this often result in a core/rim texture where feldspar in the core shows brittle deformation, while quartz in the rim shows ductile deformation. At high grade, quartz and feldspar shows dislocation creeps, and have similar strength.*

### 6.3 SMB in the field area

The SMB-rocks is referred to as Deformed granite in the results-chapter.

#### 6.3.1 1070-1010 Ma Magmatism

1070 to 1010 Ma magmatism emplaced a voluminous 50 km wide granitic belt that peaked between 1050 and 1030 Ma, coined by Slagstad et al. (2013a) as the Sirdal Magmatic Belt (SMB). Slagstad et al. (2013a) speculates that SMB is due to basaltic underplating; high-aluminium megacrystic orthopyroxenes from the nearby Rogaland Igneous Complex are estimated to have formed from a mantle/crustal source at  $1041 \pm 17$  Ma (Bybee et al., 2014). As mentioned in 6.1, Granseth et al. (2019) estimates that mantle-derived content could be as high as 50%, and still the  $\epsilon_{\text{Hf}}$ -values would be within the values of Roberts et al. (2013) from the Sauda-Suldal region. At Flåt, less than 40 km north of the field area, a  $1025 \pm 13$  Ma diorite serves as one of the first evidence of mafic magmatism during SMB(Slagstad et al., 2018). In Moi, southwest SMB granulite facies overprint of the mineral assemblage show the presence of high-grade post-SMB metamorphism (Coint et al., 2015); such metamorphism is not present in the SMB-rocks examined in the field area. They have experienced strain, and thin sections reveal granoblastic textures and recrystallisation of quartz; this is consistent with the overall description of SMB given by Coint et al. (2015).

The field area lies along the eastern border of SMB. The U-Pb geochronology of the SMB unit varies somewhat. Three samples (HAL193061, HAL193063, and VAG084362) collected well within the border between SMB and the disperse migmatite yield ages between 1025 and 1050 Ma; which fit well with the peak magmatism set by Slagstad et al. (2018). The samples VAG128010, and VAG128011 yields ages at  $1066 \pm 67$  Ma, and  $1078 \pm 14$  Ma. These samples are collected at border between SMB and the disperse migmatite, dominated by a mixture of SMB intrusions and migmatic xenoliths. We interpret 1078 Ma to mark the onset of SMB magmatism. The age of SMB is not yet fully constrained, and there is possible that it will be moved back as far as 1100 Ma, but this is yet to be documented.

#### 6.3.2 Late SMB migmatization

The  $> 1.3$  Ga units described shows at least two generations of migmatization. The first generation of leucosomes is 1-3 cm wide fine-grained, follows foliation, and is a common feature. Deformation in the deformed granite (SMB), and the eastern gneisses (i.e. augen-gneiss, and flaser-gneiss) follows the same deformation without the partial melting; however, locally the augen-gneiss phenocrysts are stretched out creating thin layers, but these are generally less than 10 cm long and is not interpreted to be due to partial melting. The

undeformed HBG suite granites cuts this foliation and is believed to be emplaced sometime after. The presence of similar foliation in the SMB granites and lack of them in the HBG granites implies that the migmatization happened sometime between the emplacement of these units. The second generation of leucosomes are 1-5 cm thick medium-grained, and cuts foliation. They are less common but have been observed in the disperse-migmatite, augen-gneiss, and SMB; it has not been observed in the HBG suite granites.

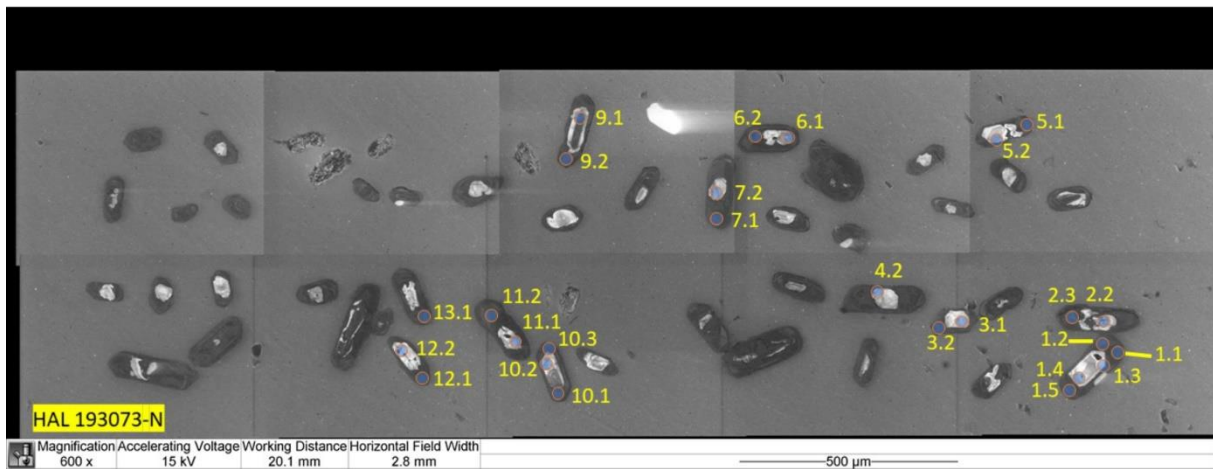


Figure 6.4: A CL-image map created to show the 31 data point of HAL 193073-N (leucosome). The zircon shows a clear core/rim-texture, and attempts was made to sample core and rim separately. The size of the analytical spots are  $28 \mu\text{m}$ .

Before separating zircon from the migmatite samples sampled during this study, the leucosome was separated from the mesosome to retrieve zircons that contained traces of partial melting (i.e. core/rim texture) (see figure 6.4). By targeting the rim specifically for U-Pb geochronology with a SHRIMP analysis, we were able to determine an age of migmatization of the first generation at  $1011 \pm 9 \text{ Ma}$ . Coint et al. (2015) describes a similar generation of migmatization in SMB host-rock/xenoliths at Konsmo, Vest-Agder; LA-ICP-MS analysis of these yielded an age of  $1026 \pm 14 \text{ Ma}$ . Further studies needs to be done to determine the age constraint of the migmatization; but for now, the migmatization seems to reflect a  $1030 - 1010 \text{ Ma}$  partial melting. The second generation has not been sampled, based on field relations we interpret 1011 Ma to reflect maximum age, and  $945 \pm 14 \text{ Ma}$  (HBG suite) to be the minimum age.

#### 6.4 HBG-suite in the field area

HBG-suite is referred to as *undeformed granite* in the results chapter.

##### 6.4.1 Widespread granitic intrusion

The HBG suite is the name given to a geographically widespread group of 990-930 Ma (Jensen and Corfu, 2016, Vander Auwera et al., 2011) ferroan A-type hornblende-biotite

granites first described by Vander Auwera et al. (2003). The general interpretation is that the suite comes from an extensional setting, with authors disagreeing it being either a gravitational driven orogenic collapse (Bingen et al., 2008a, Bingen et al., 2006, Vander Auwera et al., 2011) or a continental back-arc setting (Slagstad et al., 2013a).

Throughout the area there are fine- to medium-grained equigranular biotite-granite intrusions, ranging from 1-2 meters and up 20-30 meters. They are relatively undeformed compared to the units they cross-cut, the disperse migmatite and 1200 Ma gneisses. They are interpreted to be related to the HBG-suite. U-Pb geochronology of zircons separated from HAL193066 yields an age at  $945 \pm 14$  Ma; which puts it well within the constrained age of HBG.

A previously undocumented 2 km long biotite granitic batholith has been mapped at Try in the south-eastern corner of the field area that has been coined Fidje-granite after a local farm. This sample will undergo U-Pb geochronology sometime in the future.

#### 6.4.2 HBG-suite as the source of pegmatites

Müller et al. (2017) define (modified from Ihlen and Müller (2009)) seven individual pegmatite districts in southern Norway (including *Østfold-Halland pegmatite district* that stretches into Sweden); the field area lies within the *Mandal Pegmatite district*. Measurements taken from pegmatites at Hidra yields an age of the district at  $911 \pm 3$  Ma (Müller et al., 2017); these pegmatites have no potential nearby Sveconorwegian parental granites, Müller et al. (2017) concludes that these pegmatites are formed from anatexis. Extensive study of the nearby *Evje-Iveland Pegmatite district* concludes that these pegmatites show no apparent link to the granitic intrusions and are instead formed from partial melting of amphibolite rocks at 910 Ma (Müller et al., 2015). Müller et al. (2017) separates the pegmatitic emplacement in southern into four time periods: (I) 1094-1060 Ma, (II) 1041-1030 Ma, (III) 992-984 Ma, and (IV) 922-901 Ma.

At location 123, a HBG-suite granite ( $945 \pm 14$  Ma) is the possible source of a 10 cm thick pegmatite vein (see figure 6.5). From the granite towards the pegmatite grain size increases, and there are no clear boundary between the two. We conclude that the age of the granite reflects the age of the pegmatite. There is a significant gap between this age and the 922-901 Ma period defined by Müller et al. (2017). This could reflect an isolated event and not be related to the larger pegmatite swarms found at other locations in the Mandal pegmatite district. There are no swarm-like pegmatite complexes in the field area equal to that found in Evje-Iveland and Hidra; they are also generally much smaller and further apart. This could

mean that they come from a local short-lived emplacement during the end of HBG-suite emplacement in the area. More research is needed.



*Figure 6.5: Picture taken from location 123. The grain-size increases as you move from the fine-grained granite in the bottom-right towards the pegmatite in the upper-right. Also, there is no cutting relationship between the two units. In the upper-left corner, there is SMB-granite that is cut by the pegmatite.*

## 6.5 Mafic magmatism

Mafic magmatism is present at several stages of the Sveconorwegian orogeny, e.g. 950-920 RIC (Schärer et al., 1996, Vander Auwera et al., 2011, Bybee et al., 2014),  $985.6 \pm 1.6$  Ma gabbros at Finse (Jensen and Corfu, 2016),  $991 \pm 11$  Ma diorite at Kvås/Konsmo (Høy, 2016),  $1040 \pm 41$  Ma amphibolite near Bergen (Wiest et al., 2018), and  $1031 \pm 5$  Ma meta-quartz diorite at Gyadalen (Slagstad et al., 2018). It is believed that underplating from mafic magma served as a heat source for the long-lived magmatic events during the Sveconorwegian orogeny (Slagstad et al., 2018).



Figure 6.6: Mafic intrusion cutting foliation of a flaser-gneiss at location 129, it itself is being cut by a granitic intrusion and a leucocratic medium-grained vein.

Mafic intrusions are found sporadically all over the field area, with a cutting relationship with migmatite and flaser gneiss. At location 129 (see figure 6.6) a amphibolite cuts foliation in an flaser-gneiss while being itself cut by a undeformed granite. The mafic intrusions vary in size from 10 cm to 20-30 meters. Zircons were separated from one sample that yielded an age at  $968 \pm 14$  Ma; it is uncertain if these zircons reflects a magmatic age or a metamorphic age, but at very least it reflects a minimum age of the intrusions, while the age of the flaser-gneiss host rock  $1208 \pm 16$  reflects the maximum age. The Lu-Hf data lie between  $\epsilon_{\text{Hf}}$  4.5 and 9.5, this is considerably lower than what's calculated for a depleted mantle at 970 Ma. If the zircons comes from the emplacement of the mafic intrusion, then this indicates some crustal content; if the zircons comes from a later metamorphic event, then it's still an open question.

## 6.5 Structural data

Structural data from Knaben (west of the field area) shows an overall eastward dip (Stormoen, 2015). Slagstad et al. (2018) combines these with previous mapping (Marker et al., 2012, Marker and Slagstad, 2018) (see figure 2.4) to argue that the Rogaland region includes a massive dome structure with RIC in the centre. When moving eastwards and into the field area, the dip-direction has turned  $180^\circ$ . The dip-direction in the field area is based on multiple generations of recumbent folding that took place in late SMB; this is not compatible with the dome structure found in Rogaland, meaning that the field area lies east of the affected zone.

## 7. Conclusions

The project has resulted in a more detailed mapping of the field area with detailed description of each of the seven (including the pegmatites) lithological units found in the area. But more importantly, new geochronological data from a less studied area of the Sveconorwegian domain. Based on these results, the project draws the following conclusions:

- U-Pb geochronology of disperse migmatite in the field area reveals the presence of  $1565 \pm 11$  Ma magmatism within the Telemark lithotectonic unit. This is significantly older than the believed first onset of Telemarkian magmatism. It also questions the validity of using Gothia- and Telemark- orogens as a spatial divide between 1.66-1.52 Ga rocks, and 1.52-1.48 rocks. Gothia-Telemarkia is rather one orogen younging to the west.
- Horizontal magnetic gradient mapping and U-Pb geochronological data reveal two layers of protolith within the disperse migmatite. The inner layer yields an age at  $1469 \pm 45$  Ma, while the outer layers yields an age at  $1565 \pm 11$  Ma
- Lu-Hf isotope data suggest that the rocks found in the area originate from a juvenile mantle-input at 1.75 Ga. This is about 250 Ma older than measurements from the Suldal arc further west and much younger than crustal input of coeval magmatism in the Eastern Segment. This trend is compatible with an orogen that youngs westward.
- The augen- and flaser- gneiss units reflect 1210 Ma emplacement of porphyritic magmatism. Difference in deformation reveals that the flaser-gneiss unit has been subjected to a higher temperature ( $> 600^\circ\text{C}$ ) than the augen-gneiss
- U-Pb geochronology reveals two phases of HBG-suite magmatism in the area. One early SMB ( $1078 \pm 14$  Ma) phase of granitic intrusion in Gothia-Telemark host rock, and a latter phase of 1050-1025 plutonic granitic magmatism.
- SHRIMP-analysis of zircon-rims from the disperse migmatite reveals that the late-SMB migmatisation event happened at  $1011 \pm 9$  Ma. There are at least two generations of migmatisation. One fine-grained pre- or syn-foliation, and one medium-grained post foliation.
- $945 \pm 14$  Ma HBG-suite granites is common in the area, these may or may not be the source for the pegmatites. If so, the pegmatites found in the area is does not belong to the Mandal pegmatite district.
- One new previously undocumented HBG-suite 2 km long 500 meters wide pluton has been described; coined the Fidje-granite.

## 8 References

- ALLMENDINGER, R. W. 2019.  
<http://www.geo.cornell.edu/geology/faculty/RWA/programs/stereonet.html> [Online].  
[Accessed 30/07/2019].
- ANDERSEN, T. 2005. Terrane analysis, regional nomenclature and crustal evolution in the Southwest Scandinavian Domain of the Fennoscandian Shield. *GFF - Upsala*, 127, 159-168.
- ANDERSEN, T., ANDERSSON, U. B., GRAHAM, S., ÅBERG, G. & SIMONSEN, S. L. 2009b. Granitic magmatism by melting of juvenile continental crust: new constraints on the source of Palaeoproterozoic granitoids in Fennoscandia from Hf isotopes in zircon. *Journal of the Geological Society*, 166, 233-247.
- ANDERSEN, T. & GRIFFIN, W. L. 2004. Lu-Hf and U-Pb isotope systematics of zircons from the Storgangen intrusion, Rogaland Intrusive Complex, SW Norway: implications for the composition and evolution of Precambrian lower crust in the Baltic shield. *Lithos*, 73, 271-288.
- ANDERSEN, T., GRIFFIN, W. L., JACKSON, S. E., KNUDSEN, T.-L. & PEARSON, N. J. 2004. Mid-Proterozoic magmatic arc evolution at the southwest margin of the Baltic shield. *Lithos*, 73, 289-318.
- ANDERSEN, T., GRIFFIN, W. L. & PEARSON, N. J. 2002. Crustal Evolution in the SW Part of the Baltic Shield: the Hf Isotope Evidence. *Journal of Petrology*, 43, 1725-1747.
- ANDERSEN, T., GRIFFIN, W. L. & SYLVESTER, A. G. 2007. Sveconorwegian crustal underplating in southwestern Fennoscandia: LAM-ICPMS U-Pb and Lu-Hf isotope evidence from granites and gneisses in Telemark, southern Norway. *Lithos*, 93, 273-287.
- ANDERSSON, J., MÖLLER, C. & JOHANSSON, L. 2002. Zircon geochronology of migmatite gneisses along the Mylonite Zone (S Sweden): a major Sveconorwegian terrane boundary in the Baltic Shield. *Precambrian Research*, 114, 121-147.
- ANDERSSON, M., LIE, J. E. & HUSEBYE, E. S. 1996. Tectonic setting of post-orogenic granites within SW Fennoscandia based on deep seismic and gravity data. *Terra Nova*, 8, 558-566.
- ANDERSSON, U. B., BEGG, G. C., GRIFFIN, W. L. & HÖGDAHL, K. 2011. Ancient and juvenile components in the continental crust and mantle: Hf isotopes in zircon from Svecofennian magmatic rocks and rapakivi granites in Sweden. *Lithosphere*, 3, 409-419.
- ANDERSSON, U. B., SJÖSTRÖM, H., HÖGDAHL, K. & EKLUND, O. 2004. The Transscandinavian Igneous Belt; Evolutionary model. *The Transscandinavian igneous Belt (TIB) in Sweden; a review of its character and evolution*, 2004, 104-112.
- BINGEN, B., ANDERSSON, J., SÖDERLUND, U. & MÖLLER, C. 2008b. The Mesoproterozoic in the Nordic countries. *Episodes*, 31, 1-7.
- BINGEN, B., BELOUSOVA, E. A. & GRIFFIN, W. L. 2011. Neoproterozoic recycling of the Sveconorwegian orogenic belt: Detrital-zircon data from the Sparagmite basins in the Scandinavian Caledonides. *Precambrian Research*, 189, 347-367.
- BINGEN, B., BOVEN, A., PUNZALAN, L., WIJBRANS, J. R. & DEMAFFE, D. 1998. Hornblende 40Ar/39Ar geochronology across terrane boundaries in the Sveconorwegian Province of S. Norway. *Precambrian Research*, 90, 159-185.
- BINGEN, B., DAVIS, W. J., HAMILTON, M. A., ENGVIK, A. K., STEIN, H. J., SKÅR, Ø. & NORDGULEN, Ø. 2008c. Geochronology of high-grade metamorphism in the Sveconorwegian belt, S. Norway: U-Pb, Th-Pb and Re-Os data. *Norwegian journal of geology*.
- BINGEN, B., NORDGULEN, Ø., SIGMOND, E. M. O., TUCKER, R., MANSFELD, J. & HÖGDAHL, K. 2003. Relations between 1.19–1.13 Ga continental magmatism, sedimentation and metamorphism, Sveconorwegian province, S Norway. *Precambrian Research*, 124, 215-241.
- BINGEN, B., NORDGULEN, Ø. & VIOLA, G. 2008a. A four-phase model for the Sveconorwegian orogeny, SW Scandinavia. *Norwegian journal of geology*, 88, 43-72.

- BINGEN, B., SKÅR, Ø., MOGENS, M., SIGMOND, E. M. O., NORDGULEN, Ø., RAGNHILDSTVEIT, J., MANSFELD, J., TUCKER, R. D. & LIÉGEOIS, J.-P. 2005a. Timing of continental building in the Sveconorwegian orogen, SW Scandinavia. *Norwegian journal of geology*, 85, 87-116.
- BINGEN, B., STEIN, H. J., BOGAERTS, M., BOLLE, O. & MANSFELD, J. 2006. Molybdenite Re–Os dating constrains gravitational collapse of the Sveconorwegian orogen, SW Scandinavia. *Lithos*, 87, 328-346.
- BINGEN, B. & VAN BREEMEN, O. 1998. Tectonic regimes and terrane boundaries in the high-grade Sveconorwegian belt of SW Norway, inferred from U Pb zircon geochronology and geochemical signature of augen gneiss suites. *Journal of the Geological Society*, 155, 143-154.
- BINGEN, B. & VIOLA, G. 2018. The early-Sveconorwegian orogeny in southern Norway: Tectonic model involving delamination of the sub-continental lithospheric mantle. *Precambrian Research*, 313, 170-204.
- BLACK, L. P., KAMO, S. L., ALLEN, C. M., DAVIS, D. W., ALENIKOFF, J. N., VALLEY, J. W., MUNDIL, R., CAMPBELL, I. H., KORSCH, R. J., WILLIAMS, I. S. & FOUDOULIS, C. 2004. Improved 206Pb/238U microprobe geochronology by the monitoring of a trace element related matrix effect: SHRIMP, ID-TIMS, ELA-ICP-MS, and oxygen isotope documentation for a series of zircon standards. *Chemical Geology*, 205, 115-140.
- BLEREAU, E., JOHNSON, T. E., CLARK, C., TAYLOR, R. J. M., KINNY, P. D. & HAND, M. 2017. Reappraising the P-T evolution of the Rogaland-Vest Agder Sector, southwestern Norway. *Geoscience Frontiers*, 8, 1-14.
- BOGDANOVA, S. V., BINGEN, B., GORBATSCHEV, R., KHERASKOVA, T. N., KOZLOV, V. I., PUNCHOV, V. N. & VOLOZH, Y. A. 2008. The East European Craton (Baltica) before and during the assembly of Rodinia. *Precambrian Research*, 160, 23-45.
- BOUVIER, A., VERVOORT, J. D. & PATCHETT, P. J. 2008. The Lu-Hf and Sm-Nd isotopic composition of CHUR: Constraints from unequilibrated chondrites and implications for the bulk composition of terrestrial planets. *Earth and Planetary Science Letters*, 273, 45-57.
- BRANDER, L. 2011. *The Mesoproterozoic Hallandian event - a region-scale orogenic event in the Fennoscandian Shield*. Doctoral, University of Gothenburg.
- BRANDER, L. & SÖDERLUND, U. 2009. Mesoproterozoic (1.47-1.44 Ga) orogenic magmatism in Fennoscandia; Baddeleyite U-Pb dating of a suite of massif-type anorthosite in S. Sweden. *International Journal of Earth Sciences*, 98, 499-516.
- BREWER, T. S., DALY, J. S. & ÅHÄLL, K.-I. 1998. Contrasting magmatic arcs in the Palaeoproterozoic of the south-western Baltic Shield. *Precambrian Research*, 92, 297-315.
- BREWER, T. S., ÅHÄLL, K.-I., MENUGE, J. F., STOREY, C. D. & PARRISH, R. R. 2004. Mesoproterozoic bimodal volcanism in SW Norway, evidence for recurring pre-Sveconorwegian continental margin tectonism. *Precambrian Research*, 134, 249-273.
- BYBEE, G. M., ASHWAI, L. D., SHIREY, S. B., HORAN, M., MOCK, T. & ANDERSEN, T. B. 2014. Pyroxene megacrysts in Proterozoic anorthosites: Implications for tectonic setting, magma source and magmatic processes at the Moho. *Earth and Planetary Science Letters*, 389, 74-85.
- CHERNIAK, D. J. & WATSON, E. B. 2003. Diffusion in Zircon. In: HANCHAR, J. M. & HOSKIN, P. W. O. (eds.) *Zircon*. Reviews in Mineralogy and Geochemistry.
- CHESTER, F. M. & LOGAN, J. M. 1987. Composite planar fabric of gouge from the Punchbowl Fault, California. *Journal of Structural Geology*, 9, 621-634.
- CLAOUÉ-LONG, J. C., COMPSTON, W., ROBERTS, J. & FANNING, C. M. 1995. Two Carboniferous ages: a comparison of SHRIMP zircon dating with conventional zircon ages and 40Ar/39Ar analysis, in Time Scales and Global Stratigraphic Correlation. *Geochronology, Time Scales and Global Stratigraphic Correlation*, 54.
- CLOUGH, P. W. L. & FIELD, D. 1980. Chemical variation in metabasites from a proterozoic amphibolite-granulite transition zone, South Norway. *Contributions to Mineralogy and Petrology*, 73, 227-286.
- COINT, N., SLAGSTAD, T., ROBERTS, N. M. W., MARKER, M., RØHR, T. S. & SØRENSEN, B. E. 2015. The Late Mesoproterozoic Sirdal Magmatic Belt, SW Norway: Relationships between magmatism

- and metamorphism and implications for Sveconorwegian orogenesis. *Precambrian Research*, 265, 57-77.
- COLLINS, W. J. 2002. Hot orogens, tectonic switching, and creation of continental crust. *Geology*, 30, 535-538.
- COMPSTON, W., WILLIAMS, I. S. & MEYER, C. 1984. U-Pb geochronology of zircons from lunar breccia 73217 using a sensitive high mass-resolution ion microprobe. *Journal of Geophysical Research*, 89, B525-B534.
- COREL. 2019. [https://www.corel.com/en/products/coreldraw/?x-vehicle=ppc\\_brkws&qclid=CjwKCAjwm4rqBRBUEiwAwaWjjHCXT2b-5zIUSHD8PLUbclxc\\_E6ZIWBFZmidkVOhd-A-5G0wBbEsExoCeo0QAvD\\_BwE](https://www.corel.com/en/products/coreldraw/?x-vehicle=ppc_brkws&qclid=CjwKCAjwm4rqBRBUEiwAwaWjjHCXT2b-5zIUSHD8PLUbclxc_E6ZIWBFZmidkVOhd-A-5G0wBbEsExoCeo0QAvD_BwE) [Online].  
[Accessed 01/08/2019].
- CORFU, F., HANCHAR, J. M., HOSKIN, P. W. O. & KINNY, P. D. 2003. Atlas of Zircon Textures. In: HANCHAR, J. M. & HOSKIN, P. W. O. (eds.) *Zircon*. Reviews in Mineralogy and Geochemistry.
- DAVIS, D. W., WILLIAMS, I. S. & KROGH, T. E. 2003. Historical Development of Zircon Geochronology. In: HANCHAR, J. M. & HOSKIN, P. W. O. (eds.) *Zircon*. Reviews in Mineralogy and Geochemistry.
- DODSON, M. H. 1973. closure temperature geochronological and petrological systems. *Contributions to Mineralogy and Petrology*, 40, 259-274.
- DRÜPPEL, K., ELSÄBER, L., BRANDT, S. & GREDES, A. 2012. Sveconorwegian Mid-crustal Ultrahigh-temperature Metamorphism in Rogaland, Norway: U<sup>238</sup> LA-ICP-MS Geochronology and Pseudosections of Sapphirine Granulites and Associated Paragneisses. *Journal of Petrology*, 52, 305-350.
- EBBING, J., AFEWORK, Y., OLESEN, O. & NORDGULEN, Ø. 2005. Is there evidence for magmatic underplating beneath the Oslo Rift? *Terra Nova*, 17, 129-134.
- EVANS, J. P. 1988. Deformation mechanisms in granitic rocks at shallow crustal levels. *Journal of Structural Geology*, 10, 437-443.
- FALKUM, T. 1985. *Geologisk kart over Norge. bergrunnskart Mandal 1:250000*. Norges Geologiske Undersøkelse.
- FAURE, G. & MENSING, T. M. 2005. *Isotopes: Principles and Applications*, Wiley.
- FINCH, R. J. & HANCHAR, J. M. 2003. Structure and Chemistry of Zircon and Zircon-Group Minerals. In: HANCHAR, J. M. & HOSKIN, P. W. O. (eds.) *Zircon*. Reviews in Mineralogy and Geochemistry.
- FINCH, R. J., HANCHAR, J. M., HOSKIN, P. W. O. & BURNS, P. C. 2001. Rare-earth element in synthetic zircon: Part 2. A single-crystal X-ray study of xenotime substitution. *American Mineralogist*, 86, 681-689.
- GAÁL, G. & GORBATSCHEV, R. 1987. An Outline of the precambrian evolution of the baltic shield. *Precambrian Research*, 35, 15-52.
- GOOGLE. 2018. *Earth.Google*.
- GOWER, C., RYAN, A. B. & RIVERS, T. 1990. Mid-Proterozoic Laurentia-Baltica: An overview of its geological evolution and a summary of the contributions made by this volume. *Geological Association of Canada, Toronto, Special Papers*, 1-20.
- GRANSETH, A. U., SLAGSTAD, T., COINT, N., ROBERTS, N., RØHR, T. & SØRENSEN, B. E. 2019. Tectonomagmatic evolution of the Sveconorwegian orogeny recorded in the chemical and isotopic composition of 1070-920 Ma granites. *Winter conference (NGU)*. Bergen.
- GRiffin, W. L., PEARSON, N. J., BELOUSOVA, E., JACKSON, S. E., ACHTERBERGH, E. V., O'REILLY, S. Y. & SHEE, S. R. 2000. The Hf isotope composition of cratonic mantle:LAM-MC-ICPMS analysis of zircon megacrysts in kimberlites. *Geochimica et Cosmochimica Acta*, 64, 133-147.
- GRiffin, W. L., WANG, X., JACKSON, S. E., PEARSON, N. J., O'REILLY, S. Y., XU, X. & ZHOU, X. 2002. Zircon chemistry and magma mixing, SE China: In-situ analysis of Hf isotopes, Tonglu and Pingtan igneous complexes. *Lithos*, 61, 237-269.

- HAWKESWORTH, C. J., DHUIME, B., PIETRANIK, A. B., CAWOOD, P. A., KEMP, A. I. S. & STOREY, C. D. 2010. The generation and evolution of the continental crust. *Journal of the Geological Society*, 167, 229-248.
- HEAMAN, L. M. & SMALLEY, P. C. 1994. A U-Pb study of the Morkheia Complex and associated gneisses, southern Norway: Implications for disturbed Rb-Sr systems and for the temporal evolution of Mesoproterozoic magmatism in Laurentia. *Geochimica et Cosmochimica Acta*, 58, 1899-1911.
- HEGARDT, E. A., CORNELL, D., CLAESSEN, L., SIMAKOV, S., STEIN, H. & HAMMAH, J. 2005. Eclogites in the central part of the Sveconorwegian Eastern Segment of the Baltic Shield: Support for an extensive eclogite terrane. *GFF*, 127, 221-232.
- HYNES, A. & RIVERS, T. 2010. Protracted continental collision - Evidence from the Greenville orogen. *Canadian Journal of Earth Sciences*, 47, 591-620.
- HÖGDAHL, K., ABDERSSON, U. B. & EKLUND, O. 2004. The Transscandinavian Igneous Belt (TIB) in Sweden: a review of its character and evolution. *Special Paper - Geological Survey of Finland*, 37, 1-125.
- HØY, I. 2016. *Sveconorwegian magmatic and metamorphic evolution of southwestern Norway*. Master thesis in geology Geology, University of Oslo.
- IHLEN, P. M. & MÜLLER, A. 2009. RARE-METAL PEGMATITES IN THE SVECONORWE-GIAN OROGEN (0.9-1.1 Ga) OF SOUTHERN NORWAY. *Estudos Geológicos*, 19, 140-144.
- IRELAND, T. R., CLEMENT, S., COMPSTON, W., FOSTER, J. J., HOLDEN, P., JENKINS, B., LANC, P., SCHRAM, N. & WILLIAMS, I. S. 2008. Development of SHRIMP. *Australian Journal of Earth Sciences*, 55.
- JACKSON, S. E., PEARSON, N. J., GRIFFIN, W. L. & BELOUSOVA, E. A. 2004. The application of laser ablation-inductively coupled plasma-mass spectrometry to in situ U-Pb zircon geochronology. *Chemical Geology*, 211, 47-69.
- JENSEN, E. & CORFU, F. 2016. The U-Pb age of the Finse Batholith a composite bimodal Sveconorwegian intrusion. *Norwegian journal of geology*, 96.
- JOHANSSON, L., MÖLLER, C. & SÖDERLUND, U. 2001. Geochronology of eclogite facies metamorphism in the Sveconorwegian Province of SW Sweden. *Precambrian Research*, 106, 261-275.
- KARLSTROM, K. E., ÅHÄLL, K.-I., HARLAN, S. S., WILLIAMS, M. L., MCLELLAND, J. & GEISSMAN, J. W. 2001. Long-lived (1.8 – 1.0 Ga) convergent orogen in southern Laurentia, its extensions to Australia and Baltica, and implications for refining Rodinia. *Precambrian Research*, 111, 5-30.
- KINNY, P. D. & MAAS, R. 2003. Lu-Hf and Sm-Nd isotope systems in zircon. In: HANCHAR, J. M. & HOSKIN, P. W. O. (eds.) *Zircon. Reviews in Mineralogy and Geochemistry*.
- KNUDSEN, T.-L. & ANDERSEN, T. 1999. Petrology and Geochemistry of the Tromøy Gneiss Complex, South Norway, an Alleged Example of Proterozoic Depleted Lower Continental Crust. *Journal of Petrology*, 40, 909-933.
- KORJA, A., LAHTINEN, R. & NIRONEN, M. 2006. The Svecofennian orogen: a collage of microcontinents and island arcs. *Geological Society London Memoirs*, 32, 561-578.
- KOŠLER, J., SLÁMA, J., BELOUSOVA, E., CORFU, F., E.GEHRELS, G., GERDES, A., HORSTWOOD, M. S. A., SIRCOMBE, K. N., SYLVESTER, P. J., TIEPOLO, M., WHITEHOUSE, M. J. & WOODHEAD, J. D. 2013. U-Pb Detrial Zircon ANalysis - Results of an Inter-laboratory Comparison. *Geostandards and Geoanalytical Research*, 37, 243-259.
- KULLERUD, L. & MACHADO, N. 1991. End of a controversy: U-Pb geochronological evidence for significant Grenvillian activity in the Bamble area, Norway. *Terra Abstracts, supplement to Terra Nova*, 3.
- KYLANDER-CLARK, A. R. C. 2017. Petrochronology by Laser-Ablation Inductively Coupled Plasma Mass Spectrometry. In: KOHN, M. J., ENGI, M. & LANARI, P. (eds.) *Petrochronology: Methods and Applications. Reviews in Mineralogy and Geochemistry*.

- KYLANDER-CLARK, A. R. C. & COTTLE, J. M. 2014. Short Course: Laser Ablation Split Stream (LASS), Geochronology and Petrochronology. *US Santa Barbara Earth Science*.
- LAMMINEN, J. 2011. Provenance and correlation of sediments in Telemark, South Norway: status of the Lifjell Group and implications for early Sveconorwegian fault tectonics. *Norwegian journal of geology*, 91, 57-75.
- LEICA. 2011. <https://www.leica-microsystems.com/products/microscope-software/p/leica-laser-downloads/> [Online]. [Accessed 13/08-2019].
- LUDWIG, K. R. 2003. A Geochronological Toolkit for Microsoft Excel.
- MARKER, M., SCHIELLERUP, H., SOLLI, A. & LUTRO, O. 2012. *Jørpeland 1213 II*, 1:50.000. NGU.
- MARKER, M. & SLAGSTAD, T. 2018. *Lyngsvatnet 1313 III*, 1:50.000. NGU.
- MÜLLER, A., IHLEN, P. T., SNOCK, B., LARSEN, R. B., FLEM, B., BINGEN, B. & WILLIAMSON, B. J. 2015. The Chemistry of Quartz in Granitic Pegmatites of Southern Norway: Petrogenetic and Economic Implications. *Economic Geology*, 220, 1737-1757.
- MÜLLER, A., ROMER, R. L. & PEDERSEN, R.-B. 2017. The Sveconorwegian Pegmatite Province – Thousands of Pegmatites Without Parental Granites. *The Canadian Mineralogist*, 55, 283-315.
- MÖLLER, A., O'BRIAN, P. J., KENNEDY, A. & KRÖNER, A. 2002. Polyphase zircon in ultrahigh-temperature granulites (Rogaland, SW Norway): constraints for Pb diffusion in zircon. *Journal of Metamorphic Geology*, 20, 727-740.
- MÖLLER, C. 1998. Decompressed eclogites in the Sveconorwegian (–Grenvillian) orogen of SW Sweden: petrology and tectonic implications. *Journal of Metamorphic Geology*, 16, 641-656.
- NGU-COOP-PROJECT. 2017.
- NIIRONEN, M. 1997. The Svecfennian Orogen: a tectonic model. *Precambrian Research*, 86, 21-44.
- NJILAND, T. G., HARLOV, D. E. & ANDERSEN, T. 2014. The Bamble Sector, South Norway: A review. *Geoscience Frontiers*, 5, 635-658.
- PASSARELLI, C. R., BASEI, M. A. S., JR., O. S., SATO, K., SPROESSER, W. M. & LOIOS, V. A. P. 2009. Dating minerals by ID-TIMS geochronology at times of *in situ* analysis: selected case studies from the CPGeo-IGe-USP laboratory. *Anais da Academia Brasileira de Ciências*, 81, 73-97.
- PASSCHIER, C. W. & TROUW, R. A. J. 2005. *Microtectonics*, Springer-Verlag.
- PATCHETT, P. J., TODT, W. & GORBATSCHEV, R. 1987. Origin of continental crust of 1.9-1.7 ga age: nd isotopes in the svecfennian orogenic terrains of sweden. *Precambrian Research*, 35, 145-160.
- PEDERSEN, S., ANDERSEN, T., KONNERUP-MADSEN, J. & GRIFFIN, W. L. 2009. Recurrent mesoproterozoic continental magmatism in South-Central Norway *International Journal of Earth Sciences*, 98, 1151-1171.
- PETERSSON, A., SCHERSTÉN, A., ANDERSSON, J. & MÖLLER, C. 2015a. Zircon U-Pb and Hf – isotopes from the eastern part of the Sveconorwegian Orogen, SW Sweden: implications for the growth of Fennoscandia. *Geological Society, London, Special publications*, 389, 287-303.
- PETERSSON, A., SCHERSTÉN, A., BINGEN, B., GERDES, A. & WHITEHOUSE, M. J. 2015b. Mesoproterozoic continental growth: U-Pb-Hf-O zircon record in theldefjorden Terrane, Sveconorwegian Orogen. *Precambrian Research*, 251, 75-95.
- ROBERTS, N. M. W. 2010. *From crystal to crust: the Proterozoic crustal evolution of southwest Norway*. PhD, University of Leicester.
- ROBERTS, N. M. W. & SLAGSTAD, T. 2014. Continental growth and reworking on the edge of the Columbia and Rodinia supercontinents; 1.86-0.9 Ga accretionary orogeny inn southwest Fennoscandia. *International Geology Review*, 57, 1582-1606.
- ROBERTS, N. M. W., SLAGSTAD, T., PARRISH, R. R., NORRY, M. J., MARKER, M. & HORTSWOOD, M. S. A. 2013. Sedimentary recycling in arc magmas: geochemical and U-Pb-Hf-O constraints on the Mesoprotterozoic Suldal Arc, SW Norway. *Contributions to Mineralogy and Petrology*, 165, 507-523.
- ROCKWARE. 2007. <https://www.rockware.com/product/igpet/#> [Online]. [Accessed 09/08/2019].

- RUDNICK, R. I. & GAO, S. 2003. Composition of the Continental Crust. *Treatise Geochem.*
- SCHOENE, B. 2014. U-Th-Pb Geochronology. *Treatise on Geochemistry*, 4, 341-378.
- SCHÄRER, U., WILMART, E. & DUCHESNE, J.-C. 1996. The short duration and anorogenic character of anorthosite magmatism: U-Pb dating of the Rogaland complex, Norway. *Earth and Planetary Science Letters*, 139, 335-350.
- SLAGSTAD, T., ROBERTS, N. M. W., COINT, N., HØY, I. U., SAUER, S., KIRKLAND, C. L., MARKER, M., RØHR, T. S., HENDERSON, I. H. C., STORMOEN, M. A., SKÅR, Ø., SØRENSEN, B. E. & BYBEE, G. 2018. Magma-driven, high-grade metamorphism in the Sveconorwegian province, southwest Norway, during the terminal stages of Fennoscandian Shield evolution. *Geosphere*, 14, 861-882.
- SLAGSTAD, T., ROBERTS, N. M. W. & KULAKOV, E. 2017. Linking orogenesis across a supercontinent; the Grenvillian and Sveconorwegian margins on Rodinia. *Gondwana Research*, 44, 109-115.
- SLAGSTAD, T., ROBERTS, N. M. W., MARKER, M., RØHR, T. S. & SCHIELLERUP, H. 2013a. A non-collisional, accretionary Sveconorwegian orogen. *Terra Nova*, 25, 30-37.
- SLÁMA, J., KOŠLER, J., CONDON, D. J., CROWLEY, J. L., GERDES, A., HANCHAR, J. M., HORSTWOOD, M. S. A., MORRIS, G. A., NASDALA, L., NORBERG, N., SCHALTEGGER, U., SCHOENE, B., TUBRETT, M. N. & WHITEHOUSE, M. J. 2008. Plešovice zircon—A new natural reference material for U-Pb and Hf isotopic microanalysis. *Chemical Geology*, 249, 1-35.
- SPENCER, C. J., ROBERTS, N. M. W., CAWOOD, P. A., HAWKESWORTH, C. J., PRAVE, A. R., ANTONINI, A. S. M. & HORSTWOOD, M. S. A. 2014. Intermontane basins and bimodal volcanism at the onset of the Sveconorwegian Orogeny, southern Norway. *Precambrian Research*, 252, 107-118.
- STEIGER, R. H. & JÄGHER, E. 1977. Subcommission on geochronology: convention on the use of decay constants in geo-and cosmochronology. *Earth and Planetary Science Letters*, 36, 359-362.
- STERN, R. A., BODORKOS, S., KAMO, S. L., HICKMAN, A. H. & CORFU, F. 2009. Measurement of SIMS Instrumental Mass Fractionation of Pb Isotopes During Zircon Dating. *Geostandards and Geoanalytical Research*, 33, 145-168.
- STORMOEN, M. A. 2015. *Synkinematic intrusion of granitoid sheets, with implications for molybdenite deposits in the Knaben Zone*. MSc, Norwegian University of Science and Technology.
- SUN, S.-S. & McDONOUGH, W. F. 1989. Chemical and isotopic systematics of oceanic basalts: implications for mantle composition and processes. *Geological Society, London, Special publications* 1989, 42, 313-345.
- SÖDERLUND, U. & ASK, R. 2006. Evidence for two pulses (1215-1224 and ca. 1205 Ma) of bimodal magmatism along the protogine zone, SW Sweden. *Geologiska Föreningen*, 128, 303-310.
- SÖDERLUND, U., HELLSTRÖM, F. A. & KAMO, S. L. 2008. Geochronology of high-pressure mafic granulite dykes in SW Sweden: tracking the P-T-t path of metamorphism using Hf isotopes in zircon and baddeleyite. *Journal of Metamorphic Geology*, 26, 539-560.
- SÖDERLUND, U., ISACHSEN, C. E., BYLUND, G., HEAMAN, L. H., PATCHETT, P. J., VERVOORT, J. D. & ANDERSSON, U. B. 2005. U-Pb baddeleyite ages and Hf, Nd isotope chemistry constraining repeated mafic magmatism in the Fennoscandian Shield from 1.6 to 0.9 Ga. *Contributions to Mineralogy and Petrology*, 150, 174-194.
- SÖDERLUND, U., JARL, L.-G., PERSSON, P.-O., STEPHENS, M. B. & WAHLGREN, C.-H. 1999. Protolith ages and timing of deformation in the eastern, marginal part of the Sveconorwegian orogen, southwestern Sweden. *Precambrian Research*, 94, 29-48.
- TERA, F. & WASSERBURG, G. J. 1972. U-Th-Pb systematics in three Apollo 14 basalts and the problem of initial Pb in lunar rocks. *Earth and Planetary Science Letters*, 14, 281-304.
- VANDER AUWERA, J., BOGAERTS, M., LIÉGEOIS, J.-P., DEMAFFE, D., WILMART, E., BOLLE, O. & DUCHESNE, J. C. 2003. Derivation of the 1.0-0.9 Ga ferro-potassic A-type granitoids of southern Norway by extreme differentiation from basic magmas. *Precambrian Research*, 124, 107-148.
- VANDER AUWERA, J., BOLLE, O., BINGEN, B., LIÉGEOIS, J.-P., BOGAERTS, M., DUCHESNE, J. C., WAELE, B. D. & LONGHI, J. 2011. Sveconorwegian massif-type anorthosites and related granitoids

- result from post-collisional melting of a continental arc root. *Earth-Science Reviews*, 107, 375-397.
- VIOLA, G., HENDERSON, I. H. C., BINGEN, B. & HENDERSON, B. W. H. 2011. The Grenvillian–Sveconorwegian orogeny in Fennoscandia: Back-thrusting and extensional shearing along the "MyloniteZone". *Precambrian Research*, 189, 368-388.
- WESTPHAL, M., SCHUMACHER, F. C. & BOSCHERT, S. 2003. High-Temperature Metamorphism and the Role of Magmatic Heat Sources at the Rogaland Anorthosite Complex in Southwestern Norway. *Journal of Petrology*, 44, 1145-1162.
- WETHERILL, G. W. 1956. Discordant Uranium Lead Ages. *Transactions, American Geophysical Union*, 37.
- WIEDENBECK, M., ALLÉ, P., CORFU, F., GRIFFIN, W. L., MEIER, M., OBERLI, F., QUADT, A. V., RODDICK, J. C. & SPIEGEL, W. 1995. Three Natural Zircon Standards for U-Th-Pb, Lu-Hf, Trace Element and REE Analyses. *Geostandards Newsletter*, 19, 1-23.
- WIEST, J. D., JACOBS, J., KSIENZYK, A. K. & FOSSEN, H. 2018. Sveconorwegian vs. Caledonian orogenesis in the eastern Øygarden Complex, SW Norway – Geochronology, structural constraints and tectonic implications. *Precambrian Research*, 305, 1-18.
- WILLIAMS, I. S. 1998. U–Th–Pb geochronology by ion microprobe, in Applications of Microanalytical Techniques to Understanding Mineralizing Processes. *Economic Geology*, 7, 1-35.
- WILSON, J. R., ROBINS, B., NIELSEN, F. M., DUCHESNE, J. C. & AUWERA, J. V. 1996. The Bjerkreim-Sokndal Layered Intrusion, Southwest Norway. *Layered Intrusions*, 231-255.
- WINDGATE, M. T. D. & KIRKLAND, C. L. 2015. Introduction to geochronology information released in 2015. In: AUSTRALIA, G. S. O. W. (ed.).
- WINTER, J. D. 2001. *An Introduction to Igneous and Metamorphic Petrology*, Prentice Hall.
- WOLF, R. E. 2005. Introduction to ICP-MS. U. S. Geological Survey, 2015.
- ZEISS. 2009. <https://www.zeiss.com/microscopy/int/products/microscope-software/axiovision.html> [Online]. [Accessed 13/08-2019].
- ÅHÄLL, K.-I. & CONNELLY, J. N. 2008. Long-term convergence along SW fennoscandia: 330 m.y. of proterozoic crustal growth. *Precambrian Research*, 161, 452-474.
- ÅHÄLL, K.-I., CONNELLY, J. N. & BREWER, T. S. 2000. Episodic rapakivi magmatism due to distal orogenesis?: Correlation of 1.69-1.50 Ga orogenic and onboard, "anorogenic" events in the Baltic Shield. *geology*, 28, 823-826.
- ÅHÄLL, K.-I. & DALY, J. S. 1989. Age, Tectonic Setting and Provenance of Östfold-Marstrand Belt Supracrustals: Westward Growth of the Baltic Shield at 1760 Ma *Precambrian Research*, 45, 45-61.

## Appendix

Appendix A – Samples and localities

Appendix B – Geochronological data from SHRIMP

Appendix C – Geochronological data from LA-SS-ICP-MS

Appendix D – Trace element data

Appendix E - Hf-Lu data

Appendix F – Zircon data sampling map

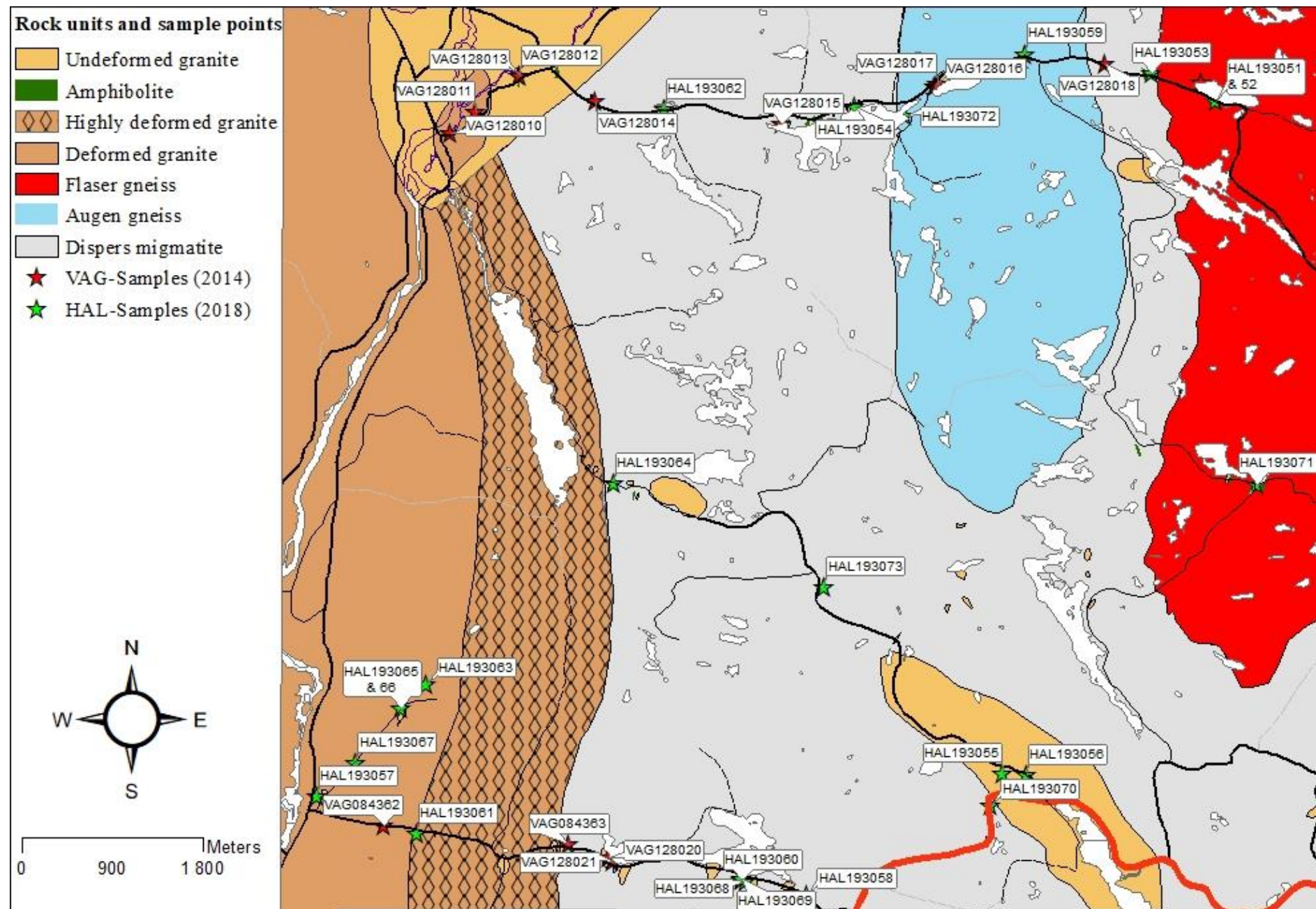
Appendix G – Thin section notes

## Appendix A – Samples and localities

		UTM- kordinater WGS 1984 EPSG				Work		
Sample	Locality	Zone+N/S	East (m)	North (m)	Rock type	Analysis	Mount	Thin section
HAL193051	10	32N	422818	6448003	Amphibolite			
HAL193052	10	32N	422818	6448003	Amphibolite	LA	C	Tpol
HAL193053	11	32N	422180	6448286	Migmatite		Shrimp	Tpol
HAL193054	18	32N	419206	6447948	Granite			
HAL193055	26	32N	420684	6441283	Migmatite			
HAL193056	34	32N	420923	6441265	Granite	LA	C	Tpol
HAL193057	35	32N	413824	6441050	Deformed granite			
HAL193058	44	32N	418725	6440065	Amphibolite			Tpol
HAL193059	73	32N	420911	6448479	Augen gneiss			Tpol
HAL193060	101	32N	418082	6440212	Migmatite			
HAL193061	37	32N	414826	6440679	Deformed granite	LA	C	Tpol
HAL193062	105	32N	417304	6447923	Migmatite	Shrimp	Shrimp	Tpol
HAL193063	111	32N	414918	6442172	Deformed granite	LA	C	
HAL193064	118	32N	416793	6444179	Migmatite			Tpol
HAL193065	123	32N	414667	6441936	Deformed granite			Tpol
HAL193066	123	32N	414667	6441936	Granite	LA	C	Tpol
HAL193067	124	32N	414218	6441384	Granite			
HAL193068	125	32N	418123	6440204	Migmatite			
HAL193069	126	32N	418078	6440229	Amphibolite			Tpol
HAL193070	30	32N	420563	6440958	Porphyritic migmatite			Tpol
HAL193071	20	32N	423237	6444177	Flaser gneiss and Amphibolite			Tpol
HAL193072	127	32N	419714	6447860	Augen gneiss			Tpol
HAL193073	128	32N	418910	6443145	Migmatite	Shrimp	Shrimp	Tpol
VAG084362	b 35-36	32N	414489	6440759	Granitic gneiss	LA	B	T
VAG084363	c 41	32N	416346	6440569	Banded gneiss	LA	B	T
VAG128010	c 2	32N	415158	6447684	Foliated Porphyritic Bt granite	LA	A	T
VAG128011	b 1-3	32N	415410	6447899	Megacrystic foliated granite	LA	A	T
VAG128012	c 4	32N	415849	6448254	Medium grained Bt granite	LA	A	T
VAG128013	c 4	32N	415850	6448256	Fine grained Bt granite		A	T
VAG128014	c 104	32N	416616	6448012	Medium grained Bt granite	LA	A	T
VAG128015	13	32N	418482	6447780	Medium grained Bt granite	LA	A	T
VAG128016	c 51	32N	420005	6448159	Migmatitic granitic gneiss	LA	A	T
VAG128017	c 51	32N	420031	6448181	Leucocratic gneiss	LA	A	T
VAG128018	c 53	32N	421718	6448384	Banded gneiss	LA	B	T
VAG128019	8	32N	422671	6448199	Porphyoclastic granitic gneiss	LA	B	T
VAG128020	b 49-50	32N	416751	6440436	Folded banded gneiss			T
VAG128021	b 49-50	32N	416790	6440396	Granitic gneiss			T

b= between, c = close to, LA = LA-SS-ICP-MS, T = Thinsection, Tpol = polished thisection

## Appendix A – Samples and localities

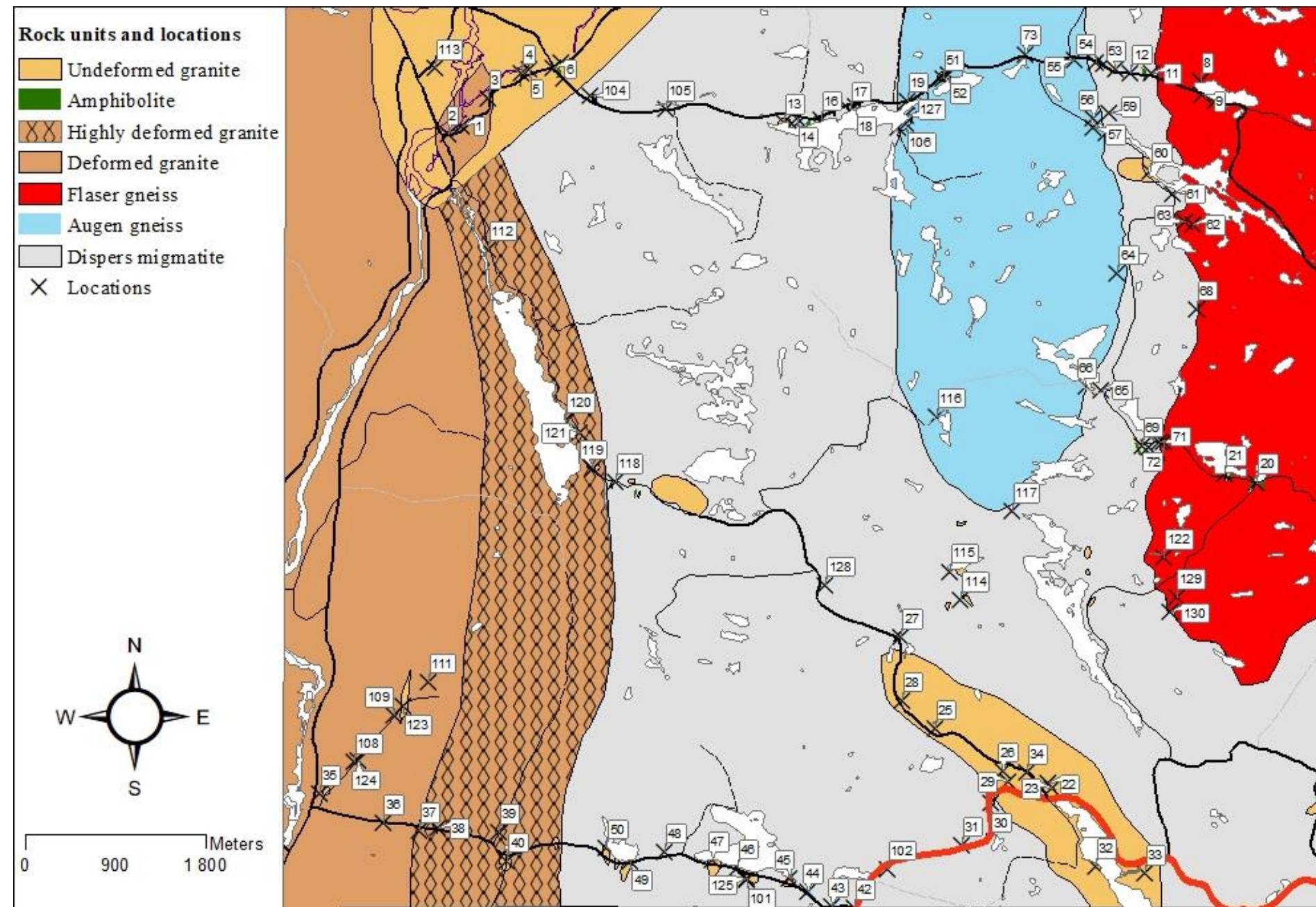


## Appendix A – Samples and localities

---

Locality	East (m)	North (m)	Samples	Locality	East (m)	North (m)	Samples	Locality	East (m)	North (m)	Samples
1	415254	6447761		36	414461	6440757		70	422153	6444524	
2	415123	6447679		37	414826	6440679	HAL193061	71	422255	6444579	
3	415516	6448035		38	415011	6440705		72	422300	6444580	
4	415856	6448288		39	415624	6440662		73	420911	6448479	HAL193059
5	415934	6448322		40	415709	6440377		101	418113	6440193	
6	416167	6448334		42	419193	6439906		102	419528	6440296	
7	416254	6448397		43	418977	6439922		103	416283	6448240	
8	422673	6448203		44	418725	6440065	HAL193058	104	416542	6448058	
9	422684	6448069		45	418545	6440205		105	417304	6447923	HAL193062
10	422818	6448003	HAL193051 & 52	46	418022	6440308		106	419717	6447781	
11	422180	6448286	HAL193053	47	417774	6440382		107	419634	6447737	
12	421972	6448290		48	417292	6440467		108	414170	6441369	
13	418488	6447791		49	416951	6440378		109	414569	6441838	
14	418619	6447836		50	416711	6440508		111	414918	6442172	HAL193063
15	418603	6447759		51	420089	6448232		112	415522	6446519	
16	418858	6447823		52	420146	6448276		113	414981	6448335	
17	419151	6447918		53	421820	6448324		114	420269	6442998	
18	419206	6447948	HAL193054	53	421708	6448377		115	420156	6443283	
19	419728	6448012		54	421625	6448390		116	420021	6444840	
20	423237	6444177	HAL193071	55	421415	6448419		117	420777	6443885	
21	422918	6444260		56	421597	6447832		118	416793	6444179	HAL193064
22	421140	6441154		57	421600	6447738		119	416571	6444321	
23	421183	6441104		58	421725	6447694		120	416297	6444796	
25	420009	6441706		59	421752	6447886		121	416443	6444679	
26	420684	6441283	HAL193055	60	422173	6447302		122	422303	6443423	
27	419666	6442622		61	422399	6447082		123	414667	6441936	HAL193065 & 66
28	419671	6441989		62	422598	6446764		124	414218	6441384	HAL193067
29	420742	6441171		63	422513	6446796		125	418123	6440204	HAL193068
30	420563	6440958	HAL193070	64	421837	6446279		126	418078	6440229	HAL193069
31	420271	6440537		65	421668	6445107		127	419714	6447860	HAL193072
32	421620	6440314		66	421530	6445142		128	418910	6443145	HAL193073
33	422109	6440248		68	422629	6445921		129	422427	6443019	
34	420923	6441265	HAL1953056	69	422086	6444543		130	422361	6442873	
35	413824	6441050	HAL193057								

## Appendix A – Samples and localities



## Appendix B – Geochronological data from SHRIMP

Sample	Analysis #	Comments	Isotopes ratios Terra-Wasserburg output				Age estimates (ma)						Concentrations				
			U238 Pb206		Pb207 $\delta$		Pb207 Pb206		U238 Pb206		$\delta$		conc.	Th/U (ppm)	U238 (ppm)	Th232 (ppm)	f204
			U238	Pb206	$\delta$	Pb206	$\delta$	Pb206	$\delta$	Pb206	$\delta$	conc.					
HAL 193062	62p-4.1	core	6.148	0.137	0.07688	0.00054	1118	14	971	21	13	0.11	694	72	0.114		
	62p-2.2	mag	3.467	0.064	0.09673	0.00030	1562	6	1634	27	-5	0.61	1410	837	0.130		
	62p-1.1	mag	3.520	0.064	0.09631	0.00049	1554	9	1612	26	-4	0.77	550	409	0.174		
	62p-1.2	mag	3.536	0.072	0.09663	0.00062	1560	12	1606	29	-3	0.38	266	99	-0.014		
	62p-5.2	mag	3.652	0.063	0.09693	0.00064	1566	12	1560	24	0	0.67	934	607	0.225		
	62p-3.1	mag	3.668	0.067	0.09715	0.00085	1570	16	1554	25	1	0.34	234	78	0.149		
	62p-2.1	mag	3.677	0.065	0.09635	0.00130	1555	25	1551	25	0	0.65	545	344	0.484		
	62p-5.1	mag/outliner	4.458	0.077	0.09236	0.00032	1475	7	1305	21	12	0.31	1753	527	0.117		
	62n-2.1	mag/outliner	6.588	0.114	0.08106	0.00043	1223	10	911	15	25	0.25	1645	395	0.321		
	62p-4.2	rim	5.871	0.101	0.07284	0.00045	1010	13	1014	16	0	0.05	1522	77	0.066		
	62n-1.1	Too high in common Pb	16.900	25.775	0.62748	0.58005	4573	1339	371	-1141	92	0.01	28892	398	74.623		
HAL 193073	73n-3.1	core	3.952	0.073	0.09322	0.00097	1492	20	1454	25	3	0.42	153	62	0.028		
	73n-5.2	core	3.825	0.078	0.09295	0.00072	1487	15	1497	28	-1	0.42	201	82	0.000		
	73n-9.1	core	4.067	0.070	0.08885	0.00024	1401	5	1417	22	-1	0.86	1839	1536	0.026		
	73p-2.1	core	4.114	0.075	0.09042	0.00078	1434	16	1403	23	2	0.39	231	87	0.112		
	73n-1.3	core/rim	4.334	0.082	0.08961	0.00141	1417	30	1338	23	6	0.32	129	40	0.374		
	73n-1.4	core/rim	4.299	0.096	0.09003	0.00218	1426	46	1348	28	5	0.33	168	53	1.415		
	73n-10.2	core/rim	4.403	0.083	0.08596	0.00183	1337	41	1319	23	1	0.65	171	108	0.718		
	73n-6.1	core/rim	4.347	0.079	0.08874	0.00074	1399	16	1335	22	5	0.36	221	77	-0.042		
	73n-11.1	Discordant	3.745	0.073	0.10049	0.00333	1633	62	1526	27	7	0.44	171	72	3.116		
	73n-2.2	Discordant	4.947	0.154	0.09132	0.00288	1453	60	1187	35	18	0.38	228	83	2.224		
	73n-7.2	Discordant	5.049	0.092	0.08743	0.00188	1370	41	1165	20	15	0.37	227	81	1.306		
	73n-10.1	Discordant	6.041	0.104	0.07528	0.00031	1076	8	987	16	8	0.11	1554	166	0.090		
	73n-4.2	Discordant	5.612	0.133	0.08275	0.00068	1263	16	1057	24	16	0.18	488	83	0.095		
	73n-12.2	no U	-8.073	-18.544	3.35545	4.98813	6891	1983	-852	112	0.02	0	130.348				
	73n-13.1	no U	-20.514	-36.069	1.98431	1.40778	6184	964	-322	105	0.02	0	147.059				
	73n-12.1	reverse discordant	5.473	0.097	0.07080	0.00067	952	19	1082	18	-14	0.05	3125	154	0.215		
	73n-5.1	reverse discordant	5.501	0.095	0.07265	0.00031	1004	9	1077	17	-7	0.03	1808	46	0.130		
	73n-9.2	reverse discordant	5.300	0.091	0.07379	0.00021	1036	6	1114	18	-8	0.03	2210	57	-0.005		
	73n-1.1	rim	5.754	0.099	0.07316	0.00026	1018	7	1033	17	-1	0.04	1741	61	-0.014		
	73n-1.2	rim	5.865	0.107	0.07359	0.00025	1030	7	1015	17	1	0.01	2214	32	0.003		
	73n-1.5	rim	6.080	0.105	0.07268	0.00026	1005	7	982	16	2	0.02	1807	33	0.004		
	73n-10.3	rim	6.424	0.114	0.06955	0.00040	915	12	933	16	-2	0.07	1631	111	0.173		
	73n-11.2	rim	5.739	0.103	0.07298	0.00033	1014	9	1035	17	-2	0.05	1244	65	0.022		
	73n-2.3	rim	5.853	0.102	0.07216	0.00042	991	12	1017	17	-3	0.06	1029	57	0.097		
	73n-3.2	rim	6.139	0.111	0.07253	0.00028	1001	8	973	17	3	0.03	2326	69	0.129		
	73n-6.2	rim	5.720	0.099	0.07350	0.00033	1028	9	1039	17	-1	0.05	1078	57	0.000		
	73n-7.1	rim	4.501	0.082	0.08819	0.00120	1387	26	1293	22	7	0.38	192	70	0.446		
	73p-1.2	rim	6.051	0.105	0.07221	0.00033	992	9	986	16	1	0.03	1164	31	-0.006		
	73p-2.2	rim	5.888	0.103	0.07302	0.00066	1015	18	1011	17	0	0.05	939	45	-0.012		
	73p-3.1	rim	6.040	0.119	0.07323	0.00031	1020	9	988	18	3	0.04	1549	56	0.016		
	73p-1.1	rim/core	5.572	0.097	0.07640	0.00039	1106	10	1064	17	4	0.06	758	47	-0.008		

## Appendix C – Geochronological data from LA-SS-ICP-MS

Sample analysis #	Comments	Isotope ratios										Age estimates (Ma)								Concentrations		
		Concordia output				Terra-Wasserburg output						Age estimates (Ma)										
		Pb207 U235	Pb206 U238	2δ	Pb206 U238	U238 Pb206	2δ	Pb207 Pb206	Pb206 2δ	2δ	Pb207 Pb206	Pb207 2δ	U235 2δ	Pb206 U238	Pb206 2δ	conc.	Th/U (ppm)	Th (ppm)	Pb (ppm)			
HAL 193052	52 - 7		1.581	0.08	0.1624	0.0041	6.157635	0.1554575	0.0705	0.003	943	87	963	31	970	23	3	0.127	546	69.5	28.2	
	52 - 8		1.532	0.092	0.1639	0.0026	6.101281	0.09678665	0.0679	0.0041	866	125	943	36	978	14	12	0.19	272	51.7	21.4	
	52 - 4		1.612	0.083	0.1604	0.0023	6.234414	0.08939621	0.0729	0.0038	1011	106	975	32	959	13	-5	0.245	333	81.7	36.2	
	52 - 1	High LREE	1.777	0.046	0.1737	0.0015	5.757052	0.04971548	0.074	0.002	1041	55	1037	17	1032	8	-1	0.312	1035	323	156	
	52 - 2	High LREE	2.171	0.095	0.2016	0.0032	4.960317	0.0787352	0.0783	0.0034	1154	86	1172	30	1184	17	2	4.708	359	1690	860	
HAL 193056	56a - 1	no clear results	1.73	0.11	0.176	0.0029	5.681818	0.09362087	0.0717	0.0046	977	131	1020	40	1045	16	6	0.233	263	61.2	61.2	
	56a - 2		1.153	0.06	0.1271	0.002	7.867821	0.1238052	0.066	0.0035	806	111	779	28	771	11	-5	0.225	870	196	196	
	56a - 3		1.434	0.044	0.1512	0.002	6.613757	0.08748355	0.0691	0.0022	902	66	903	18	908	11	1	0.333	937	312	312	
	56a - 4		0.844	0.031	0.0951	0.0016	10.51525	0.1769127	0.0644	0.0021	755	69	621	17	586	9	-29	0.113	2028	229	229	
	56a - 5		1.397	0.087	0.1426	0.0047	7.012623	0.2311313	0.0711	0.0037	960	106	888	36	859	26	-12	0.431	462	199	199	
HAL 193061	61 - 1		1.813	0.076	0.1698	0.0022	5.889282	0.076304	0.0769	0.0033	1119	86	1050	27	1011	12	-11	0.709	474.2	336	167.8	
	61a - 2		1.809	0.076	0.1767	0.0026	5.65931	0.08327224	0.0725	0.0034	1000	95	1049	27	1049	14	5	0.434	413	179.4	101	
	61a - 4		1.848	0.072	0.1703	0.0025	5.871991	0.08620068	0.0766	0.0029	1111	76	1063	25	1014	14	-10	0.655	522	342	169.7	
	61a - 5		1.719	0.072	0.171	0.0024	5.847953	0.08207654	0.0711	0.003	960	86	1016	27	1018	13	6	0.474	400	189.5	104.8	
	61a - 6		1.733	0.085	0.1728	0.0025	5.787037	0.08372449	0.0707	0.0034	949	98	1021	31	1028	14	8	0.568	292	166	87.1	
	61a - 7		2.02	0.22	0.1812	0.0033	5.518764	0.1005073	0.0783	0.008	1154	203	1122	71	1074	18	-8	1.06	215	228	151	
	61a - 8		1.842	0.064	0.1753	0.0021	5.704507	0.06833693	0.0744	0.0026	1052	70	1061	23	1041	12	-1	0.568	523	297	159	
	61a - 9		1.72	0.075	0.171	0.0021	5.847953	0.07181697	0.0724	0.0031	997	87	1016	28	1018	12	2	0.312	394	123	57.8	
	61a - 10		1.73	0.1	0.167	0.003	5.988024	0.1075693	0.0746	0.0047	1058	127	1020	37	996	17	-6	0.895	247	221	103	
	61a - 11		1.82	0.16	0.1691	0.0039	5.913661	0.1363884	0.0764	0.0068	1106	178	1053	56	1007	21	-10	0.536	166	89	39.4	
	61a - 12		1.746	0.094	0.1725	0.0024	5.797101	0.08065532	0.073	0.0041	1014	114	1026	34	1026	13	1	0.902	308.3	278	125.7	
	61a - 13		1.69	0.083	0.1695	0.0025	5.899705	0.0870163	0.0717	0.0035	977	99	1005	31	1009	14	3	0.97	299.1	290	130.1	
	61a - 14		1.781	0.07	0.1688	0.002	5.924171	0.07019159	0.0755	0.0029	1082	77	1039	25	1005	11	-8	0.764	360	275	126	
	61a - 15		1.858	0.086	0.1804	0.0027	5.543237	0.08296419	0.0746	0.0035	1058	94	1066	30	1069	15	1	0.547	360	196.8	95.7	
	61a - 16		1.773	0.081	0.1735	0.0029	5.763689	0.09633831	0.0743	0.0034	1050	92	1036	29	1031	16	-2	0.684	249.7	170.7	79.8	
	61a - 17		1.73	0.12	0.1712	0.0032	5.841121	0.1091798	0.0722	0.0051	992	144	1020	44	1019	18	3	0.651	292	190	88	
	61a - 19		1.737	0.064	0.175	0.0023	5.714286	0.07510204	0.073	0.0027	1014	75	1022	23	1040	13	2	0.54	491	265	138.6	
	61a - 1	Discordant	2	0.12	0.1755	0.003	5.698006	0.09740181	0.0807	0.0048	1214	117	1116	40	1042	16	-16	0.792	279	221	125	
	61a - 3	Discordant	2.11	0.13	0.18	0.0024	5.555556	0.07407407	0.0827	0.0048	1262	113	1152	42	1067	13	-18	0.478	343	164	110	
	61a - 18	Discordant	1.713	0.073	0.1554	0.0034	6.435006	0.1407916	0.0795	0.003	1185	75	1013	27	931	19	-27	0.763	532	406	152	

Appendix C – Geochronological data from LA-SS-ICP-MS

Sample	analysis #	Comments	Isotope ratios								Age estimates (Ma)								Concentrations						
			Concordia output				Terra-Wasserburg output				Pb207				Pb207				Pb206				U	Th	Pb
			Pb207	U235	Pb206	2δ	Pb206	U238	Pb206	2δ	Pb207	U235	Pb206	2δ	Pb207	U235	Pb206	2δ	conc.	Th/U	(ppm)	(ppm)	(ppm)		
			U235	2δ	U238	2δ	Pb206	U238	Pb206	2δ	Pb207	U235	Pb206	2δ	Pb207	U235	Pb206	2δ	Th/U	(ppm)	(ppm)	(ppm)			
HAL 193063	63a - 18	discordant	2.03	0.1	0.169	0.0026	5.91716	0.09103323	0.0859	0.0048	1336	108	1126	33	1007	14	-33	0.494	391	193	115.7				
	63a - 24	discordant	2.13	0.11	0.1753	0.0025	5.704507	0.08135349	0.0874	0.0046	1369	101	1159	35	1041	14	-32	0.998	414	413	221				
	63a - 28	discordant	1.588	0.097	0.1489	0.0039	6.715917	0.1759038	0.0765	0.005	1108	131	966	37	895	22	-24	1.051	585	615	182.8				
	63a - 3	discordant	1.947	0.088	0.1686	0.0026	5.931198	0.09146569	0.0817	0.0037	1238	89	1097	30	1004	14	-23	0.823	372	306	182				
	63a - 31	discordant	1.73	0.084	0.1631	0.0026	6.131208	0.09773845	0.0768	0.0036	1116	94	1020	31	974	14	-15	0.571	382	218	95.7				
	63a - 32	discordant	2.07	0.16	0.1827	0.0046	5.473454	0.13781	0.0823	0.0063	1253	150	1139	52	1082	25	-16	0.579	130.9	75.8	40.1				
	63a - 10		1.88	0.11	0.1768	0.0032	5.656109	0.102373	0.0764	0.0048	1106	126	1074	38	1049	18	-5	0.796	177.2	141	75.7				
	63a - 11		1.775	0.092	0.1718	0.0029	5.820722	0.09825433	0.0732	0.0039	1019	108	1036	33	1022	16	0	0.54	287	155	79.5				
	63a - 12		1.789	0.083	0.1684	0.0025	5.938242	0.0881568	0.074	0.0031	1041	85	1041	30	1003	14	-4	0.955	402	384	196				
	63a - 13		1.698	0.058	0.1673	0.0022	5.977286	0.07860149	0.0723	0.0025	994	70	1008	22	997	12	0	0.331	459	151.9	82.7				
	63a - 14		1.594	0.097	0.1699	0.0032	5.885815	0.110857	0.0753	0.0047	1077	125	968	37	1012	18	-6	0.713	230	164	91				
	63a - 15		1.973	0.098	0.1858	0.0025	5.382131	0.07241834	0.0755	0.0037	1082	98	1106	33	1099	14	2	0.712	365	260	149.5				
	63a - 16		1.706	0.076	0.1688	0.0026	5.924171	0.09124907	0.0723	0.003	994	84	1011	28	1005	14	1	0.372	360	134	69.7				
	63a - 17		1.91	0.085	0.1811	0.0031	5.521811	0.09452024	0.0756	0.0034	1084	90	1085	29	1073	17	-1	0.432	347	150	81				
	63a - 19		1.799	0.091	0.1706	0.0029	5.861665	0.09964143	0.0755	0.0039	1082	104	1045	32	1015	16	-7	0.351	318	111.6	57.2				
	63a - 2		1.645	0.091	0.1682	0.0024	5.945303	0.08483191	0.0696	0.004	917	118	988	34	1002	13	9	0.385	311.8	119.9	66.8				
	63a - 21		1.76	0.11	0.1715	0.003	5.830904	0.1019983	0.0735	0.0049	1028	135	1031	40	1020	16	-1	0.574	210	120.6	59.4				
	63a - 22		1.79	0.13	0.1768	0.0034	5.656109	0.1087713	0.0725	0.0054	1000	151	1042	46	1049	19	5	1.009	183	184.7	93.4				
	63a - 23		1.79	0.11	0.1758	0.0035	5.688282	0.1132479	0.0731	0.0047	1017	130	1042	39	1044	19	3	0.646	207	133.8	65.1				
	63a - 25		1.72	0.1	0.174	0.003	5.747126	0.09908839	0.0713	0.0043	966	123	1016	37	1034	16	7	0.54	251	135.5	58.6				
	63a - 26		1.81	0.11	0.1728	0.0032	5.787037	0.1071674	0.0749	0.0042	1066	113	1049	39	1028	18	-4	0.591	191.5	113.2	52.8				
	63a - 27		1.782	0.086	0.1766	0.0028	5.662514	0.08977939	0.0731	0.0037	1017	103	1039	31	1048	15	3	0.38	334	127	58.3				
	63a - 29		1.757	0.094	0.1721	0.003	5.810575	0.1012884	0.0745	0.0043	1055	116	1030	34	1024	16	-3	0.347	270	93.8	44.6				
	63a - 30		1.719	0.087	0.1681	0.0023	5.94884	0.081394	0.0735	0.0036	1028	99	1016	32	1002	13	-3	1.057	343.5	363	156.9				
	63a - 33		1.745	0.082	0.1723	0.003	5.803831	0.1010533	0.0743	0.0036	1050	98	1025	30	1025	16	-2	0.74	288	213.2	111.1				
	63a - 34		1.781	0.068	0.1811	0.0022	5.521811	0.06707888	0.0717	0.0029	977	82	1039	25	1073	12	9	1.007	439	442	225				
	63a - 4		1.906	0.095	0.1746	0.0029	5.727377	0.09512825	0.0777	0.0039	1139	100	1083	33	1037	16	-10	0.306	232.7	71.3	38.5				
	63a - 5		1.571	0.067	0.1729	0.003	5.78369	0.1003532	0.0728	0.0033	1008	92	959	26	1028	16	2	0.642	385	247	131				
	63a - 6		1.741	0.085	0.1657	0.003	6.035003	0.1092638	0.0743	0.0037	1050	100	1024	31	988	17	-6	0.32	388	124	66.7				
	63a - 7		1.661	0.064	0.1684	0.0021	5.938242	0.07405171	0.07	0.0027	928	79	994	24	1003	12	7	0.539	449	242	121.5				
	63a - 8		1.798	0.098	0.178	0.003	5.617978	0.09468501	0.072	0.0041	986	116	1045	35	1056	16	7	0.87	270	235	122				
	63a - 1	discordant	1.88	0.12	0.186	0.0037	5.376344	0.1069488	0.0721	0.0047	989	133	1074	41	1100	20	10	0.861	194.8	167.8	92.3				
	63a - 9	discordant	1.645	0.084	0.1708	0.0025	5.854801	0.08569674	0.0684	0.0035	881	106	988	32	1017	14	13	0.425	356.3	151.4	79				
	63a - 20	discordant	1.81	0.11	0.1854	0.0026	5.393743	0.07564041	0.0696	0.0043	917	127	1049	39	1096	14	16	0.346	276	95.5	50.4				

Appendix C – Geochronological data from LA-SS-ICP-MS

Sample	analysis #	Comments	Isotope ratios								Age estimates (Ma)								Concentrations			
			Concordia output				Terra-Wasserburg output				Pb207				Pb207				Pb206			
			Pb207 U235	Pb206 U238	2δ	Pb207 U238	Pb206	2δ	Pb207 Pb206	Pb206	2δ	Pb207 Pb206	Pb206	2δ	Pb207 U235	Pb207 U238	2δ	conc.	Th/U	U238 (ppm)	Th (ppm)	Pb (ppm)
HAL 193066	66 - 1	outliner	1.87	0.11	0.1833	0.0028	5.455537	0.08333609	0.0743	0.0043	1050	117	1071	38	1085	15	3	0.462	236	109	50.3	
	66 - 2	discordant	1.58	0.1	0.1521	0.0031	6.574622	0.1339995	0.0746	0.0059	1058	159	962	39	913	17	-16	0.484	345	167	93	
	66 - 5	discordant	1.545	0.097	0.1515	0.0028	6.60066	0.1219924	0.0732	0.0045	1019	124	949	38	909	16	-12	0.515	688	354	159	
	66 - 4		1.527	0.081	0.1608	0.0027	6.218905	0.1044219	0.0686	0.0036	887	108	941	32	961	15	8	0.425	367	156	73	
	66 - 6		1.612	0.086	0.1581	0.0035	6.325111	0.1400246	0.0733	0.0041	1022	113	975	33	946	19	-8	0.356	810	288	133	
	66 - 9		1.514	0.089	0.1574	0.003	6.35324	0.121091	0.07	0.0044	928	129	936	35	942	17	1	0.37	324	120	58.9	
	66 - 7		1.479	0.08	0.1546	0.0028	6.468305	0.1171491	0.0691	0.0041	902	122	922	32	927	16	3	0.472	443	209	97.7	
	66 - 3	outliner	1.484	0.064	0.1508	0.0029	6.6313	0.127525	0.0709	0.0033	955	95	924	26	905	16	-5	0.851	685	583	237	
	66 - 10	discordant	1.347	0.084	0.1369	0.0044	7.304602	0.2347717	0.0699	0.0037	925	109	866	36	827	25	-12	0.445	663	295	126	
VAG 084362	VAG62 - 1	high REE	1.859	0.068	0.1669	0.0024	5.991612	0.08615859	0.0801	0.003	1199	74	1067	24	995	13	-21	0.646	560	362	153	
	VAG62 - 10	high REE	1.879	0.088	0.1759	0.0023	5.685048	0.07433548	0.077	0.0038	1121	98	1074	31	1045	13	-7	0.518	372	192.6	93.7	
	VAG62 - 11	high REE	1.636	0.069	0.1665	0.0025	6.006006	0.09018027	0.0799	0.0036	1195	89	984	26	993	14	-20	0.596	406	242	109.6	
	VAG62 - 13	high REE	1.82	0.1	0.176	0.0035	5.681818	0.1129907	0.0747	0.0043	1060	116	1053	35	1045	19	-1	0.431	311	134	58.6	
	VAG62 - 14	high REE	1.604	0.054	0.1681	0.0024	5.94884	0.08493287	0.077	0.0028	1121	73	972	21	1002	13	-12	0.555	416	231	109.5	
	VAG62 - 16	high REE	1.94	0.089	0.175	0.0026	5.714286	0.08489796	0.0791	0.0036	1175	90	1095	30	1040	14	-13	0.466	335	156	79.3	
	VAG62 - 17	high REE	2.05	0.11	0.1832	0.0033	5.458515	0.09832478	0.0808	0.0042	1217	102	1132	36	1084	18	-12	0.476	294	140	68.7	
	VAG62 - 2	high REE	2.001	0.084	0.1742	0.0023	5.740528	0.07579343	0.0826	0.0035	1260	83	1116	28	1035	13	-22	0.645	445	287	136	
	VAG62 - 20	high REE	1.658	0.085	0.1716	0.0031	5.827506	0.1052755	0.078	0.0041	1147	104	993	32	1021	17	-12	0.494	401	198	96.7	
	VAG62 - 21	high REE	1.843	0.068	0.1754	0.0033	5.701254	0.1072642	0.0752	0.0029	1074	77	1061	24	1042	18	-3	0.565	520	294	136	
	VAG62 - 22	high REE	1.993	0.093	0.1699	0.0023	5.885815	0.07967849	0.0833	0.0039	1276	91	1113	31	1012	13	-26	0.48	392	188	96.8	
	VAG62 - 25	high REE	2.21	0.096	0.1739	0.0025	5.750431	0.08266865	0.0909	0.0041	1445	86	1184	30	1034	14	-40	0.56	391	219	119.5	
	VAG62 - 3	high REE	1.726	0.078	0.1704	0.0022	5.868545	0.07576759	0.0824	0.0037	1255	88	1018	29	1014	12	-24	0.519	441	229	108.1	
	VAG62 - 5	high REE	1.96	0.081	0.1727	0.0019	5.790388	0.06370433	0.0811	0.0031	1224	75	1102	27	1027	10	-19	0.627	494.8	310	147.3	
	VAG62 - 23	outliers	1.833	0.076	0.1685	0.0026	5.934718	0.09157429	0.0774	0.0033	1132	85	1057	27	1004	14	-13	0.462	409	189	85.4	
	VAG62 - 24	outliers	1.841	0.07	0.171	0.0028	5.847953	0.09575596	0.0764	0.0029	1106	76	1060	25	1018	15	-9	0.365	394	144	65.8	
	VAG62 - 7	outliers	1.972	0.097	0.1779	0.0029	5.621135	0.09163178	0.0798	0.0039	1192	96	1106	33	1055	16	-13	0.478	339	162	81.2	
	VAG62 - 8	outliers	1.607	0.076	0.1697	0.0028	5.892752	0.09722867	0.0762	0.0036	1100	95	973	29	1010	15	-9	0.544	421	229	110.6	
	VAG62 - 9	outliers	1.995	0.089	0.1816	0.0024	5.506608	0.07277455	0.0787	0.0034	1165	86	1114	30	1076	13	-8	0.433	360	156	77.5	
	VAG62 - 12		1.92	0.12	0.1787	0.0033	5.595971	0.1033391	0.0768	0.0046	1116	120	1088	41	1060	18	-5	0.361	249	90	44.7	
	VAG62 - 15		1.873	0.086	0.1753	0.0022	5.704507	0.07159107	0.077	0.0038	1121	98	1072	30	1041	12	-8	0.516	364	188	91	
	VAG62 - 18		1.829	0.077	0.1758	0.0022	5.688282	0.07118442	0.0745	0.0031	1055	84	1056	27	1044	12	-1	0.512	420	215	95.9	
	VAG62 - 19		1.859	0.09	0.1768	0.0028	5.656109	0.08957638	0.0753	0.0036	1077	96	1067	31	1049	15	-3	0.501	339	170	82.2	
	VAG62 - 4		1.883	0.089	0.1765	0.0026	5.665722	0.08346107	0.0771	0.0038	1124	98	1075	31	1048	14	-7	0.448	359	161	77.3	
	VAG62 - 6		1.9	0.082	0.1788	0.0023	5.592841	0.07194371	0.0768	0.0034	1116	88	1081	28	1060	13	-5	0.534	412	220	104.7	

Appendix C – Geochronological data from LA-SS-ICP-MS

Sample	analysis #	Comments	Isotope ratios								Age estimates (Ma)								Concentrations						
			Concordia output				Terra-Wasserburg output				Pb207				Pb207				Pb206						
			Pb207	U235	Pb206	2δ	Pb206	U238	Pb206	2δ	Pb207	U235	Pb206	2δ	Pb207	U235	Pb206	2δ	Pb206	U238	conc.	Th/U	U (ppm)	Th (ppm)	Pb (ppm)
			Pb207	Pb206	Pb206	2δ	Pb206	Pb206	Pb206	2δ	Pb207	Pb206	Pb206	2δ	Pb207	Pb206	Pb206	2δ	Pb206	Pb206	2δ	Th/U	U (ppm)	Th (ppm)	Pb (ppm)
VAG084363	VAG63 - 12	discordant	2.77	0.13	0.2158	0.0041	4.63392	0.08804019	0.0932	0.0043	1492	87	1347	34	1260	22	-18	0.234	288	67.4	52.8				
	VAG63 - 13	discordant	2.95	0.1	0.2268	0.0027	4.409171	0.05249013	0.0941	0.0034	1510	68	1395	25	1318	14	-15	0.061	385	23.4	15.8				
	VAG63 - 20	discordant	2.78	0.11	0.2199	0.004	4.547522	0.08271981	0.0916	0.0032	1459	66	1350	29	1281	21	-14	0.103	376	38.8	24.9				
	VAG63 - 24	discordant	2.494	0.094	0.2055	0.003	4.86618	0.07103912	0.0867	0.003	1354	67	1270	27	1205	16	-12	0.182	587	107	60.6				
	VAG63 - 25	discordant	2.92	0.21	0.2182	0.0059	4.582951	0.1239203	0.0949	0.0071	1526	141	1387	53	1272	31	-20	0.264	190	50.2	36.8				
	VAG63 - 6	discordant	2.93	0.14	0.2292	0.0033	4.363002	0.06281809	0.0927	0.0047	1482	96	1390	36	1330	17	-11	0.094	335	31.4	27.2				
	VAG63 - 7	discordant	2.43	0.11	0.2049	0.0046	4.880429	0.1095655	0.0871	0.0038	1363	84	1252	32	1202	25	-13	0.201	386	77.7	53.6				
	VAG63 - 1		3.261	0.082	0.2585	0.0019	3.868472	0.02843364	0.0925	0.0023	1478	47	1472	19	1482	10	0	0.644	996	641	467				
	VAG63 - 10		2.85	0.13	0.2266	0.0053	4.413063	0.1032181	0.0905	0.0032	1436	67	1369	34	1317	28	-9	0.299	633	189	127				
	VAG63 - 11		2.833	0.089	0.2329	0.0022	4.293688	0.04055867	0.0883	0.0026	1389	57	1364	23	1350	11	-3	0.176	669	117.8	81.7				
	VAG63 - 14		3.1	0.08	0.2426	0.0023	4.122012	0.03907925	0.0917	0.0021	1461	44	1433	20	1400	12	-4	0.303	917	278	194				
	VAG63 - 15		2.76	0.11	0.2243	0.0044	4.458315	0.08745691	0.0889	0.0035	1402	75	1345	29	1305	23	-7	0.246	411	101	66				
	VAG63 - 16		3.138	0.093	0.247	0.0024	4.048583	0.03933846	0.0919	0.0026	1465	54	1442	23	1423	12	-3	0.234	534	125	89.6				
	VAG63 - 17		3.11	0.11	0.2436	0.0039	4.10509	0.06572189	0.0913	0.0031	1453	65	1435	27	1405	20	-3	0.268	277.7	74.4	53				
	VAG63 - 19		2.74	0.14	0.2307	0.0061	4.334634	0.1146132	0.0856	0.0048	1329	109	1339	37	1338	32	1	0.127	277	35.3	24.8				
	VAG63 - 2		2.99	0.1	0.2406	0.0029	4.156276	0.05009643	0.0903	0.0028	1432	59	1405	25	1390	15	-3	0.203	508	103	72.7				
	VAG63 - 21		3.005	0.079	0.2406	0.0021	4.156276	0.03627672	0.0898	0.0024	1421	51	1409	20	1390	11	-2	0.419	816	342	229.2				
	VAG63 - 22		3.132	0.069	0.2453	0.0022	4.076641	0.0365618	0.0918	0.002	1463	41	1441	17	1414	11	-3	0.249	1036	258	168				
	VAG63 - 23		2.67	0.18	0.221	0.0091	4.524887	0.1863189	0.0844	0.0034	1302	78	1320	49	1287	48	-1	0.257	762	196	128				
	VAG63 - 26		3.526	0.097	0.2679	0.0029	3.732736	0.04040662	0.0937	0.0026	1502	52	1533	22	1530	15	2	0.402	411.3	165.3	119.5				
	VAG63 - 29		2.817	0.069	0.2277	0.0031	4.391744	0.05979097	0.0883	0.002	1389	43	1360	18	1322	16	-5	0.124	957	118.7	84.2				
	VAG63 - 3		2.93	0.14	0.2396	0.0043	4.173623	0.07490224	0.0895	0.0043	1415	92	1390	36	1385	22	-2	0.307	156.2	48	32.3				
	VAG63 - 30		2.792	0.098	0.2256	0.0054	4.432624	0.1061	0.0887	0.0023	1398	50	1353	26	1311	28	-7	0.286	1106	316	214				
	VAG63 - 31		2.35	0.11	0.2066	0.0033	4.840271	0.07731314	0.0815	0.0041	1234	99	1228	33	1211	18	-2	0.206	327	67.3	39.4				
	VAG63 - 32		2.49	0.13	0.2108	0.004	4.743833	0.09001581	0.0838	0.0044	1288	102	1269	37	1233	21	-4	0.128	244	31.3	19.3				
	VAG63 - 4		2.807	0.066	0.2268	0.0022	4.409171	0.04276974	0.0903	0.0023	1432	49	1357	17	1318	12	-9	0.131	905	119	88.6				
	VAG63 - 8		3.404	0.093	0.2568	0.0031	3.894081	0.04700799	0.0962	0.0026	1552	51	1505	21	1473	16	-5	0.407	695	283	194				
	VAG63 - 9		2.89	0.16	0.2347	0.0041	4.260758	0.07443166	0.0892	0.0047	1408	101	1379	41	1359	21	-4	0.245	215.3	52.8	40.4				
	VAG63 - 27	rev. disc.	2.81	0.11	0.2356	0.0027	4.244482	0.0486422	0.0859	0.0036	1336	81	1358	29	1364	14	2	0.196	307.7	60.4	42.6				
	VAG63 - 5	rev. disc.	3.467	0.063	0.2707	0.0023	3.694126	0.03138711	0.0931	0.0017	1490	35	1520	14	1544	12	4	0.827	1140	943	725				
	VAG63 - 18	rev. disc.	3.235	0.077	0.2589	0.002	3.862495	0.02983774	0.0901	0.002	1428	42	1466	18	1484	10	4	0.3	936	281	179				
	VAG63 - 28	rev. disc.	2.62	0.13	0.2275	0.004	4.395604	0.07728535	0.0828	0.0041	1265	97	1306	36	1321	21	4	0.088	276	24.17	19.1				

Appendix C – Geochronological data from LA-SS-ICP-MS

Sample analysis #	Comments	Isotope ratios										Age estimates (Ma)								Concentrations						
		Concordia output				Terra-Wasserburg output						Pb207				Pb207				Pb206				U238	Th	Pb
		Pb207 U235	Pb206 U238	2δ	Pb206 U238	2δ	U238 Pb206	2δ	Pb207 Pb206	2δ	Pb207 Pb206	2δ	U235 Pb206	2δ	U238 Pb206	2δ	conc.	Th/U (ppm)	(ppm)	(ppm)	U238	Th (ppm)	Pb (ppm)			
VAG128010	10a - 10	Discordant	1.573	0.053	0.1113	0.0024	8.984726	0.1937407	0.1048	0.0032	1711	56	960	21	680	14	-151	0.384	1770	679	415					
	10a - 11	Discordant	1.733	0.079	0.1663	0.0037	6.013229	0.133788	0.0771	0.0036	1124	93	1021	29	992	20	-13	0.477	350	167.1	78.4					
	10a - 12	Discordant	2.7	0.11	0.2176	0.0034	4.595588	0.07180607	0.0913	0.0035	1453	73	1328	30	1269	18	-14	0.156	400.9	62.6	50.7					
	10a - 14	Discordant	2.168	0.046	0.1444	0.0014	6.925208	0.0671419	0.1097	0.002	1794	33	1171	15	869	8	-106	0.461	1946	897	611					
	10a - 16	Discordant	0.916	0.033	0.0918	0.0028	10.89325	0.3322559	0.0706	0.0014	946	41	660	17	566	17	-67	0.108	6370	689	272					
	10a - 17	Discordant	1.056	0.041	0.0959	0.0025	10.42753	0.2718334	0.0776	0.0021	1137	54	732	20	590	15	-93	0.419	1688	707	226					
	10a - 2	Discordant	1.275	0.051	0.1232	0.0028	8.116883	0.1844746	0.0766	0.0023	1111	60	835	23	749	16	-48	0.188	1930	363	159.9					
	10a - 20	Discordant	1.886	0.065	0.1699	0.0023	5.885815	0.07967849	0.079	0.0027	1172	68	1076	23	1012	13	-16	0.569	768	437	203					
	10a - 21	Discordant	1.823	0.062	0.1682	0.0019	5.945303	0.0671586	0.0768	0.0028	1116	73	1054	22	1002	10	-11	0.319	489	156	81.9					
	10a - 3	Discordant	1.683	0.087	0.1436	0.0031	6.963788	0.1503325	0.0865	0.0035	1349	78	1002	32	865	17	-56	0.432	843	364	200					
	10a - 4	Discordant	1.54	0.16	0.1133	0.002	8.826125	0.155801	0.099	0.0088	1605	166	947	62	692	12	-132	0.327	1630	533	281					
	10a - 6	Discordant	1.97	0.13	0.1671	0.0025	5.98444	0.08953382	0.0882	0.0055	1387	120	1105	43	996	14	-39	0.578	414	239.2	122.7					
	10a - 8	Discordant	1.432	0.052	0.1236	0.002	8.090615	0.1309161	0.0858	0.0035	1334	79	902	21	751	11	-78	0.427	798	340.4	165.2					
	10a - 9	Discordant	1.83	0.065	0.168	0.0015	5.952381	0.05314626	0.081	0.0029	1221	70	1056	23	1001	8	-22	0.471	690	325	168					
	10a - 15	Outlier	1.61	0.055	0.1601	0.002	6.246096	0.07802744	0.0736	0.0023	1031	63	974	21	957	11	-8	0.355	1078	383	194					
	10a - 13		1.723	0.071	0.1686	0.0025	5.931198	0.08794778	0.0757	0.0033	1087	87	1017	26	1004	14	-8	0.517	505	261	128.5					
	10a - 7		1.842	0.068	0.1767	0.0026	5.65931	0.08327224	0.0769	0.0028	1119	73	1061	24	1049	14	-7	0.453	704	319	158					
	10a - 5		1.716	0.061	0.173	0.0019	5.780347	0.06348358	0.0741	0.0028	1044	76	1015	23	1029	10	-2	0.31	678	210	107					

Appendix C – Geochronological data from LA-SS-ICP-MS

Sample	analysis #	Comments	Isotope ratios								Age estimates (Ma)								Concentrations						
			Concordia output				Terra-Wasserburg output				Pb207				Pb207				Pb206				U	Th	Pb
			Pb207	U235	2δ	Pb206	U238	2δ	Pb206	2δ	Pb207	Pb206	2δ	U235	2δ	U238	2δ	conc.	Th/U	(ppm)	(ppm)	(ppm)			
VAG128011	11a - 1	Pb loss	1.354	0.045	0.1299	0.0022	7.698229	0.130378	0.0736	0.002	1031	55	869	19	787	13	-31	0.374	1330	498	184				
	11a - 12	Pb loss	1.817	0.064	0.1674	0.0022	5.973716	0.07850761	0.0765	0.0022	1108	57	1052	23	998	12	-11	0.34	1580	537	267				
	11a - 13	Pb loss	1.874	0.077	0.1613	0.0024	6.199628	0.09224493	0.0826	0.0031	1260	73	1072	27	964	13	-31	0.731	854	624	310				
	11a - 14	Pb loss	1.501	0.044	0.1402	0.0017	7.132668	0.08648741	0.0759	0.0022	1092	58	931	18	846	10	-29	0.363	1368	497	224.8				
	11a - 15	Pb loss	1.569	0.048	0.1457	0.002	6.863418	0.09421301	0.0766	0.0023	1111	60	958	19	877	11	-27	0.436	1157	505	212.2				
	11a - 16	Pb loss	1.387	0.052	0.148	0.0032	6.756757	0.146092	0.074	0.0022	1041	60	883	22	890	18	-17	0.281	1220	343	150				
	11a - 17	Pb loss	1.444	0.032	0.1381	0.0019	7.24113	0.09962452	0.074	0.0016	1041	44	907	13	834	11	-25	0.225	3100	699	399				
	11a - 18	Pb loss	1.623	0.058	0.1607	0.0023	6.222775	0.08906275	0.0799	0.0027	1195	67	979	22	961	13	-24	0.467	1062	496	256				
	11a - 19	Pb loss	1.589	0.047	0.149	0.0017	6.711409	0.07657313	0.0755	0.0024	1082	64	966	18	895	10	-21	0.282	1112	313.1	136.7				
	11a - 20	Pb loss	1.436	0.032	0.1394	0.0012	7.173601	0.06175266	0.0727	0.0018	1006	50	904	13	841	7	-20	0.411	1640	674	266				
	11a - 24	Pb loss	1.869	0.061	0.1611	0.0031	6.207325	0.1194457	0.0819	0.0026	1243	62	1070	21	963	17	-29	0.503	1076	541	222				
	11a - 26	Pb loss	1.83	0.056	0.1584	0.0024	6.313131	0.0956535	0.0815	0.0026	1234	63	1056	20	948	13	-30	0.239	1634	391.2	243				
	11a - 27	Pb loss	1.624	0.051	0.1399	0.0022	7.147963	0.1124054	0.0824	0.0027	1255	64	980	20	844	12	-49	0.509	1050	534	232.4				
	11a - 28	Pb loss	1.416	0.048	0.1249	0.0017	8.006405	0.1089743	0.0785	0.0025	1160	63	896	20	759	10	-53	0.297	2066	613.4	257.5				
	11a - 29	Pb loss	2.012	0.079	0.1788	0.0021	5.592841	0.06568773	0.0795	0.0033	1185	82	1120	26	1060	11	-12	0.269	560	150.7	94.3				
	11a - 31	Pb loss	1.766	0.044	0.1663	0.002	6.013229	0.07231785	0.075	0.0016	1069	43	1033	16	992	11	-8	0.26	1524	396	201.1				
	11a - 5	Pb loss	1.715	0.053	0.1693	0.0017	5.906675	0.05931097	0.0717	0.0021	977	60	1014	20	1008	9	3	0.193	784	151.4	79.7				
	11a - 7	Pb loss	1.765	0.067	0.1603	0.0027	6.238303	0.1050744	0.0781	0.0028	1149	71	1033	24	958	15	-20	0.473	653	309	156				
	11a - 9	Pb loss	1.492	0.058	0.1428	0.0027	7.002801	0.1324059	0.0732	0.0025	1019	69	927	23	860	15	-18	0.705	833	587	210.8				
	11a - 25		1.943	0.059	0.1835	0.002	5.449591	0.05939609	0.0751	0.0025	1071	67	1096	20	1086	11	1	1.456	654	952	487				
	11a - 4		1.88	0.061	0.1781	0.0022	5.614823	0.06935773	0.0751	0.0023	1071	62	1074	21	1057	12	-1	0.232	668	155.1	81				
	11a - 6		1.937	0.07	0.1822	0.0029	5.488474	0.08735771	0.0753	0.0026	1077	69	1094	24	1079	16	0	0.493	623	307	169				
	11a - 11		2.057	0.073	0.1838	0.0029	5.440696	0.08584341	0.0788	0.0026	1167	65	1135	24	1088	16	-7	0.424	688	292	165				
	11a - 10	discordant	3.15	0.17	0.1829	0.0029	5.467469	0.08669032	0.1208	0.0056	1968	83	1445	41	1083	16	-82	0.52	336	174.6	194.7				
	11a - 2	discordant	1.91	0.13	0.1466	0.0021	6.821282	0.09771278	0.0927	0.0058	1482	119	1085	44	882	12	-68	0.226	1098	248	175				
	11a - 21	discordant	2.98	0.48	0.1744	0.0037	5.733945	0.1216491	0.115	0.016	1880	251	1403	116	1036	20	-81	0.499	1053	525	465				
	11a - 22	discordant	2.609	0.099	0.1793	0.0019	5.577245	0.05910075	0.1026	0.0037	1672	67	1303	27	1063	10	-57	1.03	656	676	398				
	11a - 3	discordant	2.069	0.069	0.1611	0.0022	6.207325	0.08476793	0.0909	0.0025	1445	52	1139	23	963	12	-50	0.31	1300	403	301				
	11a - 30	discordant	2.172	0.084	0.1582	0.0021	6.321113	0.08390857	0.0968	0.0033	1563	64	1172	27	947	12	-65	0.337	1155	389	301				
	11a - 8	discordant	1.926	0.052	0.149	0.0019	6.711409	0.08558173	0.0917	0.0025	1461	52	1090	18	895	11	-63	0.648	755	489	231				

Appendix C – Geochronological data from LA-SS-ICP-MS

Sample	analysis #	Comments	Isotope ratios										Age estimates (Ma)							Concentrations				
			Concordia output					Terra-Wasserburg output					Pb207				Pb207			Pb206		U	Th	Pb
			Pb207 U235	Pb206 U238	2δ	Pb206 U238	2δ	U238 Pb206	2δ	Pb207 Pb206	2δ	U235 Pb206	2δ	U238 Pb206	2δ	conc.	Th/U (ppm)	(ppm)	(ppm)	U	Th (ppm)	Pb (ppm)		
VAG 128012	12a - 1	No clear results	1.647	0.044	0.1612	0.0016	6.203474	0.06157294	0.0724	0.002	997	56	988	17	963	9	-4	0.206	1133	233	107.5			
	12a - 10		1.811	0.054	0.1678	0.0022	5.959476	0.07813377	0.0767	0.0021	1113	55	1049	19	1000	12	-11	0.173	1229	213	110.8			
	12a - 11		1.66	0.046	0.1528	0.0017	6.544503	0.07281187	0.0779	0.0021	1144	54	993	17	917	9	-25	0.322	2103	678	281			
	12a - 12		1.351	0.053	0.1108	0.0016	9.025271	0.1303288	0.0868	0.0032	1356	71	868	23	677	9	-100	0.366	1491	546	202.1			
	12a - 13		1.778	0.047	0.1523	0.0025	6.565988	0.1077805	0.0832	0.0024	1274	56	1037	17	914	14	-39	0.372	1174	437	184			
	12a - 14		1.729	0.055	0.1543	0.0023	6.480881	0.09660419	0.0799	0.0024	1195	59	1019	20	925	13	-29	0.252	1129	284	136.2			
	12a - 15		1.31	0.031	0.1186	0.0025	8.431703	0.177734	0.0884	0.0018	1391	39	850	14	723	14	-93	0.181	2552	463	287			
	12a - 16		1.227	0.038	0.1144	0.0019	8.741259	0.1451782	0.0767	0.0024	1113	62	813	17	698	11	-59	0.26	1573	409	160.4			
	12a - 2		1.697	0.05	0.1524	0.0029	6.56168	0.1248614	0.0792	0.0023	1177	57	1007	19	914	16	-29	0.34	1455	494	213			
	12a - 3		1.529	0.048	0.1442	0.0023	6.934813	0.1106107	0.0753	0.0018	1077	48	942	19	868	13	-24	0.234	1853	433	190			
	12a - 4		1.692	0.049	0.1588	0.003	6.297229	0.1189653	0.0756	0.0017	1084	45	1006	18	950	17	-14	0.253	1440	364	165.4			
	12a - 5		1.717	0.054	0.152	0.0037	6.578947	0.1601454	0.0803	0.0022	1204	54	1015	20	912	21	-32	0.297	1282	381	179			
	12a - 6		1.747	0.052	0.1588	0.0038	6.297229	0.1506894	0.079	0.0024	1172	60	1026	19	950	21	-23	0.271	1266	343	180.3			
	12a - 7		1.758	0.043	0.1647	0.0016	6.071645	0.0589838	0.076	0.0018	1095	47	1030	16	983	9	-11	0.303	1282	389	180.2			
	12a - 8		1.815	0.05	0.1702	0.0016	5.875441	0.05523328	0.0754	0.0021	1079	56	1051	18	1013	9	-7	0.308	1153	355	159			
	12a - 9		2.65	0.14	0.1888	0.0027	5.299661	0.07574601	0.0982	0.0043	1590	82	1315	38	1115	15	-43	0.234	796	186	193.9			
VAG 128014	14a - 1	Uncertain source	3.565	0.086	0.2672	0.0022	3.742515	0.03081412	0.0956	0.0023	1540	45	1542	19	1527	11	-1	0.357	623	222.5	155.6			
	14a - 10		3.58	0.1	0.2576	0.0031	3.881988	0.04671647	0.1	0.003	1624	56	1545	22	1478	16	-10	0.448	449	201	149			
	14a - 11		3.148	0.075	0.2427	0.0025	4.120313	0.04244245	0.093	0.0022	1488	45	1445	18	1401	13	-6	0.474	717	340	230			
	14a - 12		3.54	0.12	0.2608	0.0027	3.834356	0.03969617	0.0972	0.0032	1571	62	1536	26	1494	14	-5	0.369	347	128	91.2			
	14a - 13		3.58	0.14	0.2612	0.0032	3.828484	0.04690333	0.099	0.0041	1605	77	1545	31	1496	16	-7	0.453	359	162.7	113.5			
	14a - 14		3.62	0.14	0.2629	0.0036	3.803728	0.05208604	0.099	0.0039	1605	73	1554	30	1505	18	-7	0.472	384	181.2	124.3			
	14a - 15		3.636	0.099	0.2618	0.0028	3.81971	0.04085251	0.0995	0.0027	1615	51	1557	21	1499	14	-8	0.515	478	246	164.2			
	14a - 16		3.526	0.088	0.2565	0.0025	3.898635	0.0379984	0.0981	0.0028	1588	53	1533	20	1472	13	-8	0.475	555	263.9	173.8			
	14a - 17		3.45	0.11	0.2521	0.0036	3.96668	0.05664438	0.0983	0.0032	1592	61	1516	25	1449	19	-10	0.363	598	217	144			
	14a - 18		3.57	0.12	0.257	0.0033	3.891051	0.04996291	0.0997	0.0036	1618	67	1543	26	1474	17	-10	0.381	300.9	114.7	78.2			
	14a - 19		3.592	0.094	0.2613	0.0027	3.827019	0.0395444	0.099	0.0027	1605	51	1548	21	1496	14	-7	0.288	590	170	123			
	14a - 2		3.88	0.18	0.2753	0.0037	3.632401	0.04881905	0.1005	0.0044	1633	81	1610	37	1568	19	-4	0.424	300.2	127.4	95.8			
	14a - 20		3.91	0.11	0.2741	0.003	3.648304	0.03993036	0.1025	0.003	1670	54	1616	22	1562	15	-7	0.403	407.5	164.2	123.9			
	14a - 3		3.57	0.18	0.2634	0.0043	3.796507	0.06197791	0.0968	0.0046	1563	89	1543	39	1507	22	-4	0.401	222	89	61.5			
	14a - 4		3.53	0.11	0.2559	0.0028	3.907776	0.04275801	0.0989	0.0029	1603	55	1534	24	1469	14	-9	0.508	535	272	178			
	14a - 6		3.725	0.098	0.2743	0.0033	3.645643	0.04385936	0.0967	0.0024	1561	47	1577	21	1563	17	0	0.232	639	148	99			
	14a - 7		3.25	0.11	0.2418	0.003	4.135649	0.05131079	0.0963	0.0035	1554	68	1469	26	1396	16	-11	0.361	427	154.1	102.9			
	14a - 8		3.54	0.11	0.2624	0.0032	3.810976	0.04647531	0.0969	0.0034	1565	66	1536	24	1502	16	-4	0.497	336	167	110.4			
	14a - 9		3.69	0.13	0.2633	0.0031	3.797949	0.04471569	0.1006	0.0035	1635	65	1569	28	1507	16	-9	0.521	293.2	152.8	106			

Appendix C – Geochronological data from LA-SS-ICP-MS

Sample	analysis #	Comments	Isotope ratios										Age estimates (Ma)						Concentrations							
			Concordia output					Terra-Wasserburg output					Pb207			Pb207			Pb206					U	Th	Pb
			Pb207 U235	Pb206 2δ	Pb206 U238	Pb206 2δ	U238 Pb206	Pb207 U235	Pb206 2δ	Pb207 Pb206	Pb207 2δ	U235 Pb206	Pb207 2δ	U238 Pb206	Pb206 2δ	conc.	Th/U	(ppm)	(ppm)	(ppm)						
VAG 128015	15a - 1	No clearer results	1.652	0.062	0.1676	0.0037	5.966587	0.1317206	0.0737	0.0021	1033	58	990	23	999	20	-3	0.451	1070	482.8	238.3					
	15a - 2		1.381	0.049	0.1166	0.0042	8.576329	0.3089244	0.0887	0.0022	1398	48	881	21	711	24	-97	0.251	2201	552	352.3					
	15a - 3		1.546	0.055	0.1506	0.0038	6.640106	0.1675458	0.0761	0.002	1098	53	949	22	904	21	-21	0.248	2120	525	239					
	15a - 4		1.315	0.074	0.1297	0.0047	7.7101	0.2793945	0.0744	0.0021	1052	57	852	32	786	27	-34	0.187	2006	376	140.1					
	15a - 5		2.193	0.082	0.1512	0.0021	6.613757	0.09185773	0.1091	0.0045	1784	75	1179	26	908	12	-97	0.478	502	240.1	195.2					
	15a - 6		1.106	0.032	0.1098	0.002	9.107468	0.165892	0.0749	0.0016	1066	43	756	15	672	12	-59	0.249	2970	741	291					
	15a - 7		2.228	0.082	0.1994	0.0027	5.015045	0.06790683	0.0834	0.0031	1279	72	1190	25	1172	14	-9	0.271	536	145.2	100.6					
	15a - 8		1.483	0.062	0.1423	0.0037	7.027407	0.1827225	0.0773	0.0021	1129	54	923	25	858	21	-32	0.175	1476	259	102.4					
	15a - 9		2.18	0.25	0.1468	0.003	6.811989	0.1392096	0.108	0.011	1766	186	1175	77	883	17	-100	0.438	1430	626	388					
	15a - 10		1.412	0.062	0.1144	0.0023	8.741259	0.1757421	0.092	0.0036	1467	74	894	26	698	13	-110	0.395	1560	616	286					
	15a - 11		1.372	0.023	0.1331	0.0014	7.513148	0.07902635	0.0768	0.0011	1116	29	877	10	806	8	-39	0.32	4850	1550	592					
	15a - 12		1.156	0.052	0.1169	0.0033	8.55432	0.2414821	0.0735	0.0024	1028	66	780	24	713	19	-44	0.228	1729	395	158.1					
	15a - 13		1.466	0.086	0.1048	0.0044	9.541985	0.4006177	0.1042	0.0042	1700	74	916	35	642	26	-165	0.305	712	217	140.1					
	15a - 14		0.797	0.019	0.09001	0.00098	11.10988	0.1209608	0.0735	0.0016	1028	44	595	11	556	6	-85	0.289	3150	910	307					
	15a - 15		1.628	0.066	0.162	0.0041	6.17284	0.1562262	0.0753	0.0029	1077	77	981	25	968	23	-11	0.5	760	380	178					
	15a - 16		1.753	0.04	0.1634	0.0018	6.119951	0.06741684	0.0803	0.0016	1204	39	1028	15	976	10	-23	0.282	2596	731	354					
	15a - 18		1.215	0.032	0.1264	0.0014	7.911392	0.08762618	0.0716	0.0017	975	48	807	15	767	8	-27	0.328	2130	699	242					
	15a - 20		1.17	0.061	0.1175	0.0049	8.510638	0.3549117	0.0751	0.0023	1071	62	787	28	716	28	-50	0.117	1413	164.8	112.1					
	15a - 21		1.204	0.059	0.1105	0.0044	9.049774	0.360353	0.0906	0.0027	1438	57	802	27	676	25	-113	0.255	1590	405	221					
	15a - 22		1.2	0.029	0.1133	0.0013	8.826125	0.1012706	0.0785	0.0018	1160	45	801	13	692	8	-68	0.212	2911	617	307					
	15a - 23		2.012	0.056	0.1707	0.0036	5.858231	0.1235479	0.0847	0.0012	1309	27	1120	19	1016	20	-29	0.261	3340	871	550					
	15a - 24		0.886	0.024	0.0908	0.0011	11.01322	0.13342	0.0705	0.0021	943	61	644	13	560	6	-68	0.192	2510	482	138.3					
	15a - 25		1.31	0.051	0.1109	0.002	9.017133	0.1626174	0.0847	0.0031	1309	71	850	22	678	12	-93	0.177	1020	180.8	135.7					
	15a - 26		0.783	0.024	0.078	0.0013	12.82051	0.2136752	0.0808	0.0016	1217	39	587	14	484	8	-151	0.276	4550	1254	516					
	15a - 27		1.695	0.095	0.1474	0.0064	6.784261	0.2945676	0.0836	0.0043	1283	100	1007	35	886	36	-45	0.272	1400	381	240					

Appendix C – Geochronological data from LA-SS-ICP-MS

Sample analysis #	Comments	Isotope ratios								Age estimates (Ma)								Concentrations					
		Concordia output				Terra-Wasserburg output				Pb207/Pb206				Pb207/Pb206				U		Th		Pb	
		Pb207 U235	2δ	Pb206 U238	2δ	U238 Pb206	2δ	Pb207 Pb206	2δ	Pb207 Pb206	2δ	U235	2δ	Pb206 U238	2δ	conc.	Th/U (ppm)	(ppm)	(ppm)	(ppm)	(ppm)	(ppm)	
VAG128016	16a - 11	discordant	2.18	0.21	0.2147	0.0064	4.657662	0.1388404	0.0748	0.0078	1063	210	1175	65	1254	34	15	0.574	79.8	45.8	29		
	16a - 16	discordant	2.13	0.21	0.1875	0.0057	5.333333	0.1621333	0.0835	0.0081	1281	189	1159	66	1108	31	-16	0.39	78.8	30.7	19.1		
	16a - 18	discordant	2.49	0.2	0.1998	0.0052	5.005005	0.1302604	0.0912	0.008	1451	167	1269	57	1174	28	-24	0.421	145	61	41.3		
	16a - 22	discordant	2.02	0.22	0.184	0.0056	5.434783	0.1654064	0.087	0.01	1360	221	1122	71	1089	30	-25	0.463	367	170	104		
	16a - 25	discordant	1.98	0.11	0.1943	0.0034	5.14668	0.09006028	0.0728	0.0043	1008	120	1109	37	1145	18	12	0.357	264	94.2	55.7		
	16a - 30	discordant	2.45	0.12	0.2259	0.0046	4.426737	0.09014162	0.0774	0.0038	1132	98	1257	35	1313	24	14	0.484	182	88	56.3		
	16a - 34	discordant	2.04	0.17	0.2049	0.0045	4.880429	0.1071837	0.0696	0.0057	917	168	1129	55	1202	24	24	0.29	121	35.1	21.1		
	16a - 39	discordant	2.16	0.21	0.2078	0.0063	4.81232	0.145898	0.0758	0.0074	1090	196	1168	65	1217	34	10	0.463	74.1	34.3	21.7		
	16a - 41	discordant	2.38	0.14	0.2218	0.0043	4.508566	0.08740683	0.0761	0.0046	1098	121	1237	41	1291	23	15	0.503	185	93	56		
	16a - 5	discordant	2.41	0.14	0.2048	0.0031	4.882812	0.07390976	0.0861	0.0052	1340	117	1246	41	1201	17	-12	0.307	193.3	59.3	35.7		
	16a - 2	outliner	1.87	0.13	0.1779	0.0042	5.621135	0.1327081	0.0745	0.0051	1055	138	1071	45	1055	23	0	0.193	145.4	28.1	15.8		
	16a - 3	outliner	2.21	0.19	0.1953	0.0051	5.120328	0.1337106	0.0828	0.007	1265	165	1184	58	1150	27	-10	0.284	139.3	39.57	29.9		
	16a - 35	outliner	2.05	0.14	0.1926	0.0037	5.192108	0.09974455	0.0761	0.0052	1098	137	1132	46	1135	20	3	0.348	174	60.6	36.5		
	16a - 36	outliner	2.07	0.1	0.1989	0.0031	5.027652	0.07835959	0.0749	0.0037	1066	99	1139	33	1169	17	9	0.345	262	90.3	52.8		
	16a - 37	outliner	2.08	0.11	0.1963	0.0036	5.094244	0.09342474	0.076	0.0041	1095	108	1142	36	1155	19	5	0.343	250	85.7	52.8		
	16a - 1		2.38	0.11	0.2118	0.003	4.721435	0.06687585	0.0819	0.0038	1243	91	1237	33	1238	16	0	0.309	300.7	93	53.8		
	16a - 10		2.4	0.21	0.2182	0.0061	4.582951	0.128121	0.082	0.0074	1246	177	1243	61	1272	32	2	0.573	84.1	48.2	30.9		
	16a - 12		2.38	0.22	0.2173	0.0055	4.601933	0.1164778	0.0815	0.0083	1234	200	1237	64	1268	29	3	0.57	87.3	49.8	29.4		
	16a - 13		2.26	0.12	0.2082	0.0034	4.803074	0.07843637	0.0807	0.0042	1214	102	1200	37	1219	18	0	0.297	243	72.1	44.7		
	16a - 14		2.421	0.091	0.2135	0.0028	4.683841	0.06142742	0.0821	0.0031	1248	74	1249	27	1247	15	0	0.214	410.1	87.8	58		
	16a - 15		2.31	0.17	0.2041	0.0044	4.899559	0.105625	0.0827	0.0062	1262	146	1215	51	1197	24	-5	0.402	117.6	47.3	30.4		
	16a - 17		2.29	0.13	0.2123	0.004	4.710316	0.08874829	0.0789	0.0048	1170	120	1209	39	1241	21	6	0.544	231	125.6	76.5		
	16a - 19		2.49	0.12	0.2243	0.0035	4.458315	0.069568	0.0799	0.0039	1195	96	1269	34	1305	18	8	0.558	206	115	76.6		
	16a - 20		2.34	0.1	0.202	0.0025	4.950495	0.0612685	0.0842	0.0034	1297	79	1225	30	1186	13	-9	0.449	414.7	186	131.5		
	16a - 21		2.4	0.11	0.2117	0.0029	4.723666	0.06470775	0.0818	0.0036	1241	86	1243	32	1238	15	0	0.752	315	237	147.5		
	16a - 23		2.57	0.19	0.221	0.0058	4.524887	0.1187527	0.0824	0.0052	1255	123	1292	53	1287	31	2	0.46	146	67.1	42.6		
	16a - 24		2.16	0.2	0.2059	0.0054	4.856727	0.1273741	0.078	0.0079	1147	201	1168	62	1207	29	5	0.472	76.5	36.1	22.3		
	16a - 26		2.39	0.11	0.2128	0.0028	4.699248	0.06183221	0.0812	0.0039	1226	94	1240	32	1244	15	1	0.661	274	181	112.4		
	16a - 27		2.42	0.1	0.205	0.0031	4.878049	0.07376562	0.0838	0.0032	1288	74	1249	29	1202	17	-7	0.424	288.2	122.2	79		
	16a - 28		2.38	0.18	0.2116	0.0049	4.725898	0.1094371	0.0807	0.0065	1214	158	1237	53	1237	26	2	0.586	112.8	66.1	40.5		
	16a - 29		2.42	0.12	0.2079	0.0035	4.810005	0.08097651	0.0835	0.0041	1281	96	1249	35	1218	19	-5	0.462	275	127.1	79.1		
	16a - 31		2.27	0.22	0.2097	0.0062	4.768717	0.1409921	0.0776	0.0071	1137	182	1203	66	1227	33	7	0.212	187	39.7	24.9		
	16a - 32		2.44	0.16	0.2166	0.0043	4.616805	0.09165403	0.0812	0.0053	1226	128	1254	46	1264	23	3	0.551	166	91.5	54		
	16a - 33		2.36	0.18	0.2151	0.0043	4.649	0.09293678	0.079	0.0062	1172	155	1231	53	1256	23	7	0.642	110.7	71.1	45.3		
	16a - 38		2.37	0.14	0.2131	0.0039	4.692633	0.08588112	0.0795	0.0051	1185	127	1234	41	1245	21	5	0.536	194	104	65.6		
	16a - 4		2.29	0.15	0.2047	0.0039	4.885198	0.09307412	0.0814	0.0055	1231	133	1209	45	1201	21	-3	0.491	125.1	61.4	36.9		
	16a - 40		2.57	0.18	0.2252	0.0044	4.440497	0.08675927	0.0811	0.0057	1224	138	1292	50	1309	23	7	0.457	134.2	61.3	40.6		
	16a - 6		2.58	0.29	0.2196	0.0068	4.553734	0.1410082	0.0858	0.0098	1334	221	1295	79	1280	36	-4	0.544	47.6	25.9	15		
	16a - 7		2.41	0.12	0.2133	0.0032	4.688233	0.07033448	0.0825	0.0042	1257	100	1246	35	1246	17	-1	0.636	233	148.2	88		

Appendix C – Geochronological data from LA-SS-ICP-MS

Sample analysis #	Comments	Isotope ratios										Age estimates (Ma)						Concentrations					
		Concordia output				Terra-Wasserburg output						Pb207			Pb207			Pb206			U238	Th	Pb
		Pb207 U235	Pb206 U238	2δ	Pb206 U238	2δ	U238 Pb206	Pb206 U238	2δ	Pb207 Pb206	Pb206 U238	2δ	Pb207 U235	Pb207 U238	2δ	conc.	Th/U (ppm)	(ppm)	(ppm)				
VAG128017	17a - 5	outlier	3.13	0.11	0.2507	0.003	3.988831	0.04773232	0.0908	0.003	1442.4	63	1440.1		1442.1	15	-0.02	0.281	408	114.5	71.9		
	17a - 13	outlier	3.19	0.16	0.2501	0.0059	3.998401	0.09432453	0.0922	0.0039	1471.5	80.3	1454.7		1439	30	-2.26	0.314	474	149	103		
	17a - 19	outlier	2.702	0.086	0.2291	0.0032	4.364906	0.0609677	0.0859	0.0027	1335.9	60.8	1329		1329.8	17	-0.46	0.213	572	122	78.4		
	17a - 6	outlier	2.581	0.085	0.2176	0.0023	4.595588	0.04857469	0.0853	0.0025	1322.4	56.8	1295.3		1269.2	12	-4.19	0.266	535	142.4	94.7		
	17a - 17	outlier	2.39	0.15	0.2167	0.0042	4.614675	0.08943993	0.0793	0.0046	1179.6	115	1239.6		1264.4	22	6.71	0.458	179.7	82.3	45		
	17a - 25	outlier	2.27	0.12	0.2158	0.0042	4.63392	0.09018751	0.0771	0.0043	1123.8	111	1203		1259.6	22	10.8	0.333	214	71.3	41.6		
	17a - 16	outlier	2.32	0.12	0.2135	0.0038	4.683841	0.08336578	0.0792	0.0041	1177.1	102	1218.4		1247.4	20	5.64	0.377	256	96.6	55.7		
	17a - 11	discordant	2.55	0.11	0.2081	0.0033	4.805382	0.0762026	0.0885	0.0036	1393.4	78	1286.4		1218.7	18	-14.3	0.542	343	186	107.9		
	17a - 8	outlier	2.3	0.12	0.2079	0.0053	4.810005	0.1226216	0.0802	0.0035	1201.9	86	1212.3		1217.6	28	1.29	0.233	451	105	63.5		
	17a - 18	outlier	2.25	0.13	0.2063	0.0043	4.84731	0.1010346	0.0786	0.0042	1162.1	106	1196.8		1209.1	23	3.89	0.308	253	77.9	44.7		
	17a - 26		2.235	0.098	0.203	0.0031	4.926108	0.07522629	0.0799	0.0032	1194.5	79	1192.1		1191.4	17	-0.26	0.368	535	197	111		
	17a - 9		2.167	0.092	0.1973	0.0036	5.068424	0.09248011	0.0794	0.0031	1182.1	77.2	1170.5		1160.8	19	-1.84	0.476	450	214	121		
	17a - 10		2.16	0.11	0.1962	0.0035	5.09684	0.09092222	0.0802	0.0041	1201.9	101	1168.3		1154.9	19	-4.07	0.316	267	84.4	47.9		
	17a - 4		2.178	0.084	0.195	0.0028	5.128205	0.07363577	0.0814	0.0033	1231.1	79.6	1174		1148.4	15	-7.2	0.267	439	117	56.8		
	17a - 3		2.156	0.09	0.1938	0.003	5.159959	0.07987552	0.0812	0.0034	1226.3	82.2	1167		1141.9	16	-7.39	0.159	328.6	52.3	29.4		
	17a - 1		2.197	0.093	0.1929	0.0023	5.184033	0.06181066	0.0832	0.0036	1273.9	84.4	1180.1		1137.1	12	-12	0.281	368	103.3	53.7		
	17a - 30		2.165	0.075	0.1925	0.0026	5.194805	0.0701636	0.0818	0.003	1240.7	71.9	1169.9		1134.9	14	-9.32	0.217	471	102	59.2		
	17a - 21		2.04	0.13	0.1921	0.0046	5.205622	0.1246531	0.0759	0.0046	1092.4	121	1129		1132.7	25	3.56	0.254	563	143	82		
	17a - 7		1.954	0.091	0.1913	0.0036	5.227392	0.09837224	0.0751	0.0037	1071.2	99	1099.8		1128.4	19	5.07	0.02	501	9.8	6.2		
	17a - 31		2.143	0.084	0.1897	0.0023	5.271481	0.06391358	0.0824	0.0033	1255	78.3	1162.8		1119.7	12	-12.1	0.228	457	104.3	67.7		
	17a - 22		2.097	0.079	0.1882	0.0023	5.313496	0.06493646	0.0803	0.003	1204.4	73.6	1147.8		1111.6	12	-8.34	0.07	507	35.5	29.3		
	17a - 20		2.004	0.085	0.1864	0.0028	5.364807	0.08058723	0.0776	0.0032	1136.7	82	1116.9		1101.8	15	-3.16	0.124	400	49.6	28.7		
	17a - 23	outlier	1.873	0.067	0.1827	0.0023	5.473454	0.068905	0.0742	0.0026	1046.9	70.7	1071.6		1081.7	13	3.22	0.036	499	17.9	11		
	17a - 2	outlier	2.051	0.076	0.1825	0.0023	5.479452	0.06905611	0.0815	0.003	1233.5	72.2	1132.6		1080.6	13	-14.2	0.129	572	73.8	38.4		
	17a - 15	discordant	2.167	0.098	0.1793	0.0027	5.577245	0.08398528	0.0872	0.0036	1364.9	79.5	1170.5		1063.1	15	-28.4	0.081	514	41.4	30.1		
	17a - 28	outlier	1.808	0.045	0.1773	0.0015	5.640158	0.04771707	0.0741	0.002	1044.2	54.4	1048.4		1052.2	8	0.76	0.014	1249	17.37	12.2		
	17a - 14	outlier	1.925	0.062	0.177	0.0019	5.649718	0.06064669	0.0786	0.0025	1162.1	63	1089.8		1050.6	10	-10.6	0.149	724	108	53.1		
	17a - 12	outlier	1.816	0.069	0.1736	0.0023	5.760369	0.07631825	0.0755	0.0027	1081.8	71.7	1051.2		1031.9	13	-4.84	0.206	558	115	59.6		
	17a - 27	outlier	1.878	0.064	0.1728	0.0025	5.787037	0.08372449	0.0787	0.0023	1164.6	57.9	1073.4		1027.5	14	-13.3	0.244	962	235.2	99.3		
	17a - 29	outlier	1.765	0.07	0.1691	0.0017	5.913661	0.05945135	0.0757	0.0028	1087.1	74.1	1032.7		1007.2	9	-7.94	0.038	647.6	24.73	12.9		
	17a - 24	outlier	2.25	0.29	0.1531	0.0028	6.531679	0.1194559	0.104	0.011	1696.7	195	1196.8		918.32	16	-84.8	0.451	1101	497	283		

Appendix C – Geochronological data from LA-SS-ICP-MS

Sample	analysis #	Comments	Isotope ratios								Age estimates (Ma)								Concentrations			
			Concordia output				Terra-Wasserburg output				Pb207				Pb207				Pb206			
			Pb207 U235	Pb206 U238	2δ	Pb206 U238	2δ	U238 Pb206	2δ	Pb207 Pb206	Pb206 2δ	2δ	U235 U238	2δ	U238 2δ	conc.	Th/U	U (ppm)	Th (ppm)	Pb (ppm)		
VAG128018	18a - 12	outlier	3.62	0.12	0.2645	0.0032	3.780718	0.04574026	0.0966	0.0031	1559	60	1554	26	1513	-3	0.341	372	127	98.1		
	18a - 15	outlier	3.56	0.17	0.2546	0.0041	3.92773	0.06325095	0.0988	0.0049	1602	93	1541	37	1462	-10	0.356	171.4	61.1	45.7		
	18a - 16	outlier	3.55	0.16	0.2647	0.004	3.777862	0.05708896	0.0944	0.0043	1516	86	1538	35	1514	0	0.366	252	92.3	73.6		
	18a - 17	outlier	3.25	0.2	0.2517	0.0067	3.972984	0.1057568	0.0902	0.0047	1430	99	1469	47	1447	1	0.232	260	60.3	45.9		
	18a - 3	outlier	3.73	0.14	0.2677	0.0034	3.735525	0.0474441	0.0995	0.0039	1615	73	1578	30	1529	-6	0.309	287.9	89	66		
	18a - 7	outlier	4.06	0.14	0.2873	0.0039	3.480682	0.04724908	0.1005	0.0037	1633	68	1646	28	1628	0	0.316	254	80.3	64.5		
	18a - 8	outlier	3.87	0.16	0.2845	0.0042	3.514938	0.05189013	0.096	0.004	1548	78	1607	33	1614	4	0.288	275	79.3	61.1		
	18a - 9	outlier	2.92	0.14	0.2304	0.0054	4.340278	0.1017253	0.0903	0.0046	1432	97	1387	36	1337	-7	0.333	264	87.8	54.1		
	18a - 1		3.72	0.14	0.2771	0.0037	3.608805	0.04818687	0.0959	0.0036	1546	71	1576	30	1577	2	0.322	286	92.2	68.2		
	18a - 10		3.74	0.14	0.2724	0.0035	3.671072	0.04716869	0.0974	0.0039	1575	75	1580	30	1553	-1	0.271	275	74.4	60.4		
	18a - 11		3.7	0.18	0.2792	0.0047	3.581662	0.06029302	0.0943	0.0051	1514	102	1571	38	1587	5	0.319	139.7	44.5	35.4		
	18a - 13		3.75	0.16	0.2794	0.0038	3.579098	0.04867778	0.0941	0.004	1510	80	1582	34	1588	5	0.306	267	81.6	70.3		
	18a - 14		3.76	0.2	0.2734	0.0048	3.657644	0.06421614	0.0966	0.005	1559	97	1584	42	1558	0	0.309	169	52.3	41.5		
	18a - 18		3.67	0.19	0.2721	0.0051	3.675119	0.06888316	0.0946	0.0049	1520	98	1565	40	1551	2	0.33	145.9	48.1	40.5		
	18a - 19		3.87	0.18	0.2753	0.0052	3.632401	0.06861055	0.0993	0.0044	1611	83	1607	37	1568	-3	0.352	210	73.9	60.1		
	18a - 2		3.69	0.1	0.2708	0.0027	3.692762	0.03681853	0.0968	0.0027	1563	52	1569	21	1545	-1	0.419	510	213.5	156.7		
	18a - 20		3.74	0.16	0.2799	0.0042	3.572705	0.05360971	0.0946	0.0041	1520	82	1580	34	1591	4	0.315	207.3	65.3	53.1		
	18a - 21		3.61	0.15	0.2757	0.0042	3.627131	0.05525553	0.0928	0.0041	1484	84	1552	33	1570	5	0.255	277	70.5	58.2		
	18a - 22		3.7	0.14	0.2749	0.0036	3.637686	0.04763795	0.0949	0.0036	1526	71	1571	30	1566	3	0.395	267.8	105.7	82.4		
	18a - 23		3.66	0.17	0.2733	0.0046	3.658983	0.06158551	0.095	0.0044	1528	87	1563	36	1558	2	0.242	221	53.5	43.8		
	18a - 4		3.87	0.17	0.2765	0.0046	3.616637	0.06016827	0.1006	0.0048	1635	89	1607	35	1574	-4	0.295	152.3	44.9	33		
	18a - 5		3.76	0.16	0.2781	0.003	3.595829	0.03878996	0.0974	0.0046	1575	88	1584	34	1582	0	0.38	272.1	103.4	78.2		
	18a - 6		3.78	0.1	0.2735	0.0028	3.656307	0.03743203	0.0976	0.0027	1579	52	1589	21	1559	-1	0.422	489.3	206.7	152		

Appendix C – Geochronological data from LA-SS-ICP-MS

VAG 128019	19a - 3	discordant	1.591	0.053	0.1485	0.0026	6.734007	0.1179018	0.0758	0.0017	1089.8	44.9	966.69		892.55	15	-22.1	0.239	1800	431	221
	19a - 44		2.2	0.1	0.1946	0.0032	5.138746	0.08450148	0.0837	0.0039	1285.6	90.7	1181		1146.2	17	-12.2	0.418	282.9	118.2	67.1
	19a - 7	discordant	2.408	0.097	0.2194	0.0031	4.557885	0.06440038	0.0778	0.0031	1141.8	79.2	1245		1278.7	16	10.7	0.328	389	127.7	78.1
	19a - 4	discordant	2.046	0.093	0.1975	0.0027	5.063291	0.06921968	0.0735	0.0033	1027.8	90.8	1131		1161.9	15	11.5	0.37	386.8	143.1	87.3
	19a - 13	discordant	1.89	0.11	0.1893	0.0048	5.28262	0.1339492	0.0713	0.0037	966.03	106	1077.6		1117.6	26	13.6	0.241	319	76.8	44.4
	19a - 8	discordant	1.97	0.12	0.2099	0.0045	4.764173	0.1021381	0.0744	0.0046	1052.3	125	1105.3		1228.3	24	14.3	0.531	177	94	58.4
	19a - 47		2.51	0.13	0.219	0.0033	4.56621	0.0688059	0.0858	0.0049	1333.7	110	1274.9		1276.6	17	-4.47	0.401	213.3	85.5	49.3
	19a - 45		2.45	0.13	0.214	0.004	4.672897	0.08734387	0.0837	0.0045	1285.6	105	1257.4		1250.1	21	-2.84	0.392	167.1	65.5	38.9
	19a - 21		2.5	0.11	0.2157	0.0033	4.636069	0.07092734	0.0831	0.004	1271.6	93.9	1272		1259.1	17	-0.99	0.302	265	79.9	49.1
	19a - 35		2.43	0.12	0.2139	0.0033	4.675082	0.07212609	0.0825	0.0042	1257.4	99.5	1251.5		1249.6	18	-0.63	0.382	256.2	97.8	59.3
	19a - 6		2.5	0.1	0.2147	0.0031	4.657662	0.06725082	0.0824	0.0035	1255	83.1	1272		1253.8	16	-0.1	0.318	267	84.9	53.1
	19a - 36		2.437	0.094	0.2154	0.0028	4.642526	0.06034852	0.0823	0.0033	1252.7	78.4	1253.6		1257.5	15	0.39	0.391	416	162.8	99.3
	19a - 33		2.34	0.15	0.2124	0.0049	4.708098	0.1086143	0.0813	0.0055	1228.7	133	1224.5		1241.6	26	1.04	0.333	115.9	38.6	24.7
	19a - 34		2.343	0.093	0.2121	0.0025	4.714757	0.05557234	0.0804	0.0031	1206.8	75.9	1225.4		1240	13	2.68	0.365	408.4	148.9	88.5
	19a - 9		2.4	0.12	0.2135	0.0027	4.683841	0.05923358	0.0804	0.0039	1206.8	95.5	1242.6		1247.4	14	3.26	0.378	267.9	101.2	62.5
	19a - 30		2.35	0.17	0.2137	0.0041	4.679457	0.08977901	0.0797	0.0059	1189.6	146	1227.6		1248.5	22	4.72	0.435	135.5	59	35.6
	19a - 27		2.36	0.069	0.2129	0.0023	4.697041	0.05074304	0.0795	0.0025	1184.6	62.1	1230.6		1244.2	12	4.79	0.346	574	198.4	127.2
	19a - 37		2.331	0.097	0.2132	0.0029	4.690432	0.06380043	0.0795	0.0032	1184.6	79.5	1221.8		1245.8	15	4.91	0.315	472	148.7	89.7
	19a - 1		2.37	0.11	0.2131	0.0029	4.692633	0.06386032	0.0794	0.0038	1182.1	94.6	1233.6		1245.3	15	5.07	0.408	270.8	110.4	66.7
	19a - 25		2.4	0.18	0.2179	0.006	4.589261	0.1263679	0.0803	0.0062	1204.4	152	1242.6		1270.8	32	5.23	0.404	110.2	44.5	28.4
	19a - 32		2.32	0.11	0.2137	0.004	4.679457	0.08758928	0.0793	0.004	1179.6	99.7	1218.4		1248.5	21	5.52	0.283	192.6	54.46	37.2
	19a - 24		2.38	0.12	0.2149	0.0035	4.653327	0.07578709	0.0793	0.0041	1179.6	102	1236.6		1254.9	19	6	0.402	224.8	90.3	58.5
	19a - 39		2.35	0.12	0.2171	0.0037	4.606172	0.07850225	0.0796	0.0044	1187.1	109	1227.6		1266.5	20	6.27	0.375	197.6	74.1	45.2
	19a - 5		2.305	0.098	0.2118	0.0028	4.721435	0.06241746	0.0773	0.0033	1128.9	85	1213.8		1238.4	15	8.84	0.368	386	142	86.8
	19a - 15		2.422	0.066	0.2186	0.0022	4.574565	0.04603863	0.0784	0.0023	1157	58.2	1249.1		1274.5	12	9.22	0.302	718	216.8	137.3
	19a - 10	Population 2	1.917	0.083	0.1818	0.0024	5.50055	0.07261452	0.0748	0.0032	1063.1	86.1	1087		1076.8	13	1.27	0.261	388.7	101.4	60.9
	19a - 20	Population 2	1.78	0.11	0.1757	0.0033	5.69152	0.1068982	0.0719	0.0043	983.11	122	1038.2		1043.4	18	5.78	0.854	219	187	44.3
	19a - 19	Population 2	1.819	0.068	0.1794	0.0022	5.574136	0.06835618	0.0718	0.0027	980.28	76.6	1052.3		1063.7	12	7.84	0.191	524	100.3	63.7
	19a - 23		2.51	0.2	0.2201	0.0054	4.543389	0.1114689	0.0823	0.0071	1252.7	169	1274.9		1282.4	28	2.32	0.463	110.5	51.2	33.3
	19a - 38		2.442	0.098	0.2224	0.0035	4.496403	0.07076174	0.0802	0.0032	1201.9	78.6	1255.1		1294.5	18	7.16	0.36	283	102	62.5
	19a - 28		2.46	0.13	0.2225	0.0037	4.494382	0.07473804	0.0798	0.0045	1192	111	1260.4		1295.1	19	7.95	0.515	231	119	81.9
	19a - 22		2.43	0.14	0.2203	0.0037	4.539265	0.07623822	0.079	0.0046	1172.1	115	1251.5		1283.5	20	8.67	0.432	196.5	84.8	56
	19a - 26		2.31	0.2	0.197	0.0046	5.076142	0.1185292	0.0821	0.0069	1247.9	165	1215.4		1159.2	25	-7.65	0.333	152.4	50.8	33.9
	19a - 43		2.29	0.11	0.2028	0.0046	4.930966	0.1118464	0.0831	0.0035	1271.6	82.2	1209.2		1190.3	25	-6.82	0.187	385	72.1	42.6
	19a - 31		2.23	0.11	0.1983	0.0032	5.042864	0.08137754	0.0818	0.0042	1240.7	101	1190.5		1166.2	17	-6.39	0.382	277	105.7	59.2
	19a - 48		2.023	0.095	0.1886	0.0032	5.302227	0.08996355	0.0794	0.0037	1182.1	92.1	1123.3		1113.8	17	-6.14	0.29	296	85.9	47.1
	19a - 46		2.39	0.12	0.2101	0.0032	4.759638	0.0724933	0.0838	0.0039	1287.9	90.6	1239.6		1229.4	17	-4.76	0.508	214.7	109.1	63.3
	19a - 41		2.13	0.17	0.2102	0.0044	4.757374	0.09958347	0.0824	0.0066	1255	157	1158.6		1229.9	23	-2.05	0.438	166	72.7	43.8
	19a - 40		2.25	0.13	0.2047	0.004	4.885198	0.09546063	0.0804	0.0045	1206.8	110	1196.8		1200.5	21	-0.52	0.416	205.2	85.3	54.6
	19a - 18		2.2	0.12	0.1992	0.0035	5.02008	0.08820422	0.0791	0.0044	1174.6	110	1181		1171	19	-0.31	0.346	247.2	85.5	53.8
	19a - 49		2.04	0.12	0.1948	0.0035	5.13347	0.09223381	0.0779	0.0048	1144.3	122	1129		1147.3	19	0.26	0.357	183.4	65.4	37.6
	19a - 16		2.21	0.11	0.2001	0.0031	4.997501	0.07742256	0.0788	0.004	1167.1	101	1184.2		1175.9	17	0.74	0.304	285.2	86.8	52.8
	19a - 14		2.26	0.14	0.2054	0.0043	4.868549	0.1019219	0.0786	0.005	1162.1	126	1199.9		1204.3	23	3.5	0.398	137.1	54.6	34.5
	19a - 17		2.238	0.094	0.2036	0.0034	4.911591	0.08202068	0.0781	0.0035	1149.4	89	1193		1194.6	18	3.78	0.272	302	82	53
	19a - 2		1.999	0.08	0.1906	0.0023	5.24659	0.06331142	0.0752	0.0031	1073.9	82.8	1115.2		1124.6	12	4.51	0.211	389.4	82	48.1
	19a - 11		2.1	0.14	0.1965	0.0037	5.089059	0.09582451	0.0759	0.0052	1092.4	137	1148.8		1156.5	20	5.54	0.312	170.4	53.1	31.7
	19a - 12		2.04	0.1	0.1946	0.0031	5.138746	0.08186081	0.0746	0.0039	1057.7	105	1129		1146.2	17	7.72	0.185	292.2	54.1	32.2
	19a - 42		1.96	0.14	0.2089	0.0038	4.786979	0.08707765	0.0767	0.0053	1113.4	138	1101.9		1223	20	8.96	0.409	194	79.4	45.9

## Appendix D – Trace element data

Sample	analysis #	Ti	La	Ce	Pr	Nd	Sm	Eu	Gd	Dy	Yb	Lu	Pb204	Pb206	Pb207	Pb208	Th	U
HAL 193052	52a - 1	95	-1.95	30.5	2.91	14.6	14	1.22	51.6	223	605	106	0.4	1413	589	117.3	314	1091
	52a - 2	381	-0.506	132	17.1	205	208	11.7	231	249	245	39.7	0.45	510	215	547	1370	339
	52a - 4	29	-0.019	0.7	0.043	0.52	0.03	0.178	1.25	7.56	47.4	11.35	0.11	373.5	140.8	23.5	69.4	297.3
	52a - 7	65	-0.033	1.14	0.151	1.03	0.69	0.226	1.7	7.79	46.6	11.17	0.13	797	262	19.2	64.1	617
	52a - 8	29	-0.031	0.92	0.002	0.54	-0.09	-0.003	0.97	6.06	34.3	8.22	0.15	546	169	20.1	66.7	391
HAL 193056	56a - 1	4.5	-0.021	32.3	0.32	3.9	3.73	1.13	11.9	45.1	164.4	33.6	0.24	395	118.1	39.8	118.6	248.9
	56a - 2	57	-7.17	144	21.7	107	53.8	9.9	92	234	480	82.8	0.084	1482	398	162	677	1245
	56a - 3	16	-5.63	114	12.34	64.3	32.1	6.16	61.4	144.7	305.4	61.6	-0.09	1456	394	229.9	783	1028
	56a - 4	95	-9.21	133.4	21.7	100.8	37.7	6.3	59.4	170	545	115.4	-0.11	2203	534	178.7	836	2398
	56a - 5	51	-16.7	175	24.1	108	38.5	7.6	66.2	186	379	71.1	0.48	1235	309	238.7	950	900
HAL 193061	61a - 1	342	-10.4	135	20.1	60	21.7	4.55	33.1	87	254	49.85	0.04	431.3	292	120.1	303	448.9
	61a - 1	66	-7.84	86	19.3	32.9	12.3	2.85	27	69.1	183	35.9	-0.08	190.7	120.4	85.6	180	251
	61a - 10	23	-2.11	65.3	5.7	22.9	13.6	4.1	34.5	92.5	246	48.2	0.1	303	205	102	274	331
	61a - 11	29	-0.78	36	1.67	6.1	4.3	1.52	14.6	48.2	148.3	30.1	-0.64	228.8	160	40.5	111	245.5
	61a - 12	41.6	-1.47	64.5	3.33	14.7	12.3	3.21	28.6	85.8	221.7	44.4	0.23	292.9	191	94.7	258	303.6
	61a - 13	3.3	-0.081	44.1	1.74	14.5	16.8	5.45	46.3	132.2	295.3	56.3	0.37	255.9	159.4	84.8	238.6	263.9
	61a - 14	79	-5.6	117	23.2	79	33.1	5.97	40.7	96.3	231	43.5	0.15	334	217	90	246	339
	61a - 15	16.2	-0.93	36.4	3.01	12.7	7.1	1.99	19	58.3	187	40.01	0.07	348.2	216	65.4	168	331.2
	61a - 16	17.2	-0.61	34.3	1.11	9.5	9.9	2.73	25.9	80.7	202.9	40	-0.12	231.4	140.7	54.8	146.7	226
	61a - 17	11.8	-0.183	33.6	1.34	8.9	9.3	3.15	28.1	80	202	40.5	0.24	326	184	66.4	179	320
	61a - 18	132	-5.91	130	21.9	69.5	25.9	5.24	33.6	81.6	240	49.8	0.4	522	326	118.9	402	562
	61a - 19	25.2	-1.61	55.8	3.02	19.7	10	2.41	20.4	66.4	211.2	44.2	-0.18	1330	161.9	68.4	216.7	430
	61a - 2	7.5	-0.58	32.3	4.69	10.3	4.63	1.11	9	26.4	123.6	27.94	-0.01	281.2	162.8	72.4	153.1	365.6
	61a - 3	1080	-0.92	36.4	2.78	7.7	5.6	1.88	19.1	59.3	159	32.5	-0.11	242.9	163.1	73.8	129	309
	61a - 4	55	-7.04	180	65.5	130	58.3	10.8	70.9	143	263	49.1	-0.23	355.1	226.2	121.1	293	479.2
	61a - 5	17	-0.595	38.3	4.17	8.9	6.5	1.63	15.8	49.5	166.9	36.04	-0.07	277.8	180.7	72.7	160.8	367.4
	61a - 6	13.3	-0.062	35.6	0.55	2.34	3.27	0.75	10	37.7	142	29.3	-0.21	203	132.5	59.5	141	263
	61a - 7	240	-0.29	40.9	2.85	13.7	13.5	4.09	37.2	106.3	248	48.5	0.01	159.5	121	97	190	198.2
	61a - 8	15.7	-1.3	53	5.7	10.9	5.7	1.32	13.3	43.9	184.1	40.4	-0.05	377.5	269	108	251	482
	61a - 9	5.5	-0.243	26	1.04	3.61	3.59	1.2	12.7	43.4	171.9	37.1	-0.22	391	267	45.5	121.2	424

## Appendix D – Trace element data

Sample	analysis #	Ti	La	Ce	Pr	Nd	Sm	Eu	Gd	Dy	Yb	Lu	Pb204	Pb206	Pb207	Pb208	Th	U
HAL 193063	63a - 1	1.1	-0.057	35.3	1.75	8.3	9.8	2.62	27.9	87.6	230.3	44.4	0.02	147.5	100.6	61.5	141.7	176.9
	63a - 10	13.8	-1.5	41.9	2.99	11.3	10.4	3.18	33.5	100.3	245	45.8	0.43	158	124	58.8	145	192
	63a - 11	3.9	-0.213	37.8	0.86	3.56	5.2	1.4	13.9	49.6	170.7	34.61	0.56	235.3	177	58	144.9	291
	63a - 12	10.1	-0.326	61.6	3.41	18	20.8	6.7	60.7	167	391	74.8	0.24	312	244	139	349	393
	63a - 13	5.6	-4.63	46.4	10.2	20	5.8	1.43	12.4	38.7	150.7	32.71	0.17	322.7	242.1	53.1	124.9	407.3
	63a - 14	25.8	-0.53	41.3	1.85	7.3	4.76	1.28	14.7	49.7	151.1	30.8	0.09	170.9	136	58.5	134	206
	63a - 15	23.8	-1.9	59.4	6.73	16.9	11.4	2.56	26.7	80.2	232.4	48.3	0.37	342	267	113.8	248	382
	63a - 16	9.6	-0.58	29.6	1.76	5.3	3.39	1.36	12.8	44.4	174.8	36.64	0.14	303	225	46.7	115.7	374
	63a - 17	17.4	-1.42	42.1	4.1	11.1	6.7	1.78	17.7	58.4	182.8	38.9	0.23	314	240	57.6	136.4	347
	63a - 18	1760	-1	41.1	3.68	10.5	8.6	1.86	18	56.9	197.8	41.5	0.07	368	328	93.2	171.7	433
	63a - 19	2.5	-0.006	23.8	-0.05	0.83	1.29	0.364	4.3	21.1	112.5	25.84	0	229.7	175	34.7	85.8	263
	63a - 2	5.8	-1.84	30.2	4	6.8	2.8	0.8	8.72	27.8	113.5	25.22	0.37	221.2	149.3	45.4	102	292.6
	63a - 20	-3.2	-0.055	23.96	0.035	0.77	1.13	0.272	3.42	15.2	78.2	17.19	-0.14	228.3	157.8	32.2	76.6	237.6
	63a - 21	10.2	-0.06	33.2	0.78	6.1	8.5	2.42	25.4	79.6	196	36.8	0.01	200.6	145.3	48.1	123.5	223.6
	63a - 22	27.5	-0.125	30.9	1.56	10.4	11.4	4.57	37.5	110.8	267	51.5	0.22	154.3	108.8	62.5	156.6	165.8
	63a - 23	-2.2	-0.135	24.7	1.01	7.1	6.9	2.42	23.4	72.5	182	36	-0.09	174.4	121.9	43.7	114.4	185.8
	63a - 24	27.6	-6.9	100.5	12.1	35.7	19.3	4.64	45.1	129	306	58.3	0.49	347	283	144	335	369
	63a - 25	8.9	-0.089	29.7	0.53	4.39	6.3	1.51	19.7	65.6	177.2	35.1	-0.1	276.5	151.3	47.5	139	261.4
	63a - 26	9.3	-0.81	37.4	2.14	10	8.2	2.74	20.4	55.6	141	27.4	0.16	213.1	107.7	39	106	183.4
	63a - 27	9.5	-0.6	29.4	1.07	6.4	5.7	1.63	17	58.5	167	33.4	-0.16	366.4	175.2	35.6	98	306.1
	63a - 28	630	-5.78	132	19.1	74.6	29.6	5.55	39	105.6	252	50.3	0.18	599	295	139.3	610	609.5
	63a - 29	12.8	-0.118	19.44	0.27	3.51	4.92	1.35	12.6	35.1	111.4	23.69	0.06	318.5	147.4	32.8	87.2	265.8
	63a - 3	22.8	-12.6	113	24.8	40.8	17.3	3.61	32.7	91.8	232.9	44.7	0.16	282	229	134	286	365
	63a - 30	14.4	-1.3	88.4	3.66	23	17.9	4.75	46.7	130.2	276	51.6	0.27	410	180	112.8	336	342
	63a - 31	12.8	-1.86	48.5	4.28	19	8	1.64	16.3	54.3	181.9	36.9	0.65	455	210	69.4	201	388
	63a - 32	4.9	-0.243	25.8	0.54	4.4	4.68	1.41	12.8	42.5	124.9	25.65	-0.11	214.9	103.1	34.5	84.2	161.5
	63a - 33	1.7	-1.59	50.5	1.8	16.9	11.4	2.82	28.5	91.3	240.9	46.7	-0.08	733	100.6	58	179.8	260.1
	63a - 34	7.5	-1.27	64.8	2.37	20.9	15.9	4.37	37.3	116.7	323.7	65.7	0.07	1274	161.9	119	382	410.6
	63a - 4	-1.9	0.004	16.69	0.39	3.16	2.76	1.38	9.9	33.7	104.2	22	-0.15	169.5	130.4	27.2	63.3	214
	63a - 5	1.7	-0.81	52.8	3.13	6.9	5.9	1.3	15.3	59.8	207	40.8	-0.42	289	209	86.8	207	358
	63a - 6	1.9	-0.149	24.4	0.5	2.58	3.3	0.78	11.5	40.5	171.6	35.35	0.59	308	233	45.9	108.7	406
	63a - 7	-8.6	-0.98	38.9	1.99	5.3	3.37	1.24	11.7	41.9	187.1	43.4	0.54	361.8	256.5	91.8	233.5	467.8
	63a - 8	8.8	-0.194	28.2	1.44	7.7	10	3.02	29.8	82.4	208	40.4	0.15	194.3	145	77.7	189	242
	63a - 9	-2.7	-10.3	84	21	42.6	13.4	2.8	26.9	72.6	203.7	41.8	0.39	275.5	192.7	57.3	140.3	346.9
HAL 193066	66 - 1	2.7	-0.192	26.8	0.146	2.59	2.25	0.56	7.3	25.4	104.4	22.8	0.4	405.9	106.1	28.1	88	220.4
	66 - 10	11.2	-4.3	66.9	7.3	37.9	12.9	3.27	20.9	80	349	79.8	0.15	2001	214	77	304	769
	66 - 2	5	-0.85	28	0.87	6	3.9	1.2	9.2	39.5	212	52.6	0.28	654	161	70	161	407
	66 - 3	6.2	-3.85	166	5.6	25.4	12	1.89	28.3	108.2	402	83.1	0.42	1158	269	161.1	579	738
	66 - 4	10.1	-0.701	39.6	1.1	8.1	6.8	1.21	14.8	51.2	213.3	49.9	-0.14	1090	183	46.3	153	515
	66 - 5	8.4	-2.07	119	2.96	16.3	7.6	1.29	18.9	65.4	317	75.7	-0.14	1436	244	95.3	334	721
	66 - 6	0.19	-12.6	104	14.5	72	16.2	1.73	23.6	57.7	273	65.3	-0.12	1742	288	77.5	257	808
	66 - 7	5.2	-1.98	49	2.24	17.9	9.5	1.87	20.4	68.3	255	58.4	-0.04	1202	176.1	71.4	238.2	544
	66 - 9	3.9	-3.14	63	3.97	19.2	6.4	1.26	15.4	55.2	235.9	55.8	-0.18	1400	191	50.9	163.8	572

## Appendix D – Trace element data

Sample	analysis #	Ti	La	Ce	Pr	Nd	Sm	Eu	Gd	Dy	Yb	Lu	Pb204	Pb206	Pb207	Pb208	Th	U
VAG 084362	VAG62 - 1	6.8	-1.31	63.2	4.11	21	13.6	3	33.5	106.7	281	55.3	-0.09	773	62.9	166	304	515
	VAG62 - 10	5.6	-1.19	43.2	2.66	11.1	7.8	1.41	21	68.5	196.8	38.2	0	404.1	47.3	98.3	165.2	338
	VAG62 - 11	9.5	-1.53	51.9	4.72	22.2	13.2	3.21	26.7	76.2	192	37.3	0.35	415	52.8	111.2	202	365
	VAG62 - 12	6.9	-0.125	21.8	0.47	1.8	2.22	0.68	9.4	31.6	118	24.1	0.13	267	34.9	47.8	79.3	230
	VAG62 - 13	5.9	-0.56	25.5	1.92	8.6	5.2	1.22	12.2	40.6	112	22	0.17	277	43.9	55.4	106	277
	VAG62 - 14	-3.4	-0.94	42.9	2.66	10.5	8.8	1.73	22.4	73.1	203	38.9	0.2	373	62.8	110.4	200	379
	VAG62 - 15	3.9	-0.158	29.4	0.5	4.13	3.69	0.93	13	51.3	163	30.8	-0.22	324	56.4	86.4	154	329
	VAG62 - 16	7.2	-1.81	34.9	2.89	8.8	5.4	1.01	12.2	43.1	128	25.7	0.02	291	54	76.1	130	302
	VAG62 - 17	9.6	-1.49	39.7	6.4	19.7	10.9	2.4	20.5	52.5	132.6	26.8	0.42	272.4	53.3	66.7	121	275
	VAG62 - 18	9.9	-0.11	36.2	0.48	4.05	4.51	0.8	16.6	65.2	187.5	35.7	-0.03	362	67.4	93.4	182.7	385
	VAG62 - 19	8.9	-0.178	32	0.6	3.63	4.75	0.83	15.4	56.6	169	31.9	-0.08	292	57.1	81.2	148	311
	VAG62 - 2	7	-2.07	64.1	5.25	26.1	15	3.65	32	96.1	224	42.2	0.48	633	55.2	151	249	416
	VAG62 - 20	12.2	-1.02	32.6	1.65	6.3	3.82	1	13.6	50.6	154	31.2	0.17	324	67.2	90.5	163	355
	VAG62 - 21	7.2	-0.59	44.3	2.56	8.4	6.2	1.39	24.2	81.5	227	43.2	0.13	430	89.8	129	248	480
	VAG62 - 22	8.6	-0.74	34.9	3.52	12.1	6.4	1.62	17.1	55.5	156	30.3	0.06	303	72	91.4	159	348
	VAG62 - 23	5.1	-0.062	31.9	0.39	2.95	3.64	0.79	14.5	58.7	175.1	35	0.23	326	75	82	163	383
	VAG62 - 24	6.4	-0.095	20.4	0.54	2.73	3.14	0.54	8.3	30.4	100.4	20.6	-0.37	346	79.9	61.7	121.8	408
	VAG62 - 25	1.6	-3.23	61.6	10.6	29.8	10.2	2.5	21.6	65.1	171.8	32.5	0.34	306	86.9	111.1	184	351
	VAG62 - 3	13.8	-0.55	39	1.63	7.9	5.95	1.39	19.4	67	191.6	36.9	-0.06	593	55.1	118.2	196.7	404
	VAG62 - 4	4.6	-0.025	23.2	0.208	2.14	3.02	0.51	10.5	43.2	141	28.3	-0.01	476	42.6	84.4	136.7	332
	VAG62 - 5	7.2	-6.9	61.6	3.11	14.2	9.7	2.08	29.9	99.4	258	48.1	0.46	621	62.3	161.3	270	458
	VAG62 - 6	2	-0.091	36.5	0.41	4.09	4.38	1.18	18.9	68.4	214	41.6	-0.17	512	51.1	111.8	189	375
	VAG62 - 7	38	-0.238	30.6	0.74	4.9	4.8	1.05	14.7	51.9	149	29	0.3	409	44.6	86.4	139	309
	VAG62 - 8	2.5	-0.129	36.7	0.35	2.86	4.52	0.93	17.8	69.5	208	40.1	-0.08	484	52.8	119	199	386
	VAG62 - 9	1.7	0.0036	28	0.133	1.65	3.46	0.66	13.3	50.1	163	32.4	0.12	419	49	79.8	130.2	330.7

VAG 084363	VAG63 - 1	103	-2.85	103	5.9	26.8	33.9	1.15	126.7	526	1316	238.3	-0.09	-5.33E+04	-1154	2816	503	852
	VAG63 - 10	26.9	-2.11	32.7	3.13	10.9	6.6	0.61	16.6	90.2	480	95.2	0.32	-6140	564	529	151	619
	VAG63 - 11	26.1	-2.11	123	2.19	7.6	3.73	0.265	14.5	80	376.2	79.3	-0.72	-5910	506	355	101.2	616
	VAG63 - 12	41	-0.98	10.38	1.13	7.6	10.5	1.35	40.9	153	395	78.8	0.19	-2282	198	234	60.8	277
	VAG63 - 13	18.4	-1.44	10.4	2.05	7.9	4.45	0.66	10.5	40.7	201.8	51	0.08	-3020	261	61.1	18.8	367
	VAG63 - 14	77	-1.82	39	2.56	12.1	10.2	0.52	40.3	202.2	740	146.5	0.26	-6560	541	744	223.8	792
	VAG63 - 15	18.7	-0.59	16.3	0.75	4.3	5.4	0.079	23.5	107	369	71.4	0.2	-2660	210	247	81	363
	VAG63 - 16	19.6	-0.084	17.9	0.334	2.41	3.3	0.089	19.1	106	460	91.7	0.17	-3596	289.6	353	107.6	477.2
	VAG63 - 17	15.8	-13.3	52	8.5	30.6	14.6	1.34	38.8	142.1	383.4	78.3	-0.15	-1940	154.4	224	71.8	274.1
	VAG63 - 18	54	-2.23	43.4	3.45	14.5	12.3	0.46	43.9	198.9	681	135.2	-0.55	-5980	465	638	226.5	834
	VAG63 - 19	11.2	-6.26	19.5	3.02	8.1	4.6	0.75	14.2	61.3	210	42.9	0.05	-1362	100.2	87.8	28.42	231
	VAG63 - 2	21.9	-1.28	21.3	1.77	6.37	3.87	0.35	16.5	89.8	401	80.3	0.85	-28000	-898	531	100.7	605
	VAG63 - 20	70	-4.7	18.9	2.93	10.1	7.26	1.43	19.7	72.5	245.3	52.06	0.1	-1840	144.1	90.3	33.33	334.9
	VAG63 - 21	44.5	-5.4	80.7	6.86	25.1	14.6	0.72	46.3	187.4	533.6	106.3	-0.47	-4426	341	858	306	772.1
	VAG63 - 22	46.3	-5.38	48.6	7.22	32.8	16.3	1.37	42.5	171	620	123.5	0.41	-5010	394	573	213	897
	VAG63 - 23	28	-0.47	25.9	0.48	3.27	4.7	0.24	22.2	120	521	103	-0.16	-2859	212.2	353	149	777
	VAG63 - 24	14.5	-1.48	22.6	2.39	10	3.6	0.52	9.5	54.4	351	74.5	-0.13	-2203	169.2	198	96	636
	VAG63 - 25	52	-7.2	36	5.83	31.6	14.1	2.31	38.2	128.1	326.8	63.9	-0.76	-806	68	158	59.3	233.5
	VAG63 - 26	36.6	-0.363	26.7	1.53	8.5	10.9	0.4	45.5	191.9	526	98.2	0.47	-1570	132.9	370	145.9	374.2
	VAG63 - 27	19.6	-1	15.3	1.48	8	7.3	1.05	25.2	102.5	303	60.4	-0.13	-1050	81.3	133.2	54.7	294.4
	VAG63 - 28	9.1	-14	57.1	12.4	50.8	15.1	1.88	22.7	63.4	173.3	36.1	0.15	-799	60.7	54.5	21.12	242.5
	VAG63 - 29	20.2	-1.24	17.6	1.61	5.8	5.7	0.48	19.5	94.8	383	83.7	0.03	-2799	228	264	110.8	869
	VAG63 - 3	118	-3.79	22.7	5.57	24	13.7	1.29	35.3	111.8	283.6	56.28	0.25	-2770	854	171	40.74	146.4
	VAG63 - 30	89	-5.9	58.1	5.6	25.2	15.9	1.46	32.4	161.5	925	192.8	-0.34	-4290	352	792	364.9	1421
	VAG63 - 31	16.4	-1.58	15.5	1.73	9.2	10.9	1.92	41.5	157	407	82.5	0.13	-868	65.2	115.7	62.5	319
	VAG63 - 32	77	-3.09	17.2	1.95	9	5.5	0.68	22.8	85.6	274.8	58.8	0.09	-879	69.9	79	39.9	326
	VAG63 - 4	16	-4.07	39.2	5.37	19.5	9	0.49	25.6	118.1	472	101.7	-0.41	-15740	3024	560	122.9	979
	VAG63 - 5	76	-14.6	123	11.4	44.9	41.8	2.01	165	640	1467	262.8	0.23	-18030	2777	3570	794	1023
	VAG63 - 6	5.7	-2.03	13.2	3.75	18	11.4	1.46	29.4	92	260	55.6	0.35	-3670	466	140	28.2	273
	VAG63 - 7	372	-7.84	35.4	6.66	22.5	13.4	1.63	35.2	129.9	362.4	71.2	0.23	-4531	489	296	75.9	409
	VAG63 - 8	67	-8.2	41	5.19	18.9	16.7	0.84	60.6	224	585	111.5	0.55	-7820	855	814	217	602
	VAG63 - 9	2.8	-16	59	11.9	44	19.9	2.26	48.4	161.9	378.4	73.8	0.25	-2565	243	213	53.1	232.2

## Appendix D – Trace element data

Sample	analysis #	Ti	La	Ce	Pr	Nd	Sm	Eu	Gd	Dy	Yb	Lu	Pb204	Pb206	Pb207	Pb208	Th	U
VAG 128010	10a - 10	72	-157.7	691	215	884	401	39.5	383	341	430	96.1	4.18	1.13E+05	-540	3710	634	1715
	10a - 11	20	-22.6	144	33.3	94	34.2	3.43	40.8	72.9	234	53.1	-0.73	1.42E+05	-245	1199	275	628
	10a - 12	21.1	-15.7	95	34.2	149	73.6	7.59	94.2	150.9	315.3	64.7	0.87	-6.33E+05	-253	384	51.7	372
	10a - 13	6.9	-9.5	73	9.5	37.6	19.2	3.32	32.8	73.9	201.9	44.9	0.1	-8.04E+04	-242	1058	247	508
	10a - 14	13.9	-38.6	184.3	25.7	66.2	14.2	2.88	23.2	68	351.9	80.8	7.34	-1.41E+05	-1344	4770	842	2007
	10a - 15	20.6	-18.3	129.3	29.9	124.6	51.6	4.57	60.2	80.2	267.8	65.2	0.37	-5.28E+04	-571	1390	342.4	1014
	10a - 16	59	-45.8	333	48.4	381	151	12.9	133	142	799	215.3	2.89	-3606	287.2	549	739	7330
	10a - 17	376	-94	551	77.7	583	240	41.9	242	262	451	102.8	0.42	-961	83.6	436	745	1877
	10a - 2	22.5	-22.7	171	41.2	174	78.4	7.08	87.3	91.1	326	85.5	0.8	2.19E+04	-191.9	3980	356.6	1930
	10a - 20	54	-6.03	112	9.25	76.5	41.6	4.75	58.6	98.2	221.6	49.6	0.15	-718	61.6	334	381	759
	10a - 21	8	-0.92	29.4	1.47	11.4	8.9	1.26	15.9	42.5	171.6	38.6	0.06	-457.8	38.2	133	138	487.1
	10a - 3	227	-9.86	101.1	19.5	83.7	45.1	6.32	61.9	112.3	303.7	67.6	1.54	12510	-127.1	4150	345	877
	10a - 4	339	-128	478	122.3	507	170.2	16.8	154.9	131.8	331.2	83	4.3	19180	-225	5.80E+03	480	1622
	10a - 5	14.3	-0.73	30.9	1.35	8.5	7.7	1.26	20.2	62.4	278.6	58.7	0.07	11270	-97.5	1530	160	588
	10a - 6	7.9	-6.82	55.2	6.37	24.9	13.8	2.48	28.4	61.1	182.5	39	0.8	7260	-73.6	1794	203.9	376
	10a - 7	6.9	-8.3	72.6	10.3	40.3	19.9	2.62	30.4	68.3	218.1	49.5	0.15	14150	-126	2250	284	649
	10a - 8	19.9	-47.7	216	44.4	164	62.9	6.62	72	91.1	245.1	54.6	1.48	12170	-119.8	2170	290.9	737
	10a - 9	84	-15.9	120.9	19.4	72.7	32.9	4.83	45.6	82.9	233	50.5	0.45	15580	-139	1960	269	634
VAG 128011	11a - 1	20.3	-11.86	141.4	19.7	103.8	49.2	6.5	67.7	93.6	297	70.3	0.14	-1729	127.1	503	475	1313
	11a - 10	18.3	-4.4	69	6.9	34.5	20.8	2.04	24.3	45.7	148	33.8	2.26	-496	63.5	462	170	329
	11a - 11	4	-1.54	48.1	2.02	12.4	8.4	1.42	15.4	38.9	152.4	35.1	0.38	-758	66.9	332	244	591
	11a - 12	460	-3.73	73.8	6.2	34.2	19.5	3.25	30.9	70	294	70.7	0.46	-1880	159	646	573	1620
	11a - 13	10.9	-5.84	127	10.7	64.4	34.6	4.35	47.3	95.3	279	59.4	0.69	-990	89.8	710	632	906
	11a - 14	31	-10.2	189	16.7	124	51.2	13.2	55.9	89.6	324.2	76.1	0.47	-1280	109.7	510	499	1355
	11a - 15	25.5	-6.53	114.9	11.74	65	32.8	3.97	42.3	79.9	228.7	54.5	1.29	-1064	92.5	441	471	1103
	11a - 16	4	-4.34	69.2	7.1	40.7	19.5	2.59	26.8	55.8	257	65.6	-0.15	-1140	95.5	304	307	1169
	11a - 17	23	-24	206	26.3	148	32.1	4.26	37.2	87.5	480.7	122.5	1.23	-2694	228.1	885	710	3060
	11a - 18	7.2	-13.6	129	10.7	55.4	28.9	3.79	45	106	297	65.5	0.76	-1049	96.3	537	482	1007
	11a - 19	32.2	-7.36	102.8	14.6	78	41.7	4.01	40.6	66.5	177.6	45.5	1.1	-1014	87.8	284	305	1088
	11a - 2	13.1	-7.06	55.1	7.97	37.3	17.6	1.72	18.1	34.8	144.4	37.97	2.23	-1583	148	487	235.8	1085
	11a - 20	18.2	-10.13	154.1	14.5	95.1	44.8	5.03	57.4	98.6	322.9	77.3	0.54	-1403	116.2	538	645	1623
	11a - 21	23.2	-9.9	148	13.5	77	39.1	4.74	58.9	122	300.7	66.8	4.7	-1026	149	1030	492	968
	11a - 22	148	-28.8	238.3	29.8	171	81.8	11.52	94	154.3	269.4	51	2.78	-725	85.7	814	656	670
	11a - 24	85	-41.9	215	21	114	46	6.7	57	104	213	46.8	1.54	-977	93.1	447	540	1040
	11a - 25	18.1	-1.3	90.8	1.73	24.2	32.3	9.4	87.3	200	432	82.2	0.69	-639	55.5	902	857	591
	11a - 26	14.2	-3.67	66.6	6.32	43.7	21.3	2.34	25.6	52.5	259.1	67.8	0.91	-1406	134.9	475	361	1544
	11a - 27	460	-17.3	228	24.1	159.8	72.2	10.02	89	126.8	279.8	59.2	1.66	-856	81.4	468	534	1066
	11a - 28	513	-10.97	159.6	16.9	118.6	55.5	7.59	57.7	92.8	311	75.7	2.07	-1213	111.5	426	504	1774
	11a - 29	3.5	-2.22	42.4	1.7	13	5.7	2.75	8.8	23.3	109.8	28.11	0.57	-501.2	45.9	165	132.3	496.8
	11a - 3	18.3	-14.05	202.7	27.6	137.6	56.9	6.55	55.6	86.5	286.4	68	1.97	-2020	186.9	800	395	1293
	11a - 30	17.1	-6.46	138	14.4	90	34.4	5.19	39.4	79.3	274.9	65.2	2.75	-1015	113.3	552	368.6	1147
	11a - 31	19.9	-4.12	68.9	6.07	39.7	20	2.16	25.4	66	318	76.7	0.42	-1369	115.9	357	367.9	1493
	11a - 4	8.8	-0.98	27.6	2.08	11.5	7.5	1.23	10.8	27.4	145	35.8	-0.24	-1126	87.2	213	147	670
	11a - 5	7.5	-0.543	21.8	0.96	4.43	3.02	0.55	7.12	26.1	158.1	38.39	-0.07	-1108	82.1	183.6	128.8	707
	11a - 6	13.9	-81.6	314	45.1	192	40.9	5.17	41.6	62	159.6	36.8	0.18	-965	75.3	432	287	601
	11a - 7	29.4	-9.7	194	27.2	147	65.1	7.3	63.3	85.5	196	43.6	0.39	-935	77	415	313	676
	11a - 8	33	-26.1	264	27.2	131.3	53.9	6.7	65.2	116.5	234.8	50.9	1.69	-1008	97.4	593	460	793
	11a - 9	55	-84	344	40.6	183	74.7	8.69	65.6	92.1	215.4	47.2	1.02	-1180	93.2	619	688	1001

## Appendix D – Trace element data

Sample	analysis #	Ti	La	Ce	Pr	Nd	Sm	Eu	Gd	Dy	Yb	Lu	Pb204	Pb206	Pb207	Pb208	Th	U
VAG 128012	12a - 1	7.1	-7.3	59.8	7.5	52	27.2	1.98	42.5	120.2	322	66	0.86	-996	78.6	182	211	1110
	12a - 10	15.6	-3.09	30.4	3.05	21.7	11	1.29	26.5	102.1	362	74.2	0.47	-1400	91.2	169.2	180	1192
	12a - 11	4.8	-15.23	115.5	12.33	90.5	40.7	8.94	72.9	173.7	450	88.6	0.82	-2437	158.3	509	696	2184
	12a - 12	542	-29.36	256.1	32.1	210.5	102.9	16.9	140.6	226.7	366.2	70.3	1.58	-1410	99.3	370	600	1715
	12a - 13	29.3	-10	148	16.2	124	75	14.2	122	239	434	84	0.53	-1247	81.2	272	382	1064
	12a - 14	38.4	-2.88	40.6	4.73	29.3	19.7	2.78	42.9	147.5	411.2	82.6	0.32	-1595	79.8	191.9	240.9	1052
	12a - 15	39.5	-10.69	105.5	14.1	96	50.1	9.8	72.9	177	508	103.5	2.95	-3290	174.7	457	458	2650
	12a - 16	24.4	-24	196	26.5	170	59.1	45.7	84.9	180	426	83.4	0.57	-2145	93.3	268	423	1718
	12a - 2	15.4	-9.3	121	13.1	96	53.5	5.41	89	207	415	82.5	0.8	-1276	101.5	359	474	1423
	12a - 3	9	-6.6	72.7	8.96	62.9	42.2	3.23	69.3	178.9	482	96.8	0.8	-1564	115.3	310	400	1802
	12a - 4	37	4.32	44.4	4.2	28.3	14.8	3.08	33	119.7	388.3	78.4	0.64	-1352	98.7	265	335	1403
	12a - 5	10.8	-12.1	117	14.9	105	67	7.8	105	245	475	91.4	0.7	-1171	88.2	289	351	1248
	12a - 6	15	-12	95	11.6	75	44.7	4.31	75	197	468	90.3	0.43	-1202	89.2	285	302	1214
	12a - 7	3.9	-1.67	42.6	2.7	19	13.9	8.14	40.8	147.6	422	82.8	0.26	-1324	91.6	279	346	1226
	12a - 8	19	-12.1	81	9	65	28.3	2.37	54.6	170.7	463.2	90.5	-0.38	-1240	83.9	241	308	1093
	12a - 9	9.40E+03	-10.8	56	6.23	34.8	17.6	1.31	37.3	126.4	359.6	73.1	1.97	-1170	102.9	389	188.1	890
VAG 128014	14a - 1	3.6	-4.2	34.8	3	21.5	8.9	0.65	29	118.2	377.7	74.2	-0.12	-1733	88.7	210.9	187	554.8
	14a - 10	-2.8	-5.1	39.1	5	32.9	19.2	1.76	51.6	174	484	93.7	0.29	-2875	69.3	193	169.4	411
	14a - 11	16.6	-14.6	89	13.8	86	32.1	5.1	68.8	205.9	523.3	101.7	0.09	-5510	106	318	313	700
	14a - 12	3.8	-2.1	21.4	2.11	13.3	8.7	1	32.5	118.3	343	68.2	0.49	-3208	54.4	117.5	108.7	314
	14a - 13	-0.44	-0.093	8.4	0.368	6.98	10.3	1.24	46	175.9	488.7	95.6	0.28	-4283	55.9	139	135.3	317.4
	14a - 14	14.5	-0.58	13.8	0.82	9	12.5	1.27	50	187	495	93.7	-0.05	-7100	66.2	163	161.2	365
	14a - 15	7.5	-0.022	12.2	0.393	8.2	12.8	1.41	58.2	220	574	111.5	0.2	-14160	77.1	201	207	426
	14a - 16	8.3	-2.94	26.6	2.75	16.6	12.4	0.94	47.2	177.6	506.5	97.9	0.05	-5.65E+04	88.4	211.6	220.7	497.3
	14a - 17	12	-0.99	16.4	1.01	6.8	8.1	0.65	33.7	141.8	452	91.4	0.41	4.05E+04	94.5	178	185	547
	14a - 18	6.7	-1.2	17.3	1.06	5	6.54	0.59	21.6	85.5	268.7	54.46	-0.12	1781	52	90	94.7	267.2
	14a - 19	0.11	-0.239	10.59	0.36	3.55	5.56	0.42	22.8	100.9	389	79.4	-0.18	3020	100.2	137.1	138	514
	14a - 2	11.6	-0.17	9.51	0.266	5.1	7.33	0.92	29.6	113.5	334.9	67.7	0.11	-945	47.8	131.9	110.1	274.9
	14a - 20	23.2	-1.24	14.6	1.89	13.7	12.7	1.07	40.1	153.8	425	82.7	-0.06	2038	81.1	145.3	140.1	371
	14a - 3	2.6	-0.161	7.33	0.56	5.45	6.9	0.82	28.5	102.6	294	58.2	0.43	-670	30.7	79.6	72.4	194
	14a - 4	4.7	-119	470	59	310	65	4.4	87	219	542.1	105.1	-0.21	-1900	83.4	255.7	247.3	519.2
	14a - 6	-1.3	-0.9	10.5	0.66	4.8	3.31	0.34	15.2	77.9	360	75.8	0.06	-2460	92.2	122	116.1	542
	14a - 7	8.6	-1.98	20	1.8	15	12.7	1.57	45	163.4	463.2	94	-0.1	-1700	57	129.1	125.8	375.2
	14a - 8	3	-0.66	16.3	0.61	7.7	10.2	1.14	42.5	162.4	445	87.2	0.6	-1585	48.2	137.3	134.5	292
	14a - 9	114	-0.041	10.4	0.282	6.16	12.2	1.26	46.2	181	464	89.1	0.15	-1689	47.2	137.1	130.9	271
VAG 128015	15a - 1	9.1	-33.1	124	29.5	101	52.4	4.26	83.3	172.3	380.5	77.8	0.2	18410	-65	-3270	462	1018
	15a - 10	5520	-166	515	157	513	194	13.6	219	320	501	93.8	3.28	16080	-106.5	-8740	646	1750
	15a - 11	326	-65.7	258	80.9	282	152	13	198	322	659	134.1	2.54	5.35E+04	-317.3	-17600	1447	4950
	15a - 12	27.7	-192	476	158.3	450	162	12.2	178	215	403	81.8	0.5	18040	-105.9	-6110	430	1921
	15a - 13	740	-92.4	226	84.7	285	110	19.5	112.3	114.3	195.8	42.2	1.3	4730	-39.5	-4880	174	617
	15a - 14	88	-168	727	218	761	391	23.3	447	502	691	135.3	2.14	25710	-161.3	-15480	944	3520
	15a - 15	26.1	-30.5	124	36	127	59.9	5.51	85.9	141.4	272	53.4	0.39	7730	-51.5	-8860	303	648
	15a - 16	20.8	-40.7	129.1	45.2	146	73.8	4.5	90	174.9	431	90.6	1.87	3.47E+04	-252	-2.85E+04	734	2710
	15a - 18	10.4	-21.5	86.3	21.6	71.2	37.6	11.7	71.6	200.2	517.6	104	0.49	21640	-148.9	-4.95E+04	653.9	2173
	15a - 2	17.7	-40.4	173	41.8	150	90	12.2	114	189	420	88.8	3.68	26280	-118.6	-5100	532	2266
	15a - 20	445	-48.2	194	64.4	222	112	11.1	119	129	285	63.4	0.39	15700	-131.8	5000	191	1588
	15a - 21	2150	-85.2	293	112	353	160	21.1	181	234	500	102.9	2.26	15330	-156	7720	383	1660
	15a - 22	24.3	-37.1	248	60.2	247	125	14.6	138	180.5	460	98.8	3.57	3.17E+04	-287	9430	624	3100
	15a - 23	19.8	-22.3	159	26.4	130	49.3	6.31	68.2	183.9	566	114.4	2.54	11390	415	786	920	3642
	15a - 24	101	-68.1	345	92.7	463	169	15.3	181	209	456.4	94.6	0.42	4000	136.2	190.2	479.3	2681
	15a - 25	25.4	-39.8	277	63.8	292	130.4	9.61	143	167	223	47	0.85	1550	69.2	167.5	164.1	939
	15a - 26	2940	-119.7	754	200	777	182	21	160.8	220	657	138.9	3.28	3764	271	662	1274	4800
	15a - 27	18.2	-14.8	127	28.7	133	64	5.81	90.8	162.1	336	67.1	0.78	1320	106	255	341	1140
	15a - 3	30.1	-161	328	92	270	105	8.84	131.4	194.4	404	83.7	0.99	3.35E+04	-137.3	-3560	488	2241
	15a - 4	29.8	-55	207	54.2	190	75.6	16.2	84.1	113	266	57.9	0.48	2.46E+04	-102.7	-2400	398	2100
	15a - 5	2390	-120	271	68.8	195	73.8	7.07	87.3	138.4	235.2	47.4	2.3	6990	-45.5	-3320	223	500.3
	15a - 6	10.1	-23	110.5	22.14	79.2	27.6	2.88	52.3	168.5	527	109.8	1.18	29620	-138.8	-5510	717	3049
	15a - 7	34.3	-36.6	62.6	26.5	80.2	29.5	1.71	39.8	91.3	288.9	61.9	-0.08	9160	-50.2	-1960	127.8	526
	15a - 8	29.5	-63.4	186	73.9	247	119	10.2	126	126	201.3	44.9	0.39	17190	-90.6	-2180	253	1441
	15a - 9	93	-33.8	152.8	40.4	130.6	77.7	6.21	119.6	224.8	425	83.2	3.7	16160	-114.7	-9.98E+03	561	1360

## Appendix D – Trace element data

VAG 128016

Sample	analysis #	Ti	La	Ce	Pr	Nd	Sm	Eu	Gd	Dy	Yb	Lu	Pb204	Pb206	Pb207	Pb208	Th	U
16a - 1		2.3	-0.34	8.04	0.4	2.7	4.06	0.323	15.5	60.9	201.9	42.4	-0.14	-1369	-36.6	-67.2	74.7	264.6
16a - 10		2.6	-0.021	5.88	0.28	2.69	5.4	0.84	25.3	99.7	260	51.6	-0.47	-372	-8.02	-44	38.7	73.5
16a - 11		11.8	0.048	6.42	0.21	2.69	5.81	0.79	25.9	98	248.8	49.5	-0.42	-333	-6.54	-40.3	35.7	67.9
16a - 12		6.1	-0.058	6.7	0.217	3.77	6.48	0.97	27.8	102.2	266	51.1	1.4	-367	-7.34	-42.7	37.7	73.4
16a - 13		0.34	-0.044	7.2	0.141	1.22	2.24	0.12	11.8	55.4	218.4	47.1	0.77	-956	-19.5	-59.4	53.4	202.3
16a - 14		0.2	-3.4	16.1	2.32	9.2	3.29	0.211	10.9	44.6	174.4	37.2	0.66	-1695	-35.3	-79	65.3	351
16a - 15		3.5	0.038	7.03	0.076	1.39	2.75	0.32	13.8	61.5	195.8	38.8	-1.04	-466	-9.52	-44.5	37.6	101.1
16a - 16		317	-96	167	42	123	20.5	0.96	20.8	54.6	151.7	30.6	0.29	-305	-6.51	-30.3	26.1	72.7
16a - 17		-1.2	-0.034	12.17	0.116	2.87	5.78	0.49	27.4	113.6	331.4	64.7	-0.43	-926	-17.8	-110.8	97.3	194.8
16a - 18		15.5	-342	457	102	304	56.1	3.11	48.1	90.5	219	42.2	0.53	-539	-11.3	-59.6	45	121
16a - 19		5.1	-0.011	9.96	0.262	3.39	7.24	0.72	30.2	115.6	302.3	58.8	0.67	-878	-16.93	-114.2	89.8	176.5
16a - 2		4.8	-0.62	5.36	0.37	1.88	2.96	0.182	9.5	40	145.9	32	0.4	-561	-14	-19.9	21.7	129.2
16a - 20		48	-37.8	84	14.7	44.8	17.1	2.11	40	132	381	75.2	-0.03	-1814	-36.4	-229	170	404
16a - 21		7.2	-0.58	15.93	1.04	9.9	16.3	1.63	66.2	242	562	107.3	-0.24	-1306	-25.1	-228	189	284
16a - 22		3	-0.15	16.3	0.41	2.8	3.9	0.2	21.1	90	291	57.7	0.38	-1090	-22	-131	111	261
16a - 23		5.9	-0.48	9.05	0.54	3.98	8	0.9	28.2	109	281.8	55.61	0.46	-550	-10.47	-63.4	50.5	118.1
16a - 24		7.4	-0.054	4.93	0.285	4.51	8.2	1.14	28.8	95.3	253.3	50.1	-0.32	-293.4	-5.17	-34.9	28.54	66.1
16a - 25		0.45	-2.18	15	1.88	9.5	7.88	0.7	28.7	103.2	286	56.7	0.23	-940	-15.56	-87.3	73.7	225.6
16a - 26		10.6	-6.2	23.6	4.2	19.7	15.3	1.47	52.2	176	432	83.3	-0.39	-1050	-19.32	-182	145.1	232
16a - 27		4.2	-28.2	68.4	13.6	54.2	17	0.93	28.7	90.5	272.3	53.6	-0.09	-1116	-21.16	-130.6	99.8	256.2
16a - 28		5.7	-1.98	10.7	1.12	7.6	7.6	1.02	30.7	109.1	288	55.2	0.32	-455	-8.05	-66.5	54.5	99.1
16a - 29		62	-4.7	22	2	12.1	8.9	0.45	35.7	121.5	320.5	62.4	0.35	-1033	-19.2	-128.5	98.1	236.3
16a - 3		1680	-0.074	5.08	0.73	4.97	8.1	1.65	31.7	113	285.3	55.2	-0.23	-644	-16.9	-42.9	35.64	138
16a - 30		2.6	-0.047	10.02	0.253	2.77	6.2	0.65	24.3	99.3	282	56.4	-0.72	-736	-11.8	-97	66.9	152
16a - 31		5	-0.117	5.1	0.147	0.63	1.41	0.29	8.5	35.5	142.4	29.9	0.35	-647	-10.5	-43.7	31.2	157
16a - 32		9.5	-0.097	7.97	0.68	8	10.5	1.38	38.1	137.4	357.9	70.4	0	-603	-10	-91.4	68	137
16a - 33		13.1	-0.028	7.73	0.51	5.7	10.6	1.77	44.3	161	386	74.9	0.64	-412	-6.65	-81.1	55.5	93.1
16a - 34		10.2	0	5.11	0.036	1.16	1.59	0.238	10.5	45.2	153	33.1	0.47	-409	-5.91	-35.4	25.5	98
16a - 35		11	-0.41	8.26	0.24	1.4	2.36	0.257	11.7	51.4	181	37.9	-0.35	-548	-8.51	-62.1	44	139
16a - 36		7.9	-0.08	11.9	0.143	0.9	3.16	0.235	14.4	68.2	232.5	46.79	-0.37	-880	-13.12	-95.8	69.46	216.2
16a - 37		-1.1	-0.022	6.52	0.211	3.79	5.63	0.57	23.9	88.5	275.1	59.1	0.01	-826	-12.37	-96.6	65.3	206
16a - 38		12	-113	217	41.7	174	37.4	1.61	46	110.6	285	56	-0.01	-709	-10.94	-123.7	80.5	164
16a - 39		4.7	-0.01	5.9	0.134	2.17	2.49	0.52	14.3	60.6	176.4	35.7	0.32	-270.3	-3.89	-41.4	26.62	63.3
16a - 4		9.4	0.078	7.5	0.27	3.54	6.26	0.65	24.3	95.7	258.2	49.9	-0.63	-557	-14.32	-47	49.3	111.1
16a - 40		2.1	-11.9	35	6.2	29	10.3	0.62	23.3	71.4	213.7	41.91	0.4	-542	-8.38	-80.5	48.9	116.1
16a - 41		5.4	-13.1	43.5	8.2	39.3	16.6	1.3	40.2	128.7	319.5	62.5	-0.12	-730	-10.69	-111.4	73.5	156.3
16a - 5		9	-15	32	7.8	27	6.4	0.46	12.5	45.6	158.9	32.43	-0.01	-842	-22.6	-45.5	47.3	169.1
16a - 6		6.9	-0.096	4.1	0.032	1.22	3.03	0.64	13.9	52.8	158.6	31.78	-0.21	-221	-6.04	-19.4	20.39	41.1
16a - 7		3.9	-0.64	11.33	0.94	8.3	10.1	1.32	46.3	174.1	422	80.7	1.09	-1054	-26.7	-112.7	117.2	202.5

## Appendix D – Trace element data

Sample	analysis #	Ti	La	Ce	Pr	Nd	Sm	Eu	Gd	Dy	Yb	Lu	Pb204	Pb206	Pb207	Pb208	Th	U
VAG 128017	17a - 1	5	-3.31	11.88	1.5	7.2	5.09	0.51	17.4	75.5	320	63.8	0.73	-1291	-49.9	-64.4	89.6	326
	17a - 10	4.7	-0.72	7.85	0.86	4.68	6.7	0.77	23.2	98.5	327	67.5	0.56	-993	-34.8	-58.9	72.1	231.2
	17a - 11	123	-0.98	13.85	0.95	5.4	9.1	0.67	35.5	141.6	417	79.8	0.77	-1373	-52	-126.1	150.5	301
	17a - 12	6.7	-1.77	8.7	1.22	6	6.2	0.5	23	97	380	79.8	0.39	-1834	-59.8	-72	96	474.2
	17a - 13	19.8	-24.8	34.8	6.4	21.4	14	0.71	50.6	208	497	92.3	0.43	-2410	-99.2	-127	125	421
	17a - 14	377	-6	14	3.47	14.1	9	1.16	22.2	98.8	440	97.5	0.65	-2633	-87.5	-71	99	659
	17a - 15	107	-305	348	115	368	94	1.49	85	112	377.1	84.6	1.16	-1955	-71.6	-43.3	39.9	485
	17a - 16	13.2	0.02078	17.5	0.141	1.59	3.17	0.114	15.3	65.7	226.1	45.8	-0.04	-1138	-37.4	-69.7	82.8	232.1
	17a - 17	4.8	0.118	11.51	0.117	1.46	2.58	0.147	13.7	66	229.2	45.3	0.51	-797	-25.9	-53.5	66.5	159.9
	17a - 18	0.061	-0.89	10.01	0.49	3.8	5.18	0.71	22.4	97.3	322.6	65.4	-0.13	-980	-31	-56.5	67	215
	17a - 19	3.6	-0.4	7.7	0.187	2.39	4.65	0.37	22.8	102.4	331	64.3	-0.14	-2595	-89.3	-92.2	96.9	488.3
	17a - 2	3.4	-5.25	11.4	2.1	8.3	4.72	0.4	12	49	236.7	52.4	0.71	-2000	-76.3	-45.9	63.6	522.8
	17a - 20	56	-1.9	8.37	1.26	3.95	3.24	0.308	13.5	70.4	344	76.9	-0.8	-1476	-45.7	-34.6	40.5	343.8
	17a - 21	4.6	-1.2	9.5	0.97	5.4	3.8	0.4	18.2	95	422	93.2	0.52	-1920	-54.6	-91	106	433
	17a - 22	41	-75.5	116.7	40.5	135	40	0.47	40.4	73.8	298.6	72.1	0.31	-2184	-65.2	-39	30.9	486.5
	17a - 23	-1.4	0.089	1.02	0.005	-0.32	-0.21	0.208	3.93	45	435	107.6	0.42	-1858	-50.3	-14.9	15.7	427
	17a - 24	39.2	-20.3	77.6	17.5	58.8	39.1	6.43	76.1	220.1	497	96.6	3.8	-3940	-143	-397	439	1066
	17a - 25	6.9	-3.9	12.3	2.56	8.7	6.1	0.47	17.9	68.1	238	48.9	0.18	-912	-25.4	-49.5	56.1	177
	17a - 26	6.9	-41	79	23.9	80	27.6	0.77	49.5	166.8	532	105.9	-0.38	-2099	-58.9	-138	160	437
	17a - 27	12.7	-37	54	14.4	42.8	26.5	2.65	58.4	177.6	333.9	63.8	1.4	-3766	-103.8	-133.2	211	901
	17a - 28	-2.8	-0.66	3.93	1.18	3.72	2.68	0.194	4.73	29.1	239.2	57.1	0.3	-4811	-123.2	-16.1	14.53	1119
	17a - 29	10.3	-3.66	9.5	3.56	13.8	10.3	0.53	15.1	50.6	303.5	71.4	0.48	-2390	-61.5	-15.9	19.98	575
	17a - 3	2.5	-0.04	6.53	0.007	0.76	1.48	0.033	7.3	40	197.2	43.2	0.6	-1236	-45.7	-36.7	46.7	301.7
	17a - 30	4.6	-4.7	17.9	3.9	13.7	10.9	0.57	26	89.9	321	67.6	0.47	-1824	-49.9	-73.2	80.1	390
	17a - 31	5.5	-37	65	16.7	53	15.2	0.48	21.4	61.7	229.4	50.9	0.5	-1874	-51	-83.8	82.1	405.9
	17a - 4	27.7	-0.83	16.5	0.56	4.26	7.5	1.01	33.2	186.4	849	159.1	-0.2	-1592	-58.4	-64.8	94	388
	17a - 5	1.5	-26.2	41.4	9.6	42.9	15	0.28	36.8	140.6	459	88.7	0.29	-1863	-77.4	-82.5	93.8	356
	17a - 6	-1.7	-2.09	15.59	1.08	6.5	5.74	0.45	18.9	70.4	226	43.91	0.87	-2245	-86.8	-109.3	118.6	480.2
	17a - 7	2.8	-0.7	2.38	0.55	1.81	1.33	0.091	4.55	35	308	74.1	0.08	-1660	-56	-7.4	7.79	419
	17a - 8	1.3	-13.3	22.9	5.9	22.8	13.1	0.57	33	117.6	413	84.9	0.39	-1732	-61.6	-79.8	92.2	392
	17a - 9	7.5	-0.69	12.7	1.23	8.3	14.9	1.58	57	209	573	109.9	0.31	-1661	-58.3	-153	190	390
VAG 128018	18a - 1	12.2	-0.447	10.99	1.05	2.83	1.48	0.6	6.55	30.8	259	65.4	-0.35	344.3	106.1	63.1	76.8	254.1
	18a - 10	2.5	0.0313	6.49	0.14	0.83	1.23	0.51	6.91	32.8	288.8	74.2	-0.13	288.8	136.6	48.4	59.9	237.2
	18a - 11	6.5	-0.006	4.01	0.2	1.66	2.07	0.41	7.16	28.7	194.6	47.6	0.24	160.6	75.6	30.5	39	128.3
	18a - 12	4.2	-0.102	10.04	1.75	3.26	3.1	0.77	7.9	34.5	279	69.8	0.17	405	236	83.1	117	349
	18a - 13	11.4	-0.411	9.17	0.82	2.8	2.1	0.66	8.4	37	302	76.4	0.04	310	181.6	59.6	74.1	253.8
	18a - 14	3.6	0.0366	4.25	0.28	1.84	1.37	0.49	7.39	29.8	211.7	53.5	0.1	177.1	109.5	30.9	42.7	149.6
	18a - 15	26.7	-0.079	5.17	1.04	2.89	3.88	1.01	9.2	34.7	227.5	56.1	-0.05	177.3	113.1	35.9	52.9	159.1
	18a - 16	22.3	-0.097	7.73	1.07	3.85	2.63	0.59	7.16	28.5	214.1	54.5	0.12	259.6	162.5	54.8	76	226.1
	18a - 17	0	-0.38	8.3	22	34	1.78	0.19	3.96	27.4	242	62.7	0.81	365	205	46.8	74.7	356
	18a - 18	-4.6	0.0215	3.99	0.17	1.25	2.06	0.51	7.17	29.7	202.3	51.2	0.11	154	102.4	30	40.2	130.6
	18a - 19	5.2	-0.8	11.38	3.27	8.1	4.05	1.14	10.1	31.4	212.9	53.7	0.18	225.2	156.7	43.4	63.1	187
	18a - 2	9	0.0181	12.45	0.34	3.25	5.04	1.33	18.7	73	484.2	118.7	0.07	590.3	190.1	140.1	175.5	447.6
	18a - 20	1.4	0.0011	4.93	0.32	2.19	2.16	0.71	8.68	36.9	258.7	65.4	-0.4	224.4	152.7	39.4	55.4	185
	18a - 21	-4.4	-0.038	6.47	0.2	0.77	2.01	0.49	5.92	32	261.7	68.2	-0.04	293.2	201	42.8	60	246
	18a - 22	-0.32	-0.017	6.8	0.65	3.75	4.14	1.02	13.6	50.9	314.2	75.7	-0.02	286.2	205.6	59.5	87	239.6
	18a - 23	11.4	-0.038	6.75	0.42	2.05	1.43	0.62	5.24	24.7	222.2	57.4	0.19	226	165	30.7	43.8	194
	18a - 3	-10	-0.065	7.88	0.4	1.36	2.41	0.5	6.66	37.5	319.6	79.9	0.19	331.8	113.1	59.5	74.1	256.6
	18a - 4	3.1	-0.02	4.22	0.074	1.47	1.58	0.57	5.84	26.2	194.5	49.29	-0.24	177.5	63	29.1	37.1	134
	18a - 5	3.9	-0.0021	7.26	0.17	1.05	1.63	0.51	7.24	35	263.4	66.6	-0.01	323.1	114.3	70	86.3	243.2
	18a - 6	0.21	-0.013	13	0.27	1.96	3.17	0.81	13	68.3	490	120.2	-0.07	571	210.3	135.2	173.8	441
	18a - 7	6.2	0.0128	6.54	0.171	0.93	1.52	0.55	6.1	32.2	254.5	64.1	-0.15	299.2	116.8	55.5	65.4	223.1
	18a - 8	0.85	-0.0005	6.98	0.134	0.58	1.53	0.55	5.92	33.1	298	77	-0.25	307	137.1	50.2	64.4	241
	18a - 9	23.4	-2.11	21.5	8.3	16.2	6.1	1.83	12.8	37.1	233	57.1	-0.18	252	107.5	47.1	76.4	247

## Appendix D – Trace element data

Sample	analysis #	Ti	La	Ce	Pr	Nd	Sm	Eu	Gd	Dy	Yb	Lu	Pb204	Pb206	Pb207	Pb208	Th	U
19a - 1		4.2	-19.8	70	14.9	80.1	29.4	1.34	41.5	106.6	293.6	59.8	0.48	-1046	-15.44	-134.8	88.4	234.5
19a - 10		1.5	-1.89	12.76	0.7	4.23	6.6	0.38	23.8	98.1	327	65.9	0.38	-1711	-17.65	-165	86.6	358.2
19a - 11		21.9	-32.3	95	24.8	136	53.3	3.65	72.9	155	335.4	66	0.33	-858	-8.7	-88.7	45.3	162.4
19a - 12		16.7	-2.98	8.98	1.13	7.1	8.4	1.19	30.4	119.4	325.6	65.1	-0.08	-1409	-13.81	-87.1	44.6	265.4
19a - 13		112	-3.6	14.8	1.19	7.3	6	0.29	20	86.4	296	63.3	1.06	-2340	-20	-142	72.7	490
19a - 14		4.4	-2.36	19.7	3.68	22	10.7	0.9	26.3	82.6	243.8	49.6	-0.1	-720	-7.05	-94.9	45.21	122.7
19a - 15		9.2	-73	191	40.3	203	61	2.18	72.8	157.8	420.3	83.5	0.06	-4113	-39.4	-379	180	643.2
19a - 16		577	-6.31	15.01	2.98	12.6	6.28	0.51	20.2	83.4	276.9	56.8	0.56	-1563	-14.67	-150.5	73.1	258.8
19a - 17		10.4	-0.48	11.69	0.55	4.21	5.22	0.41	20.6	85.1	280.8	60.7	0.27	-1608	-14.67	-147	66.4	258.6
19a - 18		35	-1.12	16.4	0.65	4.7	4.23	0.42	16.5	69.6	243.9	49.7	0.35	-1435	-12.81	-160	69	228
19a - 19		790	-34.5	80	15.2	59.7	29.2	2.4	50.8	213	591	115.3	0.2	-3520	-27.6	-240	106.1	600
19a - 2		7.2	-2.13	13.43	0.97	4.4	4.02	0.171	14.6	65.7	243.8	51.18	0.39	-1319	-18.32	-95.7	63.46	330.1
19a - 20		38	-234	331	64.8	230	47.4	3.05	60.5	160.6	391	78.9	-0.44	-1118	-8.57	-126.1	149	188.6
19a - 21		8.3	-4.08	18	2.56	11.6	5.22	0.308	15.8	68.8	241.8	50.9	0.73	-1671	-14.23	-140.9	62.58	222
19a - 22		25	-0.81	10.98	0.69	6.49	8.3	0.83	36.5	134.1	368.2	73.9	-0.05	-1335	-10.54	-164.8	67.2	168.6
19a - 23		47	-13.7	27	5.1	25	9.7	1.19	32.5	110.6	297	60	-0.28	-778	-6.16	-101	40.6	95.4
19a - 24		32	0.014	13.45	0.107	1.34	2.9	0.268	16.4	74	257.1	51.77	0.21	-1563	-11.46	-173.1	69.3	187.3
19a - 25		6.3	-0.013	6.27	0.176	3.52	5.79	0.85	25	89.7	248.9	50.9	0.24	-809	-5.72	-88.5	35.46	93
19a - 26		23	-9.7	23.6	4.1	25.4	10.7	0.96	25.4	79.5	240	49	-0.14	-975	-6.97	-98.4	36.9	121.6
19a - 27		15.2	-40.5	67.4	22.5	96.7	46.3	2.69	78.1	275	701	133.8	0.32	-4830	-31.8	-434	167.4	516
19a - 28		19.1	-3.28	16.6	1.33	7.7	8	0.68	33.7	138	390	76.6	0.55	-2120	-13.5	-283	100	206
19a - 3		111	-220	396	74.5	339	118	12.7	150	411	1110	219.6	0.22	-6376	-89.2	-574	438	2044
19a - 30		11.2	-0.012	8.71	0.197	2.26	5.31	0.53	23.7	91.2	270	54.3	0.39	-1614	-6.95	-133	44.7	112.4
19a - 31		4.4	-2.78	19.9	2.04	11.3	7.2	0.44	20.9	85.7	291	58.18	0.32	-3421	-14.27	-229	83.7	236
19a - 32		10.7	-13	34.5	8.3	38.6	16.2	0.9	25.6	83.7	248.9	50.4	0.39	-2823	-10.6	-148	43.7	166.5
19a - 33		6.8	-0.19	8.59	0.054	1.41	2.2	0.127	9.8	40.9	161.8	34.69	0.18	-1756	-6.23	-96.2	30.29	96.7
19a - 34		4	-1.29	21.03	0.89	3.76	4.95	0.166	19.9	95	328.5	65.69	0.24	-6840	-22.25	-363	115.8	345
19a - 35		9.5	0.022	13.68	0.022	0.79	3.38	0.184	15.61	73.9	262.2	55	0.37	-4774	-14.67	-252	76.68	218.1
19a - 36		-5.1	-0.035	18.49	0.121	1.88	4.61	0.159	17.9	84.9	312.7	62.6	0.28	-8620	-24.1	-431	127.5	353.1
19a - 37		26.8	-18.1	62.6	12.8	54.8	17.1	0.83	33.3	110.3	344.6	69.9	0.23	-11240	-27	-411	120.5	404.3
19a - 38		2.7	-1.66	16.98	0.89	3.8	2.73	0.202	15.4	71.2	253.1	51.58	0.09	-7780	-16.88	-288	80.96	243.3
19a - 39		13.9	-0.068	10.31	0.43	4.98	7.3	0.75	30.9	115.2	313	61.2	-0.05	-6250	-11.72	-213	58	171.9
19a - 4		6.3	-0.87	14.77	0.75	7.72	11	0.96	42.1	164.5	451	89	1.06	-1381	-18.34	-178.4	111.8	331.3
19a - 40		13.5	-8.3	40.7	10.2	48.5	20.9	1.02	35.3	102	279.8	56.1	0.13	-7530	-12.33	-279	69.8	187.7
19a - 41		3	-5.3	27.5	6.8	34.2	18.3	1.57	49.5	166	410	79	-0.36	-7190	-10.1	-225	58.5	142.6
19a - 42		3.4	-0.073	10.55	0.14	2.79	4.87	0.47	21	100.8	309.3	64.7	-0.25	-10470	-11.1	-237	62.2	165
19a - 43		7.2	-0.58	12.93	0.75	2.77	2.92	0.164	12.7	60.4	234.8	49	0.19	2.62E+04	-21	-278	56	314
19a - 44		16.9	-31	75	13.1	36	12.9	0.61	31.7	110.5	334	67.8	0.11	16430	-18.06	-482	98.7	255.6
19a - 45		337	-0.031	11.54	0.199	1.72	2.79	0.103	14.6	65	224.6	46.6	-0.2	8510	-11.8	-286	52.8	147.7
19a - 46		7.5	-0.154	14.48	0.51	3.76	6.2	0.34	25.2	104	317	63.6	-0.17	9060	-14.69	-484	89.4	188.5
19a - 47		4.3	-0.036	12.35	0.118	1.46	2.84	0.171	15.9	72.5	252	51.6	0.61	8220	-15.72	-398	70.6	188.6
19a - 48		76	-44.7	93	17.7	46.3	13.9	0.77	36.4	121	350	69.6	0.17	11570	-23.6	-494	88.6	344.5
19a - 49		15.1	-2.75	15.8	2.14	10.7	11.4	1.36	40.7	146.9	394	78.7	0.54	5260	-18.2	-569	74.2	238
19a - 5		590	-0.58	19.6	0.73	5.3	5.15	0.32	17.4	80.1	286.5	58.2	-0.25	-1560	-19.92	-191.8	110.8	329.1
19a - 6		12.4	-0.216	11.43	0.217	1.62	2.96	0.257	13.1	63	230.5	47.3	0.12	-1135	-15.35	-124.2	68.6	234
19a - 7		-0.06	-0.32	15.51	0.218	2.45	3.72	0.21	17.6	81.6	289.9	59.6	0.09	-1591	-19.8	-173.3	97.2	318.2
19a - 8		16.4	-0.095	11.77	0.41	5.3	8.1	0.82	30.7	112	321	62.6	-0.14	-720	-8.55	-125	67.9	145.7
19a - 9		8.4	0.013	14.76	0.118	1.37	3.9	0.059	18.2	75.2	260.8	52.64	-0.63	-1239	-13.96	-152.8	78.36	225.8

## Appendix E - Lu-Hf data

Sample	Analysis#	Comment	Age(Ma)	2s	$^{176}\text{Hf}/^{177}\text{Hf}$	2s	$^{176}\text{Lu}/^{177}\text{Hf}$	2s	$^{176}\text{Yb}/^{177}\text{Hf}$	2s
HAL 193052	52a - 1	Possible metamorphic age	968	14	0.28243	0.00004	0.00175	0.00014	0.0663	0.0032
	52a - 2		968	14	0.282322	0.000047	0.000716	0.000073	0.031	0.0045
	52a - 4		968	14	0.282355	0.000046	0.0002474	0.0000037	0.007077	0.000078
	52a - 7		968	14	0.282357	0.000046	0.0002198	0.0000034	0.00657	0.00015
	52a - 8		968	14	0.282431	0.000054	0.0002064	0.0000051	0.00541	0.00014
HAL 193056	56a - 1	Age not calculated	950	100	0.282208	0.000034	0.00054	0.000041	0.019	0.0016
	56a - 3		950	100	0.282187	0.000037	0.000943	0.000019	0.03058	0.0008
	56a - 4		950	100	0.282214	0.000039	0.001436	0.000046	0.0463	0.0011
	66 - 1		945	14	0.282214	0.000034	0.000863	0.00002	0.03152	0.00064
HAL 193061	66 - 4		945	14	0.2822	0.000033	0.000575	0.000067	0.0215	0.0028
	66 - 7		945	14	0.282231	0.000045	0.0011	0.00009	0.0346	0.0028
	61a - 12		1038	28	0.282222	0.000036	0.000812	0.000061	0.0283	0.0016
	61a - 13		1038	28	0.282223	0.000048	0.0011	0.000032	0.0428	0.0012
	61a - 14		1038	28	0.282227	0.000036	0.000725	0.000087	0.0279	0.0035
	61a - 15		1038	28	0.28221	0.00004	0.000674	0.00001	0.02375	0.00057
	61a - 16		1038	28	0.282178	0.000042	0.000727	0.000054	0.0274	0.0021
	61a - 18		1038	28	0.282232	0.000046	0.000957	0.000081	0.0313	0.0029
	61a - 19		1038	28	0.282218	0.00004	0.000696	0.000019	0.02461	0.00089
	61a - 2		1038	28	0.282197	0.000035	0.000418	0.000012	0.01376	0.00042
	61a - 20		1038	28	0.282255	0.000064	0.00082	0.00011	0.0294	0.0041
	61a - 3		1038	28	0.282203	0.00004	0.000494	0.000076	0.0178	0.0033
	61a - 4		1038	28	0.282167	0.000036	0.000833	0.000048	0.0322	0.0023
	61a - 5		1038	28	0.2822	0.000036	0.000568	0.000021	0.02002	0.00086
	61a - 6		1038	28	0.282199	0.000038	0.000468	0.000055	0.0166	0.002
	61a - 7		1038	28	0.282191	0.000045	0.00086	0.00011	0.0325	0.0047
	61a - 8		1038	28	0.282205	0.000043	0.000626	0.000024	0.0209	0.0011
	61a - 9		1038	28	0.282232	0.000042	0.000636	0.00003	0.019	0.0013

Appendix E - Lu-Hf data

Sample	Analysis#	Comment	Age(Ma)	2s	$^{176}\text{Hf}/^{177}\text{Hf}$	2s	$^{176}\text{Lu}/^{177}\text{Hf}$	2s	$^{176}\text{Yb}/^{177}\text{Hf}$	2s
HAL 193063	63a - 1		1025	20	0.282197	0.000038	0.000831	0.000034	0.0314	0.0015
	63a - 10		1025	20	0.282254	0.000035	0.000819	0.000065	0.0301	0.0022
	63a - 11		1025	20	0.282249	0.000035	0.000637	0.000013	0.02101	0.00073
	63a - 12		1025	20	0.282302	0.000053	0.0014	0.00015	0.0517	0.0063
	63a - 13		1025	20	0.282224	0.000043	0.000525	0.000012	0.01739	0.00048
	63a - 14		1025	20	0.282207	0.000045	0.000543	0.000054	0.0199	0.0022
	63a - 15		1025	20	0.282244	0.000043	0.000879	0.000042	0.0294	0.0012
	63a - 16		1025	20	0.282279	0.000045	0.000633	0.00003	0.02088	0.00049
	63a - 17		1025	20	0.282192	0.000046	0.00066	0.000036	0.0232	0.0015
	63a - 18		1025	20	0.282207	0.000048	0.000701	0.000021	0.0257	0.0011
	63a - 19		1025	20	0.282214	0.000032	0.000378	0.000014	0.01243	0.00048
	63a - 2		1025	20	0.282238	0.000042	0.0004095	0.0000079	0.01356	0.00042
	63a - 20		1025	20	0.282231	0.000039	0.0002552	0.0000084	0.00843	0.00034
	63a - 21		1025	20	0.282262	0.000043	0.000761	0.000094	0.0261	0.0028
	63a - 22		1025	20	0.282197	0.000049	0.000947	0.000031	0.0358	0.0012
	63a - 23		1025	20	0.282185	0.000037	0.000726	0.000056	0.0261	0.0022
	63a - 24		1025	20	0.282204	0.000039	0.001051	0.000096	0.0399	0.0043
	63a - 25		1025	20	0.28217	0.000038	0.000498	0.000023	0.01782	0.00068
	63a - 26		1025	20	0.282233	0.000041	0.000464	0.000058	0.0176	0.0023
	63a - 27		1025	20	0.282226	0.000043	0.000556	0.000089	0.0197	0.0039
	63a - 29		1025	20	0.282227	0.000036	0.000423	0.000025	0.01349	0.00057
	63a - 3		1025	20	0.282184	0.000035	0.00078	0.000036	0.0294	0.0014
	63a - 30		1025	20	0.28225	0.000036	0.001014	0.000083	0.0375	0.0029
	63a - 31		1025	20	0.282246	0.000043	0.000603	0.000029	0.01956	0.00099
	63a - 32		1025	20	0.282239	0.000036	0.000508	0.000013	0.01645	0.00068
	63a - 33		1025	20	0.282208	0.000039	0.000825	0.000023	0.03155	0.00093
	63a - 34		1025	20	0.282222	0.00004	0.001239	0.000044	0.0451	0.0017
	63a - 4		1025	20	0.282223	0.000039	0.000338	0.000031	0.0116	0.0012
	63a - 5		1025	20	0.282223	0.000039	0.000632	0.000084	0.0234	0.0034
	63a - 6		1025	20	0.282179	0.000046	0.000528	0.000023	0.0193	0.0011
	63a - 7		1025	20	0.282215	0.000044	0.000723	0.000016	0.02181	0.00096
	63a - 8		1025	20	0.282214	0.000047	0.000652	0.000059	0.0242	0.0025
	63a - 9		1025	20	0.282187	0.00004	0.000685	0.000033	0.024	0.0011
VAG 084362	VAG62 - 1		1050	6	0.28221	0.000046	0.00091	0.000073	0.0347	0.0028
	VAG62 - 10		1050	6	0.28218	0.000041	0.000609	0.000027	0.0229	0.001
	VAG62 - 11		1050	6	0.282212	0.00003	0.00058	0.000063	0.0222	0.0026
	VAG62 - 12		1050	6	0.282234	0.000038	0.000389	0.000071	0.0143	0.0027
	VAG62 - 13		1050	6	0.2822	0.000037	0.000335	0.000057	0.0121	0.0025
	VAG62 - 14		1050	6	0.282209	0.000031	0.000634	0.000066	0.0243	0.0026
	VAG62 - 15		1050	6	0.282218	0.000034	0.000468	0.000062	0.0172	0.0025
	VAG62 - 16		1050	6	0.282203	0.000038	0.000415	0.000058	0.0151	0.0023
	VAG62 - 17		1050	6	0.282193	0.000032	0.000412	0.000038	0.0152	0.0015
	VAG62 - 18		1050	6	0.282204	0.000033	0.000565	0.000047	0.0217	0.0019
	VAG62 - 19		1050	6	0.282186	0.000042	0.000521	0.000068	0.0199	0.0026
	VAG62 - 2		1050	6	0.282211	0.00003	0.000678	0.000058	0.0265	0.0024
	VAG62 - 20		1050	6	0.282202	0.00003	0.000503	0.000064	0.0185	0.0026
	VAG62 - 21		1050	6	0.282189	0.000038	0.00074	0.00013	0.0282	0.0053
	VAG62 - 22		1050	6	0.282201	0.000039	0.000495	0.000066	0.0186	0.0026
	VAG62 - 23		1050	6	0.282228	0.000043	0.000594	0.000046	0.0215	0.0018
	VAG62 - 24		1050	6	0.282244	0.00005	0.000317	0.000027	0.011	0.0013
	VAG62 - 25		1050	6	0.2822	0.000039	0.000527	0.000049	0.0201	0.0019
	VAG62 - 3		1050	6	0.28219	0.000039	0.000606	0.000049	0.0231	0.0019
	VAG62 - 4		1050	6	0.282217	0.000035	0.00044	0.000059	0.0157	0.0023
	VAG62 - 5		1050	6	0.282197	0.000038	0.000803	0.000071	0.0314	0.0026
	VAG62 - 6		1050	6	0.282199	0.000042	0.00072	0.000073	0.0271	0.0028
	VAG62 - 7		1050	6	0.282181	0.000039	0.00046	0.000058	0.0174	0.0024
	VAG62 - 8		1050	6	0.282208 <sup>18</sup>	0.00004	0.000685	0.000093	0.026	0.0036
	VAG62 - 9		1050	6	0.282217	0.000039	0.000535	0.00006	0.02	0.0024

Appendix E - Lu-Hf data

Sample	Analysis#	Comment	Age(Ma)	2s	$^{176}\text{Hf}/^{177}\text{Hf}$	2s	$^{176}\text{Lu}/^{177}\text{Hf}$	2s	$^{176}\text{Yb}/^{177}\text{Hf}$	2s
VAG 084363	VAG63 - 1		1532	11	0.282141	0.000033	0.00421	0.00012	0.175	0.0059
	VAG63 - 10		1532	11	0.282136	0.000038	0.00134	0.00013	0.0488	0.0066
	VAG63 - 11		1532	11	0.282156	0.000038	0.001173	0.000045	0.04079	0.00093
	VAG63 - 12		1532	11	0.282082	0.000038	0.001451	0.000062	0.0552	0.0026
	VAG63 - 13		1532	11	0.282085	0.00004	0.000834	0.000043	0.02446	0.00052
	VAG63 - 14		1532	11	0.282109	0.000038	0.0025	0.00015	0.0964	0.0063
	VAG63 - 15		1532	11	0.282137	0.000043	0.00125	0.00023	0.0484	0.0095
	VAG63 - 16		1532	11	0.282086	0.00004	0.00145	0.00015	0.0549	0.0066
	VAG63 - 17		1532	11	0.282066	0.000046	0.001429	0.000022	0.05102	0.00061
	VAG63 - 18		1532	11	0.282106	0.000041	0.00232	0.00013	0.0888	0.0055
	VAG63 - 19		1532	11	0.282139	0.000057	0.0007808	0.000004	0.02797	0.00031
	VAG63 - 2		1532	11	0.282151	0.000037	0.001323	0.000028	0.045	0.002
	VAG63 - 20		1532	11	0.282115	0.000033	0.0008682	0.0000072	0.03104	0.00025
	VAG63 - 21		1532	11	0.282118	0.000035	0.001788	0.000037	0.0675	0.001
	VAG63 - 22		1532	11	0.282083	0.00003	0.00194	0.00017	0.0735	0.0069
	VAG63 - 23		1532	11	0.28215	0.000049	0.00205	0.00028	0.082	0.013
	VAG63 - 24		1532	11	0.282147	0.000038	0.001062	0.000059	0.0341	0.003
	VAG63 - 25		1532	11	0.282061	0.000055	0.001545	0.000048	0.0508	0.0013
	VAG63 - 26		1532	11	0.282047	0.000037	0.001675	0.000078	0.067	0.0031
	VAG63 - 27		1532	11	0.282143	0.000039	0.001056	0.00003	0.0388	0.0011
	VAG63 - 28		1532	11	0.282085	0.000033	0.00057	0.000024	0.02087	0.00072
	VAG63 - 29		1532	11	0.282107	0.000038	0.00129	0.00011	0.0447	0.0042
	VAG63 - 3		1532	11	0.282011	0.000035	0.0010605	0.0000048	0.04027	0.00031
	VAG63 - 30		1532	11	0.282182	0.000052	0.00291	0.00024	0.0909	0.0035
	VAG63 - 31		1532	11	0.282267	0.000056	0.00166	0.00012	0.0592	0.0049
	VAG63 - 32		1532	11	0.282201	0.000043	0.001256	0.000044	0.03766	0.00089
	VAG63 - 4		1532	11	0.282153	0.000056	0.00198	0.00013	0.0606	0.0034
	VAG63 - 5		1532	11	0.282222	0.000046	0.00528	0.00024	0.2176	0.0086
	VAG63 - 6		1532	11	0.282107	0.000046	0.00097	0.00014	0.035	0.0059
	VAG63 - 7		1532	11	0.282187	0.000046	0.001411	0.000055	0.0489	0.001
	VAG63 - 8		1532	11	0.282089	0.000033	0.00198	0.00028	0.079	0.012
	VAG63 - 9		1532	11	0.282112	0.000037	0.001433	0.000019	0.0525	0.0014
VAG 128010	10a - 1		1066	67	0.282209	0.000029	0.001196	0.000071	0.0331	0.0017
	10a - 10		1066	67	0.282219	0.000039	0.001435	0.000047	0.0486	0.0015
	10a - 11		1066	67	0.282229	0.000058	0.000847	0.000083	0.0282	0.003
	10a - 12		1066	67	0.282147	0.000037	0.00106	0.000049	0.0384	0.0022
	10a - 13		1066	67	0.282197	0.000031	0.00074	0.000029	0.0238	0.0012
	10a - 14		1066	67	0.282245	0.00004	0.001238	0.00004	0.0386	0.0011
	10a - 15		1066	67	0.282194	0.000026	0.001004	0.000017	0.0308	0.00043
	10a - 16		1066	67	0.282237	0.000039	0.002225	0.000076	0.0603	0.002
	10a - 17		1066	67	0.282198	0.000043	0.00153	0.00013	0.0505	0.0045
	10a - 2		1066	67	0.282239	0.000042	0.001192	0.000064	0.0336	0.0014
	10a - 20		1066	67	0.282213	0.000034	0.000757	0.000027	0.0253	0.0016
	10a - 21		1066	67	0.282213	0.000039	0.000594	0.000014	0.0189	0.0011
	10a - 3		1066	67	0.28216	0.000037	0.001083	0.000043	0.0362	0.0021
	10a - 4		1066	67	0.282221	0.000043	0.001174	0.000032	0.0358	0.0012
	10a - 5		1066	67	0.282178	0.000032	0.000935	0.000028	0.0331	0.0013
	10a - 6		1066	67	0.282159	0.000045	0.000714	0.000044	0.0239	0.0017
	10a - 7		1066	67	0.282227	0.000037	0.000809	0.000053	0.0269	0.0017
	10a - 8		1066	67	0.282161	0.000034	0.000933	0.000019	0.03131	0.00062
	10a - 9		1066	67	0.28222	0.000038	0.000812	0.000066	0.0287	0.0029

Appendix E - Lu-Hf data

Sample	Analysis#	Comment	Age(Ma)	2s	$^{176}\text{Hf}/^{177}\text{Hf}$	2s	$^{176}\text{Lu}/^{177}\text{Hf}$	2s	$^{176}\text{Yb}/^{177}\text{Hf}$	2s
VAG 128011	11a - 1		1078	14	0.282218	0.000042	0.001032	0.000047	0.0322	0.0014
	11a - 10		1078	14	0.282205	0.000038	0.000497	0.000056	0.0165	0.0017
	11a - 11		1078	14	0.282201	0.00004	0.000538	0.00004	0.017	0.0013
	11a - 12		1078	14	0.282243	0.000043	0.00104	0.00018	0.0311	0.005
	11a - 13		1078	14	0.282213	0.000048	0.000957	0.000081	0.0329	0.0028
	11a - 14		1078	14	0.282222	0.000052	0.001241	0.000041	0.0398	0.0017
	11a - 15		1078	14	0.2822	0.000038	0.000787	0.000019	0.02456	0.0007
	11a - 16		1078	14	0.282227	0.000032	0.00093	0.000066	0.0275	0.0021
	11a - 17		1078	14	0.282251	0.000042	0.001665	0.000028	0.04945	0.00038
	11a - 18		1078	14	0.28223	0.000036	0.00109	0.00013	0.0371	0.0045
	11a - 19		1078	14	0.282212	0.000042	0.0006	0.000011	0.01795	0.00034
	11a - 2		1078	14	0.282193	0.000037	0.000514	0.000011	0.0149	0.00044
	11a - 20		1078	14	0.282229	0.000039	0.001141	0.000036	0.0356	0.0013
	11a - 21		1078	14	0.282233	0.00004	0.001109	0.000052	0.0376	0.0022
	11a - 22		1078	14	0.282212	0.000044	0.000896	0.000032	0.0344	0.0015
	11a - 23		1078	14	0.282238	0.000038	0.001422	0.000032	0.04271	0.00085
	11a - 24		1078	14	0.282216	0.000032	0.000686	0.000052	0.0231	0.0025
	11a - 25		1078	14	0.282248	0.000036	0.00161	0.00021	0.061	0.0083
	11a - 26		1078	14	0.282235	0.000035	0.000948	0.000044	0.0268	0.0013
	11a - 27		1078	14	0.282206	0.00004	0.00098	0.00003	0.0338	0.0014
	11a - 28		1078	14	0.282232	0.000034	0.00121	0.000039	0.0395	0.0017
	11a - 29		1078	14	0.282187	0.000041	0.0003916	0.0000083	0.01175	0.00028
	11a - 3		1078	14	0.282216	0.000035	0.000976	0.00005	0.0302	0.0015
	11a - 30		1078	14	0.282195	0.000035	0.000929	0.000027	0.0289	0.0011
	11a - 31		1078	14	0.282171	0.000041	0.001064	0.000039	0.0331	0.0015
	11a - 4		1078	14	0.282224	0.000038	0.000508	0.000034	0.01547	0.00072
	11a - 5		1078	14	0.282212	0.000033	0.000556	0.000011	0.01748	0.00014
	11a - 6		1078	14	0.282174	0.000042	0.00055	0.000049	0.0176	0.0016
	11a - 7		1078	14	0.282228	0.000039	0.000719	0.000061	0.0228	0.0022
	11a - 8		1078	14	0.282231	0.00003	0.000812	0.000016	0.027	0.0014
	11a - 9		1078	14	0.282173	0.000031	0.000823	0.000053	0.0257	0.0011
VAG 128012	Age not calculated	12a - 1	1050	100	0.282251	0.000038	0.000917	0.000033	0.0329	0.0013
		12a - 10	1050	100	0.282196	0.000036	0.000893	0.000051	0.0318	0.002
		12a - 11	1050	100	0.282226	0.00004	0.001181	0.000046	0.0436	0.0018
		12a - 12	1050	100	0.282218	0.000043	0.001006	0.00002	0.03678	0.00037
		12a - 13	1050	100	0.282191	0.000036	0.001156	0.000021	0.04497	0.00091
		12a - 14	1050	100	0.282198	0.000035	0.001098	0.000014	0.04081	0.0009
		12a - 15	1050	100	0.282221	0.000033	0.001145	0.000036	0.0417	0.0012
		12a - 16	1050	100	0.282277	0.00004	0.00125	0.000086	0.0466	0.0034
		12a - 2	1050	100	0.282207	0.000043	0.001079	0.000047	0.0416	0.002
		12a - 3	1050	100	0.282229	0.000028	0.001115	0.000029	0.04165	0.00096
		12a - 4	1050	100	0.282222	0.000024	0.001042	0.000025	0.0386	0.0011
		12a - 5	1050	100	0.282216	0.00003	0.001226	0.000029	0.047	0.0013
		12a - 6	1050	100	0.282216	0.000034	0.001188	0.000034	0.0448	0.0016
		12a - 7	1050	100	0.282207	0.00004	0.001123	0.000027	0.0423	0.0014
		12a - 8	1050	100	0.282212	0.000035	0.001236	0.000018	0.0466	0.001
		12a - 9	1050	100	0.282246	0.000042	0.000954	0.000027	0.0345	0.0015

Appendix E - Lu-Hf data

Sample	Analysis#	Comment	Age(Ma)	2s	$^{176}\text{Hf}/^{177}\text{Hf}$	2s	$^{176}\text{Lu}/^{177}\text{Hf}$	2s	$^{176}\text{Yb}/^{177}\text{Hf}$	2s
VAG 128015	15a - 1	Age not calculated	1050	100	0.2822	0.000038	0.001101	0.000018	0.0417	0.001
	15a - 10		1050	100	0.282237	0.000045	0.00143	0.00012	0.0551	0.0048
	15a - 11		1050	100	0.282258	0.000037	0.001862	0.000044	0.0698	0.002
	15a - 12		1050	100	0.282246	0.000033	0.000997	0.000069	0.0358	0.0029
	15a - 13		1050	100	0.282176	0.000035	0.000699	0.000039	0.0247	0.0016
	15a - 14		1050	100	0.282257	0.00005	0.00199	0.00013	0.0753	0.0045
	15a - 15		1050	100	0.282237	0.000031	0.000873	0.000034	0.0333	0.0015
	15a - 16		1050	100	0.282228	0.000039	0.00124	0.00013	0.0451	0.005
	15a - 17		1050	100	0.282227	0.000042	0.001203	0.000071	0.0419	0.0029
	15a - 18		1050	100	0.282264	0.000036	0.001597	0.000021	0.05975	0.00059
	15a - 19		1050	100	0.282286	0.000041	0.00174	0.00015	0.0619	0.0053
	15a - 2		1050	100	0.282221	0.000038	0.001189	0.000076	0.0435	0.0029
	15a - 20		1050	100	0.282225	0.000041	0.000836	0.000057	0.0259	0.0017
	15a - 21		1050	100	0.282225	0.000043	0.001518	0.000086	0.0537	0.0033
	15a - 22		1050	100	0.282219	0.000034	0.001253	0.000081	0.0441	0.0026
	15a - 23		1050	100	0.282254	0.000049	0.001764	0.000064	0.064	0.0022
	15a - 24		1050	100	0.282235	0.000037	0.0010767	0.0000088	0.03817	0.00051
	15a - 25		1050	100	0.282193	0.00004	0.0006122	0.0000083	0.02184	0.00045
	15a - 26		1050	100	0.282281	0.000045	0.001741	0.000084	0.0598	0.0036
	15a - 27		1050	100	0.282238	0.000056	0.000924	0.000067	0.0343	0.0023
	15a - 3		1050	100	0.28223	0.000042	0.00119	0.00011	0.0433	0.0044
	15a - 4		1050	100	0.282249	0.000044	0.00073	0.000097	0.025	0.0036
	15a - 5		1050	100	0.282202	0.000041	0.000785	0.000045	0.0294	0.0016
	15a - 6		1050	100	0.282232	0.000039	0.001686	0.000066	0.0616	0.0023
	15a - 7		1050	100	0.282191	0.000039	0.000979	0.000059	0.0342	0.0018
	15a - 8		1050	100	0.282182	0.000031	0.000556	0.000029	0.0192	0.0012
	15a - 9		1050	100	0.28226	0.000039	0.001274	0.000059	0.0497	0.0024

Appendix E - Lu-Hf data

Sample	Analysis#	Comment	Age(Ma)	2s	$^{176}\text{Hf}/^{177}\text{Hf}$	2s	$^{176}\text{Lu}/^{177}\text{Hf}$	2s	$^{176}\text{Yb}/^{177}\text{Hf}$	2s
VAG 128016	16a - 1		1241	41	0.282128	0.000039	0.000581	0.000018	0.02088	0.00059
	16a - 10		1241	41	0.282145	0.000036	0.000888	0.000083	0.035	0.0035
	16a - 11		1241	41	0.282182	0.000043	0.0009	0.000065	0.035	0.0026
	16a - 12		1241	41	0.282139	0.000032	0.000981	0.000055	0.0382	0.0023
	16a - 13		1241	41	0.282168	0.000032	0.000761	0.000024	0.0269	0.0011
	16a - 14		1241	41	0.282127	0.000025	0.000592	0.000017	0.0209	0.001
	16a - 15		1241	41	0.28216	0.000029	0.000669	0.00003	0.025	0.0012
	16a - 16		1241	41	0.282122	0.000033	0.000588	0.000041	0.0217	0.0015
	16a - 17		1241	41	0.282157	0.000036	0.001092	0.000047	0.0422	0.0018
	16a - 18		1241	41	0.28217	0.000036	0.000716	0.000054	0.0274	0.0024
	16a - 19		1241	41	0.282155	0.00004	0.000957	0.00004	0.0371	0.0016
	16a - 2		1241	41	0.282194	0.000035	0.000508	0.000017	0.01749	0.00088
	16a - 20		1241	41	0.282137	0.00004	0.00132	0.00014	0.0496	0.0053
	16a - 21		1241	41	0.282208	0.000043	0.00199	0.00021	0.0787	0.0084
	16a - 22		1241	41	0.282147	0.000037	0.00147	0.00019	0.0563	0.0071
	16a - 23		1241	41	0.282153	0.000033	0.000999	0.00002	0.03882	0.00075
	16a - 24		1241	41	0.282145	0.000044	0.000988	0.000035	0.0377	0.0014
	16a - 25		1241	41	0.282134	0.000037	0.000977	0.000025	0.0374	0.00092
	16a - 26		1241	41	0.28218	0.000039	0.00147	0.00017	0.0577	0.0071
	16a - 27		1241	41	0.282126	0.000038	0.00088	0.000029	0.0328	0.0011
	16a - 28		1241	41	0.282175	0.000038	0.00103	0.000051	0.0402	0.0021
	16a - 29		1241	41	0.282161	0.000042	0.001111	0.000052	0.0425	0.0021
	16a - 3		1241	41	0.282169	0.000054	0.001064	0.000044	0.0405	0.0016
	16a - 30		1241	41	0.282153	0.000038	0.000909	0.000075	0.0352	0.0031
	16a - 31		1241	41	0.282176	0.000033	0.000464	0.000027	0.0167	0.0011
	16a - 32		1241	41	0.28218	0.00003	0.001346	0.000095	0.0518	0.0036
	16a - 33		1241	41	0.282188	0.000044	0.00146	0.00018	0.0567	0.0065
	16a - 34		1241	41	0.282153	0.000037	0.000525	0.000044	0.0192	0.0018
	16a - 35		1241	41	0.28215	0.000028	0.00064	0.000058	0.0236	0.0025
	16a - 36		1241	41	0.282152	0.000032	0.0007363	0.0000033	0.02798	0.00026
	16a - 37		1241	41	0.282167	0.00004	0.001108	0.000042	0.0399	0.0019
	16a - 38		1241	41	0.282136	0.000037	0.000999	0.000046	0.0384	0.0021
	16a - 39		1241	41	0.282136	0.000032	0.000673	0.000036	0.0256	0.0017
	16a - 4		1241	41	0.282159	0.000036	0.000914	0.00003	0.0352	0.0015
	16a - 40		1241	41	0.282154	0.000038	0.0007528	0.0000065	0.02862	0.00029
	16a - 41		1241	41	0.282161	0.000039	0.001116	0.000053	0.0433	0.0019
	16a - 5		1241	41	0.282142	0.000037	0.000515	0.000011	0.01871	0.00054
	16a - 6		1241	41	0.282131	0.000038	0.000618	0.000012	0.02334	0.00055
	16a - 7		1241	41	0.282171	0.000035	0.0015	0.000058	0.0588	0.0026
	16a - 8		1241	41	0.282176	0.000029	0.00074	0.000015	0.02788	0.00059
	16a - 9		1241	41	0.282171	0.00004	0.000852	0.000056	0.0315	0.0022

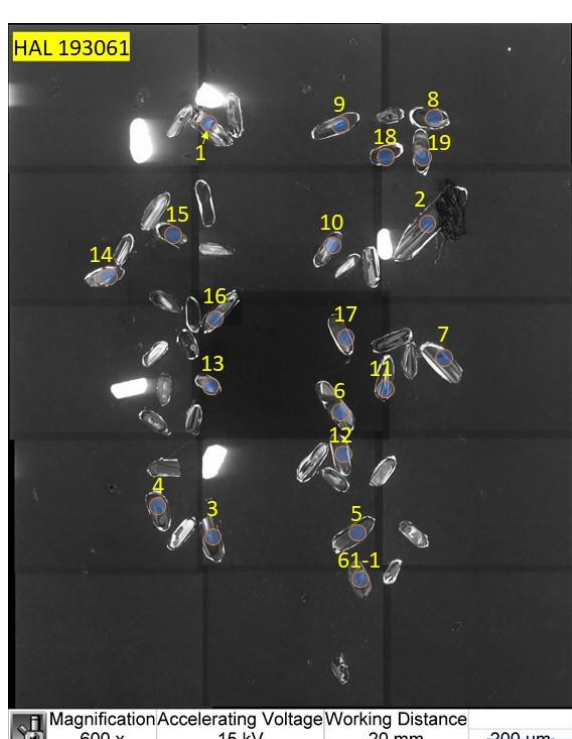
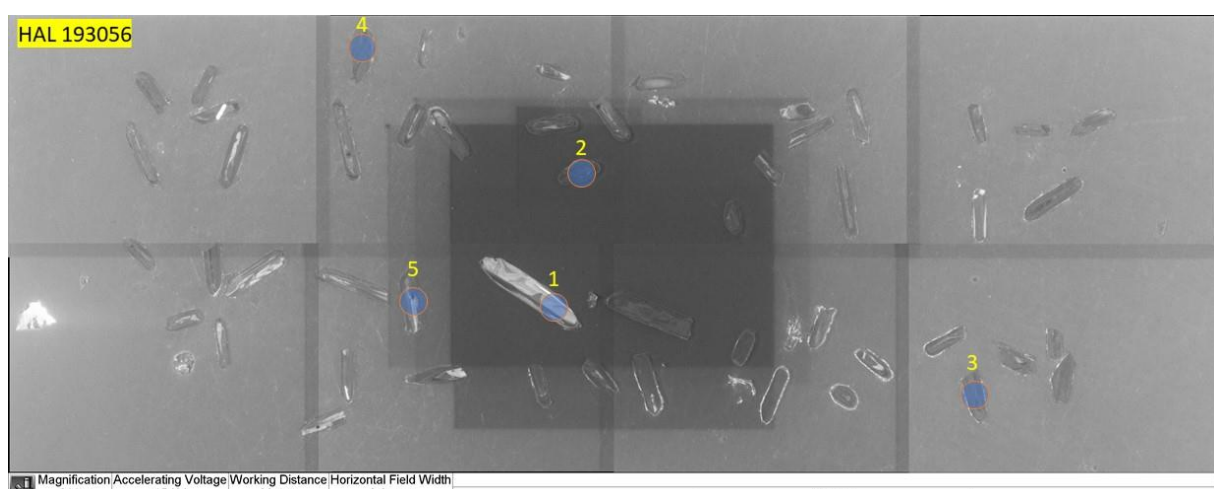
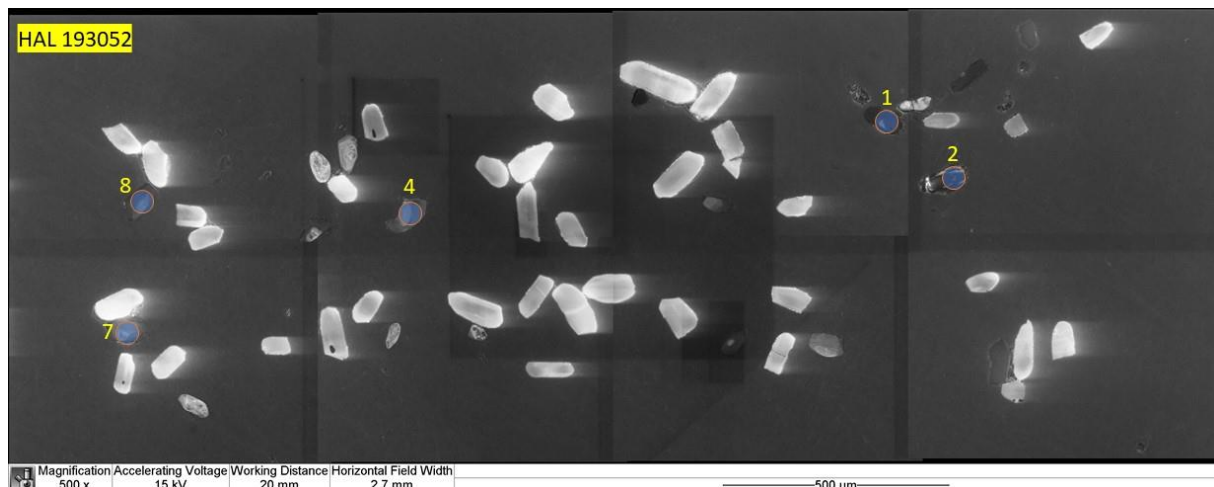
Appendix E - Lu-Hf data

Sample	Analysis#	Comment	Age(Ma)	2s	$^{176}\text{Hf}/^{177}\text{Hf}$	2s	$^{176}\text{Lu}/^{177}\text{Hf}$	2s	$^{176}\text{Yb}/^{177}\text{Hf}$	2s
VAG 128017	17a - 1		1210	31	0.282174	0.000031	0.000962	0.000098	0.0346	0.0035
	17a - 10		1210	31	0.2822	0.00004	0.001104	0.00005	0.0386	0.002
	17a - 11		1210	31	0.28216	0.000044	0.001322	0.000075	0.0504	0.0033
	17a - 12		1210	31	0.282232	0.000036	0.00119	0.00012	0.0414	0.0049
	17a - 13		1210	31	0.282124	0.000043	0.00162	0.00026	0.065	0.011
	17a - 14		1210	31	0.282246	0.000036	0.001435	0.000069	0.0464	0.0024
	17a - 15		1210	31	0.282234	0.000033	0.001152	0.000031	0.0366	0.001
	17a - 16		1210	31	0.282145	0.000036	0.000709	0.000026	0.02566	0.00053
	17a - 17		1210	31	0.282151	0.000039	0.00072	0.000023	0.02694	0.00087
	17a - 18		1210	31	0.282182	0.000045	0.001082	0.000043	0.039	0.0019
	17a - 19		1210	31	0.282072	0.000043	0.001036	0.000078	0.0384	0.003
	17a - 2		1210	31	0.282194	0.000034	0.0007295	0.000095	0.02408	0.00025
	17a - 20		1210	31	0.282287	0.000026	0.001125	0.00004	0.037	0.0013
	17a - 21		1210	31	0.282171	0.000037	0.001212	0.000096	0.0429	0.0038
	17a - 22		1210	31	0.282251	0.000033	0.0010185	0.000086	0.0312	0.00055
	17a - 23		1210	31	0.282236	0.000034	0.00152	0.000082	0.0453	0.0022
	17a - 24		1210	31	0.282224	0.000033	0.001397	0.000046	0.0523	0.002
	17a - 25		1210	31	0.282188	0.000035	0.000821	0.000068	0.0296	0.0028
	17a - 26		1210	31	0.282224	0.000031	0.00173	0.00013	0.0641	0.0042
	17a - 27		1210	31	0.282157	0.000032	0.00089	0.000037	0.0341	0.0015
	17a - 28		1210	31	0.282281	0.000032	0.000798	0.000023	0.02472	0.00086
	17a - 29		1210	31	0.282242	0.000031	0.000964	0.000027	0.0302	0.00085
	17a - 3		1210	31	0.282211	0.000024	0.000618	0.000042	0.0205	0.0012
	17a - 30		1210	31	0.282214	0.00004	0.001028	0.000063	0.0364	0.0026
	17a - 31		1210	31	0.282141	0.000032	0.000696	0.000028	0.0234	0.0012
	17a - 4		1210	31	0.282333	0.000041	0.00253	0.00011	0.0977	0.0046
	17a - 5		1210	31	0.282081	0.000035	0.001377	0.000047	0.0512	0.0018
	17a - 6		1210	31	0.282194	0.000037	0.000729	0.000014	0.02781	0.00074
	17a - 7		1210	31	0.282264	0.000039	0.0011	0.00014	0.0329	0.0046
	17a - 8		1210	31	0.282228	0.00004	0.001423	0.000095	0.0504	0.0023
	17a - 9		1210	31	0.282233	0.000031	0.00196	0.00029	0.074	0.012
VAG 128018	18a - 1		1566	7	0.282087	0.000045	0.00132	0.0001	0.038	0.0032
	18a - 10		1566	7	0.282078	0.000046	0.001552	0.000048	0.0439	0.0015
	18a - 11		1566	7	0.282049	0.000048	0.000996	0.000038	0.0292	0.0012
	18a - 12		1566	7	0.282082	0.000042	0.0012	0.00016	0.0348	0.0048
	18a - 13		1566	7	0.282084	0.000055	0.001571	0.00008	0.0448	0.0025
	18a - 14		1566	7	0.282018	0.000042	0.001107	0.000045	0.032	0.0017
	18a - 15		1566	7	0.28203	0.000031	0.001179	0.000034	0.0348	0.00086
	18a - 16		1566	7	0.282049	0.000048	0.00111	0.000047	0.0321	0.0017
	18a - 17		1566	7	0.282036	0.00004	0.00111	0.000046	0.0308	0.0014
	18a - 18		1566	7	0.282035	0.000036	0.001048	0.000018	0.03052	0.00063
	18a - 19		1566	7	0.282026	0.000051	0.000983	0.000063	0.0287	0.0017
	18a - 2		1566	7	0.282108	0.000038	0.002428	0.000039	0.0725	0.0014
	18a - 20		1566	7	0.282053	0.000042	0.001342	0.000014	0.03897	0.00051
	18a - 21		1566	7	0.28209	0.000044	0.001413	0.000038	0.04	0.0011
	18a - 22		1566	7	0.282034	0.000046	0.00154	0.000015	0.04624	0.00084
	18a - 23		1566	7	0.28206	0.000041	0.001156	0.000064	0.0325	0.002
	18a - 3		1566	7	0.282059	0.000053	0.001796	0.000018	0.05183	0.00044
	18a - 4		1566	7	0.282035	0.000047	0.00106	0.000013	0.03052	0.0004
	18a - 5		1566	7	0.28206	0.000032	0.001469	0.000048	0.0428	0.0013
	18a - 6		1566	7	0.282087	0.000044	0.002661	0.00008	0.0792	0.0022
	18a - 7		1566	7	0.282068	0.000046	0.001369	0.000018	0.03945	0.0007
	18a - 8		1566	7	0.282043	0.000034	0.00158	0.000087	0.045	0.0028
	18a - 9		1566	7	0.282059	0.000047	0.00121	0.000084	0.035	0.0026

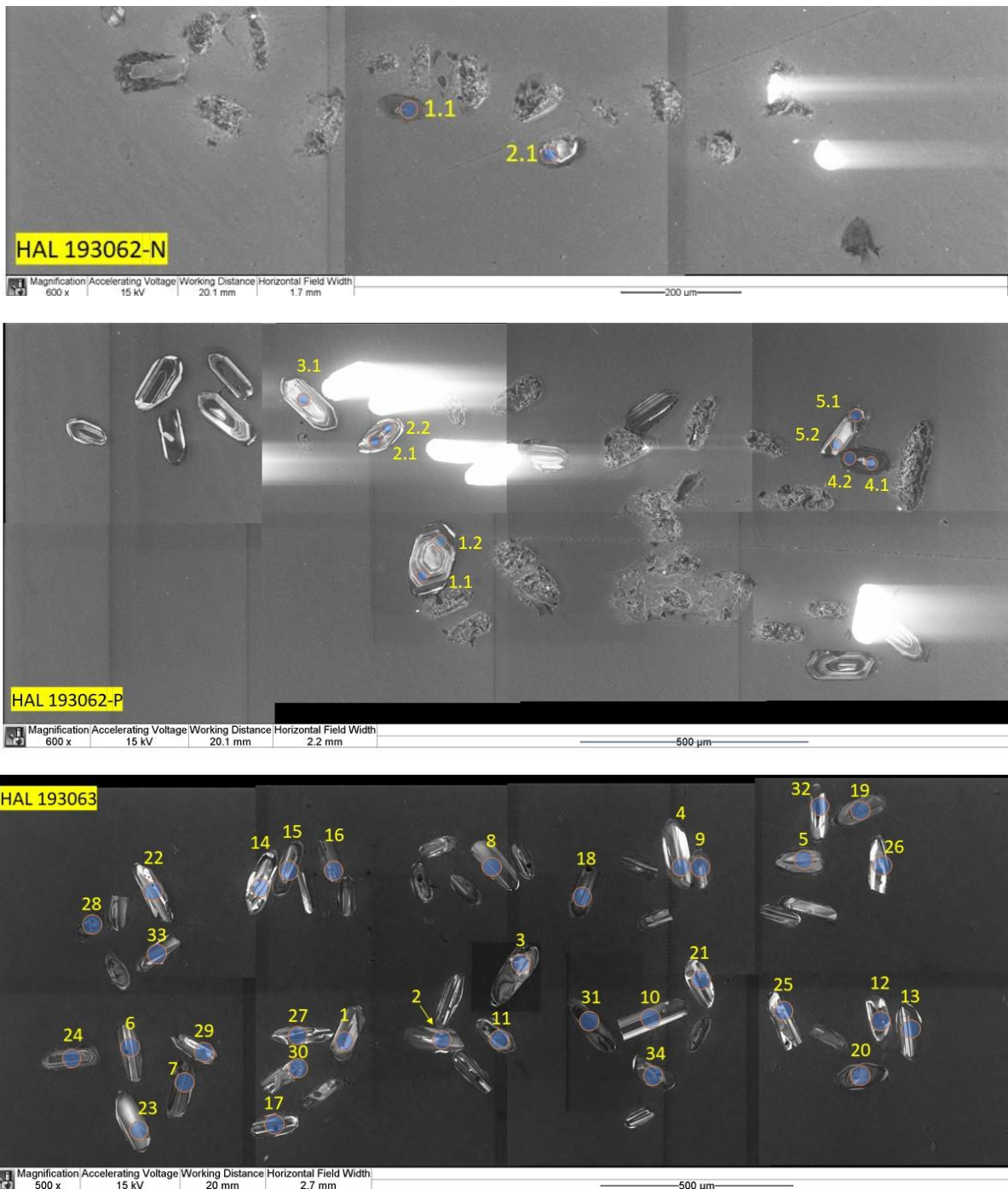
Appendix E - Lu-Hf data

Sample	Analysis#	Comment	Age(Ma)	2s	$^{176}\text{Hf}/^{177}\text{Hf}$	2s	$^{176}\text{Lu}/^{177}\text{Hf}$	2s	$^{176}\text{Yb}/^{177}\text{Hf}$	2s
VAG 128019	19a - 1		1208	16	0.282179	0.000038	0.000994	0.000017	0.03762	0.00058
	19a - 10		1208	16	0.2822	0.000035	0.001114	0.000055	0.042	0.0021
	19a - 11		1208	16	0.282181	0.000033	0.00128	0.000047	0.0489	0.002
	19a - 12		1208	16	0.282146	0.000036	0.00115	0.000013	0.04436	0.00061
	19a - 13		1208	16	0.28223	0.000054	0.00112	0.00011	0.0381	0.0023
	19a - 14		1208	16	0.282144	0.000035	0.000913	0.00003	0.0342	0.0011
	19a - 15		1208	16	0.282133	0.000034	0.001204	0.000015	0.04609	0.00072
	19a - 16		1208	16	0.282138	0.000042	0.00092	0.000018	0.03349	0.00073
	19a - 17		1208	16	0.28217	0.000047	0.000969	0.000036	0.0355	0.0015
	19a - 18		1208	16	0.282148	0.000037	0.000863	0.000033	0.0318	0.0013
	19a - 19		1208	16	0.282204	0.000043	0.00208	0.00019	0.0744	0.0059
	19a - 2		1208	16	0.282152	0.000037	0.0008077	0.0000036	0.02999	0.00019
	19a - 20		1208	16	0.28214	0.000033	0.001497	0.000079	0.0577	0.0029
	19a - 21		1208	16	0.282128	0.000032	0.000795	0.000012	0.0294	0.00054
	19a - 22		1208	16	0.282145	0.000038	0.001343	0.000042	0.0512	0.0015
	19a - 23		1208	16	0.28215	0.000045	0.00115	0.00011	0.0439	0.004
	19a - 24		1208	16	0.282135	0.000047	0.0008983	0.0000037	0.03345	0.00022
	19a - 25		1208	16	0.282157	0.000039	0.000939	0.00003	0.0354	0.0011
	19a - 26		1208	16	0.282187	0.000049	0.00096	0.000068	0.0349	0.0024
	19a - 27		1208	16	0.282135	0.000037	0.00206	0.00012	0.0832	0.0049
	19a - 28		1208	16	0.282169	0.000035	0.00131	0.00019	0.0512	0.0077
	19a - 3		1208	16	0.282257	0.000049	0.00341	0.00012	0.1216	0.0018
	19a - 30		1208	16	0.282159	0.000034	0.000968	0.000057	0.0368	0.0023
	19a - 31		1208	16	0.282153	0.000034	0.0009951	0.0000038	0.03781	0.00018
	19a - 32		1208	16	0.282158	0.000036	0.000796	0.000019	0.02994	0.00056
	19a - 33		1208	16	0.282136	0.000036	0.000567	0.000014	0.0205	0.00047
	19a - 34		1208	16	0.28213	0.000042	0.00102943	0.0000009	0.03887	0.00022
	19a - 35		1208	16	0.282117	0.000028	0.0008865	0.0000092	0.03314	0.0002
	19a - 36		1208	16	0.282123	0.000037	0.001002	0.000019	0.03762	0.00088
	19a - 37		1208	16	0.282157	0.000035	0.0011	0.000021	0.0418	0.001
	19a - 38		1208	16	0.282167	0.000043	0.000856	0.0000037	0.03191	0.00031
	19a - 39		1208	16	0.282119	0.000035	0.001093	0.000098	0.043	0.0043
	19a - 4		1208	16	0.282186	0.000038	0.001591	0.000057	0.063	0.0023
	19a - 40		1208	16	0.282168	0.000041	0.000997	0.000051	0.038	0.0021
	19a - 41		1208	16	0.282198	0.000046	0.00155	0.00014	0.06	0.0056
	19a - 42		1208	16	0.282168	0.000035	0.001089	0.000032	0.0411	0.0013
	19a - 43		1208	16	0.282161	0.00004	0.000762	0.000015	0.02792	0.00069
	19a - 44		1208	16	0.282175	0.000041	0.001163	0.000041	0.0445	0.0015
	19a - 45		1208	16	0.282115	0.000034	0.000778	0.000026	0.029	0.0012
	19a - 46		1208	16	0.28215	0.00004	0.001127	0.000079	0.043	0.003
	19a - 47		1208	16	0.28214	0.000029	0.000811	0.000044	0.0303	0.0017
	19a - 48		1208	16	0.28224	0.000038	0.00145	0.00012	0.0497	0.0052
	19a - 49		1208	16	0.282159	0.00004	0.001596	0.000042	0.0539	0.0012
	19a - 5		1208	16	0.282138	0.000021	0.00091	0.000011	0.034	0.0007
	19a - 6		1208	16	0.28213	0.000038	0.000759	0.000015	0.02803	0.00072
	19a - 7		1208	16	0.282146	0.00003	0.00095	0.000018	0.03579	0.00089
	19a - 8		1208	16	0.282155	0.000043	0.00126	0.0002	0.0488	0.0083
	19a - 9		1208	16	0.282144	0.000039	0.000876	0.0000054	0.03277	0.00035

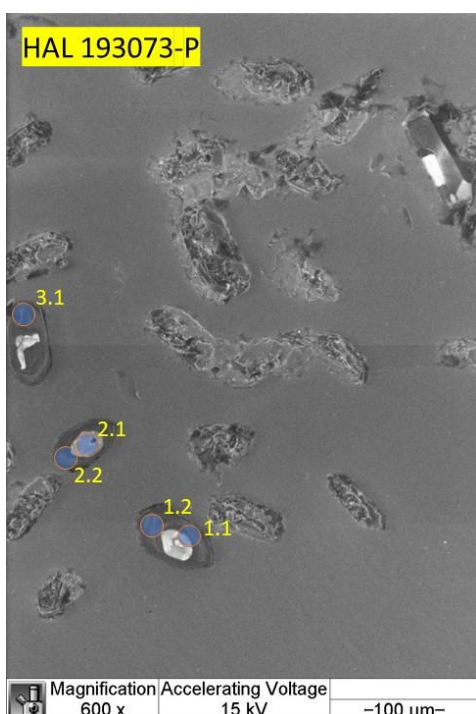
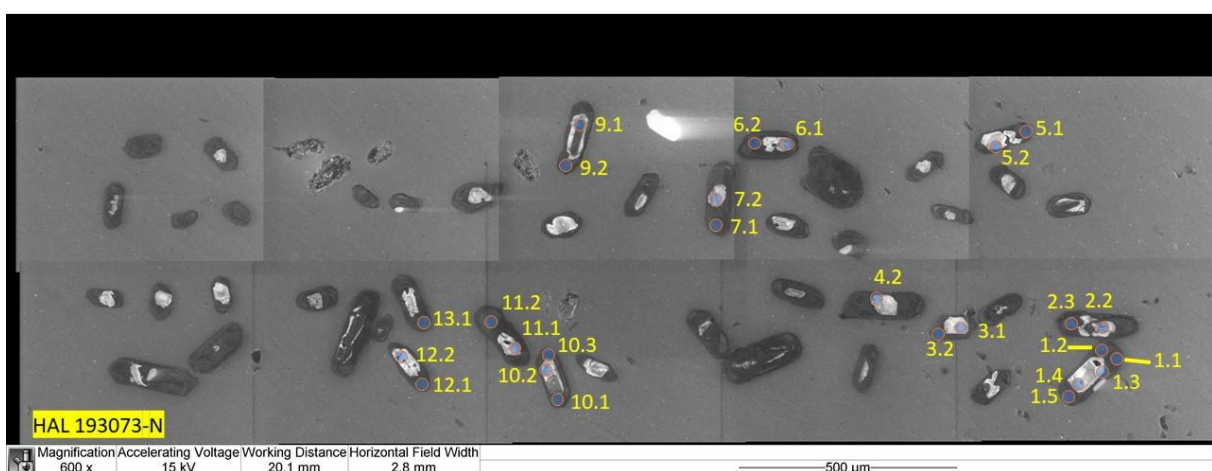
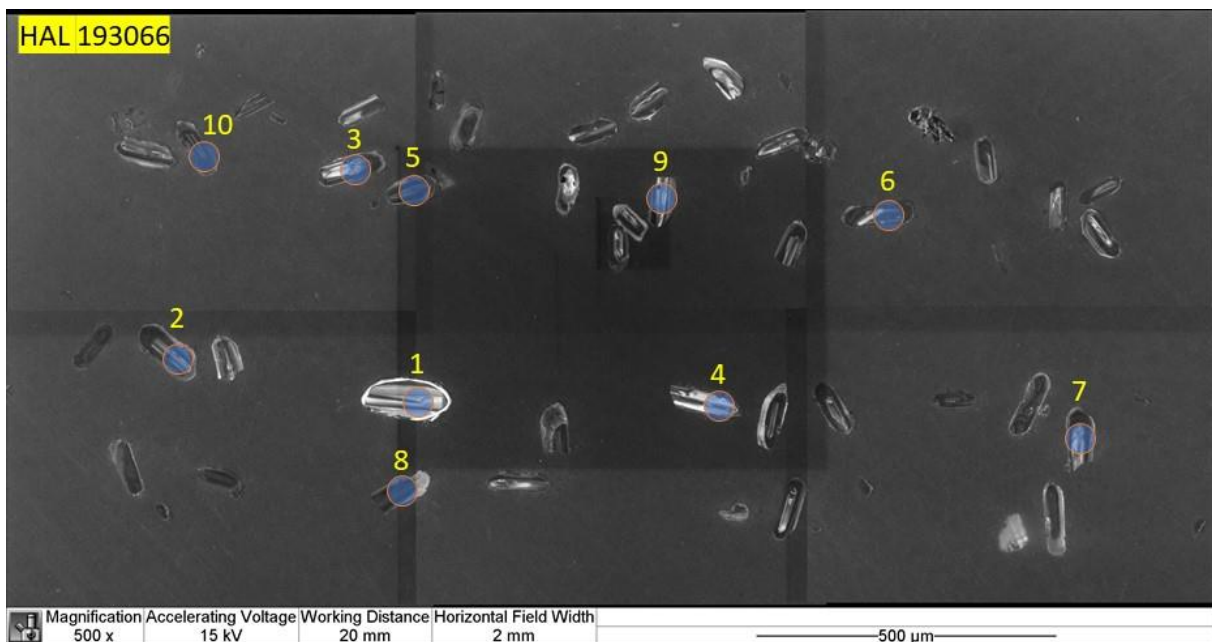
Appendix F – Zircon data sampling map



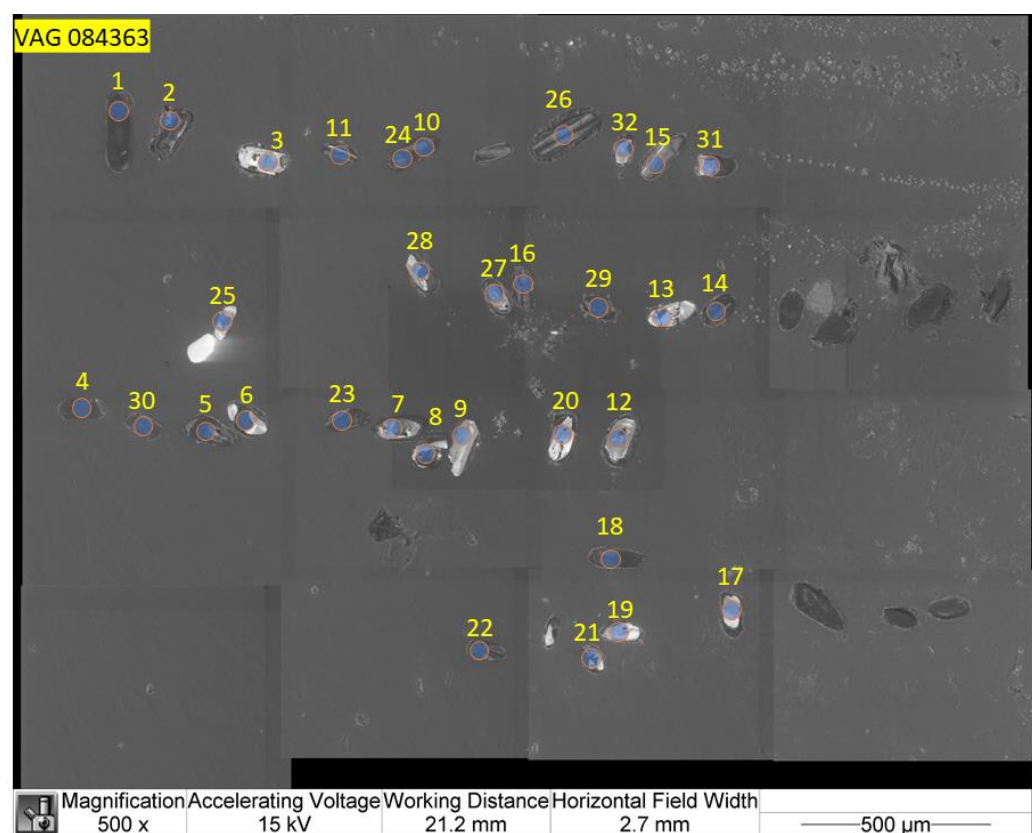
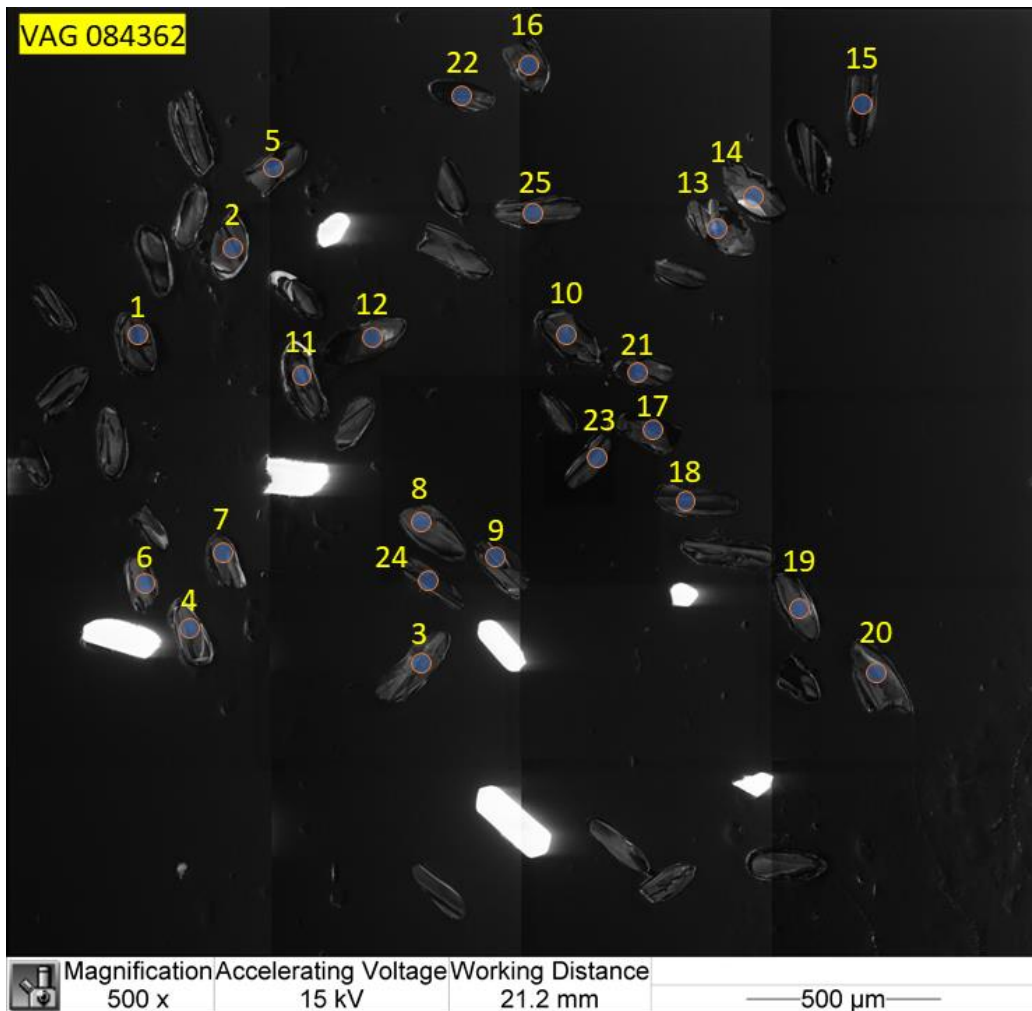
## Appendix F – Zircon data sampling map



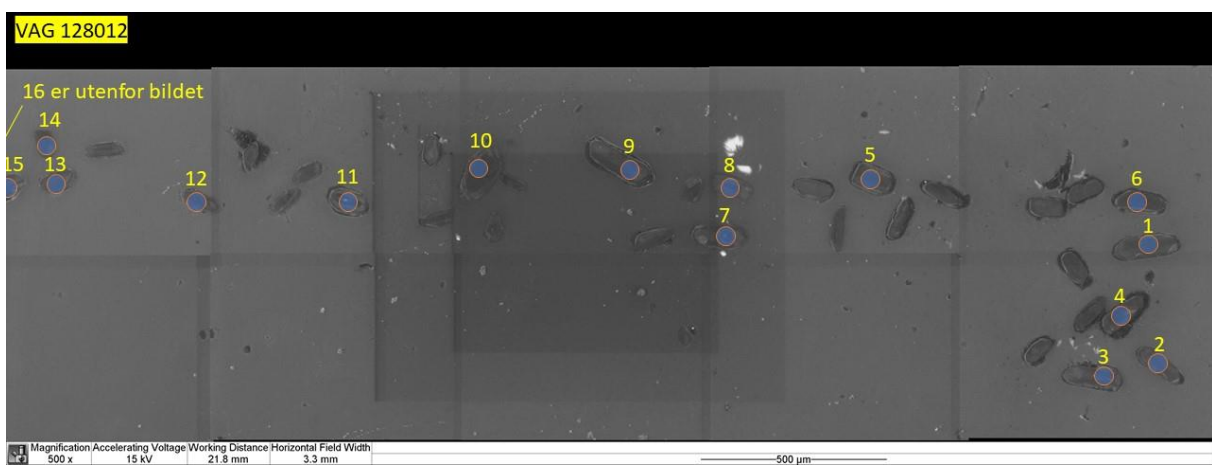
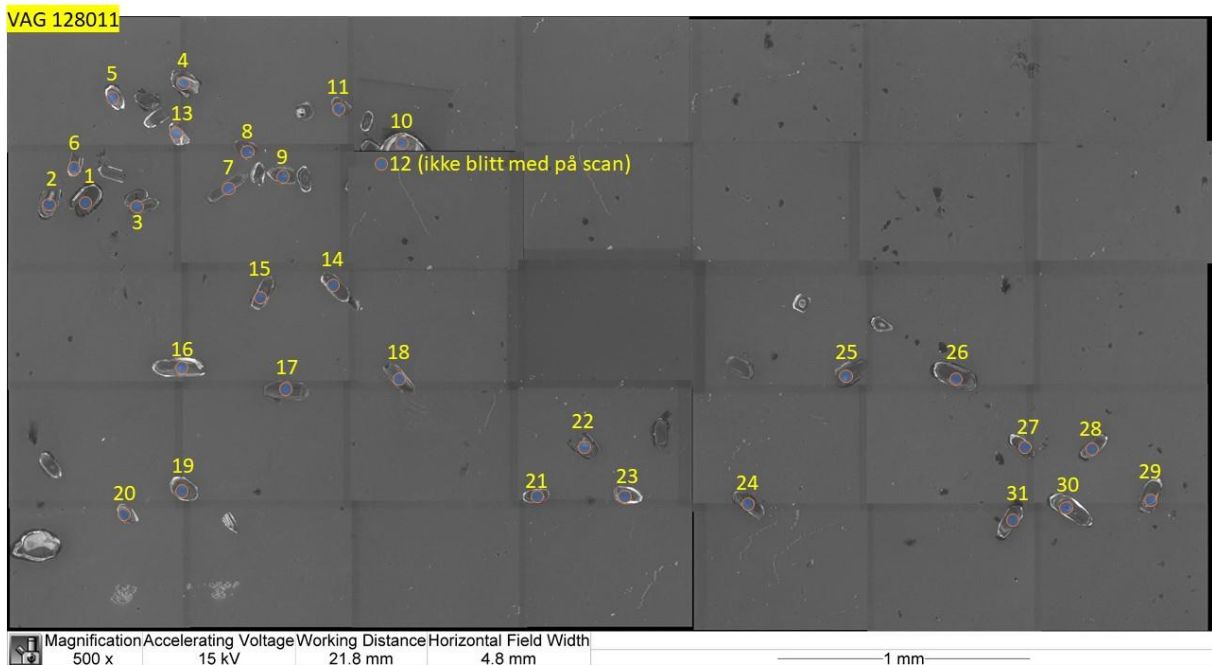
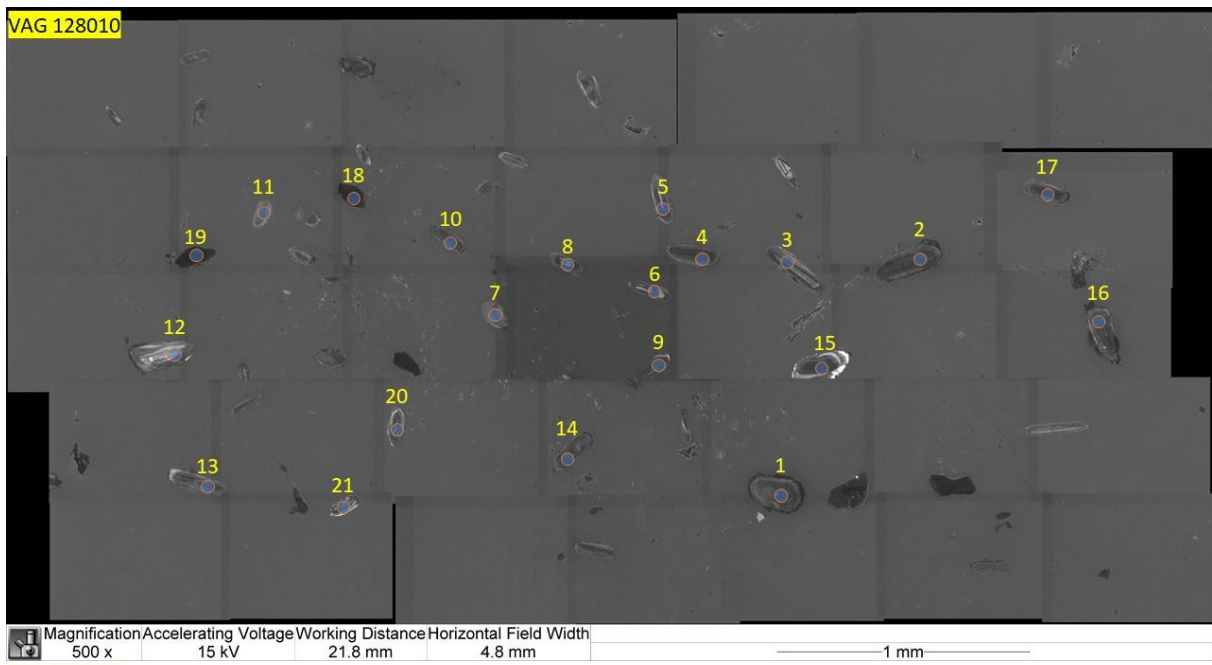
## Appendix F – Zircon data sampling map



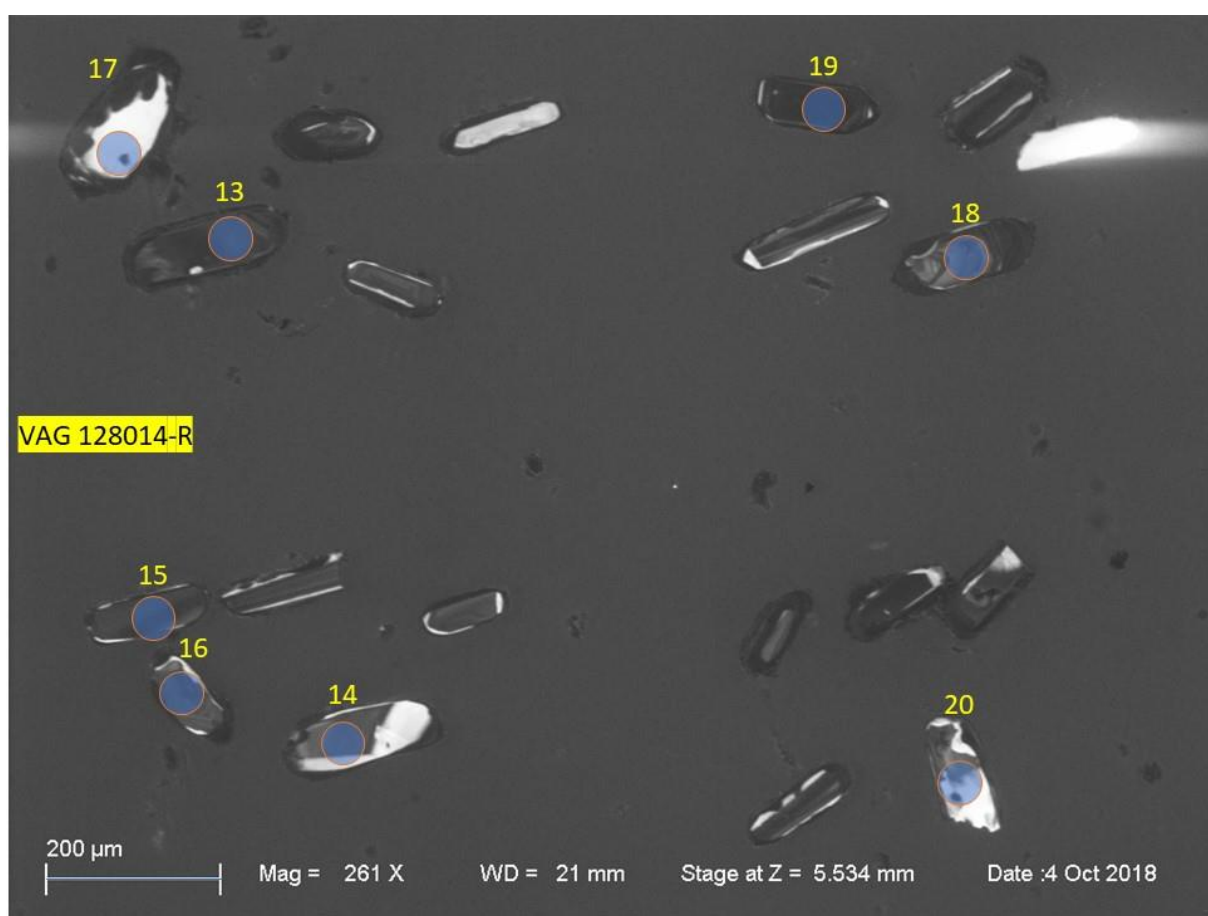
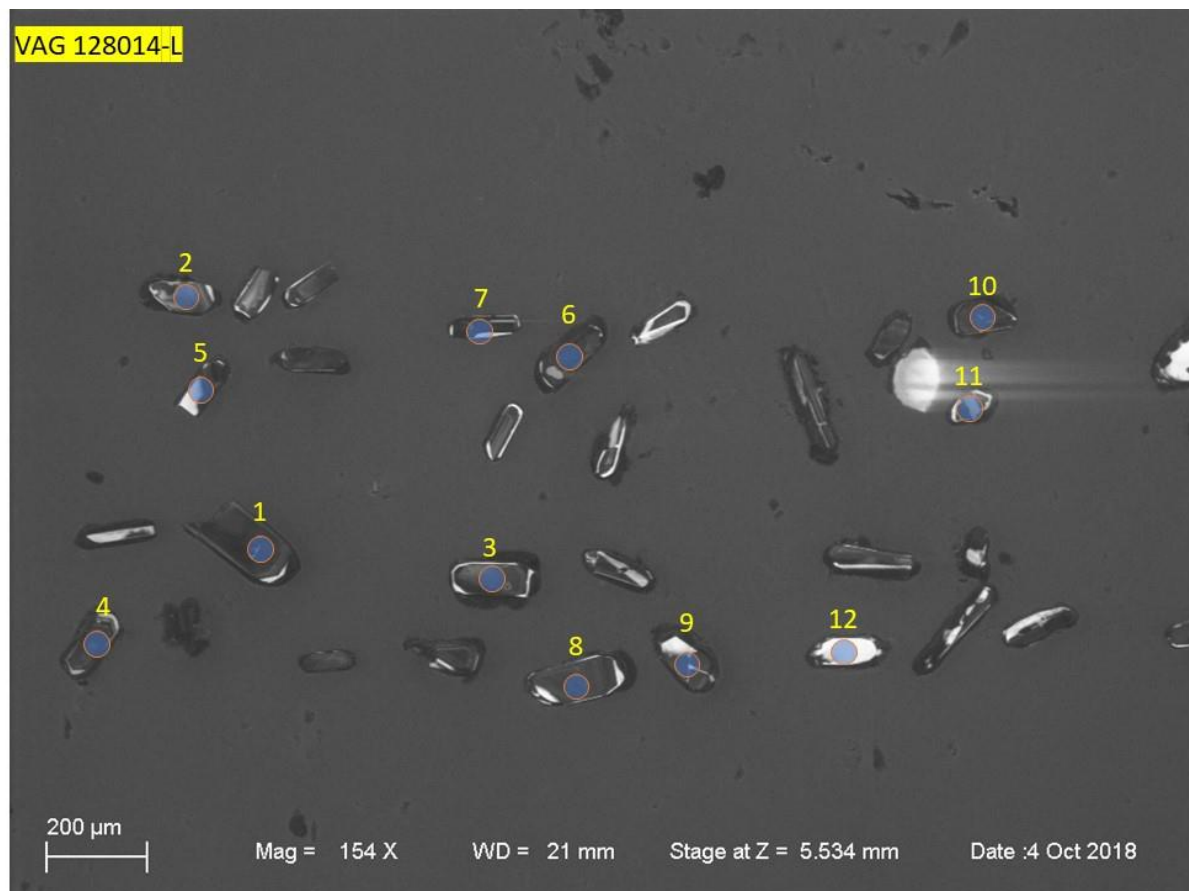
Appendix F – Zircon data sampling map



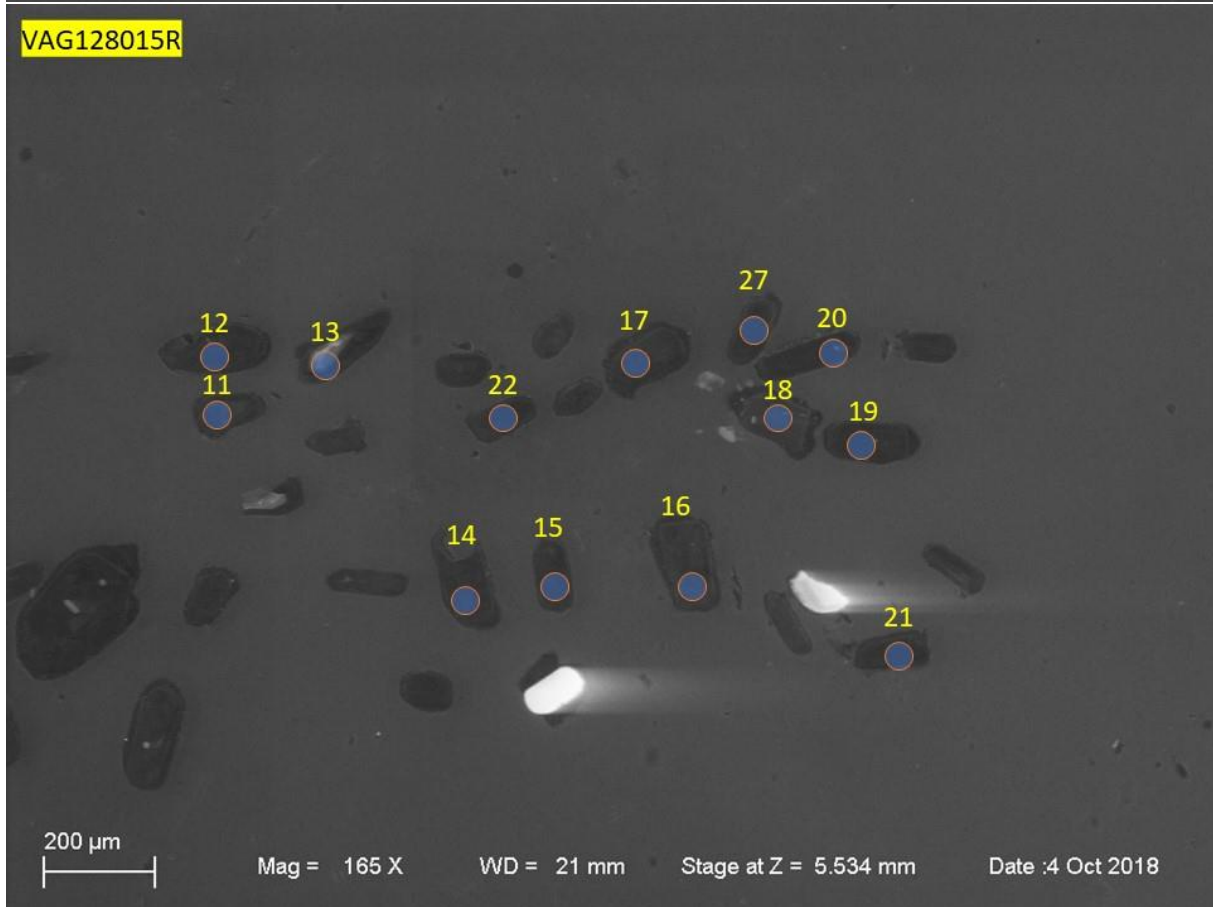
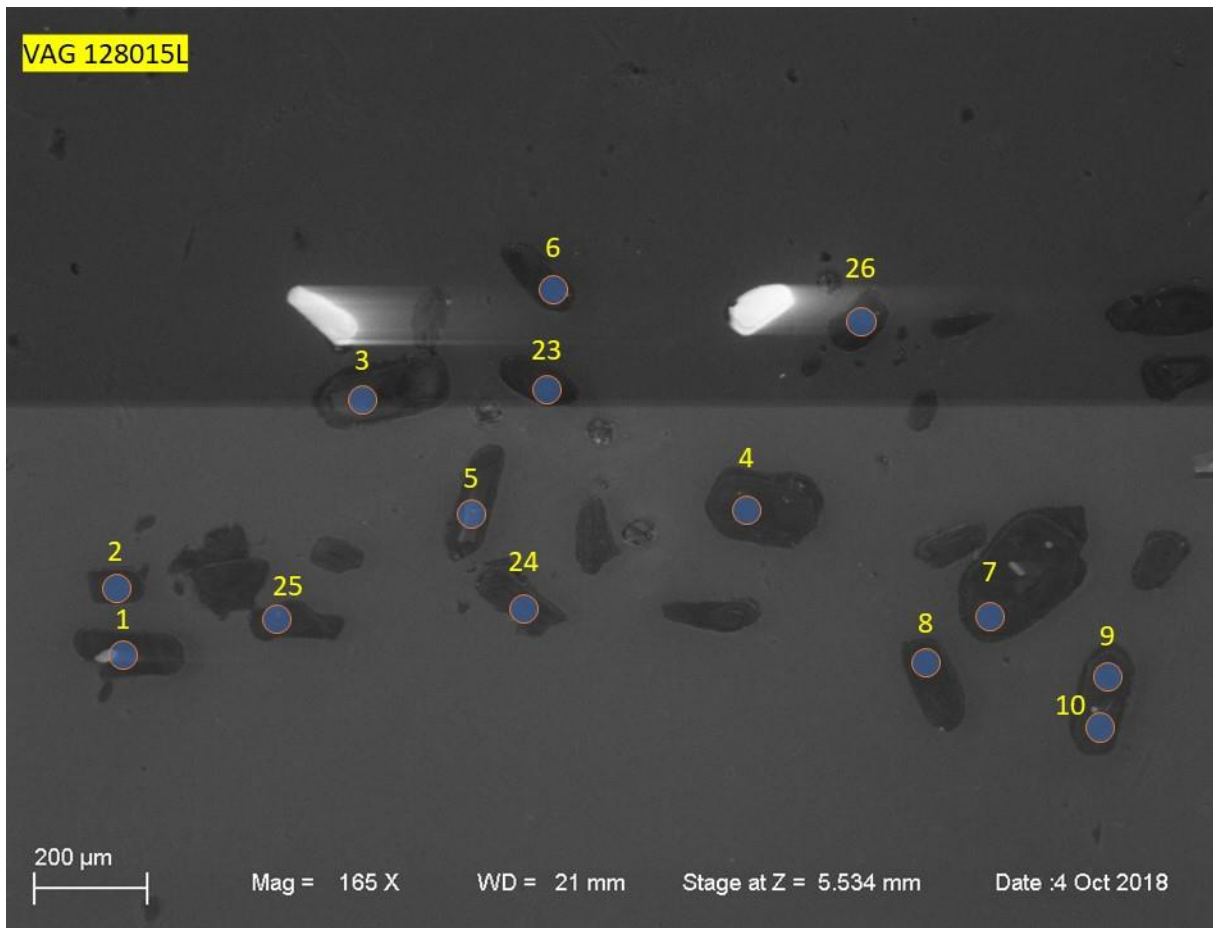
## Appendix F – Zircon data sampling map



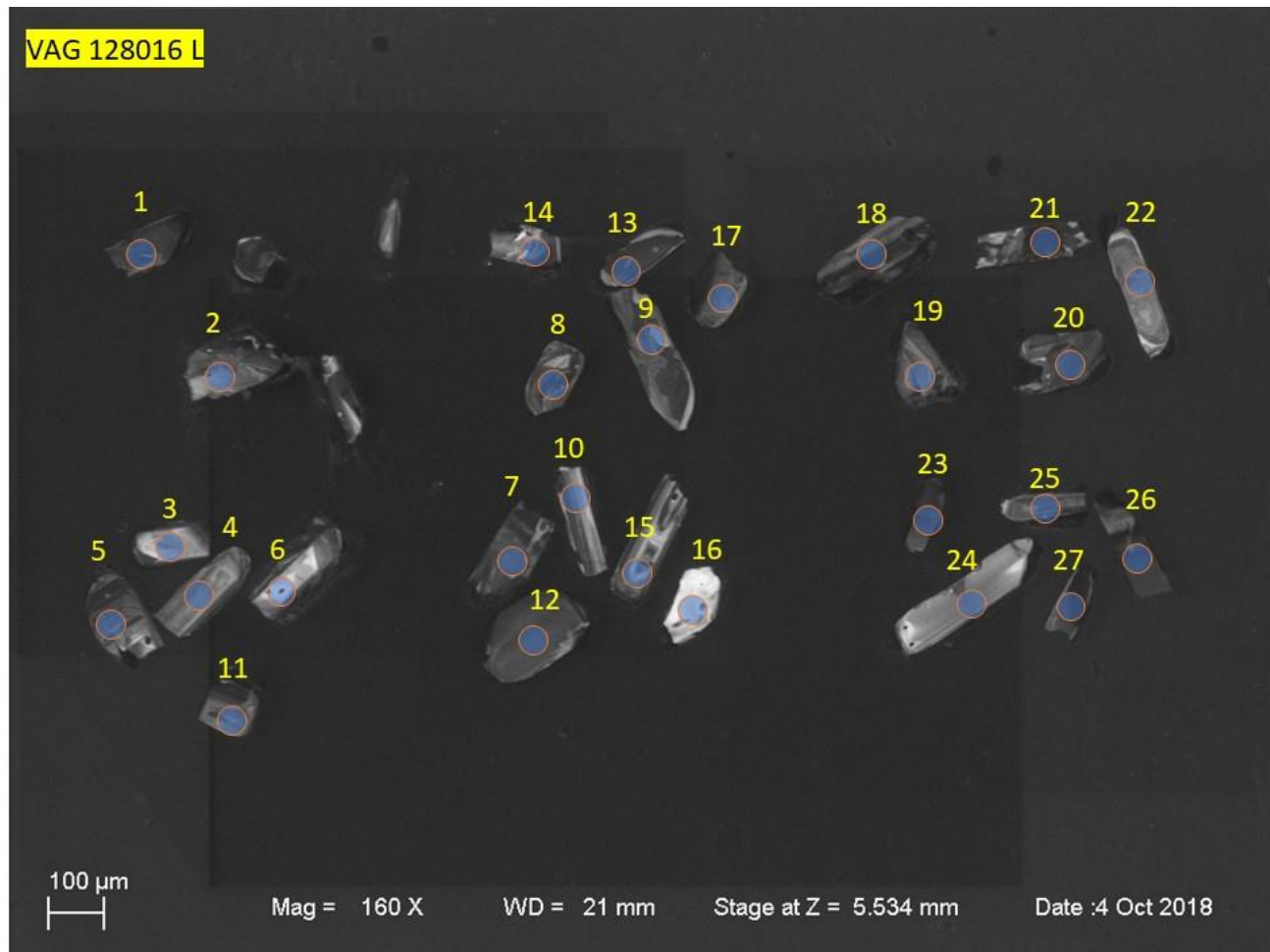
Appendix F – Zircon data sampling map



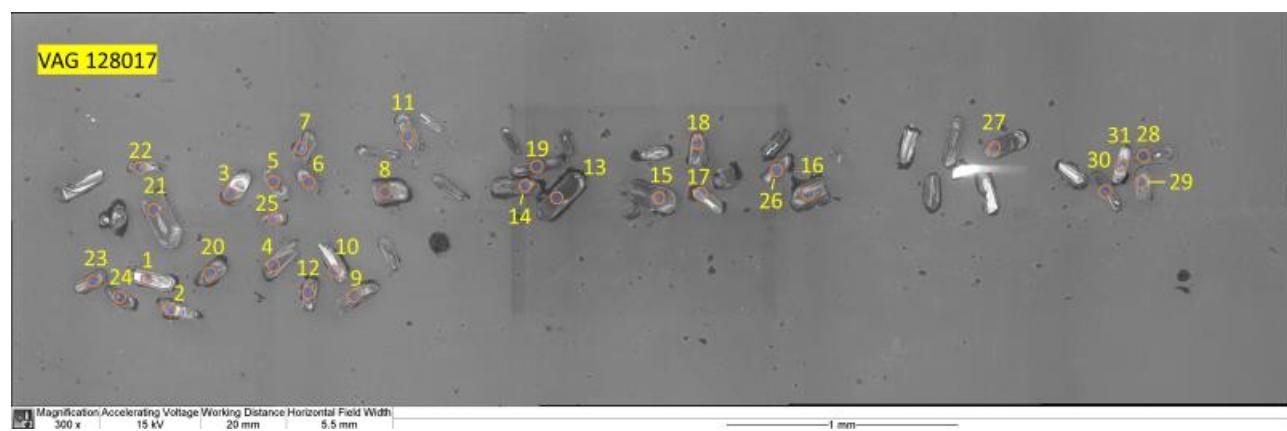
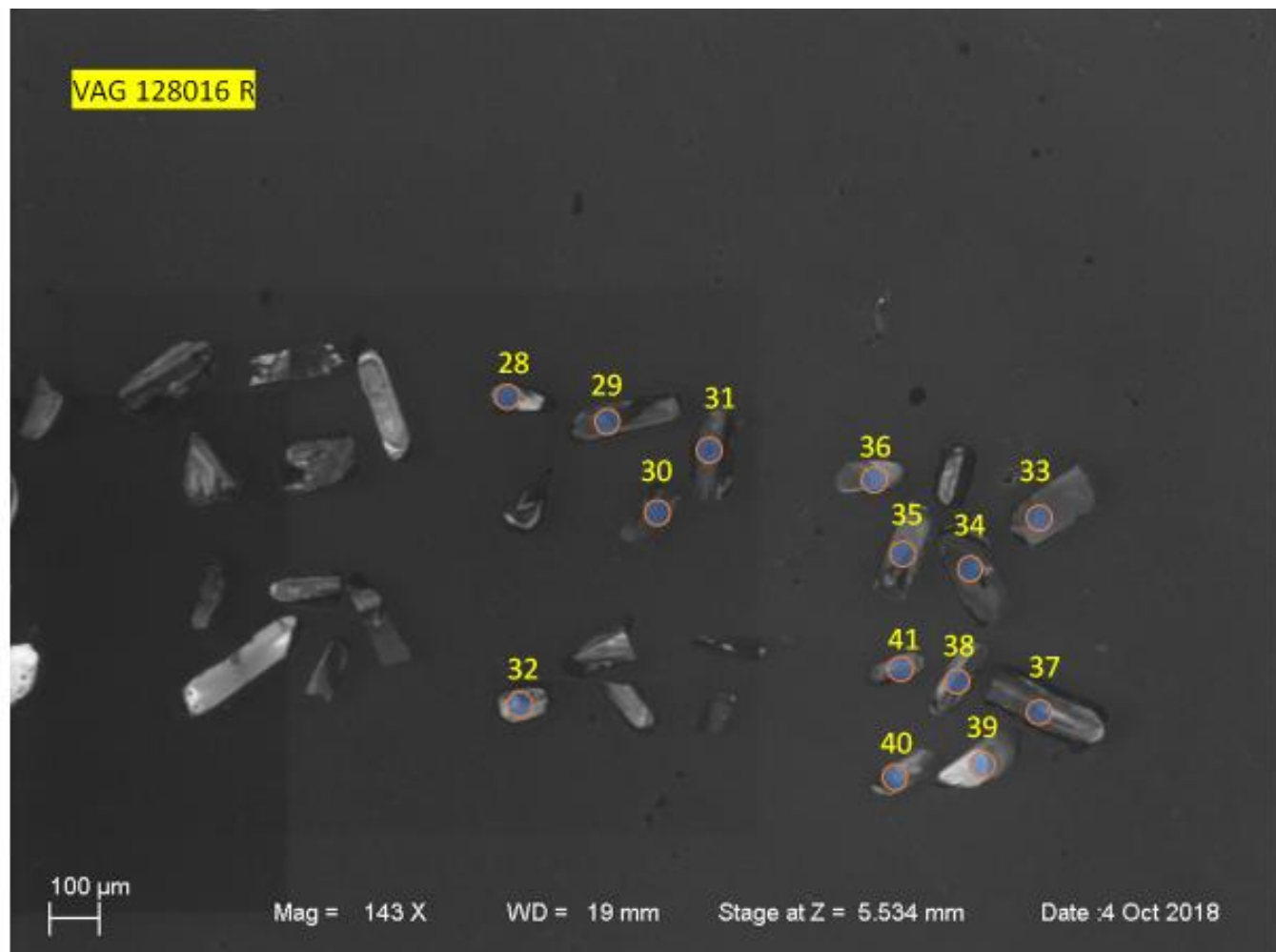
Appendix F – Zircon data sampling map



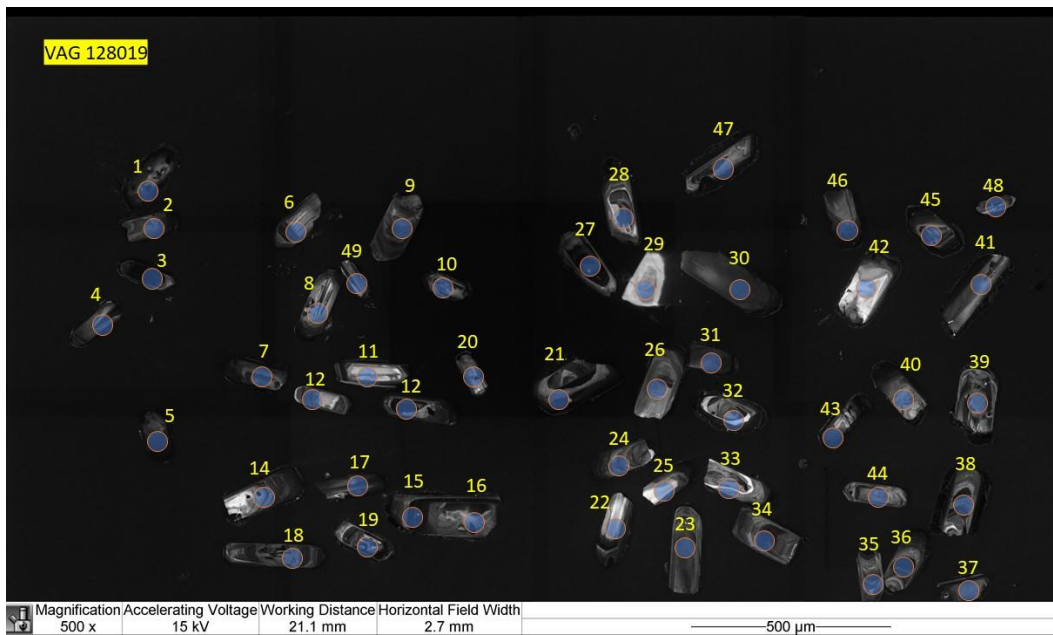
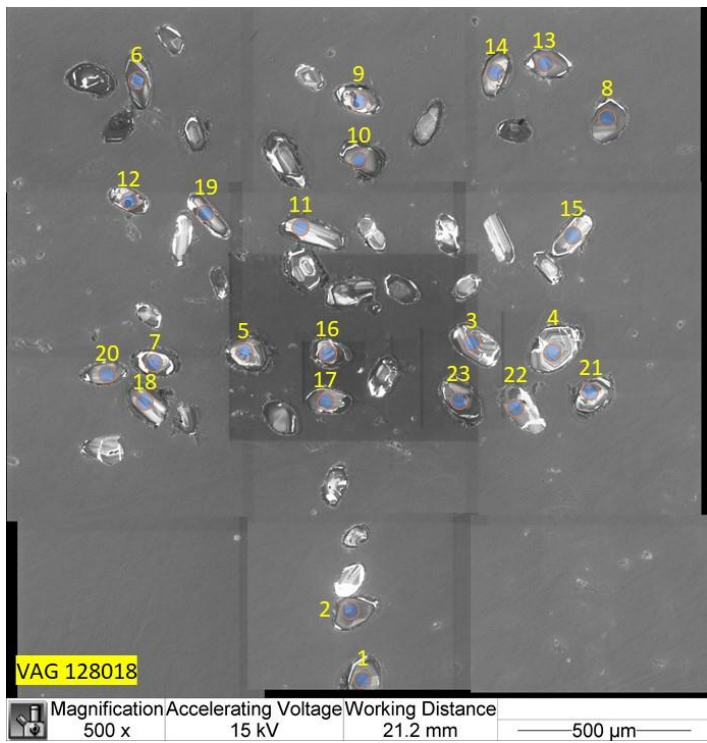
Appendix F – Zircon data sampling map



Appendix F – Zircon data sampling map



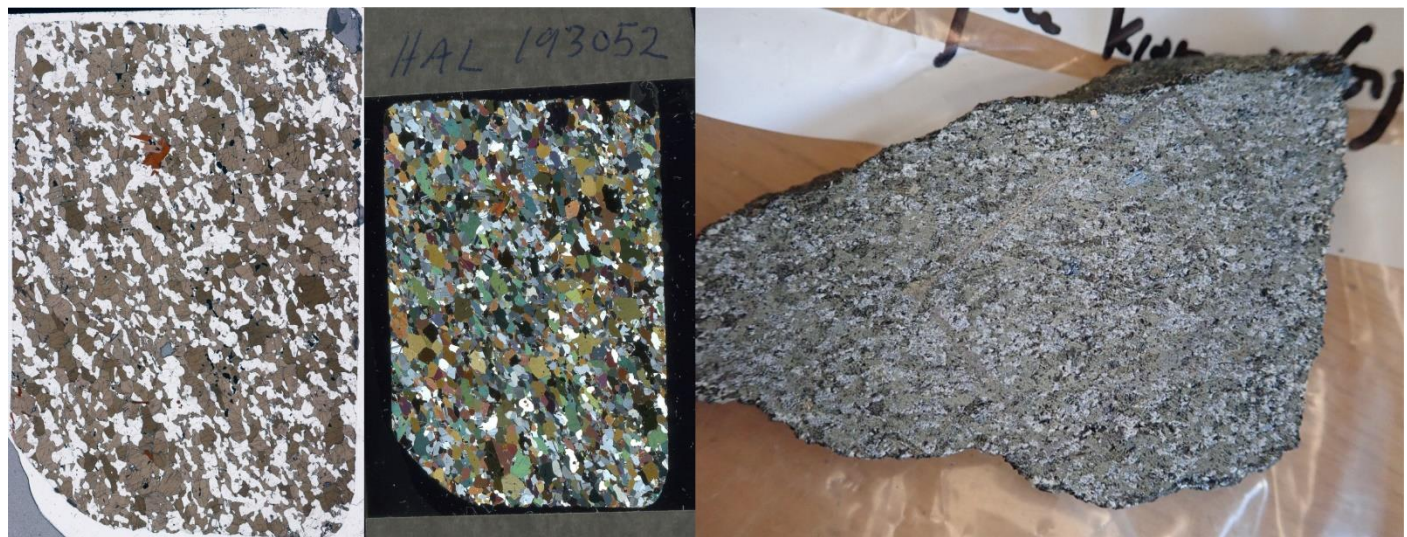
## Appendix F – Zircon data sampling map



## Appendix G – Thin section notes

### Mineral abbreviations

Apa	Apatite
Plg	Plagioclase
A-Fds	Alkalifeldspar
Qtz	Quartz
Zrn	Zircon
Amp	Amphibole
Bt	Biotite
Ser	Sericite
Aln	Allanite
Fds	Feldspar
Msc	Microcline



**Sample:** HAL193052

**Location:** 10

**Unit:** Amphibolite

**Major minerals:** amp (55%), plg (45%)

**Accessory minerals:** Qtz, Ttn, Bt, Zrn, Apa, A-Fds, Msc, Op

- Medium to fine-grained Amphibolite. Grain size varies up to 2 mm in size with recrystallization resulting in smaller grain size.
- Carlsbad twinning in Amp.
- Bt appears as thin needles <0.25 mm in length.
- Inclusions of Qtz in Amp
- 'Ttn seems retrograde and turning into Amp



**Sample:** HAL193053

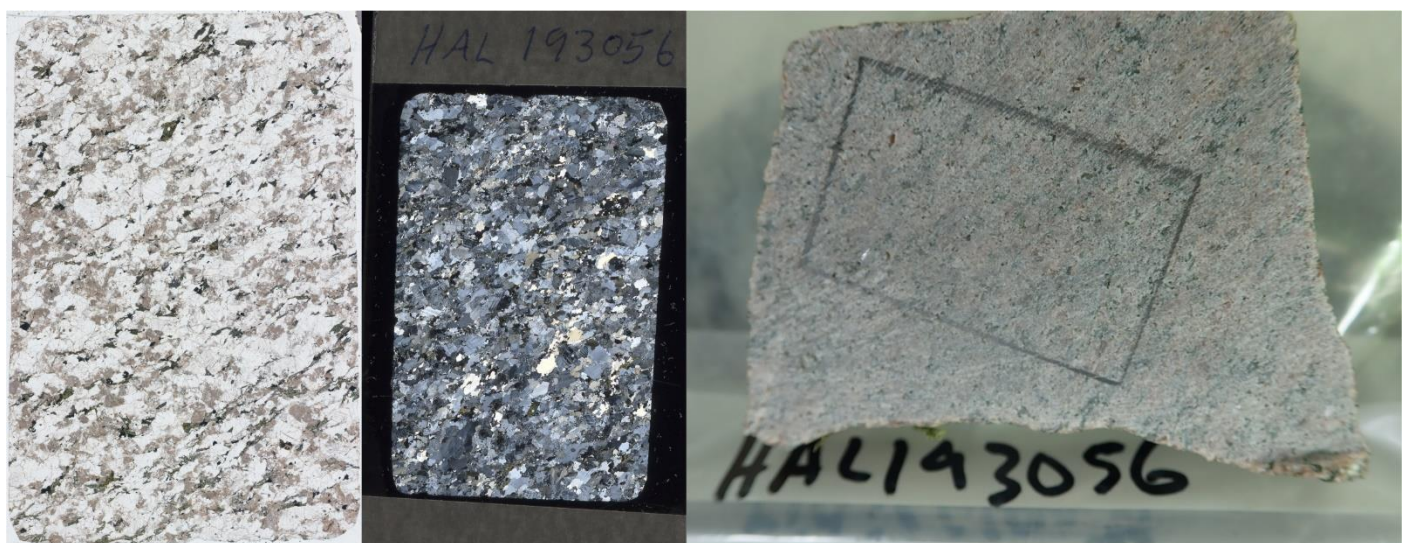
**Location:** 11

**Unit:** Disperse migmatite

**Major minerals:** Qtz (60%), Plg (25%), Bt (10%), A-Fds (5%)

**Accessory minerals:** Apa, Zrn, Op, Ser

- Mesosome: fine-grained Bt, Qtz, Fds
- Leucosome: medium-grained Qtz, and Fds
- Melanosome: Slightly more Bt than in Mesosome
- Seritization of microcline, Myrmekite, boundary migration, recrystallisation of quartz
- Bt and leucosome follows foliation Myrmekite



**Sample:** HAL193056

**Location:** 34

**Unit:** Fidje-granite

**Major minerals:** Qtz (35%), A-Fds (30%), Plg (30%), Op (2%), Bt (2%)

**Accessory minerals:** Zrn, Msc

- Sericitization of Plg
- Green Bt
- Myrmekite
- Perthite
- Microcline
- Recrystallization of Qtz



**Sample:** HAL193058

**Location:** 44

**Unit:** Amphibolite

**Major minerals:** Amp (60%), Plg (30%), Bt (10%),

**Accessory minerals:** Ttn, Apa

- Secondary alteration of Plg, possibly seritization
- Granoblastic textures
- Equigranular fine to medium-grained
- Alteration of Ttn
- Clear linear foliation



**Sample:** HAL193059

**Location:** 73

**Unit:** Augen-gneiss

**Major minerals:** Qtz (80%), A-Fds (10%), Plg (5%), Amp (5%)

**Accessory minerals:** Bt, Apa, Zrn, Op

- Myrmekite
- Radiogenic haloes in Bt from Zrn
- High degree of recrystallization
- Phenocrysts are aggregates of coarse Qtz
- Recrystallization of quartz
- Bulging
- Retrograde ampMicrocline and perthite



**Sample:** HAL193061

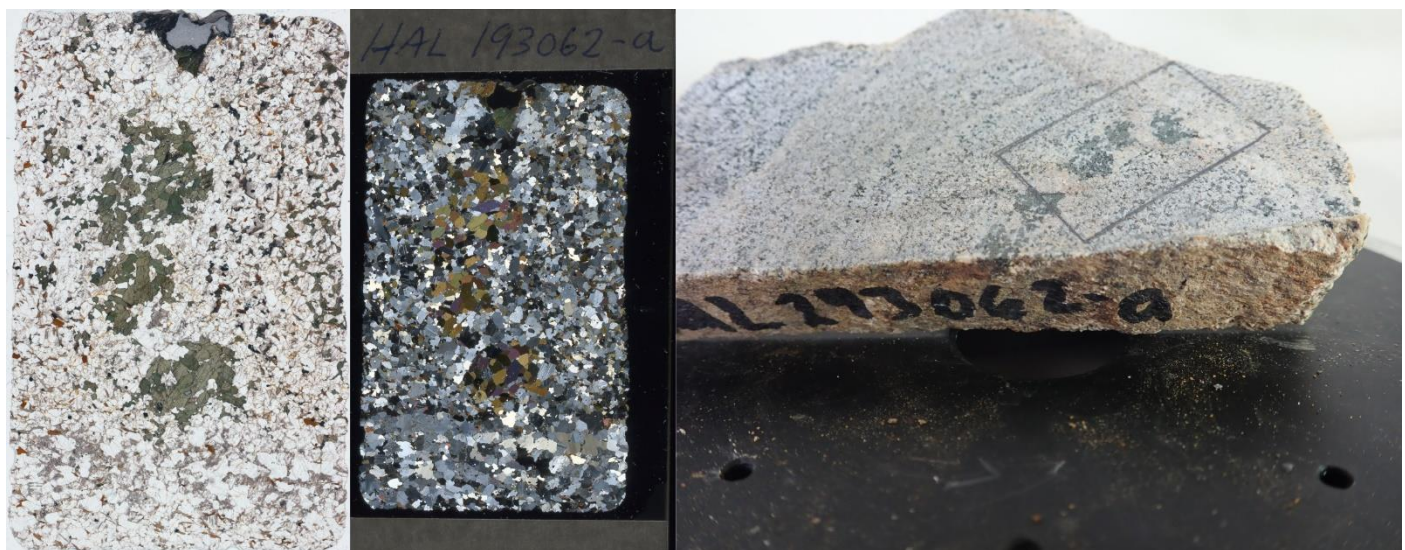
**Location:** 37

**Unit:** Deformed granite

**Major minerals:** A-Fds (70%), Qtz (10%), Amp (10%), Plg (5%), Bt (5%)

**Accessory minerals:** Apa, Ser, Zrn

- Large Perthite crystal and smaller phenocrysts of Qtz with zoned alteration
- Alteration of Plg Sericite
- Myrmekite
- Carlsbad in Amp
- Foliation
- Recrystallization of Qtz



**Sample:** HAL193062-a

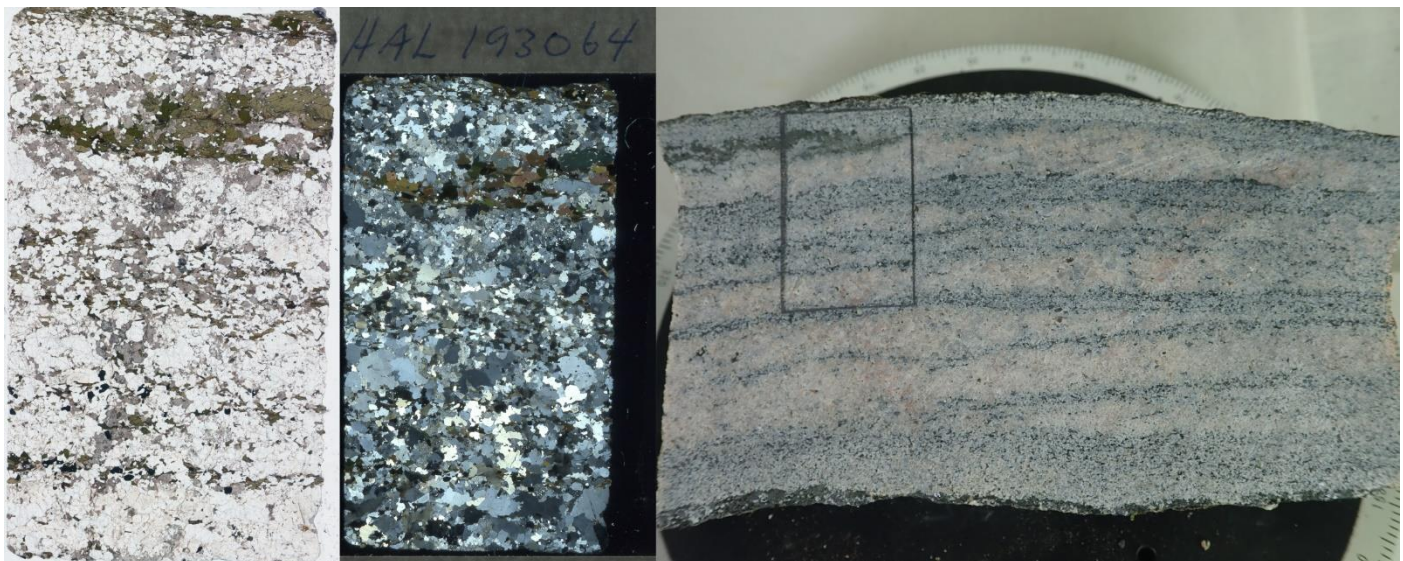
**Location:** 105

**Unit:** Disperse migmatite

**Major minerals:** Qtz (50%), Amp (25%), Plg (15%), Bt (5%), A-Fds (5%)

**Accessory minerals:** Apa, Zrn, Ser

- Seritization
- Aggregates of medium-grained Amp
- Fine-grained
- Areas lacks Amp; others have fine-grained amp like the rest of the minerals
- Recrystallization, granoblastic textures and bulging of quartz



**Sample:** HAL193064

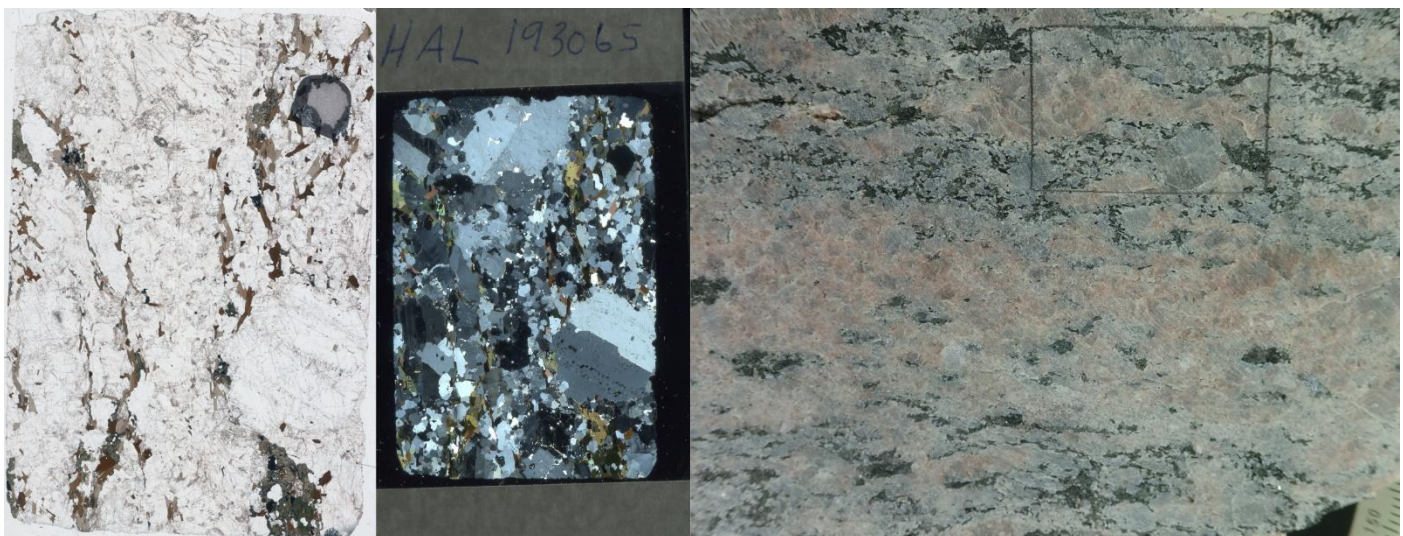
**Location:** 118

**Unit:** Disperse migmatite

**Major minerals:** Qtz (50%), Plg (25%), Amp (15%), A-Fds (5%), Bt (5%)

**Accessory minerals:** Apa, Zrn, Ser

- Phenocrysts of medium-grained quartz and seritized plg.
- Phenocrysts of fine to medium-grained Amp
- Inclusions of Apa in Amp, and A-Fds in Plg
- Fine-grained Bt
- Bulging in qtz



**Sample:** HAL193065

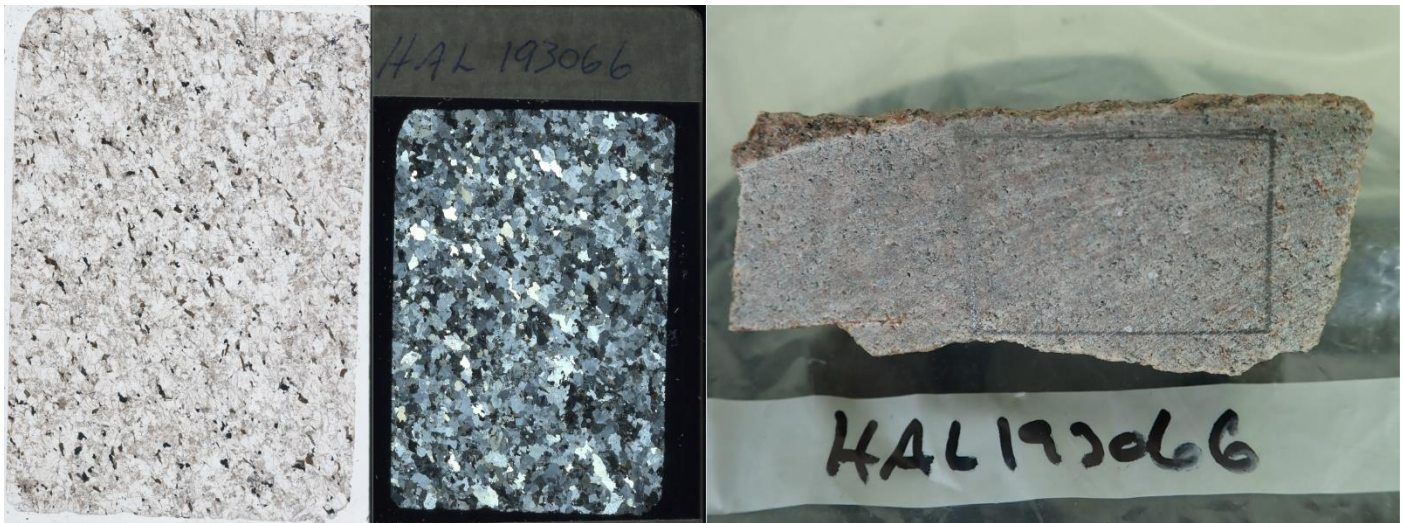
**Location:** 123

**Unit:** Deformed granite

**Major minerals:** Plg (30%), A-Fds (30%), Qtz (25%), Bt (10%), Amp (5%)

**Accessory minerals:** Apa, Zrn, Ser

- A-Fds intergrowth within Plg, and opposite
- Large Fds grains, with small Amp/Bt following foliation
- Perthite, Microcline
- Colourless high interference phases in cracks within Fds
- Some green Bt
- Metamorphic textures such as granoblastic texture and border migration



**Sample:** HAL193066

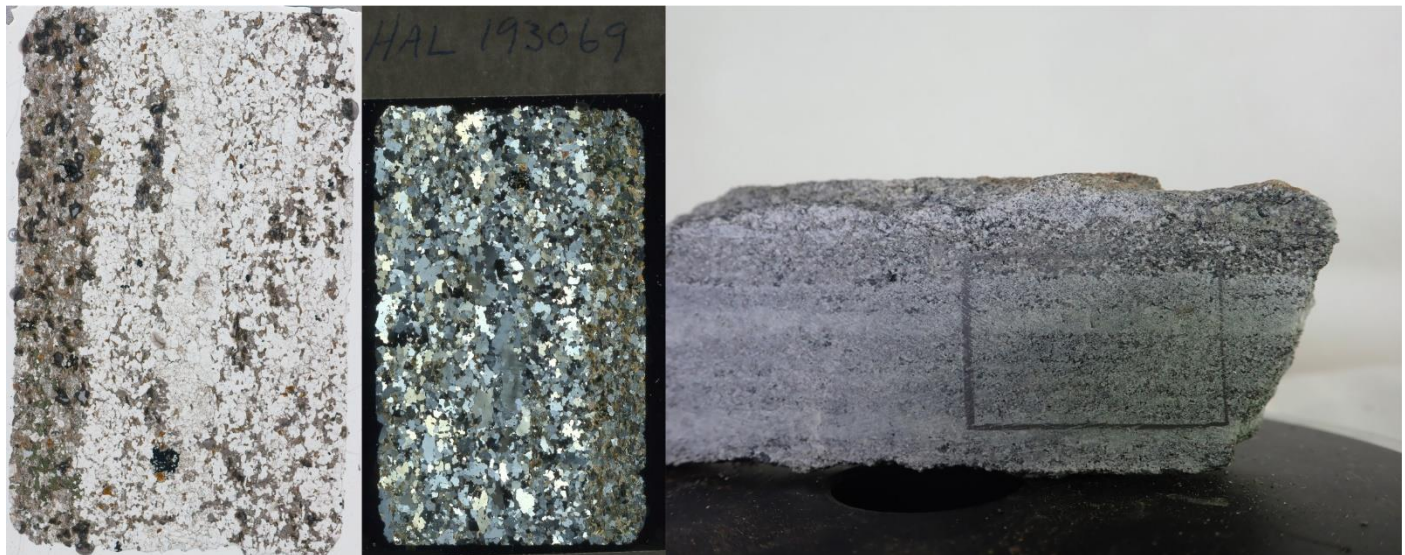
**Location:** 123

**Unit:** Undeformed granite

**Major minerals:** A-Fds (45%), Qtz (33%), Plg (20%), Bt (2%)

**Accessory minerals:** Apa, Zrn

- Fine-grained with leucocratic being 1mm and melanocratic being <0.5 mm
- Green and brown Bt
- Myrmekite, bulging, granoblastic, melttexture
- A slight preferred orientation
- Microcline, Perthite
- Secondary alteration of Fds: Colourless yellow in xpl



**Sample:** HAL193069

**Location:** 126

**Unit:** Migmatite and amphibolite

**Major minerals amphibolite:** Plg (50%), Bt (25%), Amp (15%), Qtz (10%)

**Accessory minerals amphibolite:** Ser

**Major minerals migmatite:** Qtz (55%), Plg (25%), Bt (20%),

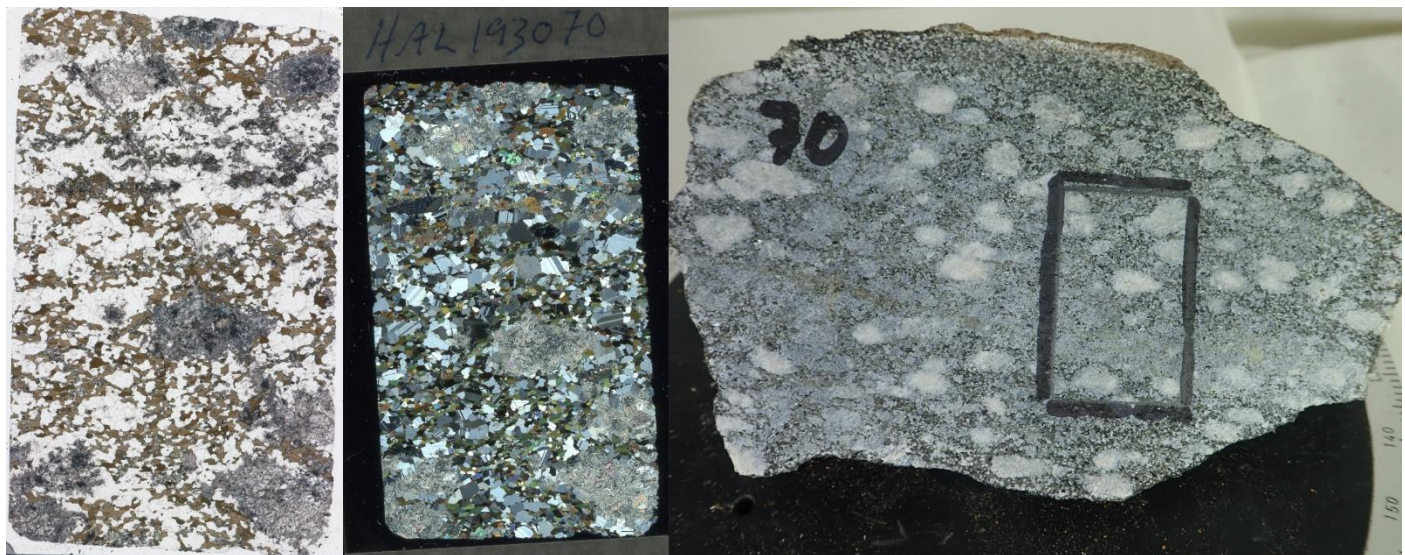
**Accessory minerals migmatite:** Apa, Op

Amp:

- Fds has heavy alteration making it difficult to determine
- Follows clear foliation
- Fine grained

Mig:

- Realy fine-grained disperse Bt and medium-grained Qtz and Fds
- Bt shows orientation
- Recrystallization, and Boundary migration of quartz
- Secondary alteration of Plg, Qtz inclusions in Plg



**Sample:** HAL193070

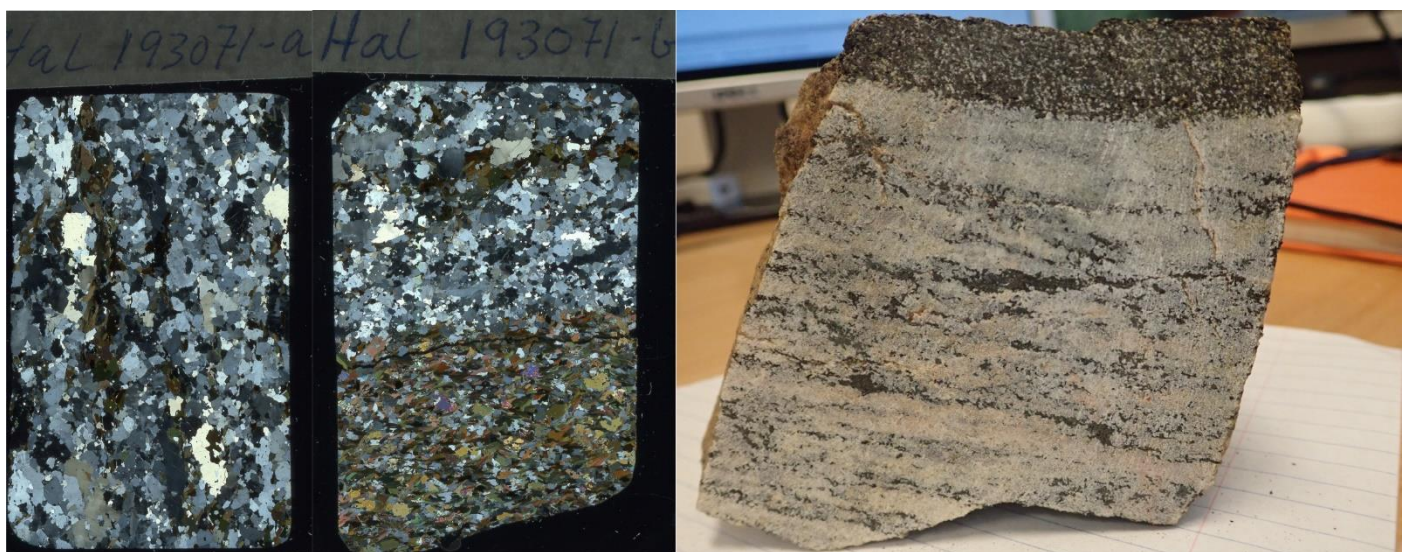
**Location:** 30

**Unit:** Migmatite (porphyritic layer)

**Major minerals:** Plg (70%), Amp (20%), Ttn (10%)

**Accessory minerals:** Msc, Apa

- Strongly altered phenocrysts, possibly Plg. Now fine-grained white micas
- Groundmass of fine to medium-grained Plg, and fine-grained Amp and Ttn
- Alteration in the groundmass seems dedicated to cracks in Ttn and Plg, but in a much less extent than in the phenocrysts



**Sample:** HAL193071-a

**Location:** 20

**Unit:** Flaser-gneiss

**Major minerals:** Qtz (60%), A-Fds (15%), Plg (15%), Amp (15%), Bt (15%)

**Accessory minerals:** Ttn, Apa, Zrn

- Amp and Bt appears as fine to medium-grained linear aggregates along foliation.
- Apa seems to be associated with Amp/Bt
- Zircon as inclusions in Bt
- Leucocratic grains are mostly 1-2 mm with some Qtz extending above 5 mm
- Myrmekite
- Bulging and recrystallization of Qtz

**Sample:** HAL193071-b

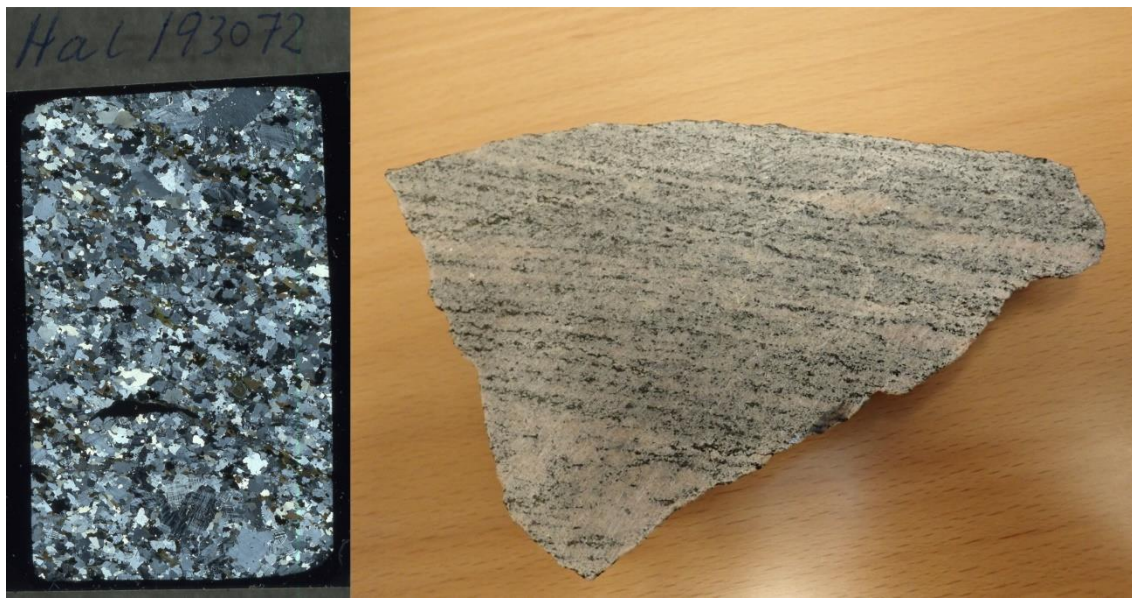
**Location:** 20

**Unit:** Flaser-gneiss and amphibolite (looking at the amphibolite)

**Major minerals:** Bt (45%), Amp (20%), Ttn (15%), Plg (10%), Qtz (10%)

**Accessory minerals:** A-Fds, Zrn, Apa

- Fine-grained disperse with a clear orientation



**Sample:** HAL193072

**Location:** 127

**Unit:** Augen-gneiss

**Major minerals:** A-Fds (50%), Qtz (45%), Amp (5%)

**Accessory minerals:** Bt, Apa, Zrn

- Aggregates of A-Fds up to 0,5 cm
- Recrystallizing of Qtz and bulging
- Myrmekite
- Fine-grained Amp and Bt appears along oriented bands
- The area between the aggregates are dominated by fine-grained Qtz and A-Fds



**Sample:** HAL193073

**Location:** 128

**Unit:** Migmatite

**Major minerals:** Qtz (60%), A-Fds (30%), Amp (5%), Bt (2%)

**Accessory minerals:** Plg, Zrn, Apa

- Mesosome is fine-grained disperse Bt and Leucocratic minerals
- Melanosome consists of medium-grained Amp and Leucocratic minerals
- Leucosome consists of relatively larger leucocratic minerals (up to 4 mm) and some odd Amp, Fds is mostly A-Fds, with some few Plg.
- Intergrowths of Plg inside A-Fds, myrmekite, and recrystallisation of Quartz and bulging



**Sample:** VAG084362

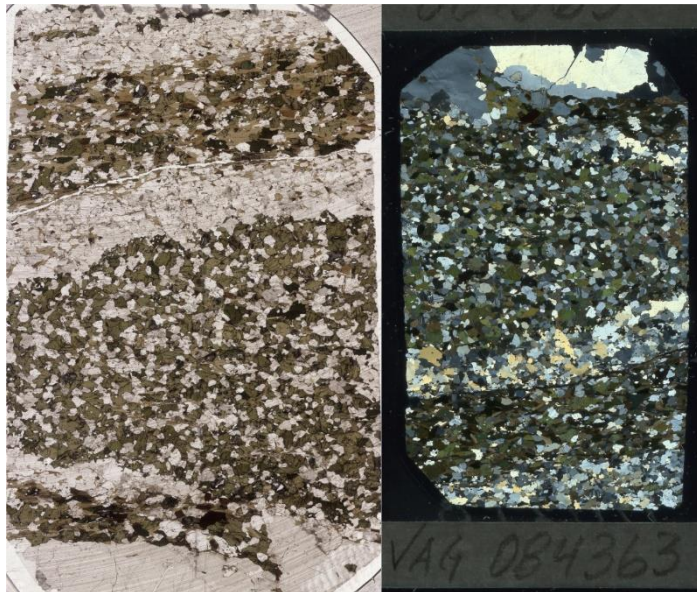
**Location:** Between 35 and 36

**Unit:** Deformed granite

**Major minerals:** Qtz (40%), Plg (35%), Amp (20%), Bt (5%)

**Accessory minerals:** Apa, Zrn, Op

- Aggregates of fine-grained Plg, and recrystallized Qtz
- Bands of fine-grained Amp and Bt with one orientation
- Secondary alteration of Plg
- Bulging of Quartz



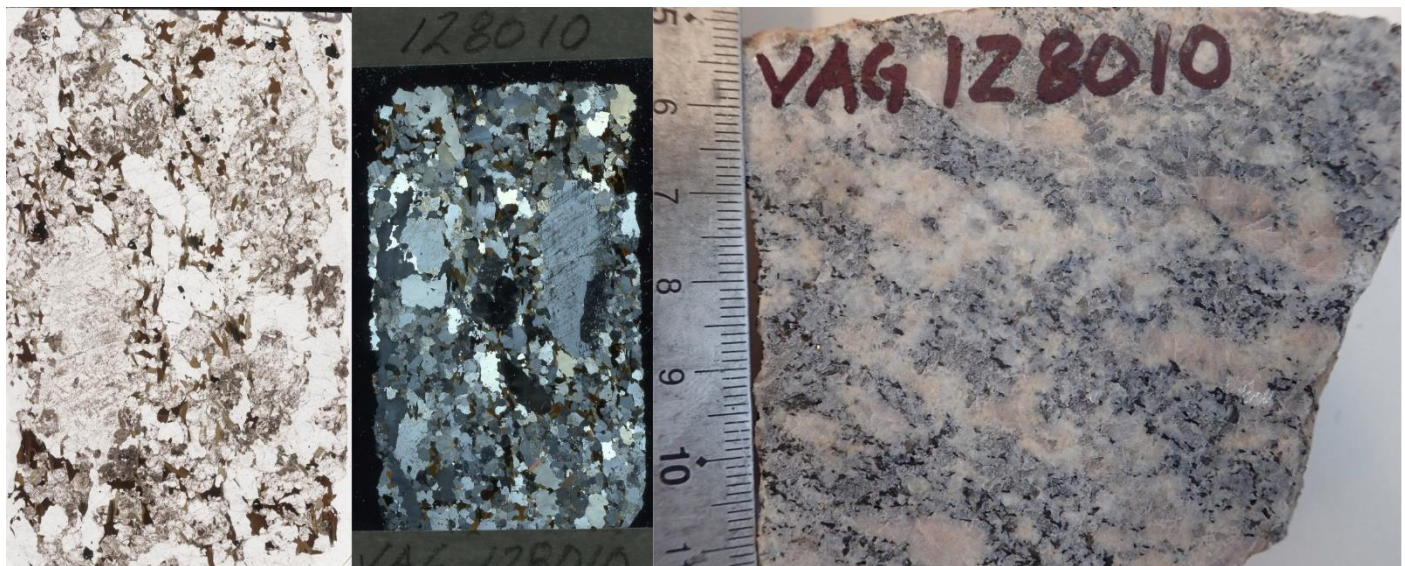
**Sample:** VAG084363

**Location:** Close to 41

**Unit:** Alternating between migmatite and amphibolite

Split into 4 zones:

- Zone 1 consist of coarse-grained Qtz
- Zone 2 consist of fine-grained Amphibolite with Amp(60%), Bt(<1%), Qtz(20%), Plg(20%), Apa(<1%)
- Zone 3 Medium grained Qtz and Plg with some Bt. Qtz in recrystallized and bulges
- Zone 4 is Bt(50%) rich, with some Amp(20%), Qtz(25%) Plg(5%), Apa(<1%)



**Sample:** VAG128010

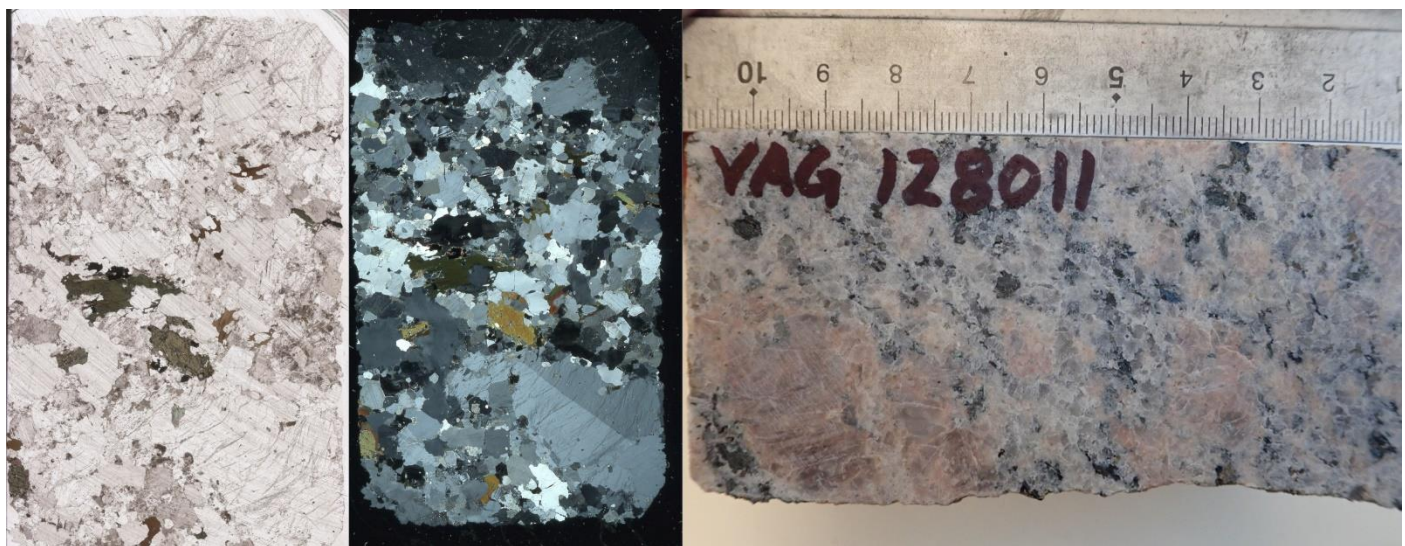
**Location:** Close to 2

**Unit:** Deformed granite

**Major minerals:** A-Fds (60%), Qtz (30%), Plg (5%), Bt (5%)

**Accessory minerals:** Zrn, Apa, Op

- Large microcline phenocrysts
- - very weakly preferred orientation on the Biotite
- Clear Zonation in Zircon
- Myrmekite
- Sweeping undulose extinction in the Quartz, some instances of Bulging



**Sample:** VAG128011

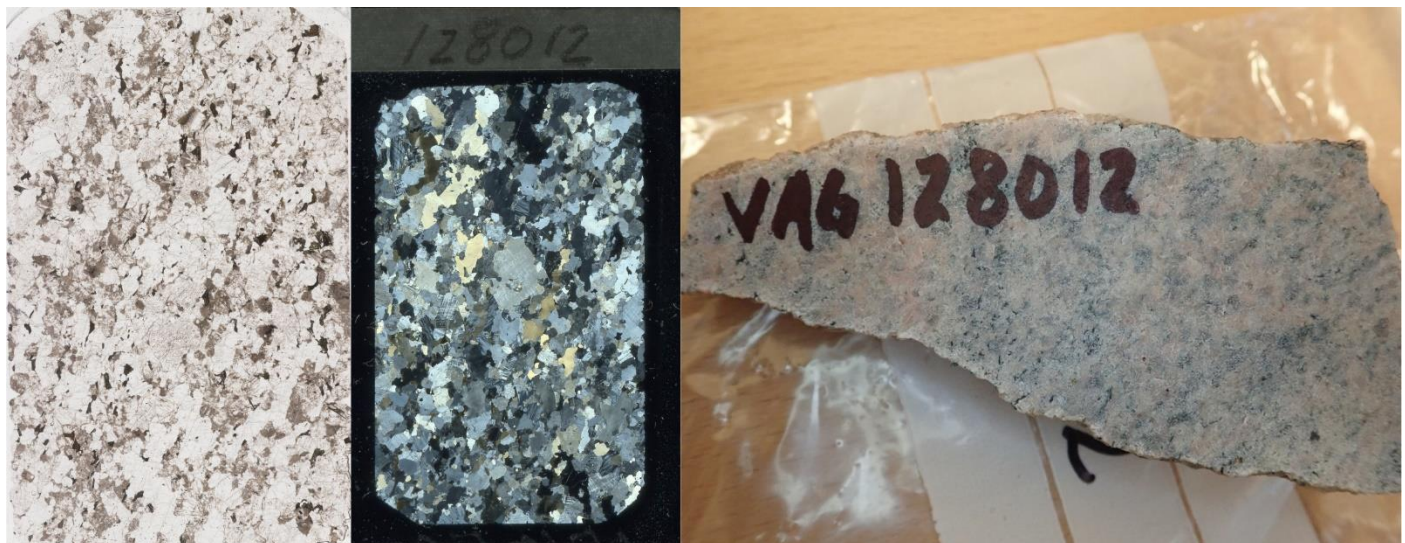
**Location:** Between 1 and 3

**Unit:** Deformed granite

**Major minerals:** A-Fds (80%), Qtz (13%), Plg (5%), Amp (1%)

**Accessory minerals:** Bt, Zrn, Apa, Msc

- Granoblastic textures, melt textures and myrmekites
- Amp and Bt are interstitial megacrystic
- Carlsbad, and perthite
- Msc in association with amp
- Some zoned Zircons



**Sample:** VAG128012

**Location:** Close to 4

**Unit:** Deformed granite

**Major minerals:** A-Fds (64%), Qtz (34%), Plg (1%), Bt (1%)

**Accessory minerals:** Zrn, Apa, Msc

- Bulging
- some green Bt
- Bt's are interstitial and has no preferred orientation.
- Bt's are fine-grained, while the A-Fds are medium-grained
- Sericitization



**Sample:** VAG128013

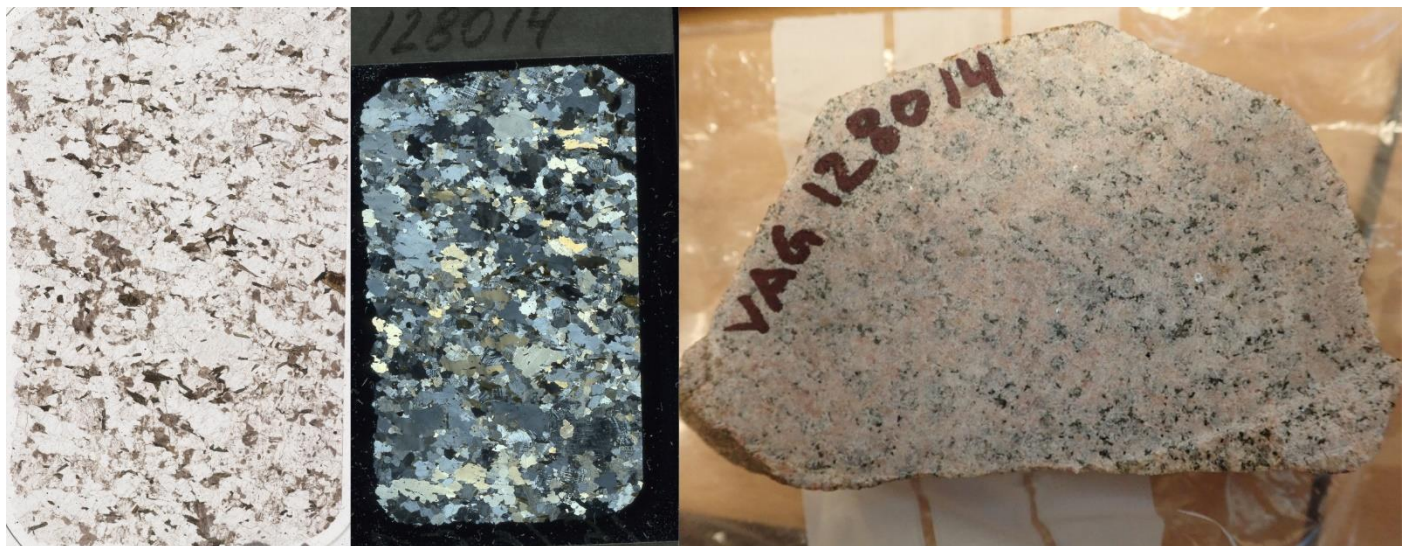
**Location:** Close to 4

**Unit:** Deformed granite

**Major minerals:** A-Fds (40%), Qtz (30%), Plg (25%), Bt (5%), Amp (1%)

**Accessory minerals:** Apa, Zrn

- Foliated
- Amp is concentrated along the central foliation band
- Along central foliation band, Bt and Amp is around 1 to 1,5 mm
- Scattered Bt outside central foliation band is around 0,5
- Grain boundary migration
- Qtz recrystallisation
- Qtz and Fds is mostly fine-grained, less than 1 mm



**Sample:** VAG128014

**Location:** Close to 104

**Unit:** Undeformed granite

**Major minerals:** A-Fds (50%), Qtz (45%), Plg (5%), Bt (1%)

**Accessory minerals:** Aln, Zrn, Apa

- Bt's are scattered with no preferred orientation

- Green and brown Bt

- Grain boundary migration

- Sweeping undulose extinction in Qtz

- Myrmekite

- Secondary alteration of Fds to Ser



**Sample:** VAG128015

**Location:** 13

**Unit:** Undeformed granite

**Major minerals:** A-Fds (45%), Qtz (30%), Plg (25%), Bt (1%)

**Accessory minerals:** Aln, Zrn, Apa

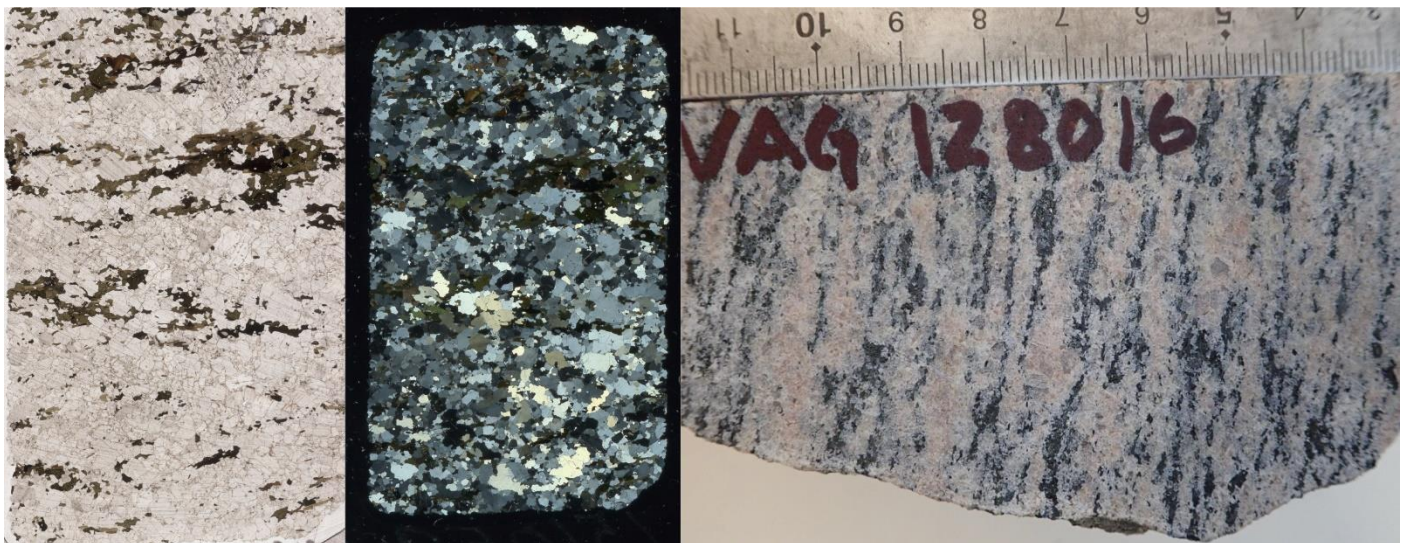
- A few bigger Bt at around 3mm

- Myrmekite

- Bt is scattered with no preferred orientation

- Th level at Allanite grain is measured to 3,05 mol% at Texas Tech

- Grain boundary migration



**Sample:** VAG128016

**Location:** Close to 51

**Unit:** Augen-gneiss

**Major minerals:** Qtz (80%), Plg (30%), A-Fds (15%), Amp (10%), Bt (2%)

**Accessory minerals:** Apa

- Foliated

- Bulging

- Myrmekite



**Sample:** VAG128017

**Location:** Close to 51

**Unit:** Augen-gneiss

**Major minerals:** Qtz (45%) A-Fds (30%), Plg (20%), Bt (5%)

**Accessory minerals:** Amp, Zrn, Msc, Apa

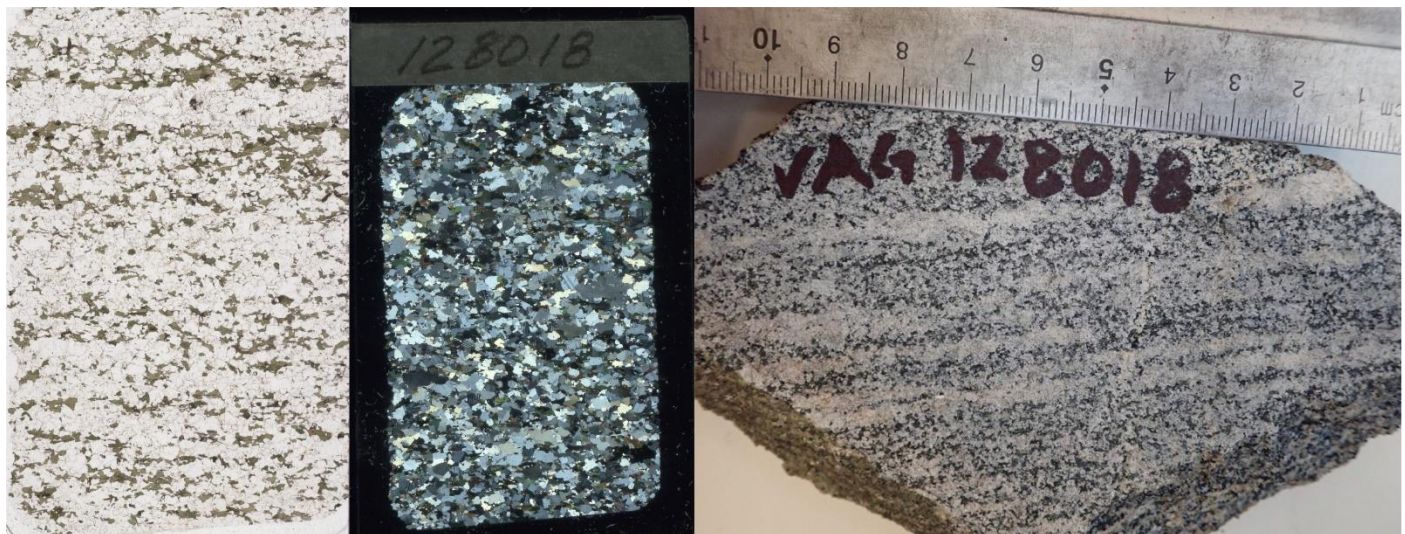
- Foliated

- most of the Amp and Bt are concentrated along on foliation band

- The biggest Bt are found along the band

- Bulging

- Alteration of Fds to White mica



**Sample:** VAG128018

**Location:** Close to 53

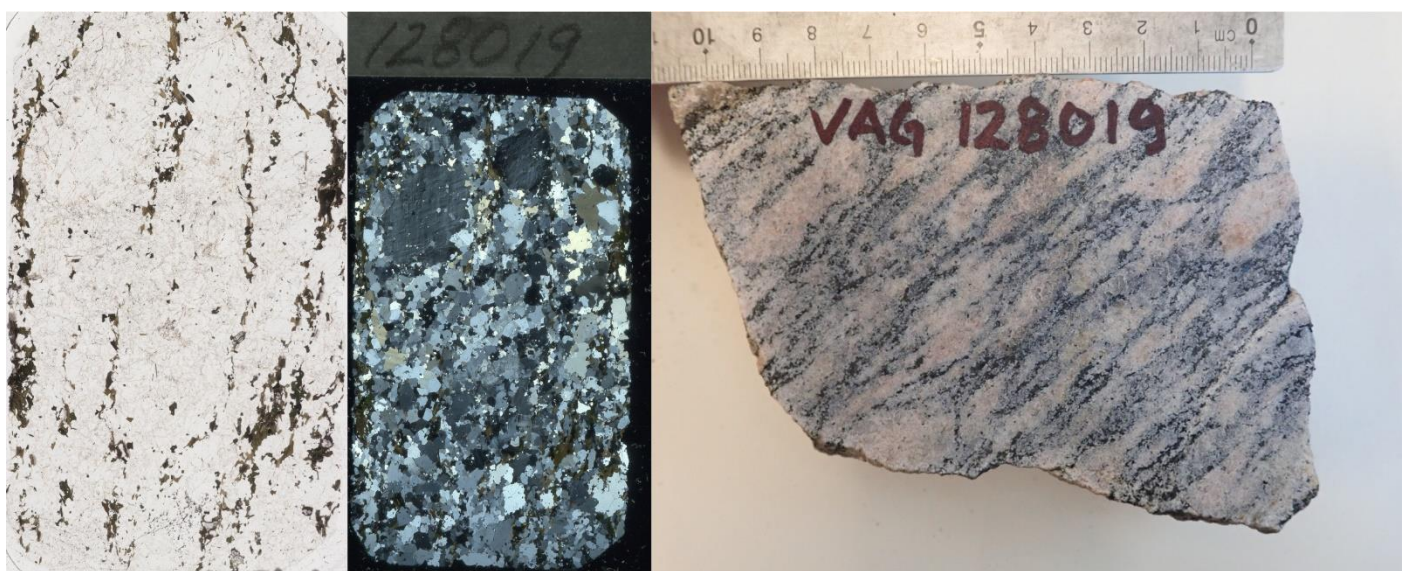
**Unit:** Migmatite

**Major minerals:** Plg (40%), Qtz (30%), Amp (20%), Bt (5%), A-Fds (5%)

**Accessory minerals:** Zrn

Description: Migmatite with >90 % mesosome with the rest consisting with <1 cm thick quartzofeldspathic leucosomes and a thin Amp/Bt melanosome. Both magmatic and metamorph textures are present. The Amp/Bt in follows an orientation similar to that of the leucosomes.

- Granoblastic textures
- Melt textures
- Recrystallisation



**Sample:** VAG128019

**Location:** 8

**Unit:** Flaser-gneiss

**Major minerals:** A-Fds (40%), Plg (34%), Qtz, Amp (5%), Bt (1%)

**Accessory minerals:** Zrn

- Foliated bands of Bt and Amp
- Myrmekite
- Bulging
- Large Aggregates of medium grained quartz and A- Fds
- fine-grained Amp and Bt in oriented bands



**Sample:** VAG128020

**Location:** Between 49 and 50

**Unit:** Migmatite

**Major minerals:** Qtz (40%), Plg (30%), A-Fds (30%)

**Accessory minerals:** Zrn, Ser, Apa

Dominated by medium-grained Microcline and recrystallized Quartz, and Plg effected by Seritization



**Sample:** VAG128021

**Location:** Between 49 and 50

**Unit:** Migmatite

**Major minerals:** A-Fds (35%), Qtz (30%), Plg (30%), Bt (1%)

**Accessory minerals:** Zrn, Ser, Apa

- Green and Brown fine-grained disperse Bt
- Dominated by medium-grained Microcline, Recrystallised Quartz, and Altered Plg
- Sericitisation
- Bt follows one orientation
- Myrmekite